1-1-1973

Light scattering and deformation studies of crystalline polymers.

Do Yeung Yoon
University of Massachusetts Amherst

LIGHT SCATTERING AND DEFORMATION STUDIES OF CRYSTALLINE POLYMERS

A Dissertation Presented

by

Do Yeung Yoon

Submitted to the Graduate School of the
University of Massachusetts in
Partial fullfillment of the requirements for the degree of

DOCTOR OF PHILOSOPHY

April 1973

Major Subject: Polymer Science and Engineering

LIGHT SCATTERING AND DEFORMATION STUDIES OF CRYSTALLINE POLYMERS

A Dissertation Presented

by

Do Yeung Yoon

Approved as to style and content by:

Richard S. Stein
(Chairman of Committee)

(Member)

(Member)

Robert L. Rowell
(Member)

April 1973

ACKNOWLEDGEMENT

The author wishes to express his sincere appreciation to Professor Richard S. Stein, thesis director, for his guidance, encouragement, and many helpful discussions throughout the course of this work.

The helpful advice and suggestions of other members of the thesis committee, Professors Fraser P. Price, William J. Macknight, and Robert L. Rowell are also gratefully acknowledged.

Special thanks are given to a number of coworkers at the Polymer Research Institute for the cooperation and discussions to finish this work; Mr. Robert Prud'homme in the light scattering studies, Mrs. Catherina Chang and Dr. Ronald Finkelstein in the wide angle x-ray and deformation of spherulitic polymers studies, and Dr. Pierre Labarbe in the small angle x-ray studies.

The author express his sincere thanks to University of Massachusetts for awarding assistantship during this work and for awarding the grant for the computer calculation at the University of Massachusetts Computing Center.

Financial assistance of Petroleum Research Fund of American Chemical Society and Office of Naval Research are also sincerely appreciated.

The author thanks to his wife, Kiseup, for the innumerable assistance and encouragement during this work.

TABLE OF CONTENT

LIGHT SCATTERING AND DEFORMATION STUDY OF CRYSTALLINE POLYMERS

(April 1973)

Do Yeung Yoon

Directed by: Professor Richard S. Stein

ABSTRACT

A number of theoretical calculations and an experiment were made, concerning their application to the study of the structure of polymer-related systems and its change upon deformation.

Anisotropic sectors were taken as a model of liquid crystals in the cholestric phase, and the light scattering patterns were predicted from these sectors, which are randomly oriented or arranged in a regular array. These results show good agreement with the experimental results in the small angle region, but differ in the wide angles, which indicate that the local orientation correlation of liquid crystals is more complicated.

The effect of inter-spherulitic interference and truncation was considered for the V_v scattering. It was found that the single spherulite model is sufficient to describe the scattering patterns when the parameters are correctly known.

Light scattering pattern and intensity was calculated, applying the fluctuation theory to the system where the size and number of anisotropic disks are changing untill these disks are volume filling. These results were applied to interpret the change of light scattering during the crystallization of polymers.

The effect of disorder of crystal orientation on the light scattering was considered to interpret the quantitative light scattering measurements. A two dimensional spherulite composed of lattice cells was built by the computer simulation so that the crystal orientation in each lattice cell is correlated with its neighbors. The light scattering intensity distribution from such a spherulite was calculated for different disorder parameters, and the calibration curves were made to relate the experimental results to such disorder parameters.

The change of disorder of crystal orientation in spherulites upon annealing the quenched polyethylene polyethlene sample was studied by the photometric light scattering experiment. It is found that the disorder of crystal orientation increased due to annealing.

A model was proposed to explain the crystal orientation in the deformed spherulitic polymers. Three processes of crystal reorientation were considered; chain tilting, lamellar twisting, and crystal rotation. The model was sucessful in predicting the experimental observation of the 110 and 200 plane diffraction intensity distribution of the low density

polyethylene. It was also applied to the relaxation and dynamic x-ray diffraction experiments, and the time dependence of the orientation processes were determined.

A theoretical consideration was made for the purpose of obtaining the lamellar orientation distribution in deformed spherulites by the small angle x-ray technique. Previous model developed by Tsvankin, and Buchanan was applied, and the peak intensity was calculated for different structural parameters so that lamellar distribution can be obtained by comparing the theoretical and experimental peak intensity.

Local strain in deformed crystalline polymers was calculated, employing the composite theory. The distribution of the crystalline and amorphous strain was obtained, based on assumptions about the geometry of the crystalline phase. The dominant effect of the crystalline morphology and also the crystallinity in determining the local strain distribution was noticed.

INTRODUCTION

A. GENERAL INTRODUCTION

This thesis is concerned with a number of inter-related theoretical studies which have come about as a result of experimental problems carried out in the laboratory of Professor Richard S. Stein. A common thread which unites all of these studies is that they are concerned with application of electromagnetic radiation to the studies of the polymer-related structures.

The application of various types of electromagnetic radiation to study the structures of solid polymer systems and the change of the structures upon deformation will be discussed together with the application of composite theory analysis to the crystalline polymer systems.

The relationship between different kinds of radiation and the size of the objects that are investigated can be approximated as follows:

a) wide angle x-ray; 0.5 - 200(Å)

b) small angle x-ray; 200 - 2,000(Å)

c) wide angle light scattering; 1,000 - 5,000(Å)

d) small angle light scattering; 5,000 - 100,000(Å)

In this thesis, the research work done related to the radiation will be discussed according to the above-mentioned

categories of radiation.

In Part(I), the theoretical and experimental studies concerning the light scattering will be discussed. In Part (II), the model of deformation of spherulitic polymers which is primarily concerned with the wide angle x-ray scattering experiment will be discussed. The theoretical consideration of the application of previous theories of small angle x-ray scattering to characterize the lamellar orientation is presented in Part(III). And the application of composite theory analysis to the crystalline polymers in relating the morphology to the properties of the system will be discussed in Part(IV).

B. MORTHOLOGY OF CRYSTALLINE POLYMERS

The existance of high polymers in the solid state, in the highly ordered crystalline phase and specially disordered amorphous phase, has been well known as evidenced by the electron or x-ray diffraction studies.

The crystalline phase is highly ordered due to the regular molecular packing as can be represented by the basic unit, that is, the unit cell(e.g. for polyethylene[57], orthorombic unit cell with a=7.4Å, b=4.9Å, c=2.9Å[1,2,5]). The classical two phase fringe-micelle model of crystalline polymers was proposed to explain their physical properties and is shown in Fig.(A-1). The crystals were considered as being dispered in the amorphous matrix and acting as inert filler particles binding the amorphous chains together. The polymer chains were believed to pass from one crystal to another. Several drawbacks of this simple model have been noticed[3], and influenced by two significant discoveries, this fringe-micelle model has been changed. One was the discovery of polymer single crystals[4,5,6] in the thin flat platelets with the thickness of the order of 100Å. In these single crystals, the chains were found to be perpendicular to the faces of the platelets, which suggested that the long polymer chains were folded. Another discovery was the recognition of polymer crystallization in the radially growing expanding spheres[9]. Therefore, the structure of crystalline phase in the thin

ribbonlike form(lamellae), and the aggregation of the lamellae into superstructure has been recognized.

Based on these ideas, the following concepts have been formed: In the bulk, polymers crystallize from primary nuclei which are often foreign impurities or amorphous parts where the previous strain has not been completely relaxed. The crystallization proceeds radially outward, leading to expanding spheres(spherulites) which are partially crystalline. The crystalline lamellae form the radii of the spherulites with one crystal axis lying in the radial direction. The lamellae often twist and are branched. Since one crystal axis remains radial, the spherulites are optically anisotropic, the radial and tangential refractive index being different, giving rise to a maltese cross [10] pattern under the polarizing microscope.

Since the structure of crystalline polymers have its order in different dimensions, their properties are also related to the structural order in different dimensions; that is, arrangement of molecules in the unit cell, presence of crystalline phase in the ribbonlike lamellae, and the aggregation of these lamellae into superstructures such as spherulites. Therefore, different kinds of experiments are needed, as mentioned in the preceding section, in order to understand the structure-property relationship, and the change of its structure upon deformation.

The presence of amorphous phase as the crystal defects, [7]

tie chains and loose loops between the crystalline lamellae, and the portions excluded from the crystallization process[8] has been well conceived. Also the amorphous phase has been understood to be in the completely disordered state. However, recently the possibility of certain order in the amorphous phase has been raised.[92] It seems that no definite conclusion can be made about the order in the amorphous phase, based on the previous work. Much more research work is needed to understand its structure and its role in determining the physical properties of crystalline polymers.

Another important feature of the studies of crystalline polymers is the understanding of the interface[79] between the crystalline and the amorphous phase which has recieved little attention so far. It is strongly felt that many assumptions concerning this interface should be cleared and their role in determing properties should be understood.

PART I SMALL ANGLE LIGHT SCATTERING

Introduction

Most crystalline polymers are turbid and give rise to light scattering. The scattering of light is the result of optical heterogenities[15] which involve both the density fluctuations and orientation fluctuations of the medium. In crystalline polymers, density vatiations in the amorphous phase and crystalline phase give rise to density fluctuations, while the orientation fluctuations arise from the aggregation of the anisotropic crystals which have the correlation distance comparable with the wavelength of the light.

Debye and Bueche[11] developed the theory of light scattering from an isotropic medium where there are local fluctuations in density. This theory has been extended by Goldstein and Michalik,[12] and Stein and Wilson[14] to include the fluctuations in orientation of anisotropic scattering elements in the medium as well as the density fluctuations. The attempts to separate the density, and orientation fluctuation were made by Stein and Wilson,[14] assuming the random orientation fluctuations. In this theory, it is assumed that the probability of the optic axes of two scattering elements being parallel is independent of angle β, which the optic axis makes with the separation vector $\underset{\sim}{r}$, but only depends upon the separating

distance. Several theoretical approaches[15,16,21,26] were attempted to include the non-random orientation fluctuations, which imply that orientation correlation depends upon the angle, β. However, the complexity of the theories and the difficulties in characterizing the parameters necessary make the practical analysis inapplicable at present.

Another line of approach to the light scattering from the crystalline polymers was to recognize the superstructure in which polymer crystals are arranged in order(e.g. spherulite, rod and sheaf). The theoretical analysis and the appropriate experimental techniques were developed by Stein and coworkers for the anisotropic spheres[16], disks[17] and rods[20] in which the crystals are arranged in perfect order. The good qualitative agreement between the theories and the experiments made the application of the small angle light scattering technique very powerful in studying the superstructure of crystalline polymers and their changes[16,27] during the deformation.

However the simplicity of the models is such that there is not quantitative agreement between the theoretical and experimental results: that is, the deviations[19] from the perfect order of crystal arrangement should be considered for the quantitative applications of the small angle light scattering results. For these purposes, a simple model of considering spherulitic polymers as a composite[18] of perfect

spherulite and the randomly oriented crystals was developed by Keijzers, van Aartsen and Prins. Also more rigorous attempts were made by Stein and Chu[19], taking into account the fluctuations of crystal orientation inside the spherulites for very simple cases.

One of the important applications of the small angle light scattering technique has been to the studies of the deformation behavior of the crystalline polymers; that is, the change of the light scattering pattern due to the deformation of the polymers is interpreted[17,27,28] in order to understand the morphological or the structural changes occuring inside the polymer specimen. However the lack of theoretical interpretations has limited the application to very qualitative studies. Again, the necessity of more quantitative theoretical developments is strongly felt in order to make the better use of the informations available through the light scattering techniques.

CHAPTER I LIGHT SCATTERING FROM ANISOTROPIC SECTORS

Introduction

The structure of liquid crystals in the cholestric mesophase is believed to consist of focal conic arrangement[34,35] of molecules. The small angle light scattering has been applied to study the morphology of the cholestric phase of cholesteryl myristate by Jabarin[33] and Stein. Small angle four-leaf clover pattern with 45° orientation surrounded by weaker clover pattern with 90° orientation has been observed for the H_v scattering(polarizer and analyzer crossed). The small angle patterns have been interpreted to originate from the spherulitic morphology, and the outer pattern has been assumed to originate from the microstructure of the spherulites which are small focal-conic groups arranged in a radially symmetrical array.

A theoretical model calculation is attempted to test these ideas, and to look for the possible applications to the studies of liquid crystals. The focal-conic texture[35] has the geometry of cones whose bases are ellipses and whose apices are the meeting points of a number of hyperbolas and the cones lie with the bases in various inclinations to the surface. Therefore simple two dimensional anisotropic

sector is assumed as a model for the focal-conic. Light scattering intensities are calculated for such sectors which are randomly oriented. Then scattering pattern for a two dimensional spherulite in which those sectors are regularly arranged, is calculated to compare with the experimental observations

Theory

The amplitude of scattering from an anisotropic system is given by the equation[16,18]

$$E = \frac{4\pi^2}{R\lambda_0^2} \int (\underset{\sim}{M}\cdot\underset{\sim}{O}) \exp\left[ik(\underset{\sim}{r}\cdot\underset{\sim}{s})\right] d\underset{\sim}{r} \qquad \text{(I-1)}$$

where $\underset{\sim}{M}$ is the induced dipole moment, $\underset{\sim}{O}$ is the unit vector perpendicular to the scattered ray and in the plane of polarization of the analyzer, k is the wave number $(2\pi/\lambda)$, λ being the wavelength of light in the medium, λ_0 is the wavelength of light in vacuum, and $\underset{\sim}{s}$ is the propagation vector, $\underset{\sim}{s}_o-\underset{\sim}{s}'$, where $\underset{\sim}{s}_o$ and $\underset{\sim}{s}'$ are the unit vectors of the incident and the scattered ray.

The induced dipole moment, $\underset{\sim}{M}$, is given as[41]

$$\underset{\sim}{M} = (\alpha_1 - \alpha_2)\ (\underset{\sim}{a}\cdot\underset{\sim}{E}_o)\ \underset{\sim}{a} + \alpha_2\underset{\sim}{E}_o \qquad \text{(I-2)}$$

where α_1 and α_2 are the polarizabilities along and perpendicular to the optic axis, $\underset{\sim}{a}$ is the unit vector along the optic axis, and $\underset{\sim}{E}_o$ is the electric field of the incident light

Equations(I-1) and (I-2) are further developed for the sector lying in the plane perpendicular to the incident light and whose axis is oriented by angle γ as shown in Fig.(I-1) from the polarization direction of polarizer(Z axis). The angle β characterizes the aperture of the sector. When the optic axis is shifted by angle δ from the radial direction vector $\underset{\sim}{r}$, it can be shown that

$$\underset{\sim}{a} = \sin(\alpha + \delta)\ \underset{\sim}{j} + \cos(\alpha + \delta)\ \underset{\sim}{k} \qquad \text{(I-3)}$$

where α is the angle between the vector $\underset{\sim}{r}$ and the Z axis. Also the vector $\underset{\sim}{O}$[17] is given for the H_v scattering as

$$\underset{\sim}{O}_{Hv} = \cos\rho_2 \underset{\sim}{j} + \sin\rho_2 \underset{\sim}{i} \qquad \text{(I-4)}$$

where $\cos\rho_2 = \dfrac{\cos\theta}{\sqrt{\cos^2\theta + \sin^2\theta\sin^2\mu}}$

and θ and μ are the scattering and azimuthal angles as shown in Fig.(I-2).

Inserting Eqs.(I-2), (I-3) and (I-4) into Eq.(I-1), the H_v scattering amplitude from the sector whose axis is oriented by γ as shown in Fig.(I-1) is obtained

$$E_{H_v}(\gamma) = C' \int (\underset{\sim}{M} \cdot \underset{\sim}{O}_{H_v}) \exp\left[ik(\underset{\sim}{r} \cdot \underset{\sim}{s})\right] d\underset{\sim}{r}$$

$$= C' E_o \int_0^R \int_{\gamma-\beta/2}^{\gamma+\beta/2} \cos\frac{\rho}{2}(\alpha_1 - \alpha_2) \sin(\alpha+\delta) \cos(\alpha+\delta) \exp\left[ikr \sin\theta \cos(\mu-\alpha)\right] r\, dr\, dr\, d\alpha$$

$$= C' E_o (\alpha_1 - \alpha_2) \frac{R^2}{2W^2} \cos\rho_2 \int_{\gamma-\beta/2}^{\gamma+\beta/2} \frac{\sin\left[2(\alpha+\delta)\right]}{\cos^2(\mu-\alpha)} \left[A \sin A + \cos A - 1 + i(-A \cos A + \sin A)\right] d\alpha \qquad \text{(I-5)}$$

where $A = W \cos(\mu-\alpha)$

$W = KR \sin\theta$

The scattering intensity, $I_{H_v}(\gamma)$, is then given by

$$I_{H_v}(\gamma) = E^*_{H_v}(\gamma) \cdot E_{H_v}(\gamma) \qquad \text{(I-6)}$$

where $E_{H_v}(\gamma)$ is the complex conjugate of $E_{H_v}(\gamma)$.

For the randomly oriented sectors, the total scattering intensity is obtained by averaging the scattering intensity

$$I_{Hv} = \frac{1}{2\pi}\int_0^{2\pi} I_{H_v}(\gamma)\, d\gamma \qquad (I\text{-}7)$$

Next the light scattering pattern is calculated for the disk in which the sectors are arranged as shown in Fig.(I-3). The total scattering amplitude, E_{H_v}, can be expressed as

$$E_{H_v} = \sum_i E_{oi} \qquad (I\text{-}8)$$

where E_{oi} is the scattering amplitude from the ith sector in the disk. In Fig.(I-4), it is seen that

$$\underset{\sim}{r} = \underset{\sim}{r}_o + \underset{\sim}{r}_s \qquad (I\text{-}9)$$

Therefore from Eqs.(I-1) and (I-9),

$$E_{oi} = \int_{\underset{\sim}{r}_o} (\underset{\sim}{M}\cdot\underset{\sim}{O}) \exp\left[ik(\underset{\sim}{r}\cdot\underset{\sim}{s})\right] d\underset{\sim}{r}_o$$

$$= \exp\left[ik(\underset{\sim}{r}_s\cdot\underset{\sim}{s})\right]\int_{\underset{\sim}{r}_o} (\underset{\sim}{M}\cdot\underset{\sim}{O}) \exp\left[ik(\underset{\sim}{r}_o\cdot\underset{\sim}{s})\right] d\underset{\sim}{r}_o \qquad (I\text{-}10)$$

From Eq.(I-5),

$$E_{oi} = \exp\left[ik(\underset{\sim}{r}\cdot\underset{\sim}{s})\right] E_{H_v}(\gamma) \qquad (I\text{-}11)$$

The summation in Eq.(I-8) can be approximated by the integration, assuming that the density of the sectors is constant

throughout the disk. Therefore Eq.(I-8) can be written from Eqs.(I-8), (I-9), (I-10), and (I-11)

$$E_{H_v} = \int_{r_s} E_{oi}\, d\underset{\sim}{r}_s$$

$$= \int_{r_s=0}^{R_s} \int_{\gamma=0}^{2\pi} \exp\left[ik(\underset{\sim}{r}_s \cdot \underset{\sim}{s})\right] E_{H_v}(\gamma)\, r_s dr_s d\gamma \qquad \text{(I-12)}$$

Inserting Eq.(I-5) into Eq.(I-12) and integrating with r_s, Eq.(I-12) becomes

$$E_{H_v} = C' E_o(\alpha_1-\alpha_2)\cos\rho_2 \frac{R^2 R_s^2}{W^2 W_s^2} \int_o^{2\pi} \left\{ \frac{1}{\cos^2(\mu-\gamma)} \left[A_s \sin A_s + \cos A_s - 1 + i(-A_s \cos A_s + \sin A_s) \right] \int_{\gamma-\beta/2}^{\gamma+\beta/2} \frac{\cos(\alpha+\delta)\sin(\alpha+\delta)}{\cos^2(\mu-\alpha)} \left[A\sin A + \cos A - 1 + i(-A\cos A + \sin A) \right] d\alpha \right\} d\gamma$$

(I-13)

where $A_s = kR_s \sin\theta \cos(\mu-\gamma)$

$W_s = kR_s \sin\theta$

R_s = radius of the disk

If we define

$$ZR' = A_s \sin A_s + \cos A_s - 1$$

$$ZR = A\sin A + \cos A - 1$$

$$ZI' = -A_s \cos A_s + \sin A_s$$

$$ZI = -A\cos A + \sin A \qquad \text{(I-14)}$$

then the following relationships are noticed;

$$ZR'(\gamma) = ZR'(\gamma+\pi)$$
$$ZR(\gamma) = ZR(\gamma+\pi)$$
$$ZI'(\gamma) = -ZI'(\gamma+\pi)$$
$$ZI(\gamma) = -ZI(\gamma+\pi) \qquad \text{(I-15)}$$

As a result, the imaginary terms in Eq.(I-13) vanishes and Eq.(I-13) becomes

$$E_{Hv} = C' \cos E_o(\alpha_1-\alpha_2)\frac{R_s^2 R^2}{W_s^2 W^2}\int_{\gamma=0}^{\pi}\int_{\alpha=\gamma-\beta/2}^{\gamma+\beta/2}\frac{\sin[2(\alpha+\delta)]}{[\cos(\mu-\alpha)\cos(\mu-\gamma)]^2}$$
$$\left[ZR'.ZR - ZI'.ZI\right] d\alpha d\gamma \qquad \text{(I-16)}$$

and the scattering intensity, I_{H_v}, is given by

$$I_{H_v} = E_{H_v}^2 \qquad \text{(I-17)}$$

Results

The light scattering pattern from the randomly oriented anisotropic sectors is calculated from Eqs.(I-5), (I-6) and (I-7), using the CDC 3600 at the University Massachusetts Computing Center. The H_v scattering contour diagrams are shown in Figs.(I-5) and (I-6) for different apertures of the sector, β, and δ values of 0° and 45°.

As the sector aperture, β, decreases, the scattering pattern becomes diffused and when β is very small(β=5), it is simillar to that of rods.[20] These results are very similar to the results obtained by Stein and Picot[24] for the two dimensional sheaf. Also in Fig(I-5), it is seen that when the optic axis is oriented by 45° with respect to the sector radius, the scattering pattern also rotates 45 and shows the 90° orientation. In Fig.(I-7), the H_v scattering intensity at μ=45 is plotted for different values of sector aperture, when δ is zero. The scattering intensity curves become smoother and show less significant maxima as the sector aperture decreases. Again the results are similar to those for the sheaf, except that when the sector aperture is less than 90°, the scattering intensity decreases continuously and shows no maximum. It is believed that this difference is due to the loss of symmetry in case of sectors.

The light scattering pattern from the disk composed of

sectors as shown in Fig.(I-3) are calculated from Eqs.(I-15), (I-16) and (I-17). The scattering intensity at $\mu=45^{\circ}$, when δ is zero is shown in Fig.(I-8), and compared with that for a homogeneous two dimensional spherulite. It is seen that two curves are very much the same except there is little difference at the very high scattering angles, and this tendency is the same at other azimuthal angles. When the optic axis is oriented by 45° to the radius of the sector($\delta=45^{\circ}$), the whole scattering pattern rotates by 45°. The maximum scattering intensity position correspond to the dimension of the disk, and no significant effect of the sector structure is noticed in the light scattering patterns.

Discussion

A theoretical model calculation has been made to predict the scattering patterns from the focal-conics. Two dimensional anisotropic sectors are chosen as simple models of focal-conics. When these sectors are oriented randomly, the light scattering patterns which are very similar to those from the sheaves or rods, depending upon the aperture are predicted. When these sectors are arranged in a regular array to form a spherulitic structure, the scattering pattern predicted is almost the same as that for the polymer spherulites. Therefore, the experimental results obtained by Jabarin and

Stein cannot be predicted based on these sector models. It is believed that the small angle four-leaf clover pattern comes from the structure which is very similar to the spherulite, while the wide angle clover pattern which is rotated by 45° from the small angle pattern is the result of strong local orientation correlation[15] of molecules with the correlation distance comparable with the wavelength of light. In other words, the orientation of the optic axes inside the spherulitic structure is not perfect as assumed in the light scattering model. There is disorder of optic axes orientation as will be discussed in CHAPTER IV, and the local orientation correlation of this disorder is believed to be the cause of the wide angle maxima. Further research work is needed in this direction to understand the local orientation correlation of liquid crystals in the cholestric mesophase.

Kawai et al.[36] also calculated the light scattering pattern from the randomly oriented anisotropic sectors. Their mathematical approach is unique in that the calculation is performed in terms of the series expansion of the shape factor of the scattering object, and the same result as shown in Figs.(I-5),(I-6) and (I-7), has been obtained.

CHAPTER II EFFECTS OF INTER-SPHERULITIC INTERFERENCE AND TRUNCATIONS ON THE SMALL ANGLE LIGHT SCATTERING(V_v SCATTERING)

Introduction

The small angle light scattering from the polymeric films has been applied to the study of the morphology of polymers(e.g. spherulite, rod) and its change during crystallization and deformation.[16,27,37] The experimental results have been interpreted by the model calculations based on a single three or two dimensonal spherulite, or randomly oriented rods.

Good qualitative agreement has been noticed between the theory and experiments, and the single model calculations are justified if the sperulite or the rod concentration is very dilute. However, in most experimental systems, the specimen is filled with the spherulites. As a result, the spherulites are impinging upon each other, resulting in the polygonal shape rather than spherical or circular. Also there is the possibility of strong inter-spherulitic interference effect.

Considering these discrepencies in previous theories, the truncation and the interference effects have been considered separately by Stein and Picot.[22,23] The main effect of truncation was found to be the broadening of the maximum

peak region. The possibility of changing the scattering pattern due to inter-spherulitic interference was noticed, using a simple interference function.

More thorough considerations of the truncation and interference effects were attempted by calculating the scattering intensity by computer simulation. The scattering specimen is simulated, based on the assumption that the nucleation sites are randomly located, and the nucleation is heterogenious with constant growth rate of spherulites. Two dimensional spherulites lying in the plane perpendicular to the incident beam with the optic axis oriented along the radius are considered for the computational simplicity. The V_v scattering(polarizer and analyzer parallel) results are reported here. Similar calculation for the H_v scattering (polarizer and analyzer crossed) will be reported by Prud'homme[39].

Theory

The amplitude of light scattering from an anisotropic medium is given by the equation

$$E = C' \int (\underset{\sim}{M}.\underset{\sim}{O}) \exp\left[ik(\underset{\sim}{r}.\underset{\sim}{s})\right] d\underset{\sim}{r} \qquad \text{(II-1)}$$

For the system as shown in Fig.(II-1), the scattering amplitude can be represented as the sum of the amplitude of scattering from the area occupied by the spherulites, E_{sp} and the area surrounding these spherulites, E_{su}

$$E = E_{sp} + E_{su} \qquad \text{(II-2)}$$

The scattering amplitude from the spherulites, E_{sp}, can be given by summing up the scattering amplitude from each spherulite

$$E_{sp} = \Sigma E_i \qquad \text{(II-3)}$$

where E_i is the scattering amplitude from the ith spherulite and from Eq.(II-1),

$$E_i = \int_{\underset{\sim}{r}_i} (\underset{\sim}{M}.\underset{\sim}{O}) \exp\left[ik(\underset{\sim}{r}.\underset{\sim}{s})\right] d\underset{\sim}{r}_i \qquad \text{(III-4)}$$

where the integration is performed over the area occupied by the ith spherulite.
As shown in Fig.(II-1),

$$\underset{\sim}{r} = \underset{\sim}{r}_{oi} + \underset{\sim}{r}_i \qquad \text{(II-5)}$$

where $\underset{\sim}{r}_{oi}$ is the vector from the reference point to the

center of the ith spherulite.

By inserting Eq.(II-5) into Eq.(II-4),

$$E_i = \int_{\underset{\sim}{r}_i} (\underset{\sim}{M}\cdot\underset{\sim}{0}) \exp\left[ik(\underset{\sim}{r}_{oi}+\underset{\sim}{r}_i)\cdot\underset{\sim}{s}\right] d\underset{\sim}{r}_i$$

$$= \exp\left[ik(\underset{\sim}{r}_{oi}\cdot\underset{\sim}{s})\right]\int_{r_i} (\underset{\sim}{M}\cdot\underset{\sim}{0}) \exp\left[ik(\underset{\sim}{r}_i\cdot\underset{\sim}{s})\right] d\underset{\sim}{r}_i \qquad \text{(II-6)}$$

The area surrounding the spherulites can be obtained by subtracting the area occupied by spherulites from the whole area. Therefore the scattering amplitude from this area, E_{su} can be expressed as

$$E_{su} = \int (\underset{\sim}{M}_s\cdot\underset{\sim}{0}) \exp\left[ik(\underset{\sim}{r}\cdot\underset{\sim}{s})\right] d\underset{\sim}{r} - \sum_{i=1} \int_{\underset{\sim}{r}_i} (\underset{\sim}{M}_s\cdot\underset{\sim}{0})$$

$$\exp\left[ik(\underset{\sim}{r}\cdot\underset{\sim}{s})\right] d\underset{\sim}{r}_i \qquad \text{(II-7)}$$

where $\underset{\sim}{M}_s$ is the induced dipole moment in the area surrounding the spherulites. The first term in Eq.(II-7) vanishes since there is no scattering if the medium is completely homogeneous. The second term is identical with Eq.(II-4) except that $\underset{\sim}{M}_s$ is replaced for $\underset{\sim}{M}$. Therefore from Eqs. (II-2),(II-3), (II-4), (II-6), and (II-7), total scattering amplitude, E, becomes

$$E = E_{sp} + E_{su} = \sum_{i=1} \int_{\underset{\sim}{r}_i} \left\{(\underset{\sim}{M}-\underset{\sim}{M}_s)\cdot\underset{\sim}{0}\right\} \exp\left[ik(\underset{\sim}{r}\cdot\underset{\sim}{s})\right] d\underset{\sim}{r}_i$$

$$= \sum_{i=1} \exp\left[ik(\underset{\sim}{r}_{oi}\cdot\underset{\sim}{s})\right] \int_{\underset{\sim}{r}_i} \left\{(\underset{\sim}{M}-\underset{\sim}{M}_s)\cdot\underset{\sim}{0}\right\} \exp\left[ik(\underset{\sim}{r}_i\cdot\underset{\sim}{s})\right] d\underset{\sim}{r}_i$$

$$= \sum_{i=1} \exp\left[ik(\underset{\sim}{r}_{oi}\cdot\underset{\sim}{s})\right] E_i' \qquad \text{(II-8)}$$

where $E_i' = \int_{\underset{\sim}{r}_i} \left\{(\underset{\sim}{M}-\underset{\sim}{M}_s)\cdot\underset{\sim}{0}\right\} \exp\left[ik(\underset{\sim}{r}_i\cdot\underset{\sim}{s})\right] d\underset{\sim}{r}_i$ (II-9)

The Eq.(II-9) was further developed by Stein and Picot[23] for the truncated spherulites as shown in Fig.(II-2)

$$E' = E_{cd} - \sum_i E_t(G_i, \gamma_i) \qquad \text{(II-10)}$$

where E_{cd} is the amplitude scattered by the complete disk, G_i is $\frac{d_i}{R}$, d_i is the distance from the center of the spherulite to the center of the ith truncation, R is the radius of the complete disk and $E_t(G_i, \gamma_i)$ is the amplitude scattered by the ith truncation oriented at an angle γ_i with respect to the reference axis Z, supposing that there is no overlapping of the truncations. Eq.(II-10) is developed for the V_v scattering, for which the amplitude scattered from a complete disk, E_{cd}, is given as[17]

$$(E_{cd})_{V_v} = 2C' \cos\rho_1 \, (A/W^2) \left((\alpha_r-\alpha_s) \left[1-J_o(W) + (\alpha_t-\alpha_s)\right.\right.$$

$$\left.\left[WJ_1(W)+J_o(W)-1\right] - (\alpha_r-\alpha_t) \cos^2\mu \left\{2\left[1-J_o(W)-WJ_1(W)\right\}\right)\right.$$

(II-11)

where W is the reduced variable, $(2\pi R/\lambda)\sin\theta$, A is the area of the disk, $J_n(W)$ is the nth order Bessel function of W, and α_r, α_t are the polarizabilities along the radial and tangential direction of the spherulite. The V_v scattering amplitude from the truncated area, $E_t(G_i, \gamma_i)_{V_v}$, is given as[23]

$$E_t(G_i, \gamma_i)_{V_v} = C' \cos\rho_1 R^2 \left\{(\alpha_r-\alpha_t)\int_{\alpha_1}^{\alpha_2} \cos^2\alpha \left[T_R(\alpha,\gamma)+ iT_I(\alpha,\gamma)\right] d\alpha + (\alpha_t-\alpha_s)\int_{\alpha_1}^{\alpha_2} \left[T_R(\alpha,\gamma)+ iT_I(\alpha,\gamma)\right] d\alpha\right\} \quad \text{(II-12)}$$

with

$$T_R(\alpha,\gamma) = 1/b^2 \left\{\cos b-\cos\left[bG\sec(\alpha-\gamma)\right] + b\sin b - bG\sec(\alpha-\gamma)\sin\left[bG\sec(\alpha-\gamma)\right]\right\} \quad \text{(II-13)}$$

$$T_I(\alpha,\gamma) = 1/b^2 \left\{\sin b-\sin\left[bG\sec(\alpha-\gamma)\right] + b\cos b + bG\sec(\alpha-\gamma)\cos\left[bG\sec(\alpha-\gamma)\right]\right\} \quad \text{(II-14)}$$

and $$b = W\cos(\mu-\alpha) \quad \text{(II-15)}$$

From Eqs.(II-10) (II-15), the Vv scattering amplitude from the truncated spherulite, $(E_i')_{V_v}$, can be expressed by the real part, E_{iR}, and the imaginary part, E_{iI}

$$(E_i')_{V_v} = E_{iR} + i\, E_{iI} \qquad \text{(II-16)}$$

Inserting Eq.(I-16) into Eq.(8), the total V_v scattering amplitude, E_{V_v}, is given as

$$E_{V_v} = \sum_{i=1} \cos\left[k(\underset{\sim}{r}_{oi}\cdot\underset{\sim}{s})\right] E_{iR} - \sin\left[k(\underset{\sim}{r}_{oi}\cdot\underset{\sim}{s})\right] E_{iI}$$

$$+ i\left\{\cos\left[k(\underset{\sim}{r}_{oi}\cdot\underset{\sim}{s})\right] E_{iI} + \sin\left[k(\underset{\sim}{r}_{oi}\cdot\underset{\sim}{s})\right] E_{iR}\right\} \qquad \text{(II-17)}$$

Finally the scattering amplitude, I_{V_V} is obtained by

$$I_{V_v} = E_{V_v}\cdot E_{V_v}^{*} \qquad \text{(II-18)}$$

where $E_{V_v}^{*}$ is the complex conjugate of E_{V_v}.

Computer Simulation

The nucleation site of each spherulite is chosen by the random selection of the coordinates in two dimensional space. Due to the limitation in computing time, 20 spherulites were considered within a circle of 20 μ in radius. On the assumption of the heterogeneous nucleation, each has the same radius. Once the radius of the spherulite is determined, the boundary between the spherulites, i.e., the

truncation parameter, G_i is calculated between the spherulites whose centers are separated by the distance shorter than the diameter of the spherulite. In Fig.(II-3), the simulated spherulites distribution and resulting truncations are shown. For such a given set of spherulites, the V_v scattering intensity is calculated from Eqs.(II-10), (II-18). It is shown for a single spherulite that the scattering is proportional to the square of the area of the spherulite. Therefore for the purpose of comparison with single spherulite calculation, the scattering intensity calculated above should be normalized to that of a single spherulite with the same area. The area of the truncated spherulite A_{TD}, is given

$$A_{TD} = \pi R^2 - A_T \qquad \text{(II-19)}$$

where A_T is the area of truncation, and for the single truncation as shown before ,

$$A_T = \frac{1}{2} R^2(2\epsilon - \sin 2\epsilon) \qquad \text{(II-20)}$$

The area of each spherulite is calculated from Eqs.(II-19) and (II-20), and the average area, $\overline{A_{TD}}$ is obtained. Then, the normalized scattering intensity I_{vv}' is given as

$$I_{V_V}' = \frac{I_{V_V}}{N(\overline{A_{TD}})^2} \qquad \text{(II-21)}$$

These calculations are repeated for 40 different sets of spherulites. The normalized scattering intensity, I_{V_V}', is averaged over these 40 sets of spherulites to eliminate the effects of statistical fluctuations in locating the spherulites.

Throughout these calculations, the polarizabilities, α_r, α_t, α_s remained constant. The effect of increasing volume fraction and also different truncations are considered by increasing the value of radii of the spherulites.

Results

First, the effect of inter-spherulitic interference is considered by neglecting the truncations: that is, each spherulite is considered as a complete disk whose center is chosen randomly as mentioned before and shown in Fig.(II-3). The result is shown in Fig.(II-4) and compared with the single disk case. It is seen that except for the very small angle region, the normalized intensity curve is almost the same as the scattering intensity curve for a single spherulite.

The scattering intensity, calculated considering both the truncations and interference is shown in Fig.(II-5)

and (II-6). Two different values of radius of spherulite, 1μ and 3μ were considered. As mentioned before, increasing the radius results in more severe truncations between the spherulites. These effects are clearly seen in Fig.(II-5) where the scattering intensity from the 3μ spherulites has less significant maximum and minimum, compared with that of 1μ spherulites. However it is clearly noticed that despite the complicated effects of truncation and interference, the normalized scattering intensities is not significantly different in magnitude and angular variation from those of a simple single spherulite with same α_r, α_t, and α_s.

Discussion

From the results shown in Fig.(II-4), it is seen that there is not any significant effect of inter-spherulitic interference. The absence of any significant interference effect is believed to come about as the result of random nucleation assumption. If the truncation is neglected, Eq.(II-18) is given, as shown by Stein and Picot,[22]

$$I_{V_v} = E_{cd}^2 \left[N + \sum_i \sum_{j \neq i} \exp \left[ik(\underset{\sim}{R}_{ij} \cdot \underset{\sim}{s}) \right] \right] \qquad \text{(II-22)}$$

where N is the number of spherulites considered, and R_{ij} is the vector connecting the centers of the ith and jth

spherulite. When the nucleation site is randomly located, the second term in parenthesis in Eq.(II-22) becomes zero, since there is equal probability of this term being positive and negative. The difference noticed in very small angles is believed to come about due to the fact that only those spherulites within a circle of 20μ in radius are considered due to the limitation on computing time. In other words, the big disk of 20μ in radius resulted in excessive scattering at very small angles, and this should be eliminated if a larger area is considered. The change of scattering pattern due to inter-spherulitic interference as reported by Stein and Picot[22] is believed to result from the interference function they used, in which the spherulites were considered as hard spheres which cannot be penetrated.

As shown in Figs.(II-5) and (II-6), the effects of interference and truncation are not so significant when normalized intensity is considered. Also it should be noted that increasing the volume fraction of spherulites in the field of 20μ in radius as introduced by increasing the radius of each spherulite does not affect the change of the scattering pattern in any significant way. This is in contradiction with the experimental results as obtained during the crystallization process. Experimental V_V scattering patterns[16,37] show a change from the isotropic circular pattern to the oriented anisotropic

pattern. This difference can be explained on the ground that the polarizability of the surroundings, α_s, depends on the volume fraction of the spherulites, since this term includes the contribution from the field outside the chosen area of 20μ radius. A more thorough analysis of the nature of the surrounding polarizability, α_s, and change in scattering pattern and scattering intensity when the volume fraction of the spherulites change will be considered in the next chapter. However at this point, it is concluded that when the correct value of surrounding polarizability, α_s, is employed, the scattering pattern calculated on the basis of a single spherulite is not significantly different from the scattering pattern calculated considering the truncation and inter-spherulitic interference. This point may be applied to the real system where the spherulites are volume filling, and previous interpretations based on a single two or three dimensional spherulite model are justified.

CHAPTER III LIGHT SCATTERING DURING THE CRYSTALLIZATION OF POLYMERS

Introduction

In most polymers, the crystallization starts from the heterogeneous nuclei, and proceeds radially outwardly, leading to expending spheres(spherulites). Since the dimensions of these spherulites are comparable with the wavelength of light and their growth rate is fast, the small angle light scattering experiments have proven to be a very powerful technique in study of the morphology and kinetics[16,38] of polymer crystallization.

When the polymer melt is cooled, the V_v scattering pattern which first develops is circular without any orientation, and continues to intensify. Then the scattering intensity decreases to reach a minimum after which a new pattern develops which is extended along the polarization directs. With H_v polarization, a weak cloverleaf pattern appears, which continues to decrease in size,and intensify as the crystallization further proceeds.

The H_v patterns are easily interpreted, since the cloverleaf pattern decreases in size and its intensity increases as the spherulite radius increases. The V_v patterns have been qualitatively interpreted to explain the polymer crystallization. In the begining, the spherulites are of low crystallinity so

that the anisotropy in spherulites is much lower than the polarizability difference between the melt and the spherulites. Therefore the spherulites are similar to isotropic spheres located in the medium of different density. As a result, the V_v pattern is circular, which intensifies as the volume fraction of spherulites increases, and then decreases to a minimum when the field is completely filled with these nearly isotropic spherulites. As the crystallization continues inside the spherulites, the anisotropy increases, and therefore the extended pattern is obtained.

However the appropriate theories which can substantiate these experimental observations have not been avaiable. Although the simple theories based on a single two[17] or three[16] dimensional spherulite model have been successful in explaining the scattering patterns, these model approaches are not satisfactory if the volume fraction of spherulites is appreciable, especially for the V_v scattering. Since the V_v scattering comes not only from spherulites, but also from isotropic medium, the total scattering intensity becomes very complicated. As has been mentioned in Chapter II, extensive computer simulation calculation has been restricted to small number of spherulites due to the limittations on computing time, and also the nature of the surrounding polarizability, α_s, was uncertain.

Similar problems concerning isotropic spheres have been solved successfully by Sturgill,[43] who applied the fluctuation theory of Debye and Bueche[11] in calculating the scattering intensity from the isotropic spheres of appreciable concentrations. After a long computer calculation, Sturgill has found that if the isotropic spheres can randomly overlap, the Debye correlation function, $\gamma(r)$, for the whole field is the same as that for a single sphere.

Sturgill's method can be extended to the anisotropic spherulites, where the Debye correlation function should be expressed as vector functions. For the mathmatical simplicity, the problem is restricted to the two dimensional anisotropic disks, where the optic axis is perfectly oriented along the radius. The H_v and V_v scattering patterns and intensity changes are calculated as a function of volume fraction of spherulites in the field. The polarizability of surroundings, α_s, is also defined.

Theory

The amplitude of scattering from the system where there is fluctuations of electron density, ρ, is expressed as

$$E = K \int \rho \exp\left[ik(\underset{\sim}{r}\cdot\underset{\sim}{s})\right] d\underset{\sim}{r} \qquad \text{(III-1)}$$

where K is the proportionality constant and other terms have been defined in Eq.(I-1). In terms of average density ρ_o, the density at any point is given as

$$\rho = \rho_o + \eta \qquad \text{(III-2)}$$

the quanty η being a measure of the density fluctuation. Then, Debye and Bueche showed that the scattering intensity, I, can be given as

$$I = E.E^* = K^2 \int_V \eta_n \eta_m \exp\left[ik(\underset{\sim}{r}_n - \underset{\sim}{r}_m)s\right] d\underset{\sim}{r}_n \, d\underset{\sim}{r}_m \qquad \text{(III-3)}$$

By introducing the Debye correlation function, $\gamma(\underset{\sim}{r})$, which can be defined as

$$\gamma(\underset{\sim}{r}) = \frac{1}{\overline{\eta^2} V} \int_V \eta(\underset{\sim}{x}) \eta(\underset{\sim}{x}+\underset{\sim}{r}) \, d\underset{\sim}{x} \qquad \text{(III-4)}$$

the scattering intensity from the isotropic medium where the correlation function is independent of orientation, is given as

$$I = K^2 \, \overline{\eta^2} \, V \int \gamma(\underset{\sim}{r}) \exp\left[ik(\underset{\sim}{r}.\underset{\sim}{s})\right] d\underset{\sim}{r} \qquad \text{(III-5)}$$

$$= 4\pi K^2 \, \overline{\eta^2} \, V \int_0^\infty \gamma(r) \frac{\sin hr}{hr} r^2 \, dr \qquad \text{(III-6)}$$

where $\bar{\eta}^2$ is the average square fluctuation and h is the phase factor given by, $h = 4\pi(\sin\theta/2)/\lambda$.

Sturgill applied this fluctuation theory to calculate the scattering intensity from isotropic spheres which can overlap randomly. The correlation function, $\gamma(r)$, obtained from Eq.(III-4) by a long computer caculation has been found to be almost the same for all sphere concentrations as that for a single sphere given as[30]

$$\gamma(r) = 1 - \frac{3}{4}\left(\frac{r}{R}\right) + \frac{1}{16}\left(\frac{r}{R}\right)^3 \qquad \text{(III-7)}$$

where R is the radius of the sphere. The average square fluctuation depends upon sphere concentration, and therefore the scattering intensity changes accordingly from Eq.(III-6).

The amplitude of scattering from an anisotropic system is given by Eq.(I-1) as

$$E = C' \int (\underset{\sim}{M}.\underset{\sim}{O}) \exp\left[ik(\underset{\sim}{r}.\underset{\sim}{s})\right] d\underset{\sim}{r} \qquad \text{(III-8)}$$

Comparing Eq.(III-8) with Eq.(III-1), it is noticed that the anisotropic system can be treated similarly by the fluctuation theory if one recognizes that the term, $(\underset{\sim}{M}.\underset{\sim}{O})$, which is similar to ρ in Eq.(III-1), depends upon the orientation of volume elements inside spherulites. In this respect, Eq.(III-8) can be rewritten as

$$E = C' \int \sigma(\underset{\sim}{r}) \exp\left[ik(\underset{\sim}{r}.\underset{\sim}{s})\right] d\underset{\sim}{r} \qquad \text{(III-9)}$$

and $\sigma(\underset{\sim}{r}) \cong (\underset{\sim}{M}.\underset{\sim}{O})$ (III-10)

Eq.(III-9) is further developed by the fluctuation theory for the H_v and V_v scattering

a. H_v scattering

With H_v polarization, from Eq.(I-3) and (I-4) the term, $(\underset{\sim}{M}.\underset{\sim}{O})$, is given as

$$(\underset{\sim}{M}.\underset{\sim}{O})_{H_v} = \tfrac{1}{2}E_o(\alpha_r - \alpha_t)\sin 2\alpha \qquad \text{(III-11)}$$

where α is the angle between the optic axis and the polarization direction of the incident beam. When the volume element is in the isotropic field surrounding spherulites, there is no scattering. Therefore σ, defined in Eq.(III-10) is zero. When the volume element is inside spherulites, σ is given by Eq.(III-11). The average of σ for the volume elements inside spherulites, $\overline{\sigma}_{sp}$ is given by

$$\overline{\sigma}_{sp} = \frac{\frac{1}{2}E_o(\alpha_r - \alpha_t)\int_o^{2\pi} \sin 2\alpha \, d\alpha}{2\pi} = 0 \qquad \text{(III-12)}$$

Therefore the average value of σ for the whole field, $\overline{\sigma}$, is

also zero. Therefore the fluctuation of from the average defined similarly as in Eq.(III-2) by

$$\eta = \sigma - \bar{\sigma} \qquad \text{(III-13)}$$

is zero for the volume elements in the isotropic field. And for the volume elements inside the spherulites, the fluctuation of σ, η_{sp}, is given by

$$\eta_{sp} = \frac{1}{2} E_o(\alpha_r - \alpha_t) \sin 2\alpha \qquad \text{(III-14)}$$

Therefore the average square fluctuation for the H_v scattering, $\bar{\eta}^2_{H_v}$ is given by

$$\bar{\eta}^2_{H_v} = \phi \bar{\eta}^2_{sp} = \phi \frac{\frac{1}{\pi} E_o^2 (\alpha_r - \alpha_t)^2 \int_o^{2\pi} \sin^2 2\alpha \, d\alpha}{2\pi}$$

$$= \frac{1}{8} \phi E_o^2 (\alpha_r - \alpha_t)^2 \qquad \text{(III-15)}$$

where ϕ is the volume fraction of spherulites in the field.

Since Eq. (III-9) can be developed in the same way as done for Eq.(III-1), the H_v scattering intensity, I_{Hv}, is given similar to Eq.(III-5) by

$$I_{H_v} = C'^2 \bar{\eta}^2_{H_v} V \int \gamma(\underset{\sim}{r}) \exp\left[ik(\underset{\sim}{r}.\underset{\sim}{s})\right] d\underset{\sim}{r} \qquad \text{(III-16)}$$

$$= \frac{1}{8} c'^2 E_o^2 (\alpha_r - \alpha_t)^2 V\phi \int \gamma(\underset{\sim}{r}) \exp\left[ik(\underset{\sim}{r}\cdot\underset{\sim}{s})\right] d\underset{\sim}{r} \qquad \text{(III-17)}$$

According to Sturgill's results, the correlation function, $\gamma(\underset{\sim}{r})$, can be obtained from Eqs.(III-4) and (III-14) by performing the integration in Eq.(III-4) over only one spherulite, if the spherulites are randomly located. In that case, Eq.(III-4) can be calculated numerically.

b. V_v scattering

With V_v polarization, the term, $(\underset{\sim}{M}\cdot\underset{\sim}{O})$ is given by

$$(\underset{\sim}{M}\cdot\underset{\sim}{O})V_v = E_o \left[(\alpha_r - \alpha_t)\cos^2\alpha + \alpha_t \right] \qquad \text{(III-18)}$$

Therfore, the value of σ in Eq.(III-9) is given by Eq.(III-18), if the volume elements are inside spherulites, and it is given by $\alpha_m E_o$, α_m being the polarizability of the isotropic field outside spherulites, if the volume elements are outside spherulites. Then, the average value of σ for the whole field, $\bar{\sigma}$, is given by

$$\bar{\sigma} = E_o(1-\phi)\alpha_m + \frac{\phi E_o \int_o^{2\pi} \left[(\alpha_r - \alpha_t)\cos^2 + \alpha_t \right] d\alpha}{2\pi}$$

$$= E_o(1-\phi)\alpha_m + \frac{\phi E_o}{2}(\alpha_r + \alpha_t) \qquad \text{(III-19)}$$

Therefore for the volume elements inside spherulites, the fluctuation of δ, η_{sp}, is given by

$$\eta_{sp} = E_o\left[(\alpha_r-\alpha_t)\cos^2\alpha + \alpha_t\right] - \bar{\sigma}$$

$$= E_o\left[\left(\cos^2\alpha - \frac{\phi}{2}\right)(\alpha_r-\alpha_t) + (1-\phi)(\alpha_t-\alpha_m)\right] \quad \text{(III-20)}$$

and the fluctuation outside spherulites, η_m, is given by

$$\eta_m = E_o\alpha_m - \bar{\sigma} = \phi\, E_o\left[\frac{1}{2}(\alpha_r+\alpha_t) - \alpha_m\right] \quad \text{(III-21)}$$

Therefore the average square fluctuation for the whole field, $\overline{\eta^2}_{V_V}$, can be obtained by

$$\overline{\eta^2}_{V_V} = \phi\frac{\int_o^{2\pi}\eta_{sp}^2\, d\alpha}{2\pi} + (1-\phi)\eta_m^2 \quad \text{(III-22)}$$

$$= E_o^2\left[\phi(1-\phi)(\alpha_t-\alpha_m)(\alpha_r-\alpha_m) + (\alpha_r-\alpha_t)^2\left(\frac{3}{8}-\frac{\phi}{4}\right)\right] \quad \text{(III-23)}$$

In Eq.(III-23), it is found that the first term shows the contribution from density fluctuation, and the second term is due to the orientation fluctuation.

As shown in H_v scattering, the V_v scattering intensity, I_{V_v}, can be obtained by

$$I_{V_v} = C'^2 E_o^2 \left[\phi (1-\phi)(\alpha_r-\alpha_m)(\alpha_t-\alpha_m) + (\alpha_r-\alpha_t)^2(\frac{3}{8} - \frac{\phi}{4}) \right] V$$

$$\int \gamma(\underset{\sim}{r}) \exp\left[ik(\underset{\sim}{r}.\underset{\sim}{s}) \right] d\underset{\sim}{r} \qquad \text{(III-24)}$$

In Eq.(III-24), the scattering intensity dependence on volume fraction of spherulites is clearly noticed.
Also the correlation function, $\gamma(\underset{\sim}{r})$, is calculated in the same way as done for the H_v scattering, from Eqs.(III-20), and (III-4).

Results

a. H_v scattering

The correlation function, $\underset{\sim}{\gamma}(\underset{\sim}{r})$, for the H_v scattering and scattering intensity, I_{Hv}, are calculated from Eqs.(III-4), (III-14), and (III-17) by numerical calculations and the computer programs are shown in Appendix(III).
The correlation function is shown in Fig(III-1), and it is seen that the correlation function for the anisotropic system depends upon not only the separation distance but also the angle α, which the separation vector $\underset{\sim}{r}$, makes with respect to the polarization direction. The scattering intensity is plotted in Figs(III-2) and (III-3), and it is found that these results are in good agreement with those obtained from the model calculation. As expected from Eq.(III-14), the correlation function is independent of the volume fraction of spheru-

lites. Also, as shown in Fig(III-1), the correlation function can be expressed as a single function of α and r/R, for all volume fractions of spherulites. As a result, the shape of the scattering pattern is also independent of spherulite concentration, but the size and intensity are changing as the number of spherulites per unit volume, N_s, and the radius of spherulite, R, vary. This relationship can be shown from Eq.(III-17) as follows.

In Eq.(III-17), for two-dimensional spherulites,

$$\phi = N_s(\pi R^2) \tag{III-25}$$

If one replaces r with p by

$$p = r/R$$

Eq.(III-17) can be expressed by

$$I_{H_V} = \frac{\pi}{8} C'^2 E_o^2 (\alpha_r - \alpha_t)^2 V N_s R^4 \int \gamma(\underset{\sim}{p}) \exp\left[ikR(\underset{\sim}{p}.\underset{\sim}{s})\right] d\alpha\, p\, dp$$

$$= \frac{\pi}{8} C'^2 E_o^2 (\alpha_r - \alpha_t)^2 V N_s R^4 \int \gamma(\underset{\sim}{p}) \exp\left[iWp\cos(\mu-\alpha)\right] d\alpha\, pdp \tag{III-26}$$

The integration over p needs to be done up to p=2, since the correlation function is zero, when $p > 2$ as shown in Fig.(III-1). As has been mensioned,

correlation function expressed as a function of p is the same for all volume fractions of spherulites. Therefore, the integration term in Eq.(III-26) can be uniquely defined as the function of W and μ, I^o_{Hv}. Then Eq.(26) is further simplied to be given by

$$I_{H_v} = K'^2(\alpha_r-\alpha_t)^2 N_s R^4 I^o_{H_v} \qquad \text{(III-27)}$$

where $K' = \frac{\pi}{8}C'^2E_o^2V$

The exact expression for $I^o_{H_v}$ can be obtained by comparing with the results obtained based on a complete disk model,[17] since both results show the same scattering pattern. Therefore $I^o_{H_v}$ is found to be given as

$$I^o_{H_v} = \frac{8\pi}{W^4}\left[2- 2J_o(W) - WJ_1(W)\right]^2 \sin^2 2\mu \qquad \text{(III-28)}$$

where J_o and J_1 indicate the zero and first order Bessel functions.

Eq.(III-27) is valid for all volume fractions of spherulites in the field, and the H_v scattering pattern during the crystallization of polymers can be interpreted by Eq.(III-27).

b. V_v scattering

For the V_v scattering, scattering intensity change during the crystallization of polymers is complicated as shown in

the expression for the average square fluctuation in Eq.(III-23) The average square fluctuation is plotted in Fig.(III-4), as a function of volume fraction of spherulites for several combinations of $(\alpha_r-\alpha_m)$, and $(\alpha_r-\alpha_t)$. As is shown, the average square fluctuation, and therefore the scattering intensity as related shown in Eq.(III-24) goes through maximum in certain cases. More careful consideration of Eq.(III-23) indicates that the scattering intensity goes through maximum when the polarizability of the isotropic field(e.g. supercooled melt) has the value that is not between the polarizabilities along the radial and tangential direction of the spherulite (i.e. $(\alpha_r-\alpha_m)(\alpha_t-\alpha_m) < 0$). This is the case for most experiments of polymer crystallization.

In contrast to the H_v case,where the correlation function and the shape of scattering pattern are independent of the spherulite concentration, it is expected from Eq.(III-20) that the correlation function and therefore the the shape of scattering pattern is very much dependent upon the volume fraction of spherulites for the V_v scattering.
Eq.(III-20) can be rewritten as

$$\eta_{sp} = E_o\left[\left(\cos^2\alpha - \frac{\phi}{2}\right)(\alpha_r-\alpha_t) + (1-\phi)(\alpha_t-\alpha_m)\right]$$

$$= E_o\left[\cos^2\alpha(\alpha_r-\alpha_t) + \alpha_t - \alpha_b\right] \qquad \text{(III-29)}$$

where $\alpha_b = \phi(\frac{\alpha_r+\alpha_t}{2}) + (1-\phi)\alpha_m$ (III-30)

The correlation function is shown in Figs(III-5), (III-6), and (III-7) for several values of $(\alpha_t-\alpha_b)$, while $(\alpha_r-\alpha_t)$ remains constant, which shows the effect of spherulites volume fraction. For the bulk crystallization, the supercooled melt has lower polarizability than α_r, or α_t. Therefore as the spherulites volume fraction increases, α_b increases and $(\alpha_t-\alpha_b)$ decreases. When the spherulites are volume filling, from Eq.(III-30) and (III-29),

$$\eta_{sp} = E_o\left[\cos^2\alpha(\alpha_r-\alpha_t) + (\frac{\alpha_t-\alpha_r}{2})\right]$$

$$= \frac{E_o}{2}(\alpha_r-\alpha_t)\cos 2\alpha \qquad \text{(III-31)}$$

Therefore, the correlation function is given as the 45° rotation of the H_v correlation function as shown in Fig.(III-7). And the V_v pattern is predicted to be a cloverleaf pattern with 90° orientation. At the early stage of crystallization, $(\alpha_t-\alpha_b)$ is much bigger than $(\alpha_t-\alpha_r)$ as in Fig.(III-5). In that case, the correlation function is very close to that of isotropic spheres as given by Eq.(III-7). Therefore, circular scattering pattern is predicted. As the spherulites volume fraction increases, $(\alpha_t-\alpha_b)$ decreases as shown in Fig.(III-6). Then the correlation function

as shown in Fig.(III-6) shows slight anisotropy, and the scattering pattern is also slightly extended along the polarization direction, as shown in Fig.(III-8).

It can be also shown that the shape of the scattering pattern calculated by the fluctuation theory is the same as that obtained from the model calculation when the polarizability, α_s, is given by α_b defined by Eq.(III-30).

Therefore the total intensity function for the V_v scattering can be developed, combining the fluctuation theory with the model calculation.[17]
Since the correlation function is obtained from Eq.(III-4) where the integration is restricted over one spherulite, the denominator is replaced by $\overline{\eta}_{sp}^2(\pi R^2)$ in calculating the the H_v and V_v correlation functions as shown before. Therefore from Eqs.(III-24), (III-20), and (III-30), I_{V_v} can be given by

$$I_{V_v} = C'^2 E_o^2 \left[\phi(1-\phi)(\alpha_r-\alpha_m)(\alpha_t-\alpha_m) + (\alpha_r-\alpha_t)^2(\tfrac{3}{8} - \tfrac{\phi}{4})\right] V$$

$$\frac{\overline{\eta}_{sp}^2 \pi R^2 \int \gamma(\underset{\sim}{r}) \exp\left[ik(\underset{\sim}{r}.\underset{\sim}{s})\right] d\underset{\sim}{r}}{\pi \overline{\eta}_{sp}^2 R^2}$$

$$= C'^2 E_o^2 \left[\phi(1-\phi)(\alpha_r-\alpha_m)(\alpha_t-\alpha_m) + (\alpha_r-\alpha_t)^2(\tfrac{3}{8} - \tfrac{\phi}{4})\right] V$$

$$\frac{\left\{\int \eta_{sp} \exp\left[ik(\underset{\sim}{r}.\underset{\sim}{s})\right] d\underset{\sim}{r}\right\}^2}{\pi R^2 \overline{\eta}_{sp}^2} \qquad \text{(III-32)}$$

$$= C^{\prime 2} E_o^2 \frac{\phi(1-\phi)(\alpha_r-\alpha_m)(\alpha_t-\alpha_m) + (\alpha_r-\alpha_t)^2(\frac{3}{8}-\frac{\phi}{4})}{(1-\phi)^2(\alpha_r-\alpha_m)(\alpha_t-\alpha_m) + (\alpha_r-\alpha_t)^2(\frac{3}{8}+\frac{\phi^2}{4}-\frac{\phi}{2})} V$$

$$\pi (2/W^2)^2 R^2 \left\{ (\alpha_r-\alpha_b)\left[1-J_o(W)\right] + (\alpha_t-\alpha_b)\left[WJ_1(W) \right.\right.$$

$$\left.\left. -(1-J_o(W))\right] - (\alpha_r-\alpha_t)\cos^2\mu \left[2(1-J_o(W)) - WJ_1(W)\right]\right\}^2$$

(III-33)

where $\alpha_b = \phi(\alpha_t+\alpha_r)/2 + (1-\phi)\alpha_m$ as defined in Eq.(III-30).

Discussion

The H_v and V_v light scattering patterns have been calculated as a function of volume fraction of spherulites in the field. It is found that the fluctuation theory predicts the experimental result in detail as observed during the crystallization of polymers. Also the complicated equations which need to be calculated numerically, can be replaced by simple ones, combining the fluctuation theory with the analytically computable model calculations. This is very useful, especially for the V_v scattering, since the surrounding polarizability is well defined, and also the intensity contribution from the isotropic medium is included.

It is also found that the experimental V_v patterns which are usually extended along the polarization direction can be explained if the spherulites are not completely volume-

filling. If the spherulites are completely volume filling, two lobes which are perpendicular to each other are expected to have the same intensity.

The theory presented here is a strictly two dimensional analysis, and extension to the three dimension would be possible without much difficulty. Also it has been assumed that the anisotropy remains constant, while the volume fraction of spherulites is increasing. In real system, this assumption would not be valid, but this difference would not change the interpretation of light scattering during crystallization of polymers in a significant way. Also it would be possible to determine the value of spherulite anisotropy during crystallization, if the absolute scattering intensity is measured.

Among the four variables which are changing during the crystallization process, namely, size, number, crystallinity, and crystal disorder of spherulites, the size can be determined from the peak position of H_v pattern. Therefore, if the absolute intensity of the H_v scattering maximum, and the shape and absolute maxium scattering intensity of V_v pattern are measured, it would be possible to determine the remaing three variables.

CHAPTER IV SCATTERING OF LIGHT BY DISORDERED SPHERULITES

Introduction

The light scattering patterns from polymer films have been interpreted to result from the superstructure such as spherulites, into which the crystals are arranged with certain order. Theories of light scattering based on two[17] or three[16] dimensional perfect spherulites have been successful in predicting the qualitative features of small angle light scattering patterns. In these perfect spherulites, it is assumed that the crystals are oriented making a definite angle with respect to the spherulite radius. However, the quantitative studies by photometric experiments showed a difference from the theoretical predictions in three important aspects.[19] The theory predicts: (1) more rapid intensity decrease with angle at larger angles and almost zero scattering intensity at wide angles (2) less scattering at very small angles, (3) a greater azimuthal angle dependence of scattering intensity than is experimentally found.

These differences are easily understood, noticing the fact that in reality, the spherulites are partially crystalline and crystalline lamellae are twisted and branched, therefore possibly possessing internal density and orientation fluctuations. It is shown by Stein et al. that the largest contribu-

tion to the light scattering is from orientation fluctuations.[31,32] The theoretical analysis of orientation fluctuations inside the spherulites was first attempted by Wilson et al.,[25] who adopted a model for correlated crystal growth based on two dimensional circular lattice cells with only two orientation states allowed for the cells. This model was further extended by Stidham,[30] who considered the orientation fluctuation by building larger number of square lattice cells with four orientation states allowed in each cell. Both analyses were able to predict the uniform decrease of scattering intensity with increasing scattering angles at wide angles, which is observed experimentally. However, due to the limitted small number of orientation states allowed within the lattice cells, and neglecting the fact that the crystal orientations are strongly correlated with respect to the spherulite radius, the small angle light scattering pattern such as the four-leaf clover pattern in the H_v scattering could not be predicted.

Another line of attempts to take into account these differences were made by Keijzers, van Aartsen, and Prins,[18] who considered the total scattering to be a sum of perfect spherulitic scattering and random orientation fluctuation scattering. Although this model is simple in mathematical analysis, the predictions have not been adequate in describing the experimental results, especially the azimuthal angle dependence of scattering intensity, as discussed by Chu.[93]

This type of "composite model" has been further extended by Chu, who considered the non-spherulitic part by the non-random fluctuation theory, to find that the quantitative description of experimental results still unachievable.

More specific models, originating the deviation from the perfect spherulite to the disorder of crystal orientation has been proposed by Stein and Chu.[19] In these models, the crystal orientations are conceived to fluctuate around a definite angle with respect to the spherulite radii with exponential correlation. Considerations of simple cases where the disorder occurs in the radial direction or in the angular direction only have been computed. It is found that excess scattering in the small angle part is due to the angular disorder, while the excess scattering at large angles is due to the radial disorder. It is certain that in real spherulites, the disorder is affected in both angular and radial correlation. However the mathmatical complexities prevent this model from quantitative description of scattering patterns.

An alternate approach to the light scattering by disordered spherulites is proposed to achieve the quantitative description of the light scattering pattern. The spherulites divided into circular lattice cells are built by computer simulation, such that the crystal orientation in the lattice cells fluctuate from the perfect orientation, correlated with its neighbors. The light scattering patterns and average

birefringence are calculated from such spherulites and compared with the experimental results.

The Model

The orientation of the optic axis vector $\underset{\sim}{a}$ of a unaxial crystal with respect to the spherulite radius is described by the angles β and ω defined in Fig.(IV-1). The considerations are restricted to two dimensional spherulites lying in the YZ plane perpendicular to incident beam which is propagating in the X direction. The equation describing the scattering amphlitude is given as developed previously[17]

$$E_{H_V} = 1/2\ C \int_{\underset{\sim}{r}} \{\cos\rho_2[\ (\cos^2\beta - \sin^2\beta\ \cos^2\omega)\ \sin 2\alpha + \sin 2\beta\ \cos\omega\ \cos 2\alpha\ ] + \sin\rho_2[\sin^2\beta\ \sin 2\omega\ \sin\alpha - \sin 2\beta\ \sin\omega\ \cos\alpha\ ]\}\ \exp[\ ik(\underset{\sim}{r}\cdot\underset{\sim}{s})]\ d\underset{\sim}{r} \qquad (IV\text{-}1)$$

$$E_{V_V} = C'E_o \int_{\underset{\sim}{r}} \{\cos\rho_1[\ (\alpha_1-\alpha_2)(\cos\beta\ \cos\alpha - \sin\beta\ \cos\omega\ \sin\alpha\ )^2 + \alpha_2 - \alpha_s] + \sin\rho_1[\ (\alpha_2-\alpha_1)(\cos\beta\ \cos\alpha - \sin\beta\ \cos\omega\ \sin\alpha\ )(\ \sin\beta\ \sin\omega\ )]\}\ \exp[\ ik(\underset{\sim}{r}\cdot\underset{\sim}{s})]\ d\underset{\sim}{r} \qquad (IV\text{-}2)$$

where $C = C'(\alpha_1-\alpha_2)E_o$, α_1 and α_2, α_s are polarizabilities along and perpendicular to the optic axis and surrounding polarizability, $\underset{\sim}{E}_o$ is the incident field strength, $k = 2\pi/\lambda$, λ is the wavelength of light in the medium, $\underset{\sim}{s} = \underset{\sim}{s}' - \underset{\sim}{s}$, $\underset{\sim}{s}_o$ and $\underset{\sim}{s}'$ being the unit vector along the incident and scattered

$$\cos \rho_2 = \cos\theta/(\cos^2\theta + \sin^2\theta \sin^2\mu)^{1/2}$$

$$\cos \rho_1 = \cos\theta/(\cos^2\theta + \sin^2\theta \cos^2\mu)^{1/2} \qquad \text{(IV-3)}$$

(1) When the Optic Axis Twist Angle, ω is Zero

When ω is zero, Eqs.(IV-1) and (IV-2) reduce to

$$E_{H_v} = -(C/2) \cos\rho_2 \int_{r=0}^{R}\int_{\alpha=0}^{2} (\cos 2\beta \sin 2\alpha + \sin 2\beta \cos 2\alpha)$$

$$\exp\left[ik(\underset{\sim}{r}\cdot\underset{\sim}{s})\right] dr \qquad \text{(IV-4)}$$

$$E_{V_v} = C' \cos\rho_1 \int_{r=0}^{R}\int_{\alpha=0}^{2} \left\{(\alpha_1-\alpha_2)\cos^2(\alpha+\beta) + \alpha_2-\alpha_s\right\}$$

$$\exp\left[ik(\underset{\sim}{r}\cdot\underset{\sim}{s})\right] dr \qquad \text{(IV-5)}$$

a. Scattering from Perfect Spherulite

When the crystal orientation with respect to the radius is the same everywhere in the spherulites, that is $\beta = \beta_o = 90^\circ$, Eqs.(IV-4), (IV-5) reduces to

$$E_{H_v} = C \cos \rho_2 \sin 2\mu \, (R^2/W^2) \left[2 - 2J_o(W) - WJ_1(W) \right]$$

$$E_{V_v} = 2C' \cos \rho_1 (R^2/W^2) \left[(\alpha_2 - \alpha_s)(1 - J_o(W)) + (\alpha_1 - \alpha_s) WJ_1(W) - (\alpha_2 - \alpha_1) \cos^2 \mu \left\{ 2(1 - J_o(W)) - WJ_1(W) \right\} \right] \quad \text{(IV-6)}$$

where $W = kR \sin \theta$ and $J_o(W)$ and $J_1(W)$ are the zero and first order Bessel functions.

b. Disordered Spherulite

The spherulite is divided into lattice cells as shown in Fig.(IV-2), and the optic axis orientation defined by β_i in the i cell are represented as a sum of perfect orientation angle β_o, and orientation disorder angle $\Delta\beta_i$,

$$\beta_i = \beta_o + \Delta\beta_i \quad \text{(IV-7)}$$

The light scattering amplitude from a spherulite divided into lattice cells is obtained, simply replacing integral in

Eqs.(IV-4) and (IV-5) by a summation over all lattice cells. When β_o is 90°, as shown by Keller[42] for the polyethylene spherulites, Eqs.(IV-4), (IV-5) become,

$$E_{H_v} = +C/2 \cos\rho_2 \sum_i \sin\left[2(\alpha_i+\Delta\beta_i)\right] \exp\left[ik(\underset{\sim}{r}_i \cdot \underset{\sim}{s})\right]$$

$$E_{V_v} = C' \cos\rho_1 \sum_i \left[(\alpha_1-\alpha_2)\sin^2(\alpha_i+\Delta\beta_i) + \alpha_2-\alpha_s\right] \exp\left[ik(\underset{\sim}{r}_i \cdot \underset{\sim}{s})\right]$$

and $\underset{\sim}{r}_i \cdot \underset{\sim}{s} = r_i \sin\theta \cos(\mu-\alpha_i)$ (IV-8)

The scattering I, is given by,

$$I = E \cdot E^* \qquad \text{(IV-9)}$$

where E^* is the complex conjugate of the amplitude, E.

Also the effect of spherulite size distribution can be considered, following the method of Stein and Stidham[94],

$$I(\theta) = \int I(\theta,a)\, P(a)\, da \,/ \int P(a)\, da \qquad \text{(IV-10)}$$

where $I(\theta)$ is the scattering intensity at scattering angle θ. $I(\theta,a)$ is the scattering intensity at angle θ by the sphrulite with radius a, P(a) is the spherulite size distribution function and for Gaussian distribution,

$$P(a) = \exp\left[-\left(\frac{a-\bar{a}}{b}\right)^2\right] \qquad \text{(IV-11)}$$

Eqs.(IV-4) and (IV-5) by a summation over all lattice cells. When β_o is 90°, as shown by Keller[42] for the polyethylene spherulites, Eqs.(IV-4), (IV-5) become,

$$E_{H_v} = +C/2 \cos\rho_2 \sum_i \sin\left[2(\alpha_i+\Delta\beta_i)\right] \exp\left[ik(\underset{\sim}{r}_i \cdot \underset{\sim}{s})\right]$$

$$E_{V_v} = C' \cos\rho_1 \sum_i \left[(\alpha_1-\alpha_2) \sin^2(\alpha_i+\Delta\beta_i) + \alpha_2-\alpha_s\right] \exp\left[ik(\underset{\sim}{r}_i \cdot \underset{\sim}{s})\right]$$

and $\underset{\sim}{r}_i \cdot \underset{\sim}{s} = r_i \sin\theta \cos(\mu-\alpha_i)$ (IV-8)

The scattering I, is given by,

$$I = E \cdot E^* \qquad \text{(IV-9)}$$

where E^* is the complex conjugate of the ampltude, E.

Also the effect of spherulite size distribution can be considered, following the method of Stein and Stidham[94],

$$I(\theta) = \int I(\theta,a)\, P(a)\, da \Big/ \int P(a)\, da \qquad \text{(IV-10)}$$

where $I(\theta)$ is the scattering intensity at scattering angle θ. $I(\theta,a)$ is the scattering intensity at angle θ by the sphrulite with radius a, P(a) is the spherulite size distribution function and for Gaussian distribution,

$$P(a) = \exp\left[-\left(\frac{a-\bar{a}}{b}\right)^2\right] \qquad \text{(IV-11)}$$

where $\bar{a}$ is the average radius of spherulites, and b is the half-width of the distribution function.

c. Disorder of Crystal Orientation

For many crystalline polymer systems, it is found experimentally that the orientation correlation function f(r) may be fitted by the empirical exponential function.[32]

$$f(r) = \exp(-r/a) \qquad \text{(IV-12)}$$

where $f(r) = \dfrac{3\langle \cos^2 \theta_{ij} \rangle_r - 1}{2}$

θ_{ij} is the angle between the optic axis of ith volume element and that of jth which is separated by distance r and a is correlation distance. This type of orientation correlation has been explained theoretically by Stein[29] using the lattice model. The orientation of optic axis in the lattice cells differ with that of the adjacent cells separated by distance d, by $+\delta$ or $-\delta$ as shown in Fig.(IV-3). It is found that in the one dimensional lattice model, the correlation distance a can be represented by

$$a = d/(2\,\delta^2) \qquad \text{(IV-13)}$$

To discribe the disorder of crystal orientation, a two dimensional spherulite is divided into circular lattice cells as shown in Fig.(IV-2). For this type of two dimensional lattice model, it is assumed that the disorder angle $\Delta\beta$ differs with the average disorder of adjacent cells which are already filled by $+\delta$ or $-\delta$. Further to avoid the formation of domains whose orientation is too far away from the perfect orientation, it is assumed that the farther away the crystal orientation, the greater the tendency to return to the original orientation becomes.

The disorder of orientation in the lattice cell, $\Delta\beta$ is determined in the following way.

First, the spherulite of a given radius is divided into the lattice cells with the same dimension 1, in the tangential and radial direction so that all the lattice cells have almost the same area. The orientation fluctuation $\Delta\beta$, is assigned from the innermost layer. The way of assigning the lattice cells proceeds clock- or counterclockwise in a continuous way until all the cells in the layer are filled. On proceeding to the next layer, the first cell to be assigned is chosen by random selection. The same process is repeated until all the lattice cells are filled. The fluctuation, $\Delta\beta$, in the lattice cell(e.g. cell(3) in Fig.(IV-2)) deviates from the average fluctuation of the average fluctuation of the nearest neighbors which have already been filled(e.g. cell (1)

and (2)) by the angle δ in either the positive or negative direction. The probability to go to the positive or negative direction is determined by the probability rule such that the optic axis orientation has the tendency to return to perfect orientation. This tendency increases as the fluctuation of the neighboring cells gets greater. The probability to go to the positive direction by δ, P_+ is assumed to be

$$P_+ = 0.5 + 0.5\left[1 - \exp(C_1 x_o)\right] \qquad \text{when } x_o < 0$$

$$P_+ = 0.5 - 0.5\left[1 - \exp(-C_1 x_o)\right] \qquad \text{when } x_o \geq 0 \qquad \text{(IV-14)}$$

where x_o is the average fluctuation of neighboring cells(cells (1) and (2)) divided by δ, and C_1 is the parameter which determines the rate which the optic axis tends to return to the perfect orientation.

After the process of describing the disorder, $\Delta\beta$ of each lattice cell is finished, the light scattering intensities are calculated from Eqs. (IV-8) and (IV-9). This procedure is repeated several times and the scattering intensities are averaged to eliminate the effects of statistical fluctuations.

First, two special cases of disorder in the radial direction and disorder in the angular direction are considered. For this purpose, one dimensional orientation fluctuation in the radial or angular direction is determined, and $\Delta\beta$ values of

the rest of lattice cells are determined according to their angular or radial position in the spherulite. The H_v scattering intensities along W(equal $kR\sin\theta$) at $\mu = 45°$, are shown in Figs. (IV-4) and (IV-5), compared with scattering curves of the perfect spherulite. The maximun intensities are matched by multiplying the disorder case by the factor indicated. The excess scattering at small angles due to angular disorder and excess scattering at wide angles due to radial disorder are in good agreement with the analytical results of Chu and Stein. The size of the lattice cells is represented by M, which is the number of lattice cells along the radius of a spherulite. In Figs. (IV-6) and (IV-7), H_v scattering intensities calculated from the lattice model as described previously are shown for different disorder parameters, δ. The higher order maxima are eliminated since spherulite distribution smoothens out these maxima. Excess scattering at small and wide angles relative to the peak intensity, and less significant azimuthal angle dependence of scattering intensity are reproduced. Also it is seen that the peak intensity in H_v scattering decreases as the disorder increases. The V_v scattering intensities are shown in Figs (IV-8) and (IV-9). It is seen that as disorder increases, the scattering peak predicted for perfect spherulite($\delta = 0$) becomes less significant, while there is rapid build-up of intensity at very small angles.

It has been found experimentally that the quantitative light scattering patterns depend upon the crystallization conditions. Such a comparision is made for the polyethylene films prepared by different cooling rate. For the slowly cooled sample, the melt is allowed to be cooled by the natural cooling rate of the press, while for the quenched sample, the polymer melt between the copper plates is plunged into the dry-ice-methanol bath. The relative H_v scattering intensity from both samples are shown in Fig.(IV-10).

Therefore for the quantitative analysis of experimental data, the disorder parameter should be determined for each sample. For this purpose, calibration curves relating the disorder parameter to the intensity drop ratio relative to the peak intensity ($I_{H_v}(W=4, \mu=45^\circ)$) along W at $\mu=45^\circ$, and along μ at W=4 are shown in Figs(IV-11) and (IV-12). Also the decrease of peak intensity due to disorder is shown in Fig.(IV-13). One simple example of fitting the experimental scattering curve is shown in Fig.(IV-14) for the slowly cooled polyethylene film. The disorder parameter $\delta=0.22$ was chosen by taking the experimental value of $I_{H_v}(W=4)/I_{H_v}(W=15)$, and using the calibration curve shown in Fig.(IV-11). The scattering curve was then somewhat modified by considering the truncation effects which will be discussed later.

Another important aspect of disorder of crystal orientation in spherulites is that the spherulite birefringence, Δ, decreases as the disorder increases. This is well illustrated in that the spherulite birefringence as experimentally measured is always

much lower than expected from the intrinsic crystal birefringence, Δ_c^0. It can be explained by the following relationship;

$$\Delta = n_r - n_t = \phi_c \Delta_c = \phi \Delta_c^0 f_c \qquad \text{(IV-15)}$$

where $\Delta_c^0 = n_c - \frac{n_a + n_b}{2}$

$$f_c = \frac{3\langle \cos^2\beta \rangle - 1}{2} \qquad \text{(IV-16)}$$

ϕ_c is the crystallinity and n_r, n_t, are the refractive indices along the radial and tangential direction of the spherulite, and n_c, n_a, n_b are the refractive indices along the c, a, and b crystal axis. When β_0 is 90°, from Eqs.(IV-7) and (IV-15) it can be shown,

$$f_c = \frac{3\langle \sin^2(\Delta\beta) \rangle - 1}{2} \qquad \text{(IV-17)}$$

Eq.(IV-17) is easily calculated from this lattice model, and the decrease of spherulites birefringence due to disorder is shown in Fig.(IV-15).

(2) Case of Twisting angle(ω) Fluctuation

In this case, β is fixed at 90° and ω is allowed to fluctuate. When β is 90°, Eq.(IV-1) becomes

$$E_{H_V} = \frac{1}{2}C \sum_i \left[\cos\rho_2(-\cos^2\omega_i)\sin 2\alpha + \sin\rho 2 \sin 2\omega_i \sin\alpha_i\right]$$

$$\exp\left[ik(\underset{\sim}{r}_i \cdot \underset{\sim}{s})\right] \qquad \text{(IV-18)}$$

The above equation is obtained in the same way as before, replacing $\Delta\beta$ in the lattice cells with ω. Since there is no preferential orientation for the twisting angle, equal probability, $\frac{1}{2}$, is assumed to fluctuate by $+\delta$ or $-\delta$. The H_V scattering results are shown in Fig.(IV-16). It is seen that twisting angle fluctuation has little effect on light scattering pattern when β is 90°.

(3) Case of Random Orientation of ω

In this case, β and ω are both fluctuating, but the ω fluctuation is so rapid that ω can be approximated to be random in the lattice cells. Then $\cos^2\omega$ and $\sin^2\omega$ become $\frac{1}{2}$, and $\sin\omega$ and $\cos\omega$ become zero. Therefore Eq.(IV-1) becomes

$$E_{H_V} = \frac{1}{2}\, C \sum_i \left[\cos\rho_2 \frac{3\cos^2\beta_i - 1}{2} \sin 2\alpha_i\right] \exp\left[ik(\underset{\sim}{r}_i \cdot \underset{\sim}{s})\right] \qquad \text{(IV-19)}$$

The results are similar to those of Case (1) and the calibration curves are shown in Figs.(IV-17) and (IV-18) and (IV-19). One sample program used in previous calculations are given in Appendix(IV).

Discussion

Three different cases of disorder of crystal orientation have been considered, concerning their effects on the light scattering pattern. As shown in Case(2), the fluctuations in twisting angle ω has little effect on light scattering. It is found that Case(1) which assumes the twisting angle is zero, and Case(3) which assumes the ω is random in the lattice cells predict quite well the experimental observations. However Case(1) is not realistic, since it means that the lamellae shoud be straight. In this respect, Case(3) is more favored in interpreting the experimental results.

As has been mentioned by Stein and Picot[23], the effect of spherulite truncation should be considered in the quantitative analysis of light scattering intensities. These aspects have been thoroughly studied by Prud'homme.[39] It is found that truncation has little effect on the scattering angle(θ) dependence at $\mu = 45^{\circ}$, but it has significant effect on the azimuthal angle dependence, especially at $\mu = 0^{\circ}$, or 90°.

Also the effect of secondary scattering is significant for thick samples, as clearly indicated by the fact that as sample thickness increases, the scattering pattern becomes more diffused. Without any appropriate theories available at present to account for the secondary scattering effect, it is felt that any attempts to interpret the light scattering

experiments quantitatively should be limitted to very thin samples.

The present lattice model of disordered spherulites can be extended to predict the change of light scattering pattern due to deformation. As the spherulites undergo deformation, the disorder of crystal orientation should change due to the crystal reorientation processes.[17,28] In this respect, the analysis of static, dynamic and relaxation light scattering experiments should be interpreted, taking into account the significant effect of spherulite disorder.

CHAPTER V PHOTOMETRIC LIGHT SCATTERING STUDY OF QUENCHED AND ANNEALED POLYETHYLENE FILMS

Introduction

The change of crystalline morphology, encountered upon annealing the polyethylene film which has been crystallized by rapid quenching, has been extensively studied by Tanaka[40] using the rheo-optical techniques. The dynamic x-ray and birefringence studies clearly showed that the deformation processes in these samples are strikingly different, although there is only slight increase(about 5%) in crystallinity due to annealing.

In quenched samples, the crystals are relatively free to change their orientation without restrictions imposed by the spherulitic superstructure. Therefore the crystal orientation is similar to that of floating rods[50]. In annealed samples, the crystal orientation is restricted by the spherulitic superstructure. Therefore the positive b axis orientation is observed at low temperature and high dynamic frequency.

Light scattering patterns from both samples showed the presence of spherulitic structure as shown in Fig.(V-5). Therefore, it is believed that the crystals in quenched samples are arranged with spherulitic order, but this order is not strong, so that the crystals can orient without restrictions.

On the other hand, the crystals in annealed samples are believed to be in better arranged spherulitic order.

As has been described in detail in CHAPTER IV, the order of crystal orientation inside spherulites can be easily studied by measuring the intensity distribution of the H_v scattering. The larger the disorder of crystal orientation, the azimuthal angle variation of I_{Hv} intensity becomes less significant, and I_{Hv} intensity at large scattering angles becomes more significant. For this purpose, photometric light scattering intensity is measured from both samples, and the disorder of crystal orientation is compared.

Experiments

a. Sample preparation

Two special research samples of low density polyethylene provided by Monsanto Company have been used, one of them being the same sample that Tanaka[40] used in the dynamic x-ray studies. Tanaka sample has a melt index of 7.0 with number and weight average molecular weights of 1.67×10^4 and 6.20×10^5. Another sample is P.E. Grade 8011 having a melt index of 2.9 with number and weight average molecular weight of 1.38×10^4 and 1.72×10^5.

Pellets of polyethylene were melted at a pressure of 10,000 p.s.i. at 155 C°. The samples were then removed from the press and plunged into a dry-ice-methanol bath.

Some samples of quenched films were annealed by reheating to 95°C for 2 hrs. for the Tanaka sample, and 42 and 110 hrs. for P.E. 8011 between the press without any pressure. Then they were allowed to cool to room temperature at the natural cooling rate of the press.

b. Photometric light scattering measurements

The H_v scattering intensity was measured, using the dynamic light scattering apparatus described by Hashimoto[96] without any strain imposed on the sample. The I_{H_v} intensity was measured along the scattering angle at $\mu=45°$, and along the azimuthal angle at the maximum scattering angle.

Results

For the Tanaka sample, the variation of I_{H_v} intensity with θ at $\mu=45°$ and the variation of I_{H_v} intensity with μ at the maximum scattering angle are shown in Figs(V-1) and (V-2). It is seen that the variation of I_{H_v} intensity with μ is less significant in the annealed sample, and also the I_{H_v} change drops more slowly with θ in the annealed sample. For P.E. 8011, longer annealing time was required to see the difference. However, the trend is the same as the Tanaka sample, and as the annealing time increased, more difference was noticed.

Discussion

The photometric light scattering results clearly show that there is more disorder of crystal orientation in the annealed sample. At first, this seems contradictory to the results of Tanaka. However, the light scattering results indicate that the crystals produced during annealing have different orientation from the crystals already present in the quenched sample, and the following interpretation is proposed.

In the quenched sample, the crystals are arranged with spherulitic order, and during annealing, the crystallization proceeds inside these spherulites, unrestricted by the spherulitic order. Therefore, the overall disorder of crystal orientation inside spherulites increases. And since the newly formed crystals tend to connect the already present crystals, the crystal orientation is more restricted by the spherulitic superstructure.

It is felt that other experiments such as electron microscopy, micro x-ray diffraction, etc. would be also desirable to substantiate the explanations given above.

PART II WIDE ANGLE X-RAY SCATTERING

CHAPTER VI AN IMPROVED MODEL FOR CRYSTALLINE ORIENTATION OF SPHERULITIC POLYMERS*

Introduction

An objective in our understanding of the behavior of crystalline polymers is to predict the change in crystal orientation occurring upon stretching. Early theories such as the floating-rod model of Kratky[50] assumed that crystal orientation could be predicted on the assumption that the crystals were initially randomly oriented and imbedded in a continuous matrix which underwent affine deformation. While these theories approximately predicted the orientation of the c crystal axis(the chain axis), they were not satisfactory in predicting the details of the orientation behavior and not able to account for differences in the orientation of the a and b axis. They were quite inadequate in their attempts to predict the reversible small strain orientation observed in dynamic x-ray diffraction experiments.[44]

A major step forward was made by Wilchinsky[45] who considered the occurrence of crystals in spherulites and attempted to account for their orientation in terms of a deformation model

*Adapted in part from the paper prepared for publication by Do Y. Yoon, C. Chang and R. S. Stein

of these spherulites. The direct observation of spherulite deformation has been made experimentally.[48,49] The model of Wilchinsky has been elaborated by several authors[17,28,46,47,51,52,53,62] who attempted to introduce various mechanisms of crystal reorientation within spherulites to account for differences among various polymers.

For many polymers at small deformations, the change in spherulite shape is close to affine. Polyethylene spherulites are negatively birefringent and have their c crystal axes directed perpendicularly[42] to the radius in the undeformed state, and the b axis parallel to the radius. It was pointed out by Sasaguri, et al.[46,47] that if the b axis remained radial during deformation, this axis should orient parallel to the stretching direction and the chain axis should orient perpendicular to the stretching direction. Indeed, this mechanism was employed to account for the initial negative birefringence found with annealed samples of the higher poly-α-olefins at low elongations.[46] To account for the birefringence becoming positive at the higher elongations, at higher temperatures, or with quenched samples, it was realized that some mechanisms of crystal reorientation within the spherulites must be introduced to allow the c axes to turn around and orient parellel to the stretching direction.

At first, unfolding of folded chain crystals was proposed.[46] We now feel that this mechanism is not important at low elongations and is probably only significant at strains where the

spherulite itself is destroyed. Additional mechanisms of twisting of lamellae about their b axes[47] and tilting of chains within the lamellae about the crystal a axis[17,28] were introduced. These processes are illustrated in Fig.(VI-1). It is evident that these processes occur to a different extent in different parts of the spherulites. The lamellae twisting process would predominate in the equatorial part of the spherulite(at $\alpha=90^\circ$ in Fig. (VI-2)) where the strain is perpendicular to the lamellar axis. In the unstretched state, the twist angle of the chain axis about the lamellae, ω, is random. Upon stretching, the chains tend to preferentially orient parallel to the stretching direction, close to $\omega=0$, or π. A two-dimensional orientation function in ω was introduced[47]

$$g = 2\langle \cos^2\omega \rangle_{av} - 1 \qquad \text{(VI-1)}$$

which was zero for random orientation and approached unity with stretching. An empirical equation was assumed for g

$$g = 1 - \exp\left[-\eta(\lambda_3^2 - \lambda_2^2)\sin^2\alpha\right] \qquad \text{(VI-2)}$$

where η is an adjustable parameter and λ_3 and λ_2 are extension ratios in the Z(stretching) and Y(transverse) directions. Uniaxial orientation was assumed so that the extension ratio λ_1 in the X(normal) direction was the same as λ_2. The factor $\sin^2\alpha$ accounts for the angular dependence of the process within

the spherulites. In the meridional region where $\alpha = 0°$, strain is parallel to the lamellae and there is no driving force for the twist process, while at $\alpha=90°$, the process occurs to the greatest extent. The parameter η is a material property which is a measure of the compliance for lamellae twisting. The larger η, the greater the extent of the process. Its value becomes smaller, for example with increased annealing of a sample. The Eq.(VI-2) is undoubtedly an over simplificatin but a more elaborate model requires the introduction of additional parameters, the use of which would not be justified at the present stage of experimental sophistication.

The process of chain tilting involves the plastic deformation of the crystal leading to the tilting of chains from their initial angle β_o with respect to their lamellae plane to some value β. Such tilting processes have been demonstrated by Geil[56] in deforming single polymer crystals on a polymer substrate. This process was assumed to occur to the greatest extent in the meridional region of the spherulite (at $\alpha=0$) and was described by the empirical equation[17]

$$\beta = \beta_o \exp\left[-K(\lambda_3^2 - \lambda_2^2)\cos^2\alpha\right] \qquad \text{(VI-3)}$$

The process occurs to the greatest extent at $\alpha=90°$.
K is a parameter describing the compliance for this process. (It is conceivable, of course, that the process may be shear induced in which case it would occur to the greatest extent

at $\alpha=45^{\circ}$)

Thus, the deformation process is characterized by the two parameters, K and η and such properties as birefringence[47] and light scattering[17,28] have been calculated as a function of them. These properties primarily depend upon the orientation of the optic axis which lies along the c-axis. It is possible to calculate the c-axis orientation function

$$f_c = \left[3\langle\cos^2\theta_c\rangle_{av} - 1\right]/2 \qquad \text{(VI-4)}$$

(where θ_c is the angle between the c axis and the stretching direction) as well as the distribution of c axis in terms of this model.

Experimentally x-ray diffraction data is most readily obtained using the more intense reflections from the 110 and 200 crystal planes. The description of the orientation of these planes is not uniquely characterized by the model. It is necessary to introduce a third orientational angle which we shall take as ϵ(in Fig. VI-2) between the b axis and the plane defined by the c axis and the vector $\underset{\sim}{r}$ along the spherulite radius.

The angle varies in a plane and may consequently be described in terms of the two dimensional orientation function, h, defined by

$$h = 2\langle\cos^2\epsilon\rangle_{av} - 1 \qquad \text{(VI-5)}$$

As with the other functions we shall propose an empirical equation describing the angular variation of h within the spherulite as

$$h = \exp\left[-P(\lambda_3^2 - \lambda_2^2)\cos^2\alpha\right] \qquad \text{(VI-6)}$$

The parameter P is a third compliance parameter. It is assumed that this process also occurs to the greatest extent in the polar region of the spherulite.

The azimuthal dependence of h is reasonable, at least in the case where $\beta_o = 90$. In the equatorial region where the b axis lies along the radius, the predominate response mechanism is for lamellae twisting, promoting the c axis orientation in which case there will be no driving force leading to the rotation of the b axis about the c. However in the polar region where the c axis will be tilted with respect to the lamellar normal, there will be some trend for a preferred b axis orientational angle, ϵ.

Calculation of Second-Order Orientation Functions

In this treatment, we have considered the three processes to be independent of each other, and each dependent upon angular orientation within the spherulite as specified by α. A more general and exact treatment would permit cross-interaction among these processes. This independence of the

orientation processes can be expressed in terms of crystal orientation distribution functions. If $N(\alpha, \beta, \omega, \epsilon)$ represents the number of crystals oriented per unit solid angle at sperulite position α, with axes at β, ω, and ϵ, then this assumption implies

$$N(\alpha,\beta,\omega,\epsilon) = N_1(\alpha,\omega)\, N_2(\alpha,\omega)\, N_3(\alpha,\epsilon) \qquad \text{(VI-7)}$$

If $\underset{\sim}{a}$, $\underset{\sim}{b}$, and $\underset{\sim}{c}$ are unit vectors directed along the three crystal axes, then these may be expressed in terms of the above angles as

$$\begin{aligned}
\underset{\sim}{a} = \{ & [-\sin\omega\cos\epsilon - \cos\omega\sin\epsilon\cos\beta]\cos\alpha\sin\Omega \\
& + [\cos\omega\cos\epsilon - \sin\omega\sin\epsilon\cos\beta]\cos\Omega \\
& + [\sin\beta\sin\epsilon\sin\alpha\sin\Omega]\}\ \underset{\sim}{i} \\
+ \{ & [-\sin\omega\cos\epsilon - \cos\omega\sin\epsilon\cos\beta]\cos\alpha\cos\Omega \\
& - [\cos\omega\cos\epsilon - \sin\omega\sin\epsilon\cos\beta]\sin\Omega \\
& + [\sin\beta\sin\epsilon\sin\alpha\cos\Omega]\}\ \underset{\sim}{j} \\
+ \{ & [\sin\omega\cos\epsilon + \cos\omega\sin\epsilon\cos\beta]\sin\alpha \\
& + [\sin\beta\sin\epsilon\cos\alpha]\}\ \underset{\sim}{k}
\end{aligned} \qquad \text{(VI-8)}$$

$$\begin{aligned}
\underset{\sim}{b} = \{ & [\sin\omega\sin\epsilon - \cos\omega\cos\epsilon\cos\beta]\cos\alpha\sin\Omega \\
& - [\cos\omega\sin\epsilon + \sin\omega\cos\epsilon\cos\beta]\cos\Omega \\
& + [\sin\beta\cos\epsilon\cos\alpha\sin\Omega]\}\ \underset{\sim}{i} \\
+ \{ & [\sin\omega\sin\epsilon - \cos\omega\cos\epsilon\cos\beta]\cos\alpha\cos\Omega \\
& + [\cos\omega\sin\epsilon + \sin\omega\cos\epsilon\cos\beta]\sin\Omega \\
& + [\sin\beta\cos\epsilon\sin\alpha\cos\Omega]\ \underset{\sim}{j} \\
+ \{ & -[\sin\omega\sin\epsilon - \cos\omega\cos\epsilon\cos\beta]\sin\alpha
\end{aligned}$$

$$+ \sin\beta \cos\epsilon \cos\alpha \Big\} \underset{\sim}{k} \qquad \text{(VI-9)}$$

$$\underset{\sim}{c} = \Big\{ \cos\omega \sin\beta \cos\alpha \sin\Omega + \sin\omega \sin\beta \cos\quad + \cos\beta \sin\alpha \sin\Omega \Big\} \underset{\sim}{i} + \Big\{ \cos\omega \sin\beta \cos\alpha \cos\Omega - \sin\omega \sin\beta \sin\Omega + \cos\beta \sin\alpha \cos\Omega \Big\} \underset{\sim}{j} + \Big\{ - \cos\omega \sin\beta \sin\alpha + \cos\beta \cos\alpha \Big\} \underset{\sim}{k} \qquad \text{(VI-10)}$$

Therefore, the cosines of the angles between the a, b, and c axes and the stretching direction are given by

$$\cos(\theta_{az}) = \underset{\sim}{a} \cdot \underset{\sim}{k} = \sin\alpha \left[\sin\omega \cos\epsilon + \cos\omega \sin\epsilon \cos\beta \right] + \sin\beta \sin\epsilon \cos\alpha \qquad \text{(VI-11)}$$

$$\cos(\theta_{bz}) = \underset{\sim}{b} \cdot \underset{\sim}{k} = \sin\beta \cos\epsilon \cos\alpha - \sin\alpha \left[\sin\omega \sin\epsilon - \cos\omega \cos\epsilon \cos\beta \right] \qquad \text{(VI-12)}$$

and

$$\cos(\theta_{cz}) = \underset{\sim}{c} \cdot \underset{\sim}{k} = - \cos\omega \sin\beta \sin\alpha + \cos\beta \cos\alpha \qquad \text{(VI-13)}$$

The orientation of the three crystal axes with respect to the stretching direction is described by the orientation functions, f_i defined by

$$f_i = \left[3 \langle \cos^2 \theta_{iz} \rangle_{av} - 1 \right] / 2 \qquad \text{(VI-14)}$$

where i = a, b, or c.

The mean squared cosine of the crystal axis orientation angle may be calculated from the crystal axis distribution function $N_i(\alpha, \Omega, r)$ by

$$\langle \cos^2\theta_{iz} \rangle_{av} = \frac{\int_{\alpha=0}^{\pi}\int_{\Omega=0}^{2\pi}\int_{r=0}^{R'} N_i(\alpha,\Omega,r) \langle \cos^2(\theta_{iz}) \rangle_{\alpha} \sin\alpha \; r^2 dr \; d\alpha \; d\Omega}{\int_{\alpha=0}^{\pi}\int_{\Omega=0}^{2\pi}\int_{r=0}^{R'} N_i(\alpha,\Omega,r) \sin\alpha \; r^2 dr \; d\alpha \; d\Omega} \qquad \text{(VI-15)}$$

where $\langle \cos^2(\theta_{iz}) \rangle_{\alpha}$ designates the average value of $\cos^2(\theta_{iz})$ at a specified angle α.

If the spherulite deforms affinely with conservation of volume, then the number of crystals in a volume element is conserved on deformation so that

$$N_i(\alpha,\Omega,r) \sin\alpha r^2 dr \; d\alpha \; d\Omega = N_{oi}(\alpha_o \Omega_o r_o) \sin\alpha_o r_o^2 dr_o d\alpha_o d\Omega_o \qquad \text{(VI-16)}$$

The distribution function N_{oi} is that in the undeformed state and is independent of angle and radius in an initially homogenious spherulite and set equal to N_i^o, the number of axes per unit volume in the uniformed state. Thus

$$\int_{\alpha=0}^{\pi}\int_{\Omega=0}^{2\pi}\int_{r=0}^{R'} N_i(\alpha,\Omega,r) \sin\alpha_o r^2 dr \; d\alpha d\Omega$$

$$= N_i^o \int_{\alpha=0}^{\pi}\int_{\Omega=0}^{2\pi}\int_{r=0}^{R} \sin\alpha_o \; r_o^2 \; dr_o \; d\alpha_o \; d\Omega_o$$

$$= (4/3) \; \pi \; R^3 \; N_i^o = V_s N_i^o$$

where V_s is the volume of the spherulite.

It is evident that $N_a^o = N_b^o = N_c^o = N^o$.

Now, it is evident from eq.(VI-11) that

$$\langle \cos^2\theta_{az} \rangle_\alpha = \sin^2\alpha \langle [\sin\varpi \cos\epsilon + \cos\varpi \sin\epsilon \cos\beta]^2 \rangle_\alpha$$

$$+ \cos^2\alpha \langle \sin^2\beta \sin^2\epsilon \rangle_\alpha$$

$$+2\sin\alpha \cos\alpha \langle \sin\varpi \sin\epsilon \cos\epsilon + \cos\varpi \sin^2\epsilon \cos \rangle_\alpha \qquad \text{(VI-18)}$$

If the distribution in ϵ and ϖ are independent cross-products vanish on averaging over these angles.

Since β depends upon α as given by eq.(VI-3), then

$$\langle \sin^2\beta \sin^2\epsilon \rangle_\alpha = \sin^2\beta \langle \sin^2\epsilon \rangle_\alpha$$

$$= \sin^2\beta(1-h)/2 \qquad \text{(VI-19)}$$

and

$$\langle [\sin\varpi \cos\epsilon + \cos\varpi \sin\epsilon \cos\beta]^2 \rangle_\alpha$$

$$= \langle \sin^2\varpi \rangle_\alpha \langle \cos^2\epsilon \rangle_\alpha + \cos^2\beta \langle \cos^2\varpi \rangle_\alpha \langle \sin^2\epsilon \rangle_\alpha$$

$$+ 2 \langle \sin\varpi \cos\varpi \rangle_\alpha \langle \sin\epsilon \cos\epsilon \rangle_\alpha \cos\beta$$

$$= \left(\frac{1-g}{2}\right)\left(\frac{1+h}{2}\right) + \cos^2\beta\left(\frac{1+g}{2}\right)\left(\frac{1-h}{2}\right) \qquad \text{(VI-20)}$$

Thus

$$\left\langle \cos^2\theta_{az} \right\rangle_{\alpha} = \sin^2\alpha\left(\frac{1-g}{2}\right)\left(\frac{1+h}{2}\right) + \sin^2\alpha\cos^2\beta\left(\frac{1+g}{2}\right)\left(\frac{1-h}{2}\right)$$

$$+ \cos^2\alpha\sin^2\beta\left(\frac{1-h}{2}\right) \qquad \text{(VI-21)}$$

Similarly

$$\left\langle \cos^2\theta_{bz} \right\rangle_{\alpha} = \cos^2\alpha\sin^2\beta\left(\frac{1+h}{2}\right) + \sin^2\alpha\left(\frac{1-h}{2}\right)\left(\frac{1-g}{2}\right)$$

$$+ \sin^2\alpha\cos^2\beta\left(\frac{1+h}{2}\right)\left(\frac{1+g}{2}\right) \qquad \text{(VI-22)}$$

$$\left\langle \cos^2\theta_{cz} \right\rangle_{\alpha} = \sin^2\alpha\sin^2\beta\left(\frac{1+g}{2}\right) + \cos^2\alpha\cos^2\beta \qquad \text{(VI-23)}$$

These values were then substituted in Eq.(VI-15) and the integrals were numerically evaluated using a CDC 3600 computer at the University of Massachusetts Computation Center. The value of β was calculated for each value of β_o as a function of α using Eq.(VI-3). Eq.(VI-16) was used for the distribution function where α was related to α_o through the affine transformation where[46,47,17]

$$\tan \alpha = (\lambda_2/\lambda_3) \tan \alpha_o \qquad \text{(VI-24)}$$

Calculations were carried out for the case of uniaxial stretching where $\lambda_1 = \lambda_2 = \lambda_3^{-1/2}$. Such theoretical values of orientation functions(to be discussed later) are compared with experimental values for particular values of the parameters K,$\eta$and P in Figs.(VI-3) and (VI-4). Those parameters were chosen numerically as shown in appendix VI to give list square deviation.

Calculation of Orientation Distribution

A more critical test of our model is the comparison of the predicted azimuthal dependence of the x-ray diffracted intensity with experiment. This variation depends upon the complete orientation distribution of the crystal axes rather than merely an average computed from this distribution.

From the dimensions of the polyethylene unit cell[57] as shown in Fig.(VI-5), it is evident that the normal to the 110 crystal plane is given by

$$\underset{\sim}{n}_{110} = \sin \partial \, \underset{\sim}{a} + \cos \partial \, \underset{\sim}{b} \qquad \text{(VI-25)}$$

where ∂ is the orientation angle of the plane normal with respect to the unit cell axes given by $\tan \partial = 4.94A/7.41A$

or $\partial = 33.4^{\circ}$. Thus the cosine of the orientation angle of this plane normal can be obtained using Eqs.(VI-11) and (VI-12) as

$$\cos(\theta_{110,z}) = (\underset{\sim}{n}_{110} \cdot \underset{\sim}{k}) = \sin\partial(\underset{\sim}{a}\cdot\underset{\sim}{k}) + \cos\partial(\underset{\sim}{b}\cdot\underset{\sim}{k})$$

$$= \sin\partial\left[\sin\beta\sin\epsilon\cos\alpha + \sin\alpha(\sin\omega\cos\epsilon + \cos\omega\sin\epsilon\cos\beta)\right]$$

$$+ \cos\partial\left[\sin\beta\cos\epsilon\cos\alpha - (\sin\alpha\sin\omega\sin\epsilon - \cos\omega\cos\epsilon\cos\beta)\right] \qquad \text{(VII-26)}$$

The distribution of crystal axes is assumed to be factorable into three independent distribution functions as expressed in Eq.(VI-7). The quantity $N_1(\alpha,\beta)\sin\alpha\, d\alpha$ is the number of crystals with their c axes at angle β with respect to the radius for radial vectors in the interval between α and $\alpha+d\alpha$. Theangle β is related to α through equation (VI-3) so that $N_1(\alpha,\beta) = N_1(\alpha)$, the density of radial vectors in the deformed state. Now from Eq.(VI-16), if we assume that the density of radial vectors is independent of Ω and r, it follows that

$$N_1(\alpha)\sin\alpha\, d\alpha = \int_{r=0}^{R'} \int_{\Omega=0}^{2\pi} N_1(\alpha,\Omega,r)\, r^2 dr\, d\Omega \qquad \text{(VI-27)}$$

From the affine condition,

$$N_1(\alpha)\sin\alpha\, d\alpha = N_1(\alpha_0)\sin\alpha_0\, d\alpha_0 \qquad \text{(VI-28)}$$

$N_1(\alpha_0)$ is the density of radial vectors in the undeformed state which is assumed constant.

The function $N_2(\alpha,\omega)\, d\omega$ is the number of c axes in the interval of ω between ω and $\omega+d\omega$ for those radial vectors in the interval between α and $\alpha+ d\alpha$. This depends upon the angle ω which varies in a plane and may consequently be expanded in a Fourier series as

$$N_2(\alpha,\omega) = \sum_{N=0}^{\infty} (b_n \sin n\omega + c_n \cos n\omega) \qquad \text{(VI-29)}$$

However, due to the symmetry of the distribution, it follows that

$$N_2(\alpha,\omega) = N_2(\alpha,\pi-\omega) = N_2(\alpha, -\omega) = N_2(\alpha, \pi+\omega) \qquad \text{(VI-30)}$$

Thus, only the even cosine terms remain giving

$$N_2(\alpha,\omega) = c_o + c_2 \cos 2\omega + c_4 \cos 4\omega + - - -$$

(VI-31)

As a first approximation, we will retain only the first two terms of this expansion. The distribution is determined by the coefficients c_o and c_2 which depend upon strain. Now

$$\int_0^{2\pi} N_2(\alpha,\omega)\, d\omega = 2\pi\, c_o = N_2^0 \qquad \text{(VI-32)}$$

$$\int_0^{2\pi} N_2(\alpha,\omega) \cos^2\omega\, d\omega = \frac{1}{2} \int_0^{2\pi} N_2(\alpha,\omega)(1+\cos 2\omega)\, d\omega$$

$$= \frac{1}{2}\left[2\pi\, c_o + \pi\, c_2\right] \qquad \text{(VI-33)}$$

Now, since

$$\left\langle \cos^2\omega \right\rangle_\alpha = \frac{\int_0^{2\pi} N_2(\alpha,\omega) \cos^2\omega\, d\omega}{\int_0^{2\pi} N_2(\alpha,\omega)\, d\omega} = \frac{1+g}{2} \qquad \text{(VI-34)}$$

it follows that

$$N_2(\alpha,\omega) = c_o\ (1 + 2g \cos 2\omega) \qquad \text{(VI-35)}$$

By the same procedure, one may show that

$$N_3(\alpha, \epsilon) = d_0(1 + 2h \cos 2\epsilon) \qquad \text{(VI-36)}$$

The number of crystals characterized by orientation angles in the interval $\sin\alpha \, d\alpha \, d\omega \, d\epsilon$ is then

$$N(\alpha, \beta, \omega, \epsilon) \sin\alpha \, d\alpha \, d\omega \, d\epsilon$$

$$= K \sin\alpha_0 (1+2g \cos 2\omega)(1+2h \cos 2\epsilon) \, d\alpha_0 \, d\omega \, d\epsilon \qquad \text{(VI-37)}$$

For diffraction to occur, the vector Bragg equation must be obeyed

$$\underset{\sim}{H} = \frac{\underset{\sim}{s} - \underset{\sim}{s}_o}{\lambda} \qquad \text{(VI-38)}$$

where $\underset{\sim}{H}$ is reciprocal lattice vector which is normal to the diffracting plane

$$\underset{\sim}{H} = h_1 \underset{\sim}{b}_1 + h_2 \underset{\sim}{b}_2 + h_3 \underset{\sim}{b}_3 \qquad \text{(VI-39)}$$

where $\underset{\sim}{b}_1$, $\underset{\sim}{b}_2$, and $\underset{\sim}{b}_3$ are the reciprocal lattice vectors of unit cell, and has a direction dependent upon the orientation of the crystal. The unit vectors $\underset{\sim}{s}$ and $\underset{\sim}{s}_o$ are in directions along the incident and diffracted rays and depend upon the diffraction angles. For diffraction at a Bragg angle θ_B and an azimuthal angle ψ defined in Fig.(VI-6), the vector $\underset{\sim}{s} - \underset{\sim}{s}_o$ is given by

$$\underset{\sim}{s} - \underset{\sim}{s}_o = (\cos 2\theta_B - 1)\underset{\sim}{i} + (\sin 2\theta_B \sin\psi)\underset{\sim}{j} + (\sin 2\theta_B \cos\psi)\underset{\sim}{k} \qquad \text{(VI-40)}$$

It may be shown that if the normal to the polymer film is tilted through the angle ϕ with respect to the incident beam(Fig.(VI-6)), such that $\phi = \theta_B$, then the angle between the crystal plane normal and the stretching direction θ_{kz} will equal the azimuthal angle of diffraction ψ. Under those conditions, the diffracted intensity $I(\theta_B,\psi)$ will be proportional to the number of crystals $N(\theta_{kz})$ oriented with their plane normals at angle θ_{kz}. That is

$$I(\theta_B,\psi) \sin\psi = K\, N(\theta_{kz}) \qquad \text{(VI-41)}$$

The determination of $N(\theta_{kz})$ is carried out as follows: The range of θ_{kz} is divided into a number of equal intervals The angles α_o, ω and ϵ are then incremented by equal intervals and, for example, $\theta_{110,z}$ is calculated for each of these combinations of angles using Eq.(VI-26). The number of crystals oriented for each of these combinations of α_o, ω and ϵ is then calculated using Eq.(VI-37) and these numbers are summed for each interval of $\theta_{110,z}$. This sum divided by $\sin\psi$ is then proportional to the diffracted intensity at a corresponding value of ψ.

A calculated variation of the relative diffracted intensity with azimuthal angle is given in Figs.(VI-7)

and (VI-8) for $K = \eta = P = 1.2$ at elongations of 15 and 20 % where it is compared with experimental values. These parameters were those chosen to best fit.the orientation function variation in Fig.(VI-3). It is noted that those same parameters fit the intensity variation with azimuthal angle reasonably well. The theory predicts a maximum in 110 intensity at an azimuthal angle at $\psi \simeq 70^\circ$, whereas the 200 maximum intensity occurs at $\psi = 90^\circ$.

Application to the Relaxation X-ray and Dynamic X-ray Diffraction

Experimental results of Stein and coworkers[54,55] indicate that the reorientation of crystals required certain amount of time. The change of x-ray intensity of 110 and 200 reflections from low density polyethylene has been measured as a function of time after the rapid stretching. The results are replotted[54] in Fig.(VI-9) and (VI-IO) as orientation functions, f_a, f_b, f_c vs. time for different strains. The changing orientation function of the a, b, and c axis cleary indicate that the reorientation, or deformation processes of crystals; chain tilting, lamellae twisting, and crystal rotation, are time dependent processes. In other words, the parameters K, η, P should be represented as functions of time. The determination of these parameters at certain time after stretching is done in the same way

as in the static orientation. The change of K, η, P with time for low density polyethylene at room temperature is plotted in Fig.(VI-11).

Another experimental technique which is useful in studying the time dependence of crystal orientation is dynamic x-ray diffraction[44]. The in-phase and out-of-phase change of diffracted intensity from the j crytal plane during the sinusoidal vibration of the sample, which is initially at certain static elongation, are measured. The in-phase orientation compliance of the j crystal plane C_j', defined as

$$C_j' = \frac{\Delta f_j'}{\Delta\lambda} \qquad \text{(VI-42)}$$

where $\Delta f_j'$ is the in-phase orientation function change and $\Delta\lambda$ is the amplitude of the dynamic strain, is replotted[54] in Fig.(VI-12) as a function of frequency.

Since the vibration strain is added to the static strain, the frequency dependent deformation starts from the already oriented states. Therefore the orientation function at the strain $\lambda + \lambda\Delta$ is calculated by modifying Eq.(VI-2),(VI-3), and (VI-6) to

$$\beta = \beta_o \exp\left\{-\left[K\, s(\lambda) + K'(s(\lambda+\Delta\lambda) - s(\lambda))\right] \cos^2\alpha\right\} \qquad \text{(VI-43)}$$

$$g = 2\overline{\cos^2\omega} - 1 = 1 - \exp\left\{-\left[\eta\, s(\lambda) + \eta'(s(\lambda+\Delta\lambda)-s(\lambda))\right]\sin^2\alpha\right\} \qquad \text{(VI-44)}$$

$$h = 2\overline{\cos^2\epsilon} - 1 = 1 - \exp\left\{-\left[P\, s(\lambda) + P'(s(\lambda+\Delta\lambda)-s(\lambda))\right]\cos^2\alpha\right\} \qquad \text{(VI-45)}$$

where $s(\lambda) = \lambda^2 - \frac{1}{\lambda}$, K, η, P are the static orientation parameters determined previously and K', η', P' are the frequency dependent dynamic orientation parameters. Then the orientation compliance is calculated by

$$C_j' = \frac{f_j(\lambda+\Delta\lambda) - f_{js}}{\Delta\lambda} \qquad \text{(VI-46)}$$

where f_{js} is the static orientation function for the j crystal plane.

It has been found by Tanaka[40] that the orientation compliance C_j' remains constant up to 5-6 % of dynamic strain. The frequency dependent K', η', P' are determined by fitting experimental C_j' values, based on the assumption of linear strain dependence. $K'(\omega)$, $\eta'(\omega)$, $P'(\omega)$ obtained from the experimental results shown in Fig.(VI-12) are plotted in Fig.(VI-13).

Comparing the results shown in Fig.(VI-11) and (VI-13), it is seen that the dynamic parameters show smaller change than the relaxation parameters. The most significant difference is found in the chain tilting parameters, K(t) and $K'(\omega)$. In the relaxation experiment, chain tilting is

the most slow process, but the magnitude of K(t) is much larger than that of dynamic parameter K(ω). It is believed that the main difference between the relaxation and dynamic experiments is that dynamic case responds to the reversible process of crystal deformation, while relaxation case responds to both the reversible and irreversible processes. Accordingly less change is observed in the dynamic orientation parameters.

Discussion

The deformation of crystalline polymers, especially polyethylene, has been studied extensively by many authors in various experiments. It has been studied in the form of single crystals[56,59,61] and bulk specimens, by compression[60], rolling[63] and simple extension[62,50-55,46,47], and combination of rolling and stretching[64,65] etc., and various mechanisms of deformation have been proposed. They are for example, chain tilting[46,47], lamellar twisting[17,28], crystal rotations, phase transformation, twinning[58-61], lamellar slip, etc.. Therefore the complete model describing the deformation of crystalline polymers should contain all these processes. However at present, the number of experimental data available limit the unique characterization of all such processes. Also one process that is dominant in one experiment may become the second order contribution in other experiments. In case of the uniaxial elongation

experiment which has been treated here, three processes defining the orientation of three crystal axes, have been considered to give good aggrement with the experimental results. Also the characterization of these process have been possible without much difficulty. A more elaborate model involving more processes such as proposed by Nomura et al.[53] could give better aggrement. However, since the unique characterization of the parameters necessary is not possible, the understanding of the deformation of crystalline polymers would become more difficult.

PART III SMALL ANGLE X-RAY DIFFRACTION

CHAPTER VII ANALYSIS OF LAMAELLAE ORIENTATION BY THE SMALL ANGLE X-RAY DIFFRACTION

Introduction

a. Analysis of Small Angle X-ray Diffraction(SAXD)

The small angle x-ray diffraction pattern of semi-crystalline polymers usually shows the appearance of one, and sometimes several, intensity maximum at angles 2θ between 0.05 and 2.0°. Direct application of Bragg's equation to the angular position of these maxima leads to the conclusion that the periodicites in electron density that are responsible for the scattering are of several hundred angstroms size.

The values which correspond to the maximum scattering angles are normally termed the long period in polymers. It is generally accepted that the long periods are directly related to the amorphous-crystalline layer structure[66,67] observed by electron microscopy. More specifically, it is usually assumed that the small angle maxima should be discribed by the periodicity of stacking of the lamaellae.

However, the simple analysis applying the Bragg equation are met with some difficiencies: the sizes calcu-

lated do not agree with those obtained from other experiments, especially electron microscopy, and quite often the positions of the first-order and second-order maxima differ by factors other than two.

These points were studied by Reinhold et al[68], who showed that a model based on the linear paracrystal was able to predict the shift of the maximum scattering angle from that given by Bragg's equation. They also showed that the positions of the first-order and second order maxima differ by factors of other than two, if the distribution function of the lamellar thickness is asymmetric.

Still, utilization of only the positions of the SAXRD maxima wastes the other information available in the experiment, partially the intensity distribution within the scattering pattern. The characterization of the size and shape of crystalline and amorphous layers from the experimental data were attempted by Tsvankin[69] and subsequently modified by Buchanan.[73]

In this method, the experimental values of position and width of the first-order maximum are compared with the results based on the one dimensional model calculations. Through the use of the calibration curves, it is possible to compute average values of the true periodicity of a superlattice composed of alternating crystalline and amorphous layers, average lengths of each layer, and a one dimensional linear crystallinity for the superlattice.

Crystal lengths and crystallities obtained in this method have been found to correspond quite closely with those obtained by other techniques.

Another line of approach based on the similar alternating two-phase model was developed by Vonk and Kortleve.[71,72] In this method, the Fourier transform of the experimental data is compared with the correlation function based on the model calculation. It was pointed out by Buchanan[73] that both methods described above show good agreement. However, Tsvankin's method is easier to apply without long computer calculations.

b. SAXRD of Deformed Spherulitic Polymers

in most melt-crystallized polymers, the specimen is completely filled with the spherulites in which crystalline lamaellae form the radius. In the undeformed state, the radial lamaellae are uniformly distributed without any preferential orientation. As a result, the SAXRD pattern is a circular ring. The change of SAXRD pattern when a polymer film is stretched have been studied by Peterlin[77,78] and Geil.[76] They observed that the small angle x-ray diffraction peak intensity and its angular position varied depending upon the azimuthal angles. In other words, it is qualitatively shown that the long period and the population of the lamaellae are different, depending upon the orientation of the lamaellae inside the spherulite. The qualitative analysis of these results

led to the conclusion that the change of long period and population of lamellae is the results of affine deformation of the spherulite shape, as is illustrated in Fig.(VII-1).

However those analysis were confined to the qualitative features of SAXRD of the deformed spherulites. No rigorous quantitative analysis concerning the change of crystalline and amorphous layer thickness and population of lamaellae has been made. It is the purpose of the present work to attempt the quantitative analysis of the SAXRD of the deformed spherulites, using the Tsvankin, Bucharan's method which is mentioned briefly in the preceding section. Theoretical considerations are presented to chmpute the lamellae orientation distribution as well as long period, and crystalline and amorphous layer thickness for the lamellae with given orientation.

Theoretical Analysis

a. Collimation Correction in SAXRD

Experimental measurements of the angular distribution of intensity of SAXRD ordinarilly represent the average intensity over a range of angles around the nominal scattering angle, though the use of slits. The results of the slit smearing is to shift the small angle maximum in a manner related to the beam geometry and the positions of the

maxima. The experimental scattering data must then be corrected for this effect. Guinier and Fournet[74] showed that the measured scattering intensity F(S) is related to the true scattering intensity by the equation,

$$F(S) = \int_0^\infty W(y)\, I(\sqrt{s^2 + y^2})\, dy \qquad \text{(VII-1)}$$

where y is the ordinate of a point in the beam, and W(y) is a weighting function, describing the fraction of the total beam power at y, and s is equal to $2\sin\theta/\lambda$, λ being the wavelength of x-ray beam.

For slits of negligible width compared with height, and for a Gaussian weighting function, Eq.(VII-1) becomes

$$I(s) = -\frac{\exp(p^2 s^2)}{p\sqrt{\pi}} \int_0^\infty \frac{F'(\sqrt{s^2 + u^2})}{\sqrt{s^2 + u^2}}\, du \qquad \text{(VII-2)}$$

where p is a constant depending upon the slit system and

$$F'(\sqrt{s^2 + u^2}) = \frac{dF(s^2 + u^2)}{d(\sqrt{s^2 + u^2})} \qquad \text{(VII-3)}$$

The numerical solution of Eq.(VII-2) has been derived by Schmidt[75] and is given in Appendix(VII). In the following discussions, all the intensity function represent the slit corrected intensity function I(s).

b. Direct Analysis of SAXRD Intensity

Tsvankin[69] used the fibril model which is a linear system formed of alternating layers of different densities (crystalline and amorphous layers), which are responsible for the long period. Scattering from such an assembly is calculated for the straight fibril. The effects of fibril curvature[70] was also considered. However slight deviation from linearity doesn't substantially change the results since the scattering is calculated from the projection of the electron density along the fibril axis. The distribution of crystal size(as projected on the fibril axis) is rectangular, with mean size a and limits of $(a - \Delta)$ and $(a + \Delta)$. A long period c is defined as the mean projected distance between crystal centers and a mean length of amorphous layer is given by $c - a$.

In general, the intensity of rays diffracted by a system of N crystallites of different sizes i.e. with different structure amplitude F, where F is the Fourier transform of electron density distribution within a crytal is given by

$$I \propto N\,(|\bar{F}^2| - |\bar{F}|^2) + |\bar{F}|^2\left\{N + \Sigma_{i\neq k}^{N}\exp(i\underset{\sim}{s}\cdot \underset{\sim}{Z}_{ik})\right\} \qquad \text{(VII-4)}$$

where $|\underset{\sim}{s}| = 4\pi \sin\theta/\lambda$ is the diffraction vector, θ being

the Bragg angle, and $\underset{\sim}{Z}_{ik}$ is the vector from the center of ith crystal to the jth crystal. To calculate the scattering amplitude F along the fibril axis, Tsvankin assumed that the projection of the electron density on the fibril axis, within a crystal could be represented by a trapezoidal function shown in Fig.(VII-2).

If $\epsilon = \partial/z$,

$$F = \int_0^x (z/\partial) \exp(iyz/l)dz + \int_{\epsilon x}^{(1-4)x} \exp(iyz/l)dz$$

$$+ \int_{(1-\epsilon)x}^{x} \left[(x-z)/\partial\right] \exp(iyz/l)dz \qquad \text{(VII-5)}$$

and

$$\bar{F} = \left(\frac{1}{2\Delta}\right) \int_{a-\Delta}^{a+\Delta} F(x)dx \qquad \text{(VII-6)}$$

$$|\bar{F}|^2 = |\bar{F}| \cdot |\bar{F}^*| \qquad \text{(VII-7)}$$

$$|\bar{F^2}| = \left(\frac{1}{2\Delta}\right) \int_{a-\Delta}^{a+\Delta} F^2(x)\, dx \qquad \text{(VII-8)}$$

where $y = \vec{s}l = 2\pi l \sin 2\theta/\lambda$

$\alpha = a/l$

$\beta = \Delta/l$

$l = c - a$ (VII-9)

The mean long period is represented by c, the mean crystal length by a, the mean amorphous length by l, and the

dispersion of crystallites size is assumed to be uniform between a-Δ and a+Δ as shown in eq.(VII-6) and (VII-8). This assumption is made for the mathematical simplicity and will be discussed later.

Eq.(VII-5)~(VII-8) were originally calculated by Tsvankin, and modified by Buchanan[73] to consider the continuous scattering contribution ($|\bar{F}^2| - |\bar{F}|^2$), which was considered constant by Tsvankin.

$$|\bar{F}|^2 = \frac{a^2}{\epsilon^2(\alpha y)^4}\left\{\left[\frac{\sin(1-\epsilon)\beta y}{(1-\epsilon)\beta y}\cos(1-\epsilon)\alpha y + \frac{\sin \epsilon\beta y}{\epsilon\beta y}\cos \epsilon\alpha y - \frac{\sin \beta y}{\epsilon\beta y}\cos \alpha y - 1\right]^2 + \left[\frac{\sin(1-\epsilon)\beta y}{(1-\epsilon)\beta y}\sin(1-\epsilon)\alpha y + \frac{\sin \epsilon\beta y}{\epsilon\beta y}\sin \epsilon\alpha y - \frac{\sin \beta y}{\beta y}\sin \alpha y\right]^2\right\} \qquad \text{(VII-10)}$$

$$|\bar{F}^2| = \frac{a^2}{\epsilon^2(\alpha y)^4}\left[4 + 2\frac{\sin(1-2\epsilon)\beta y}{(1-2\epsilon)\beta y}\cos(1-2\epsilon)\alpha y - 4\frac{\sin(1-\epsilon)\beta y}{(1-\epsilon)\beta y}\cos(1-\epsilon)\alpha y - 4\frac{\sin \epsilon\beta y}{\epsilon\beta y}\cos \epsilon\alpha y + 2\frac{\sin \beta y}{\beta y}\cos \alpha y\right] \qquad \text{(VII-11)}$$

The second term in Eq.(VII-4) describes the scattering resulting from the interference between the different crystallites and is responsible for the occurence of maxima in the scattering pattern. It is shown by Tsvankin[69] that

$$|\bar{F}|^2 \left[N + \sum_{i \neq k}^{N} \sum \exp\left(i \, \underset{\sim}{s} \cdot \underset{\sim}{Z}_{ik}\right)\right] = N|\bar{F}|^2 I_1 \qquad \text{(VII-12)}$$

where

$$I_1 = (\beta^2 y^2 + \beta^2 y^4 - \sin^2 \beta y) \,/\, (\sin^2 \beta y + \beta^2 y^2 + \beta^2 y^4 - 2\beta y \cos \alpha y \sin \beta y + 2\beta y^2 \sin \alpha y \sin \beta y) \qquad \text{(VII-13)}$$

Therefore, from Eq.(VII-4), (VII-10), (VII-11), (VII-12) and (VII-13)

$$I \propto N \left\{ (|\bar{F}^2| - |\bar{F}|^2) + |\bar{F}|^2 I_1 \right\} \qquad \text{(VII-14)}$$

Detailed calculation of Eq.(VII-14) shows that increasing the dispersion of crystallite lengths and decreasing linear crystallinity contribute to the broadening of the maxima, therefore decreasing the peak intensity. Also it is found that the effects of the boundary between the crystalline and amorphous layers are insignificant in changing the shape of the scattering pattern when ϵ is other than zero. Usually ϵ=0.2 is suggested. Therefore, it is clearly seen

in Eq.(VII-14) that scattering intensity depends upon the number of lamellae with fixed orientation as well as the size and shape of the crystallites.

As shown by Tsvankin and Buchanan, the positions and widths of the first-order maxima are employed in determining the structural parameters, c, a, l and Δ. This is done by using the calibration curves built by the model calculations and comparing with the experimental results. Among the several parameters shown in Eq.(VII-9), it is found that dimensionless variables, $\beta/\alpha = \Delta/l$ and the linear crystallinity $k = a/a+l = a/l+a$ are sufficient to characterize the intensity function.

The peak position X_m and half-width P of the first-order maximum based on the model calculation for given value of β/α, are expressed in terms of $c \sin 2\theta/\lambda$ scale. The equivalent quantities obtained from the experimental data are refered to $\sin 2\theta/\lambda$ scale(apparent long period $d = \lambda/\sin 2\theta$, half width q). Then they are related by

$$P = cq$$

$$X_m = c/d \qquad \text{(VII-15)}$$

And it is shown that

$$P/X_m = dq = \psi(P)$$

The quantity $\psi(P)$ relates the calculated and experimental curves through calibration curves which relates (1) P to $\psi(P)$, (2) P to $k=\alpha/1+\alpha$ and (3) P to X_m.

If experimental values of d and q are known, and a value of crystallite length dispersion, β/α, is assumed, then X_m and k are obtained from calibration curves. Such calibration curves for $\beta/\alpha = 0.3$ and 0.4 are shown in Fig. (VII-4) and (VII-5). For these parameters, the mean long period c, the mean crystallites length a and the mean amorphous length l are obtained.

$$\begin{aligned} c &= X_m d \\ a &= kc \\ l &= c - a \end{aligned} \qquad \text{(VII-16)}$$

At the peak position

$$y = \frac{2\pi}{1+\alpha} c \sin 2\theta/\lambda = \frac{2\pi}{1+\alpha} X_m$$

Therefore the peak intensity for single crystallite normalized for unit length can be calculated from X_m and k, using Eq.(VII-14) and the results are shown in Figs.(VII-4) and (VII-5).

Therefore, the lamellar distribution function $N(\phi)$ and orientation function $f_e = 3\langle \cos^2\phi - 1 \rangle / 2$ of the deformed spherulite are determined as follows.

The intensity function along the scattering angle at a

fixed azimuthal angle ϕ is measured as shown in Fig.(VII-3). From the slit corrected intensity function, the structural parameters are determined from Figs.(VII-4) and (VII-5). Also the intensity at the first order maximum for a single lamellae normalized for unit length, I_m^o is obtained from Figs.(VII-4) and (VII-5). The relative maximum intensity, I_m is obtained by $I_m^o a^2$. The experimental peak intensity is divided by I_m to give the relative number of lamellae oriented by ϕ with respect to the stretching direction. This process is repeated for other azimuthal angles, and the lamellae distribution function $N(\phi)$ is determined. From $N(\phi)$, the lamellar orientation function, f_e is given by

$$f_e = \frac{3\langle \cos^2\phi \rangle - 1}{2}$$

$$\langle \cos^2\phi \rangle = \frac{\int_o^{\pi/2} N(\phi) \cos^2\phi \sin\phi \, d\phi}{\int_o^{\pi/2} N(\phi) \sin\phi \, d\phi} \qquad \text{(VII-17)}$$

Discussion

The quantitative analysis of the SAXRD of deformed spherulites provides further information in understanding the deformation behavior of spherulitic polymers, combined with other experimental techniques, e.g., wide angle x-ray diffraction, light scattering, and birefringence etc..

Whether the crystallite density is uniform or more

concentrated in the polar region of the deformed spherulites has been discussed and no definite answer is given yet. Also, the validity of the affine deformation will be further checked. The change in crystallite length should result from the crystalline slip process. Therefore the SAXRD studies will provide the information on the chain tilting process[28,52,61] suggested by several workers in interpreting the wide angle x-ray pattern.

Also the change of amorphous layer thickness will give further information concerning the amorphous phase orientation in the deformed spherulites.

Future Improvement

In applying Tsvankin, Buchanan's method to SAXRD, it is necessary to assume the crystalline length dispersion, β/α beforehand. It is not known exactly, but β/α between 0.2 and 0.4 gives good agreement with other experimental results. Also the assumption that the crystallite length distribution is uniform between $a-\Delta$ and $a+\Delta$ is questionable and further modification of the present method is needed.

PART IV COMPOSITE THEORY

CHAPTER VIII ANALYSIS OF LOCAL STRAIN IN CRYSTALLINE POLYMERS

Introduction

Crystalline polymers are composed of a densely packed crystalline phase and a spacially disordered amorphous phase. The presence of a crystalline phase even at very low volume fractions results in a marked difference in physical properties, compared with purely amorphous rubbery polymers. For example, as shown by Neilson[82] the elastic modulus changes by the factor of as much as 100 at the crystallinity of 20%.

This marked contribution resulting from the presence of the crystalline phase has been the topic of study of many authors.[82-88] The crystallites were first treated as the crosslinks in the kinetic rubber-elasticity theory. The modulus predicted were much lower than the experimental results. Subsequently they were treated as spherical particles acting as crosslinks. Still the predictions fell below the experimental elastic modulus by an order of magnitude or more. These observations resulted in the suggestion that[88] the amorphous phase in crystalline polymers

is stiffer than the reference rubbery conditions. In other words, the amorphous chains are in non-Gaussian extended state due to the presence of tie molecules, running between the crystalline phase.

It is generally recognized that the crystalline polymers are present as spherulites in many cases. In the spherulites, the crystalline phase is present as ribbonlike lamellae. The crystalline lamellae form the radius and the amorphous phase remains between these lamellae. Therefore another line of approach has been to consider the crystalline polymers as blends of distinctly two phases. It is conceivable that in the polar region, the lamellae-amorphous layer acts as a parallel spring model, and in the equatorial region, it acts as a series spring model. Employing an empirical two-phase model, Takayanaki[83] considered the crystalline polymers in terms of a combined series-parallel spring model.

The development of composite theories[80,81] and micro-mechanics in recent years demonstrated that the geometry and orientation of the phase play an important role in determining the physical properties of composite materials or blends. According to these composite theories, internal morphology becomes the dominant factor, replacing the arbitrariness of series-parallel model. These results were applied to crystalline polymers by Halpin and Kardos,[95] who took into account the morphology of crystalline polymers in predicting elastic modulii. These predictions were

made based on an apriori assumption concerning the morphology of the crystalline phase, namely, the dimensions of the lamellae. However the results showed good agreement with the experimental results in relating morphology to the mechanical properties.

Since the strain and stress distribution is a basic factor in affecting the mechanical properties of any system, it becomes obvious that the strain distribution in the deformed crystalline polymers should be related to their internal morphology. The understanding of strain distribution is very important in understanding the deformation behavior. The deformation of crystalline polymers and the resulting crystal reorientation has been interpreted by various mechanisms; i.e. chain tilting, lamellar twisting, lamellar unfolding etc. It is evident that these mechanisms are affected differently depending on not only the magnitude of strain but also the type of strain; crystalline shear strain, crystalline normal strain, and amorphous strain between the crystalline phase. However in previous interpretations of the experimental results, and theoretical models, no clear distinction is made between the crystalline strain and amorphous strain. Rather these effects are considered loosely based on series or parallel models. Also the effects of crystallinity is not clear. For example, it is not clearly known whether the high density polyethylene

and low density polyethylene undergo the same deformation processes. Therefore it is the purpose of this work to compute the strain distribution of crystalline and amorphous phase of the deformed crystalline polymers, based on its internal morphology. For this purpose, composite theories and micromechanics are applied. Also the dependence of strain distribution on the crystallinity is considered.

Theoretical Analysis

As has been mentioned, most bulk crystallized polymers are filled with spherulites. The crystalline ribbon-like lamellae form the radius and the amorphous phase is present between these lamellae. This lamellae-amorphous layer polymer can be treated as a composite material whose main axis is oriented along the radius of the spherulite. The lamellae are considered as straight ribbon-shaped as shown in Fig.(VIII-1). Also the crystalline lamellae are considered as isotropic material with the same elastic moduli along all directions. In this respect it has been found that the introduction of anisotropy[90] yields only a second order contribution to the mechanical properties of composites, compared with the contribution of internal morphology.

The stiffness properties of composites which contain one phase(reinforcement) imbedded in a matrix material depends

upon the geometry and orientation of the reinforcement. If the reinforcement phase is oriented along one direction inside the matrix, this composite becomes highly anisotropic; that is, the elastic properties strongly depend upon the direction. This relationship has been developed by Halpin and Tsai.[80] In crystalline polymers, the lamellae are oriented along the radial direction, so that lamellae-amorphous layers are considered as an anisotropic composites whose orientations determined by their position inside the spherulite. For the ribbon-shaped reinforcements inside the amorphous matrix, the Halpin and Tsai[80,89] equations show that the composite modulus along the lamellar axis(radial direction of the spherulite), E_{11}, is given by

$$E_{11}/E_m = (1 + \xi\eta V_f)/(1-\eta V_f) \qquad \text{(VIII-1)}$$

$$\eta = (E_f/E_m - 1)/(E_f/E_m + \xi) \qquad \text{(VIII-2)}$$

$$\xi = 2(c/b) \qquad \text{(VIII-3)}$$

where E_f = modulus of enforcement(crystalline lamellae)

E_m = modulus of matrix phase(amorphous phase)

V_f = volume fraction of enforcement(crystallinity)

c = length of lamellae

b = thickness of lamellae

The composite modulus transverse to the lamellae, E_{22}, is given by the same equations(VIII-1) and (VIII-2), and Eq.(VIII-3) is replaced by

$$\xi = 2(a/b) \tag{VIII-4}$$

where a = transverse dimension of lamellae

Also the shear modulus, G_{12}, is given by

$$G_{12}/G_m = (1+\xi\eta V_f)/(1- V_f) \tag{VIII-5}$$

$$\eta = (G_f/G_m-1)/(G_f/G_m+\xi) \tag{VIII-6}$$

$$\log \xi = \sqrt{3} \log(a/b) \tag{VIII-7}$$

where G_f = shear modulus of the lamellae

G_m = shear modulus of amorphous matrix

The Poisson's ratio ν_{12}, is given approximately by

$$\nu_{12} = \nu_f V_f + \nu_m(1-V_f) \tag{VIII-8}$$

where ν_f and ν_m are the Poisson's ratios of the lamellae and amorphous matrix.

Therefore from Eqs.(VIII-1)~(VIII-8), all the elastic properties of the lamellae-amorphous composite are obtained from

the characteristic elastic properties, geometry and volume fraction of each phase. Then the spherulite can be considered as being composed of such composites which are oriented along the radii.

For many polymers at small deformations, the spherulite deforms affinely. Therefore the strain of the lamellae-amorphous composite is the same as the macroscopic strain. However the overall strain is distributed between the lamellae and amorphous layer, and the distribution is strongly dependent upon the orientation of the lamellae-amorphous composite as simply seen in the series or parallel model.

All the following calculations are made based on uniaxial elongation. First, the distribution of elongational strain between the lamellae and amorphous layer is computed as a function of the composite orientation. This is done in two steps. First, the elastic modulus of the composite along the stretching direction is obtained, depending upon its orientation. And then, the elongational strain in the amorphous and crystalline phase are calculated by comparing with the characteristic modulus of each phase.

The constitutive equation relating stress and strain in the reference coordinate system(X,Y) as shown in Fig.(VIII-2) can be expressed by

$$\begin{pmatrix} \epsilon_x \\ \epsilon_y \\ \epsilon_{xy} \end{pmatrix} = \begin{pmatrix} S_{11}' & S_{12}' & S_{13}' \\ S_{21}' & S_{22}' & S_{23}' \\ S_{61}' & S_{62}' & S_{66}' \end{pmatrix} \begin{pmatrix} \sigma_x \\ \sigma_y \\ \tau_{xy} \end{pmatrix} \qquad \text{(VIII-9)}$$

where ϵ_x, ϵ_y, ϵ_{xy} are the strains along X and Y direction and shear strain, and σ_x, σ_y, τ_{xy} are the normal stress along X and Y direction and shear stress. X axis is the stretching direction, and for the uniaxial stretching, one transverse direction(Y) is considered for the mathematical simplicity. The constitutive equation in the material axes can be expressed as follows for the anisotropic material whose two transverse components are equal[80]

$$\begin{pmatrix} \epsilon_1 \\ \epsilon_2 \\ \epsilon_{12} \end{pmatrix} = \begin{pmatrix} S_{11} & S_{12} & 0 \\ S_{12} & S_{22} & 0 \\ 0 & 0 & S_{66} \end{pmatrix} \begin{pmatrix} \sigma_1 \\ \sigma_2 \\ \tau_{12} \end{pmatrix} \qquad \text{(VIII-10)}$$

The compliance matrix $[S']$ in the reference coordinate and $[S]$ in the material coordinate are related by their orientation angle, θ, as shownin Fig.(VIII-2). The relationship has been derived by Pagano and Halpin[91], employing the matrix invariants. For the present purpose, only S_{11}' is needed, since the elastic modulus along the stretching

direction, E_x, is given by

$$E_x = 1/S_{11}' \qquad \text{(VIII-11)}$$

According to Pagano and Halpin,

$$S_{11}' = I_1 + I_2\cos 2\theta + I_3\cos 4\theta \qquad \text{(VIII-12)}$$

$$I_1 = 1/8(3S_{11} + 3S_{22} + 2S_{12} + S_{66}) \qquad \text{(VIII-13)}$$

$$I_2 = 1/2(S_{11} - S_{22}) \qquad \text{(VIII-14)}$$

$$I_3 = 1/8(S_{11} + S_{22} - 2S_{12} - S_{66}) \qquad \text{(VIII-15)}$$

Also the components of the compliance matrix [S] are related to the elastic properties obtained from Eqs.(VIII-1) (VIII-8) as follows.[80]

$$S_{11} = 1/E_{11} \qquad \text{(VIII-16)}$$

$$S_{22} = 1/E_{22} \qquad \text{(VIII-17)}$$

$$S_{12} = -\nu_{12}/E_{11} = -\nu_{21}/E_{22} \qquad \text{(VIII-18)}$$

$$S_{66} = 1/G_{12} \qquad \text{(VIII-19)}$$

Therefore from Eqs.(VIII-11) and (VIII-12), the elastic modulus of lamellae-amorphous composite along the stretching direction is obtained as a function of lamellar orientation.

The elongational strains in the crystalline and amorphous phase, ϵ_f and ϵ_m, are related to the composite elongational strain $\bar{\epsilon}$, composite modulus along the stretching direction, E and crystallinity, V_f, as follows,

$$\bar{\epsilon} = V_f\epsilon_f + (1-V_f)\epsilon_m \qquad \text{(VIII-20)}$$

$$\sigma_x = \bar{\epsilon}\cdot E = E_f V_f \epsilon_f + E_m(1-V_f)\epsilon_m \qquad \text{(VIII-21)}$$

where σ_x is the composite stress along the stretching direction. If we define,

$$\epsilon_f/\bar{\epsilon} = a_f, \qquad \epsilon_m/\bar{\epsilon} = a_m \qquad \text{(VIII-22)}$$

Eqs.(VIII-20) and (VIII-21) become

$$V_f a_f + (1-V_f)a_m = 1 \qquad \text{(VIII-23)}$$

$$E_f V_f a_f + E_m(1-V_f)a_m = E \qquad \text{(VIII-24)}$$

Therefore from Eqs.(VIII-22) and (VIII-23),

$$(E-E_m)/(E_f-E_m) = V_f a_f \qquad \text{(VIII-25)}$$

$$(E-E_f)/(Em-E_f) = (1-V_f)a_m \qquad \text{(VIII-26)}$$

From Eqs.(VIII-25) and (VIII-26), the elongational strain in the stretching direction is obtained, distributed in the crystalline and amorphous phase. The same procedure can be applied in determining the transverse strain perpendicular to the stretching direction by changing θ in Eq.(VIII-12) to $(90-\theta)$.

When the distribution of macroscopic elongation and transverse strain in the crystalline and amorphous phase is determined, it is possible to calculate the crystalline and amorphous strain in any coordinate system. Of special interest are the lamellar shear strain, ϵ_{12}^f, lamellar normal strain, ϵ_2^f, elongational along the lamellae, ϵ_1^f, and amorphous strain perpendicular to the lamellar surface, ϵ_2^m. These are mostly responsible for the crystal orientation processes, and ϵ_2^f, and ϵ_2^m are also responsible for the small angle x-ray diffraction from the deformed spherulites. The transformation of strain from the reference coordinate system(X, Y) to the material coordinates(1, 2) are expressed as

$$\begin{pmatrix} \epsilon_1 \\ \epsilon_2 \\ \frac{1}{2}\epsilon_{12} \end{pmatrix} = \begin{pmatrix} \cos^2\theta & \sin^2\theta & 2\sin\theta\cos\theta \\ \sin^2\theta & \cos^2\theta & -2\sin\theta\cos\theta \\ -\sin\theta\cos\theta & \sin\theta\cos\theta & \cos^2\theta - \sin^2\theta \end{pmatrix} \begin{pmatrix} \epsilon_x \\ \epsilon_y \\ \frac{1}{2}\epsilon_{xy} \end{pmatrix} \qquad \text{(VIII-27)}$$

these transformation is performed for the crystalline strain and amorphous strain. According to these analyses, the long period observed in the small angle x-ray diffraction, L, can be predicted by

$$\frac{L-L_o}{L_o} = V_f \epsilon_2^f + (1-V_f)\epsilon_2^m \qquad \text{(VIII-28)}$$

where L_o is the long period in the underformed state.

Results and Discussion

The calculations have been made, based on several assumptions concerning the charactistic properties of the crystalline and amorphous phase: the ratio of lamellar length vs. thickness, c/b, is 100 and transverse dimension vs. thickness, a/b, is 10, the elastic modulus ratio of crystalline phase vs. amorphous matrix, $\frac{E_f}{E_m}$, is 1000, and the Poisson's ratios are 0.3 and 0.5 for the crystalline and amorphous phase. These values have been adopted since they have been used with success in predicting the elastic moduli of

crystalline polymers. However as discussed by Halpin[95] and Kardos, the exact values of these parameters are not clearly known.

The elongational modulus of the lamellae-amorphous composite along the stretching direction, E_x, is obtained from Eq.(VIII-11), and E_x/E_m is plotted as function of orientation angle in Fig.(VIII-3) for several crystallinities. The crystalline and amorphous strain along the stretching direction is obtained from Eqs.(VIII-25) and (VIII-26), and $\epsilon_f/\bar{\epsilon}$, $\epsilon_m/\bar{\epsilon}$ are shown Figs.(VIII-4) and (VIII-5), $\bar{\epsilon}$ being the macroscopic strain along the stretching direction. In those three figures, it is seen that the angular profiles of E_x/E_m, $\epsilon_f/\bar{\epsilon}$, $\epsilon_m/\bar{\epsilon}$ are affected by the crystallinity. In other words, the strain distribution is very much dependent upon the crystallinity. Also the deviation from the parallel or series model is clear. The parallel model assumption at $\theta=0^\circ$, would predict $\epsilon_f/\bar{\epsilon} = \epsilon_m/\bar{\epsilon} = 1$. Similarly the series model assumption at $\theta=90^\circ$, would predict $\epsilon_f/\bar{\epsilon}=0$ and $\epsilon_m/\bar{\epsilon}=1/(1-V_f)$. However it should be noted that the results obtained here always stay between these extreme series and parallel model predictions.

The crystalline strain along the lamellar axis, ϵ_1^f, and crystalline shear strain in the lamellar coordinate, ϵ_{12}^f, are shown as ϵ_1^f/ϵ_x and $\epsilon_{12}^f/\epsilon_x$ in Figs.(VIII-6) and (VIII-7) for the case, $\epsilon_y/\epsilon_x=-0.4$, ϵ_x, ϵ_y being the macroscopic

strain in X and Y direction. Significant effects of crystallinity are seen and rapid change in crystalline strain is noticed at nigher crystallinity.

It has been suggested by several authors[56] that the crystalline shear strain, ϵ^f_{12}, is mainly responsible for the chain tilting or crystal slip process. It is assumed that the crystal shear strain, and crystal slip process has its maximum when the lamellae are oriented 45° with respect to the stretching direction. Results shown in Fig.(VIII-7) indicate that the crystal shear strain distribution depends strongly upon the crystallinity. When completely crystalline, ϵ^f_{12} has its maximum at $\theta = 45°$. However as the crystallinity decreases, ϵ^f_{12}, maximum shifts toward smaller θ, closer to the stretching direction, and the distribution profiles are changing at the same time. Therefore it is noted that the deformation processes of crystalline polymers of different crystallinities should not be uniquely defined.

The change of long period is plotted in Fig.(VIII-8) as a function of orientation as $(L-L_o)/(L_o\bar{\epsilon}_x)$. The change of long period is the same for all crystallinities. This is expected since the long period is due to the lamellar-amorphous composite, whose strain is related to the macroscopic strain by the affine deformation.

All the results obtained are based on the parameters as discussed before. More precise predictions could be made

if more informations are available on determining these parameters by other experimental techniques, e.g. electron microscopy.

It would be also possible to test the present theoretical predictions by the electron microscopic observations, micro-x-ray, and small angle x-ray diffraction experiments on the deformed spherulitic polymers. The systematic investigation of deformation behavior of low density, medium dendity, and high density polyethylene would be also desirable in this respect.

PART V SUMMARY

Several theories of light scattering, x-ray diffraction, and orientation of polymer crystals have been discussed, concerning their application to the study of structure of crystalline polymers and its change upon deformation.

And based on these theories, light scattering measurements have been applied to study the effect of annealing the quenched polyethylene films.

Composite theory has also been applied to crystalline polymers to predict the local strain, based on their morphology.

These several different theories are related with each other in that they are concerned with simple separate aspects of general complicated problem of understanding the physical properties of crystalline polymers.

BIBLIOGRAPHY

1. O. K. Gerngross, K. Horrmann, and W. Agitz, Z. Physik. Chem., B10, 371 (1930).
2. O. Kratky, and H. Mark, Z. Physik. Chem., B36, 139 (1937).
3. R. S. Stein, J. Polymer Sci. Part C, No. 15, 185 (1966).
4. E. W. Fisher, Z. Naturforshe. 12a, 753 (1957).
5. A. Keller, Phil. Mag., (8) 2, 1171 (1957).
6. P. H. Till, Jr., J. Polymer Sci., 24, 301 (1957).
7. P. H. Geil, J. Polymer Sci., 47, 65 (1960).
8. H. D. Keith, and F. J. Padden, J. Appl. Phys., 34, 2409 (1963).
9. C. W. Bunn, and T. C. Alcock, Trans. Faraday Soc. 41, 317 (1945).
10. F. P. Price, J. Polymer Sci., 39, 139 (1959).
11. P. Debye, and A. M. Bueche, J. Appl. Phys., 20, 518 (1949).
12. M. Goldstein, and E. R. Michalik, J. Appl. Phys., 26, 1450 (1955).
13. R. S. Stein, P. Erhardt, J. J. van Aartsen, S. Clough, and M. B. Rhodes, J. Polymer Sci., Part C, 13, 1 (1966).
14. R. S. Stein, and P. R. Wilson, J. Appl. Phys., 33, 1914 (1962).
15. R. S. Stein, P. Erhardt, S. Clough and G. Adams, J. Appl. Phys., 37, 3980 (1966).

16. R. S. Stein, and M. B. Rhodes, J. Appl. Phys., 31, 1873 (1960).

17. S. Clough, J. J. van Aartsen, and R. S. Stein, J. Appl. Phys., 36, 3072 (1965).

18. A. E. M. Keijzers, J. J. van Aartsen, and W. Prins, J. Appl. Phys., 36, 2874 (1965).

19. R. S. Stein, and W. Chu, J. Polymer Sci., A-2, 8, 1137 (1970).

20. M. B. Rhodes, and R. S. Stein, J. Polymer Sci., A-2, 7, 1539 (1969).

21. T. Hashimoto, and R. S. Stein, J. Polymer Sci., A-2, 8, 1127 (1970).

22. R. S. Stein, and C. Picot, J. Polymer Sci., A-2, 8, 1955 (1970).

23. R. S. Stein, and C. Picot, J. Polymer Sci., A-2, 8, 2127 (1970).

24. C. Picot, R. S. Stein, M. Motegi, and H. Kawai, J. Polymer Sci., A-2, 8, 2115 (1970).

25. P. R. Wilson, S. Krimm, and R. S. Stein, J. Phys. Chem., 65, 1749 (1961).

26. R. S. Stein, and T. Hotta, J. Appl. Phys. 35, 2237 (1964).

27. R. J. Samuels, J. Polymer Sci., Part C, 13, 37 (1966).

28. J. J. van Aartsen, and R. S. Stein, J. Polymer Sci., A-2, 9, 295 (1971).

29. R. S. Stein and S. N. Stidham, J. Appl. Phys., 35, 42 (1964).

30. S. N. Stidham, Ph. D. thesis, University of Massachusetts, Amherst, Mass. 1964.

31. R. S. Stein, "Morphology of Crystalline Aggregates in Polyethylene" in Growth and Perfection of Crystals (R. H. Doremus, B. W. Roberts, and D. Turnbull, eds.), Jhon Wiley and Sons, Inc., New York (1958).

32. R. S. Stein, J. J. Kead, F. H. Norris, F. A. Bettelheim, and P. R. Wilson, Annals of the New York Academy of Sciences, 83, article 1, 37 (1959).

33. S. Jabarin, Ph. D. thesis, University of Massachusetts, Amherst, Mass. 1971.

34. G. H. Brown, and W. G. Shaw, Chem. Rev., 57, 1049 (1957).

35. G. W. Gray, Molecular Structure and Properties of Liquid Crystals, Academic Press, N. Y. (1962).

36. S. Tatematsu, N. Hayashi, S. Nomura, and H. Kawai, presented at the 20th Annual Meeting of the Society of Polymer Science, Japan, Tokyo, May, 1971.

37. M. B. Rhodes, and R. S. Stein, J. Polymer Sci., 45, 521 (1960).

38. S. Clough, M. B. Rhodes, and R. S. Stein, J. Polymer Sci. Part C, 18, 1 (1967).

39. R. Prud'homme, Ph. D. thesis, University of Massachusetts, Amherst, Mass., 1973.

40. A. Tanaka, Ph. D. thesis, University of Massachusetts, Amherst, Mass. 1970.

41. R. S. Stein, and P. R. Wilson, ONR technical Report No. 35, Project 356-378, Contract 3357(01), Polymer Research Institute, University of Massachusetts, August, 1961.

42. A. Keller, and S. Sawada, Macro. Chemie, 74, 190 (1964).

43. D. T. Sturgill, presented at the American Ceramic Society Symposium on Nucleation, 1971.

44. T. Kawaguchi, T. Ito, H. Kawai, D. Keedy, and R. S. Stein, Macromolecules, 1, 126 (1968).

45. Z. W. Wilchinsky, Polymer, 5, 271 (1964).

46. K. Sasaguri, S. Hoshino, and R. S. Stein, J. Appl. Phys., 35, 47 (1964).

47. K. Sasaguri, R. Yamada, and R. S. Stein, J. Appl. Phys., 35, 3188 (1964).

48. I. L. Hay, and A. Keller, Kolloid-Z., 204, 43 (1965).

49. K. Kobayashi, and T. Nagasawa, J. Polymer Sci., Part C, No. 15, 163 (1967).

50. O. Kratky, Kolloid-Z. 84, 149 (1938).

51. T. Oda, N. Sakayuchi, and H. Kawai, J. Polymer Sci., Part C, No. 15, 223 (1966).

52. S. Nomura, A. Asanuma, S. Suehiro, and H. Kawai, J. Polymer Sci., A-2, 9, 1991 (1971).

53. S. Nomura, M. Matsuo, H. Kawai, J. Polymer Sci., A-2, 10, 2489 (1972).

54. R. S. Finkelstein, C. Chang, and R. S. Stein, in press.

55. T. Oda and R. S. Stein, J. Polymer Sci., A-2, 10, 685 (1972).

56. P. H. Geil, Polymer Single Crystals, J. Wiley, New York (1963).

57. C. W. Bunn, Trans. Faraday Soc., 35, 482 (1939).

58. F. C. Frank, A. Keller, and A. O'Connor, Phil. Mag. 8, 64 (1958).

59. H. Kiho, A. Peterlin, and P. H. Geil, J. Appl. Phys., 35, 1599 (1964).

60. T. Seto, T. Hara, and K. Tanaka, Japanese J. Appl. Phys., 7, 31 (1968).

61. P. Ingram, and A. Peterlin, J. Polymer Sci., Part B, 2, 739 (1964).

62. R. S. Moore, J. Polymer Sci., A-2, 5, 711 (1967).

63. J. J. Point, G. A. Homes, D. Gezovichad, and A. Keller, J. Mater. Sci., 4, 908 (1969).

64. A. Cowkiz, J. G. Rider, I. L. Hay, and A. Keller, J. Mater. Sci., 3, 646 (1968).

65. G. L. Wilkes, J. Mater. Sci., 6, 1465 (1971).

66. W. O. Statton, J. Polymer Sci., 41, 143 (1959).

67. G. Porod, Fortschr. Hochpolymeren Forch., 2, 363 (1961).

68. C. Rheinhold, E. W. Fisher, and A. Peterlin, J. Appl. Phys., 35, 71 (1964).

69. D. Ya. Tsvankin, Polymer Sci. USSR, 6, 2304, 2310 (1964).

70. A. I. Kitaigorodskii, D. Ya. Tsvankin, and Yu. M. Petrov, Vysokomol. soyed., 5, 1062 (1963).

71. C. G. Vonk, and G. Kortleve, Kolloid Z. Z. Polym., 220, 19 (1967).

72. G. Kortleve, and C. G. Vonk, Kolloid Z. Z. Polym., 225, 124 (1968).

73. D. R. Buchanan, J. Polymer Sci., A-2, 9, 615 (1971).

74. A. Guiner, and G. Fournet, Small Angle Scattering of X-ray, Wiley, New York, 1955.

75. P. Schmidt, Acta Cryst., 19, 938 (1965).

76. K. O'leary, and P. H. Geil, J. Macromol. Sci., B2(2), 179 (1968).

77. A. Peterlin, J. Appl. Phys. 40, 4238 (1969).

78. A. Peterlin, Makromol. Chem., 142, 227 (1971).

79. A. Peterlin, Croat. Chem. Acta., 42, 335 (1970).

80. J. E. Ashton, J. C. Halpin, and P. H. Petit, Primer on Composite Materials: Analysis, Technomic Pub. Co., Stamford, Conn. (1969).

81. S. W. Tsai, J. C. Halpin, and N. J. Pagano, Composite Materials Workshop, Technomic Pub. Co., Stamford, Conn. (1968).

82. L. Nielsen, J. Appl. Polymer Sci., 2, 351 (1959).

83. M. Takayanagi, In Fourth Int. Cong. on Rheology, Part I; ed. by E. H. Lee, and A. L. Copley, J. Wiley, N. Y. (1965).

84. P. J. Flory, Trans. Faraday Soc., 51, 848 (1955).

85. A. V. Tobolsky, and V. D. Gupta, Textile Res. J., 33, 761 (1963).

86. S. Newman, J. Polymer Sci., 47, 114 (1960).

87. L. E. Nielsen, and F. D. Stockton, J. Polymer Sci., A1, (1963).

88. W. R. Krigbaum, R. T. Roe, and K. J. Smith, Polymer, 5, 533 (1964).

89. J. C. Halpin, and R. L. Thomas, J. Comp. Mat. 2, 488 (1968).

90. J. C. Halpin, K. Jerina, and J. M. Whitney, J. Comp. Mat. 5, 36 (1971).

91. J. C. Halpin, and N. J. Pagano, J. Comp. Mat. 3, 720 (1969).

92. G. S. Y. Yeh, J. Macromol. Sci., B6(3), 451 (1972).

93. W. Chu, Ph.D. Thesis, University of Massachusetts, Amherst, Massachusetts, 1969.

94. R. S. Stein, S. N. Stidham, and P. R. Wilson, O.N.R. Technical Report No. 36, University of Massachusetts, Contract: Nonr 3357(00), Project; NR 356-378, August, 1961.

95. J. L. Kardos, W. L. Mcdonnell, and J. Raisoni, J. Macromol. Sci., B6(2), 307 (1972).; J. C. Halpin. and J. L. Kardos, in press.

96. T. Hashimoto, Ph.D. Thesis, University of Massachusetts, Amherst, Massachusetts, 1970.

CAPTIONS FOR FIGURES

A-1. Fringe-micelle model of crystalline polymers.

I-1. Schematic diagram of sector and its orientation.

I-2. Photographic light scattering set-up.

I-3. Model of assembly of focal conics representing the cholestric mesophase morphology of liquid crystals.

I-4. Definition of $\underset{\sim}{r}$, $\underset{\sim}{r}_s$, and $\underset{\sim}{r}_o$.

I-5. Contour diagram of $\log(I_{H_v})$ from the randomly oriented sectors with $\beta=180^\circ$, and $\delta=0^\circ$(a), and $\delta=45^\circ$(b).

I-6. Contour diagram of $\log(I_{H_v})$ from the randomly oriented sectors when $\beta=60^\circ$(a), and $\beta=5^\circ$(b).

I-7. The variation of I_{H_v} intensity with W at $\mu=45^\circ$ from the randomly oriented sectors with different values of the aperture angle.

I-8. Comparison of the variation of I_{H_v} intensity with W at $\mu=45^\circ$ for the disk composed of anisotropic sectors and the homogeneous anisotropic disk.

II-1. Definition of $\underset{\sim}{r}$, $\underset{\sim}{r}_{oi}$, and $\underset{\sim}{r}_i$.

II-2. Definition of parameters for the truncated spherulite.

II-3. One example of computer simulation of spherulites distribution within a circle of 20μ in radius.

II-4. The variation of I_{Vv}' with W at $\mu=0^\circ$ when the interference effects only is considered for 40 sets of assembly of 20 spherulites, compared with single spherulite case with $\alpha_r-\alpha_t=-3$, and $\alpha_t-\alpha_s=1$.

II-5. The variation of I_{V_V}' with W at $\mu=0^\circ$ when the interference and truncation are considered for 40 sets of assembly of 20 spherulites (a) $R=1\mu$ (b) $R=3\mu$, compared with single spherulite case with $\alpha_r-\alpha_t=-3$, and $\alpha_t-\alpha_s=1$.

II-6. The variation of I_{V_V}' with W at $\mu=90^\circ$ when the interference and truncation are considered for 40 sets of assembly of 20 spherulites of $R=3\mu$, compared with single spherulite case with $\alpha_r-\alpha_t=-3$, and $\alpha_t-\alpha_s=1$.

III-1. The H_v correlation of a spherulite, $\gamma_{Hv}(\underset{\sim}{r})$.

III-2. The variation of I_{Hv} intensity with μ at W=4 obtained from $\gamma_{H_v}(\bar{r})$ shown in Fig.(III-1).

III-3. The variation of I_{H_v} intensity with W at different azimuthal angles, obtained from $\gamma_{H_v}(\underset{\sim}{r})$ shown in Fig.(III-1).

III-4. The variation of the average square fluctuation for the V_v scattering, $\overline{\eta^2}_{V_v}$, with volume fraction of spherulites for different values of $(\alpha_r-\alpha_m)$ with $\alpha_r-\alpha_t=-3$.

III-5. The V_v correlation function of a spherulite, $\gamma_{V_v}(\underset{\sim}{r})$, with $\alpha_r-\alpha_t=-3$, and $\alpha_t-\alpha_b=9$.

III-6. The V_v correlation function of a spherulite, $\gamma_{V_v}(\underset{\sim}{r})$, with $\alpha_r-\alpha_t=-3$, and $\alpha_t-\alpha_b=4$.

III-7. The V_v correlation function of a spherulite, $\gamma_{V_v}(\underset{\sim}{r})$, when spherulites are volume-filling.

III-8. The variation of I_{V_v} obtained from the correlation function shown in Fig.(III-6).

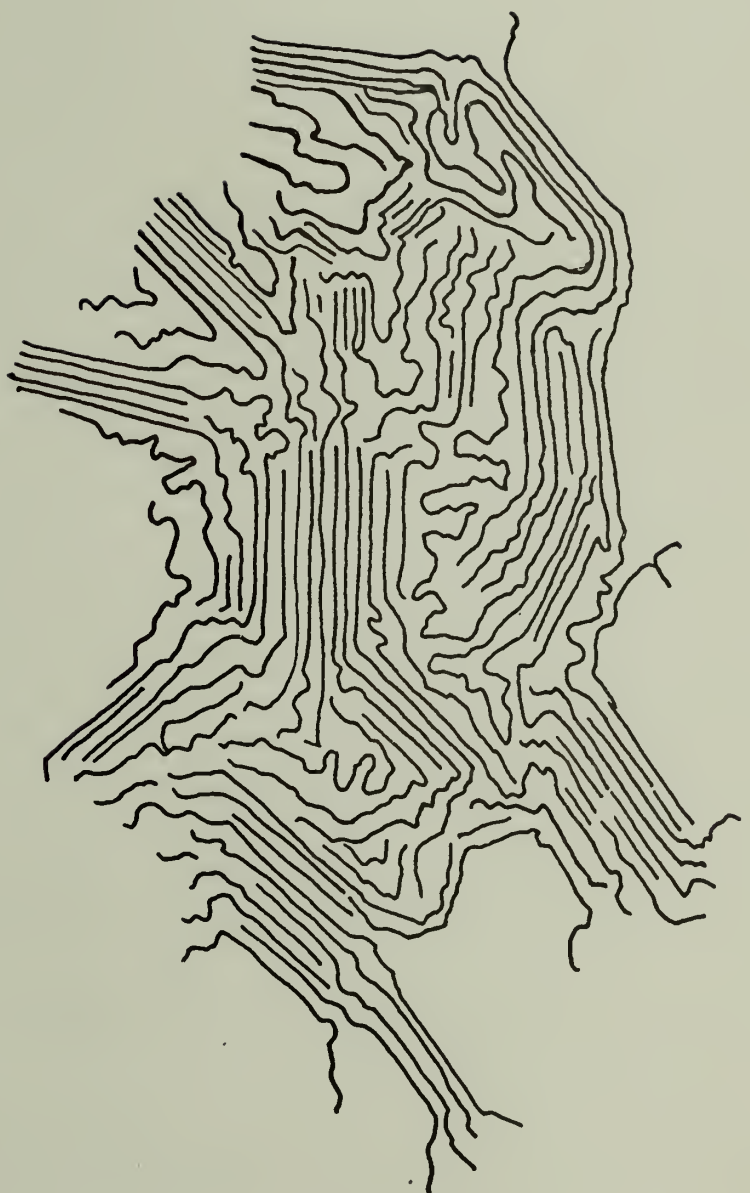

Figure A-1

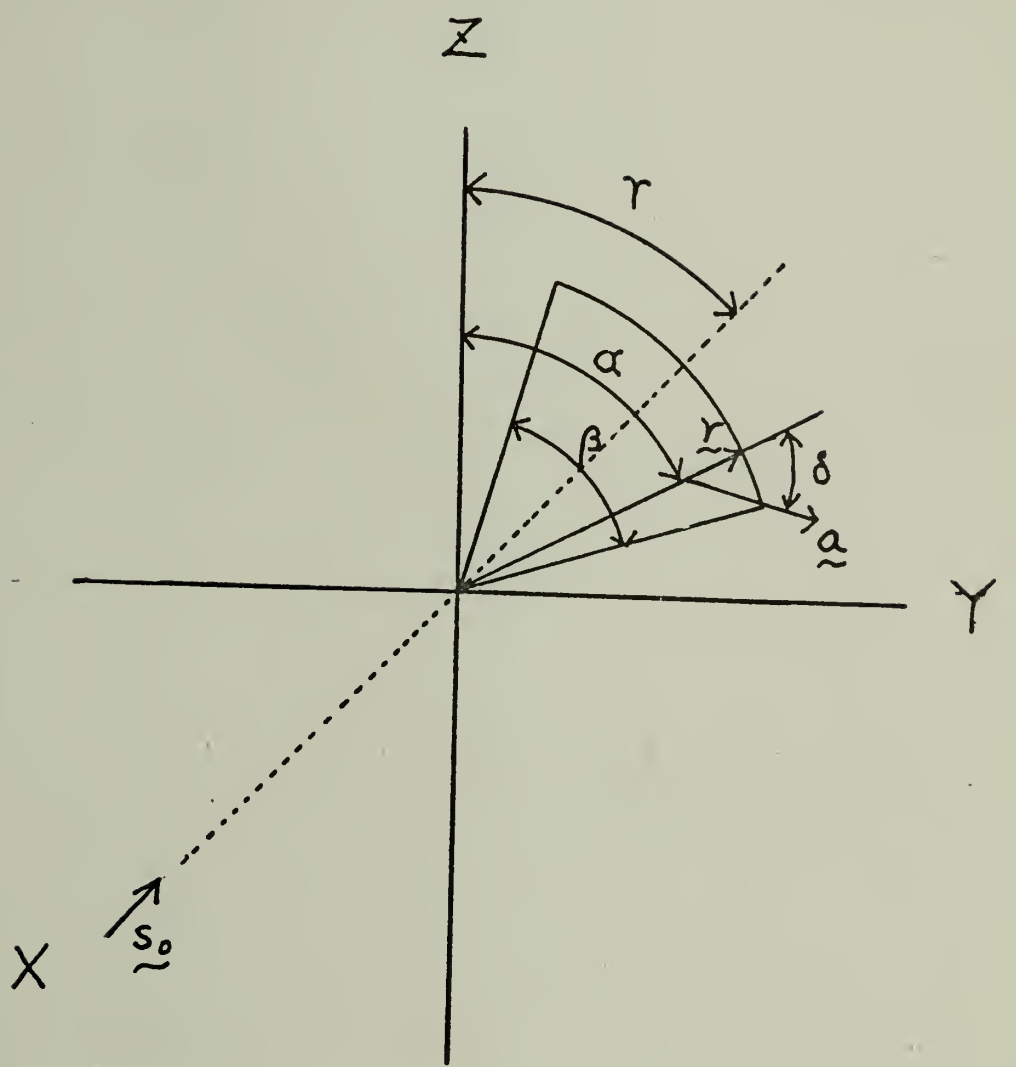

Figure I-1

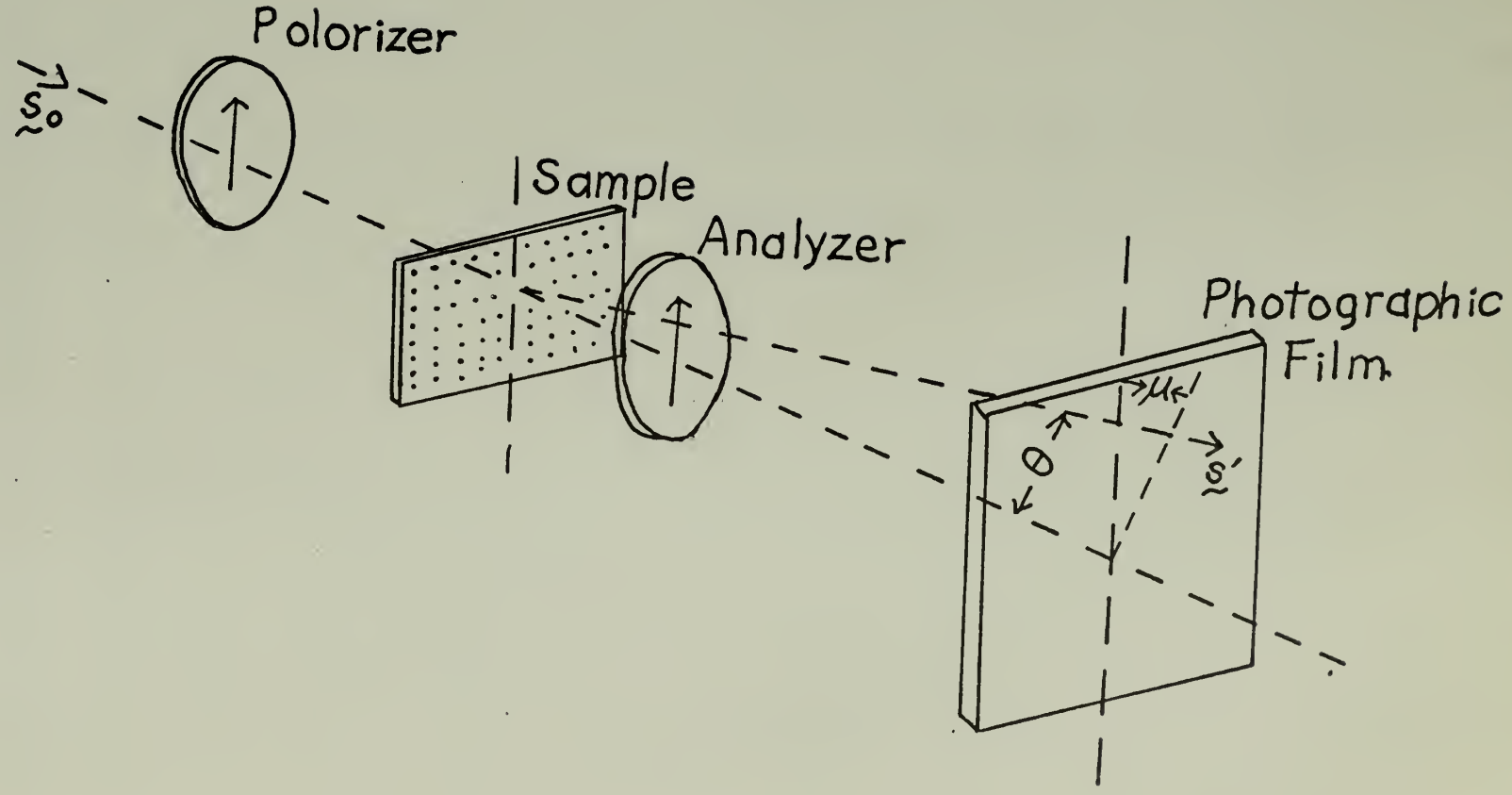
Polorizer
$\vec{s}_o$
Sample
Analyzer
Photographic
Film
$\vec{\mu}$
θ
$\vec{s}'$

Figure I-2

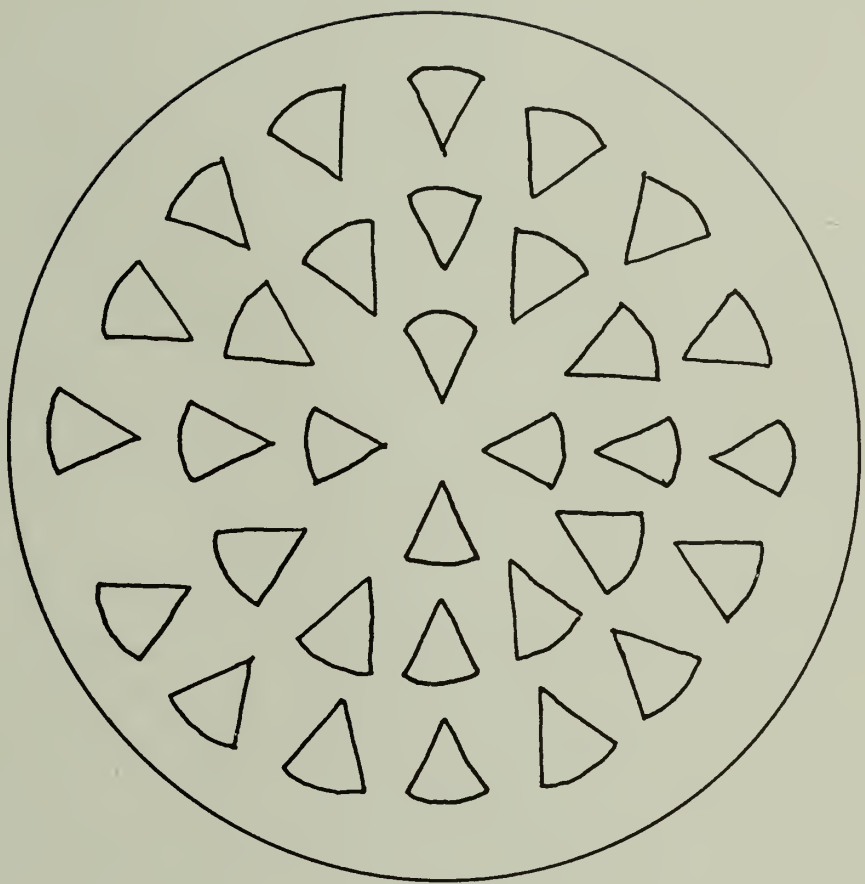

Figure I-3

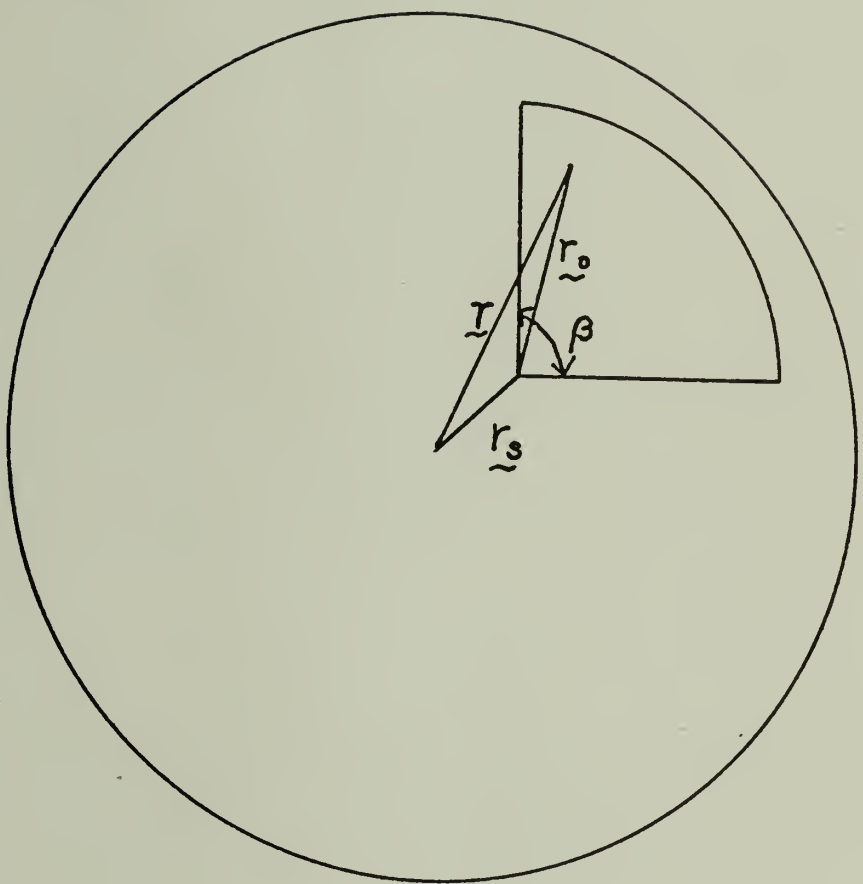

Figure I-4

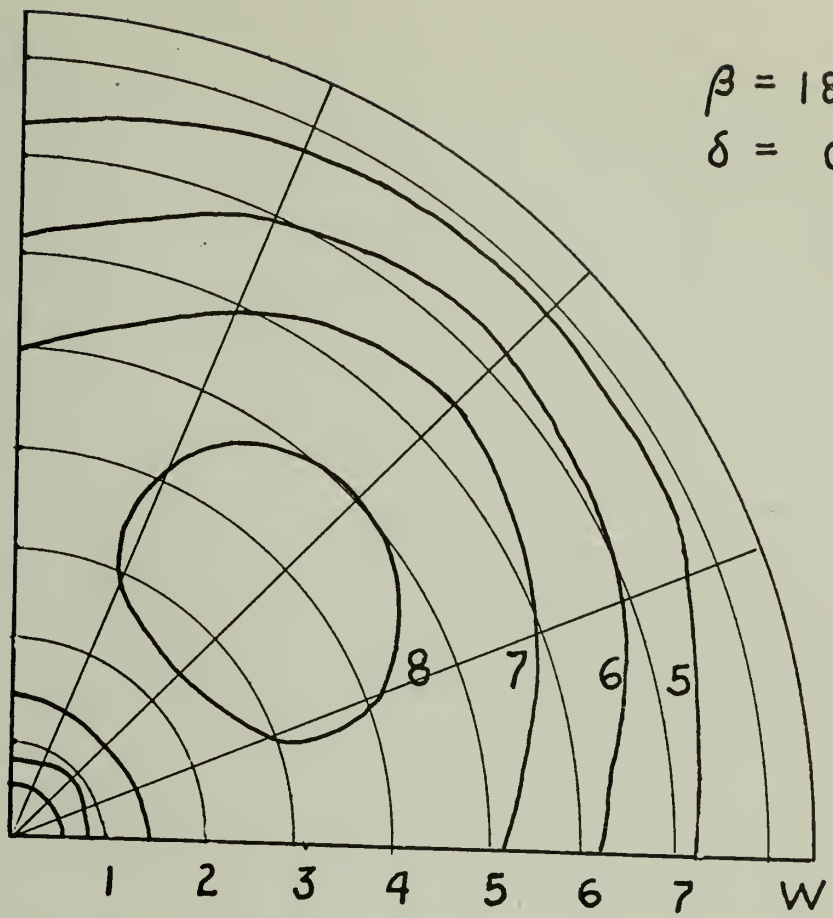

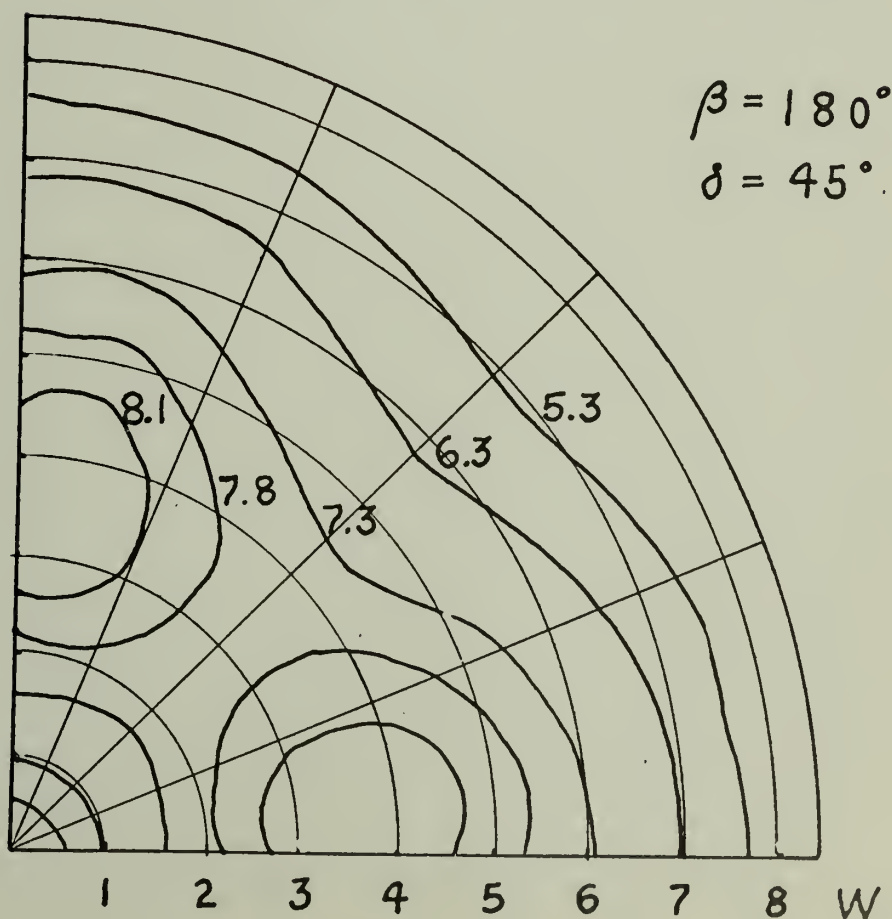

Figure I-5

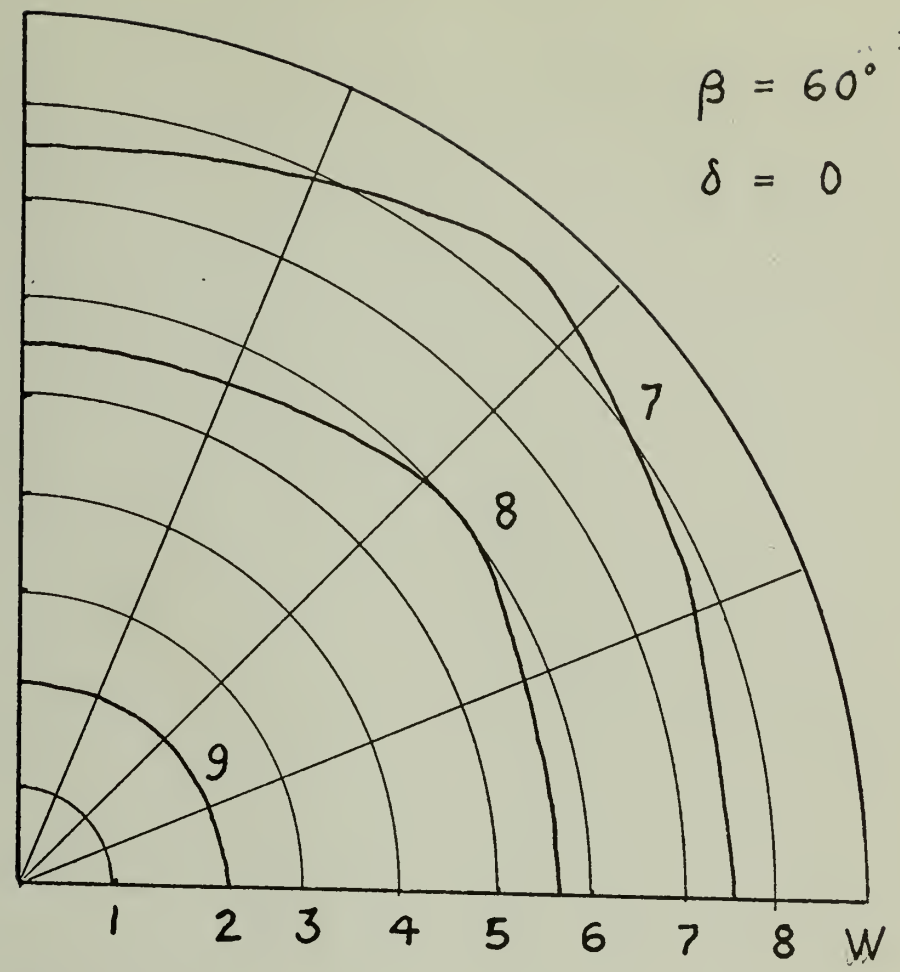

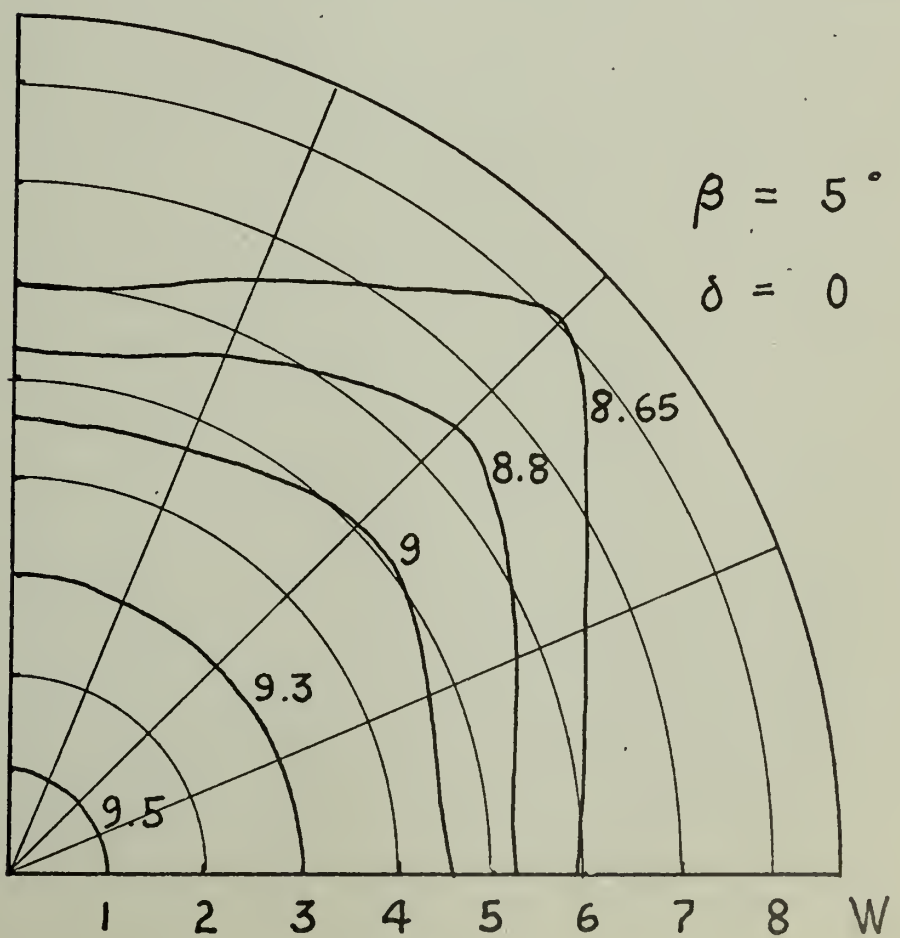

Figure I-6

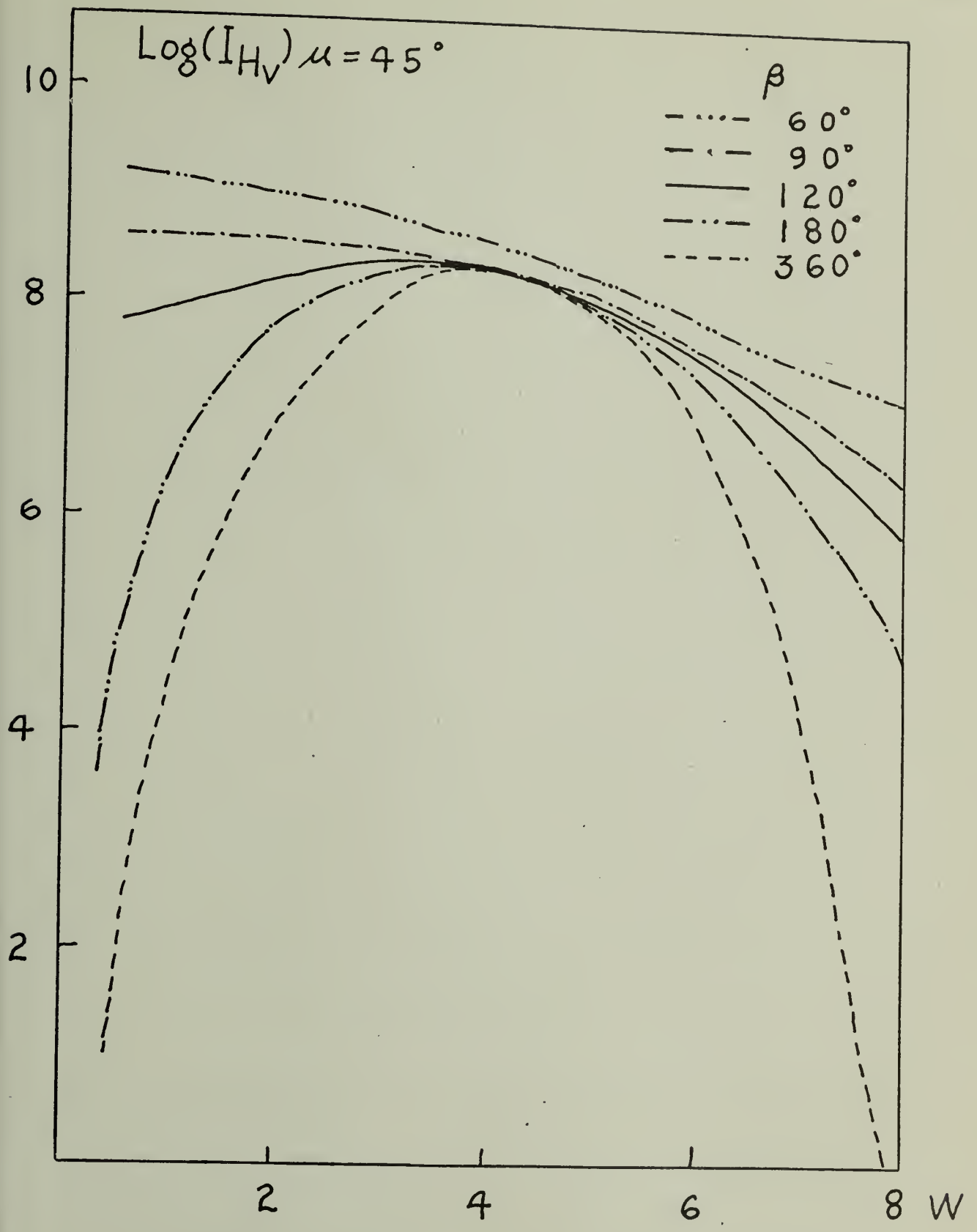

Figure I-7

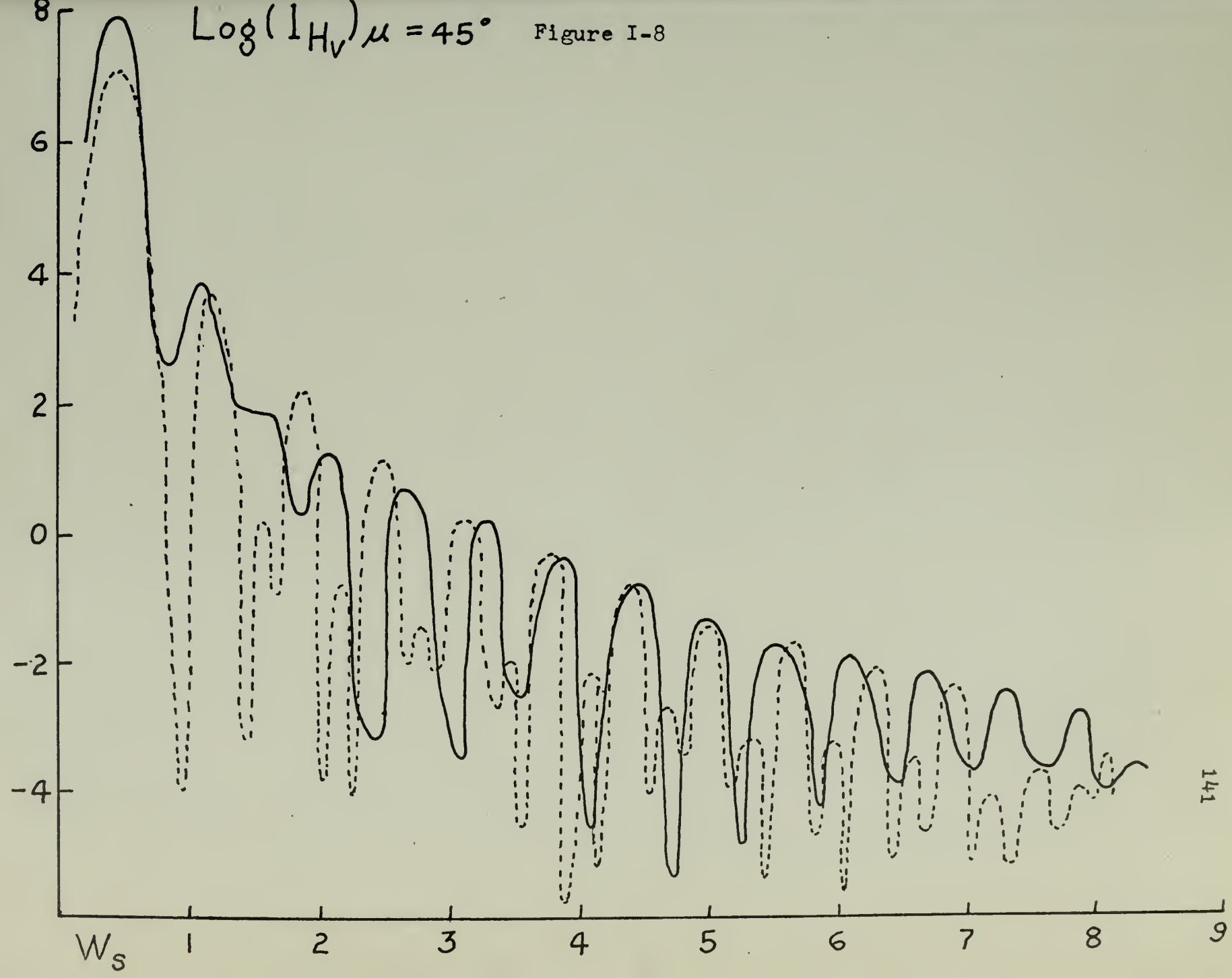

Figure I-8

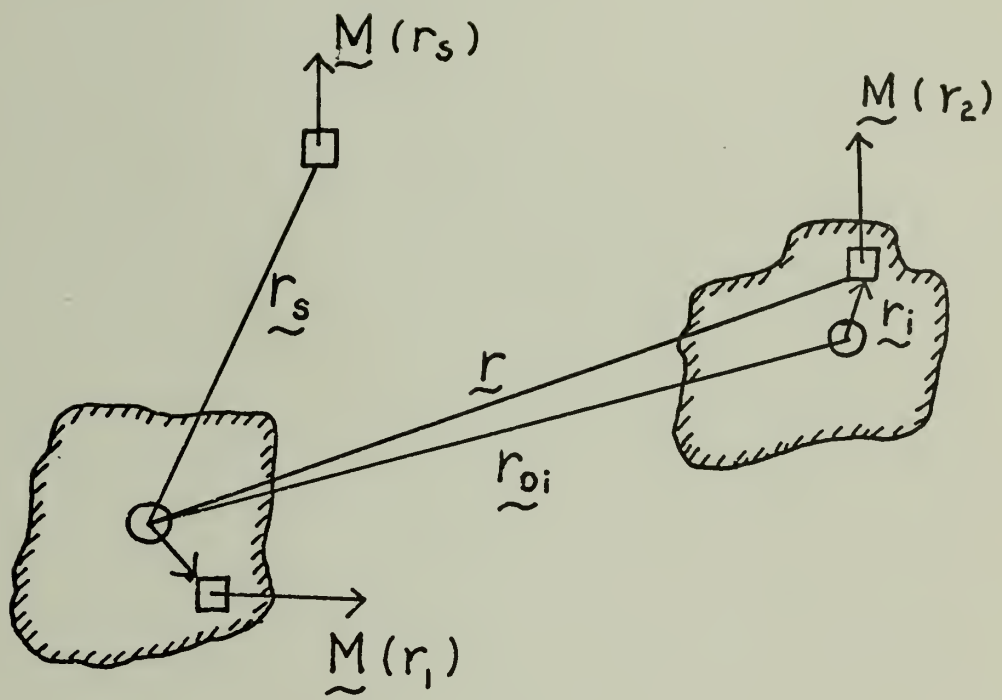

Figure II-1

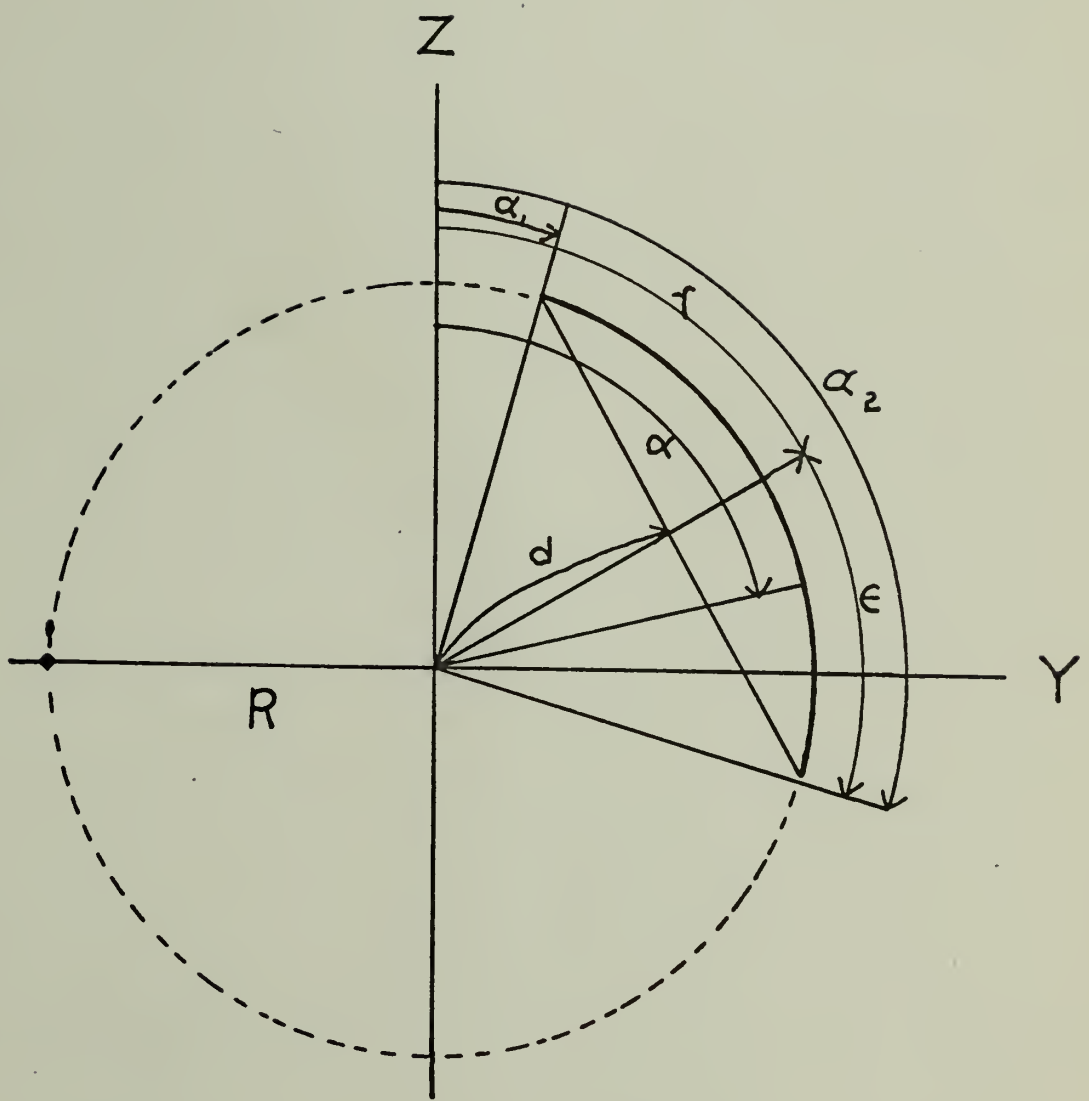

Figure II-2

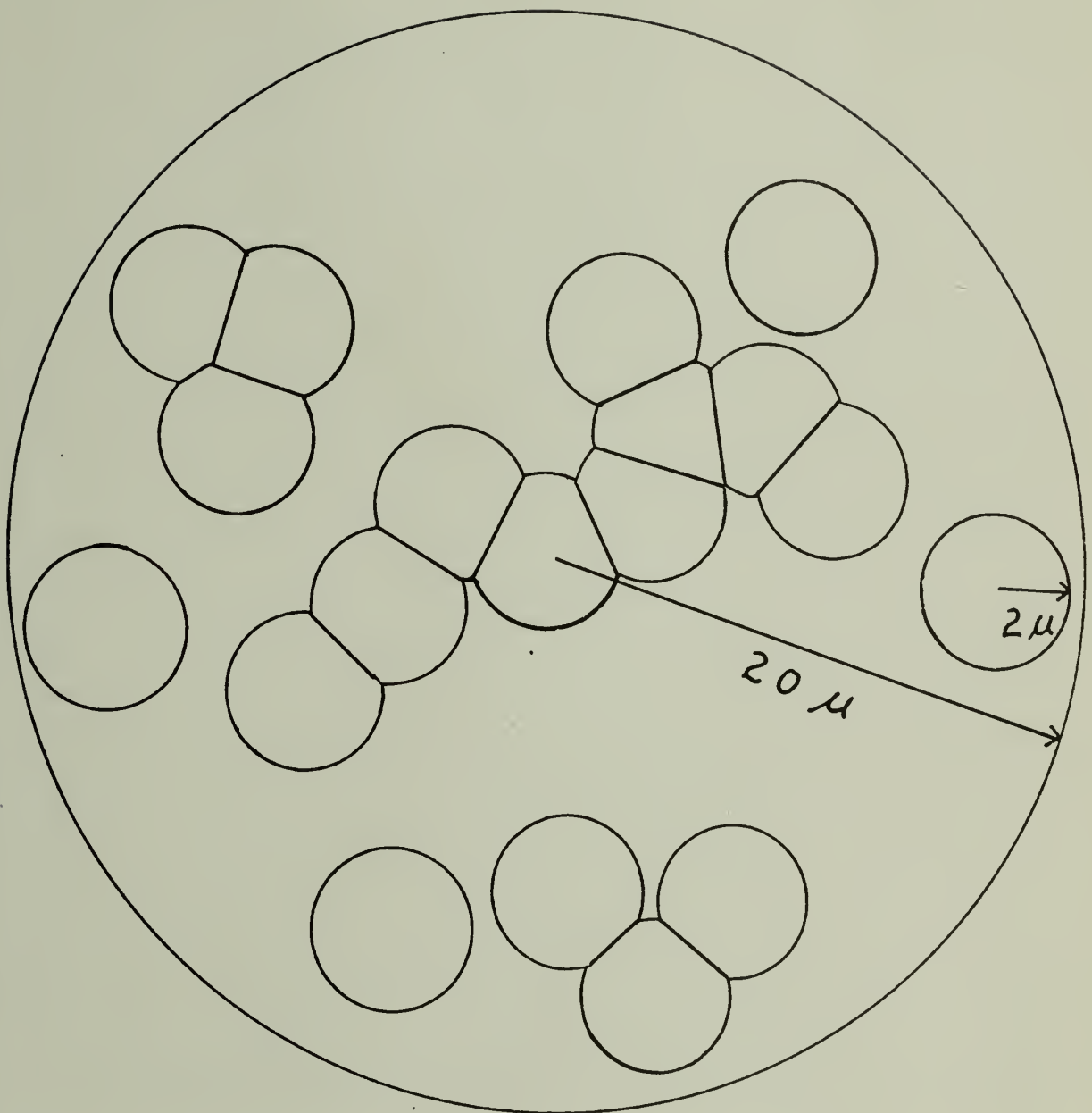

Figure II-3

Figure II-4

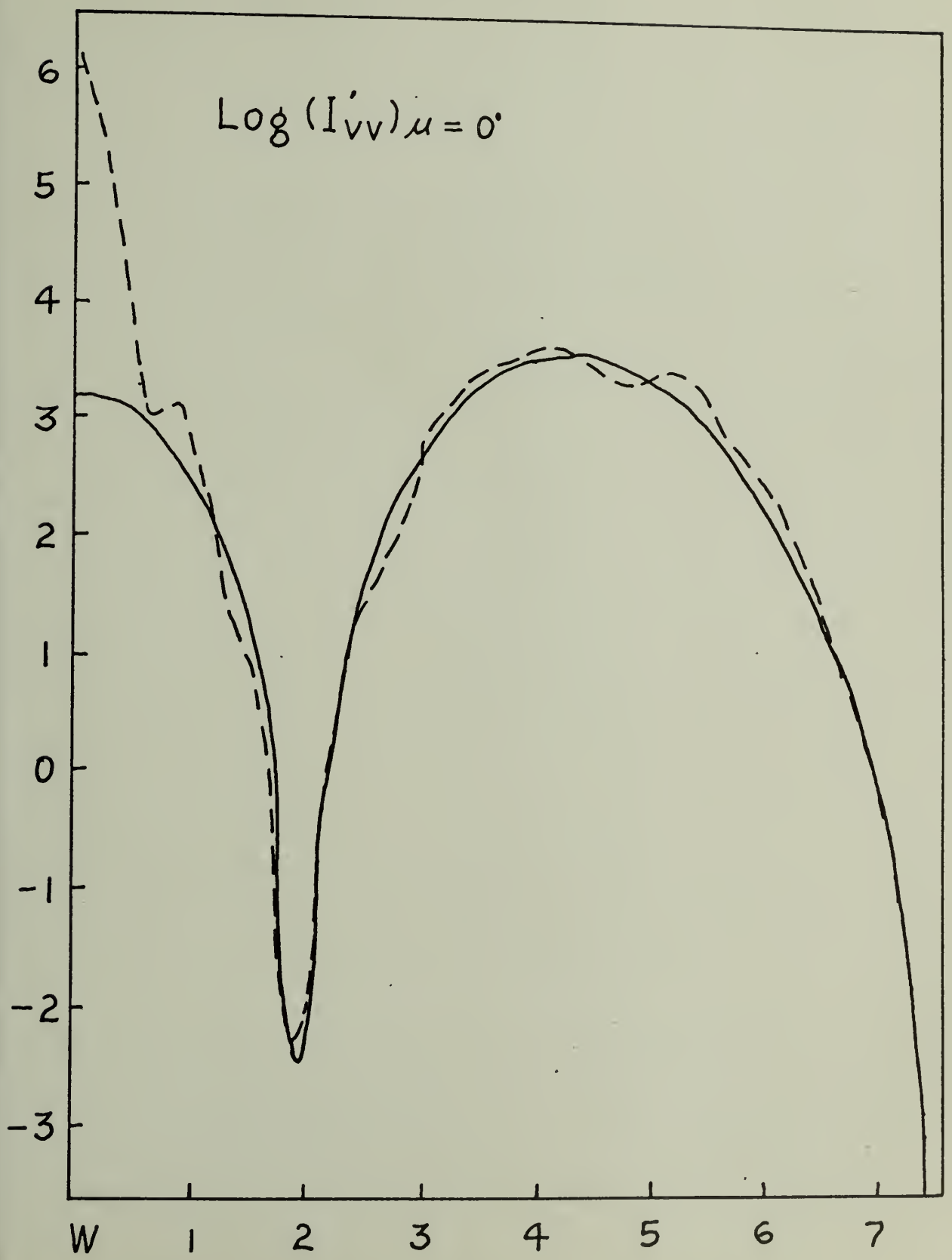

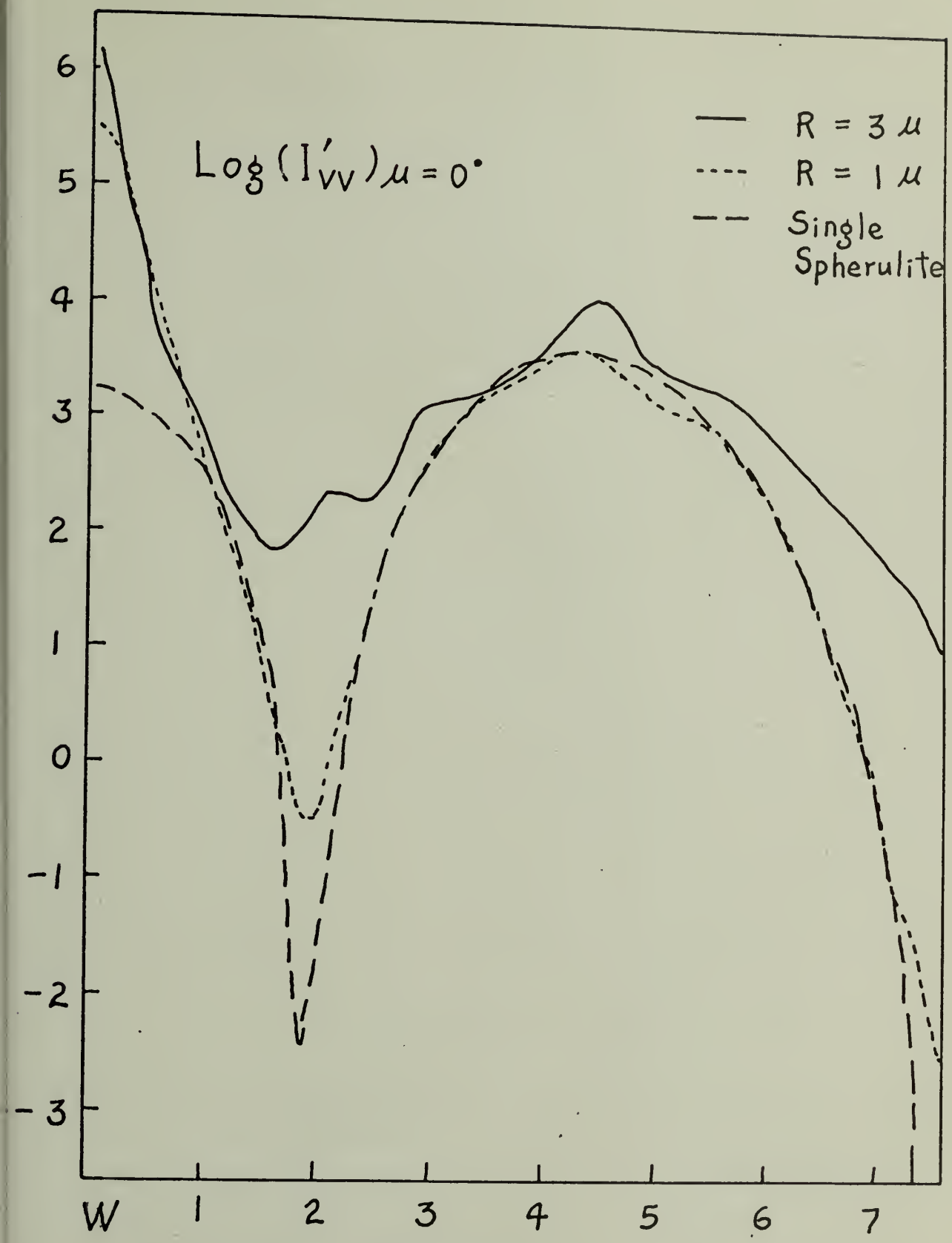
Log $(I'_{VV})_{\mu=0^\circ}$
R = 3 μ
R = 1 μ
Single Spherulite
6
5
4
3
2
1
0
-1
-2
-3
W
1
2
3
4
5
6
7

Figure II-5

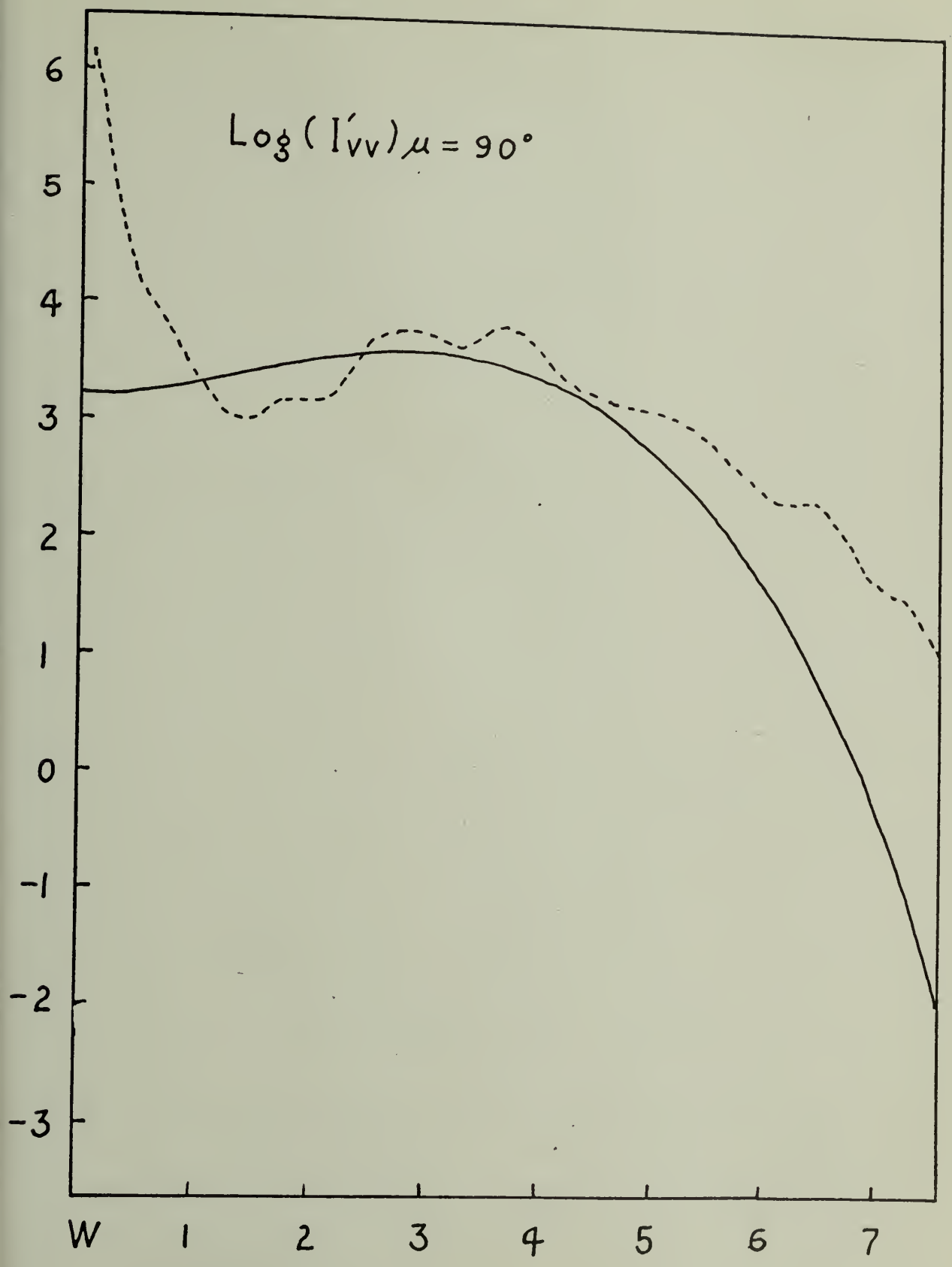

Figure II-6

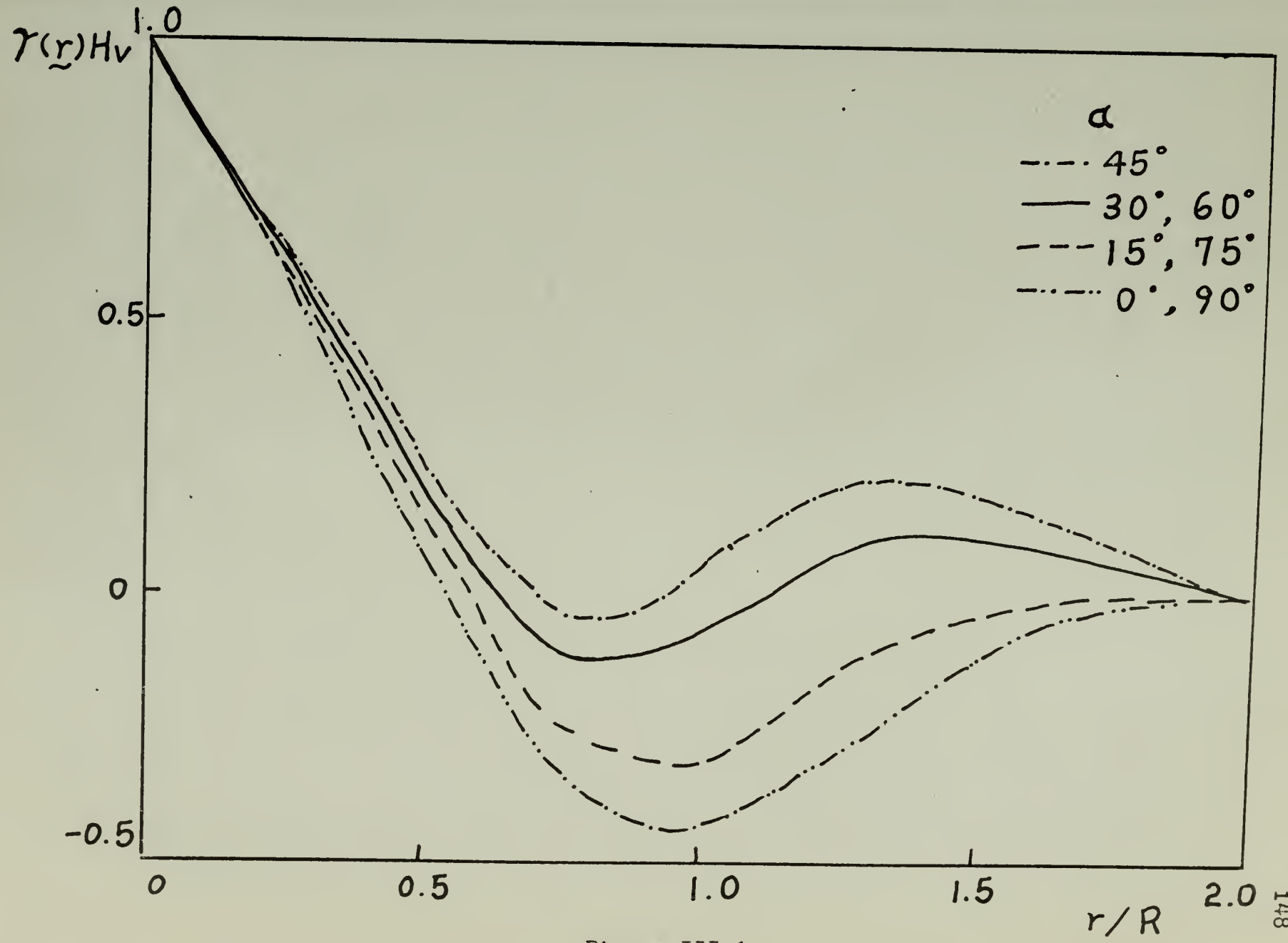

Figure III-1

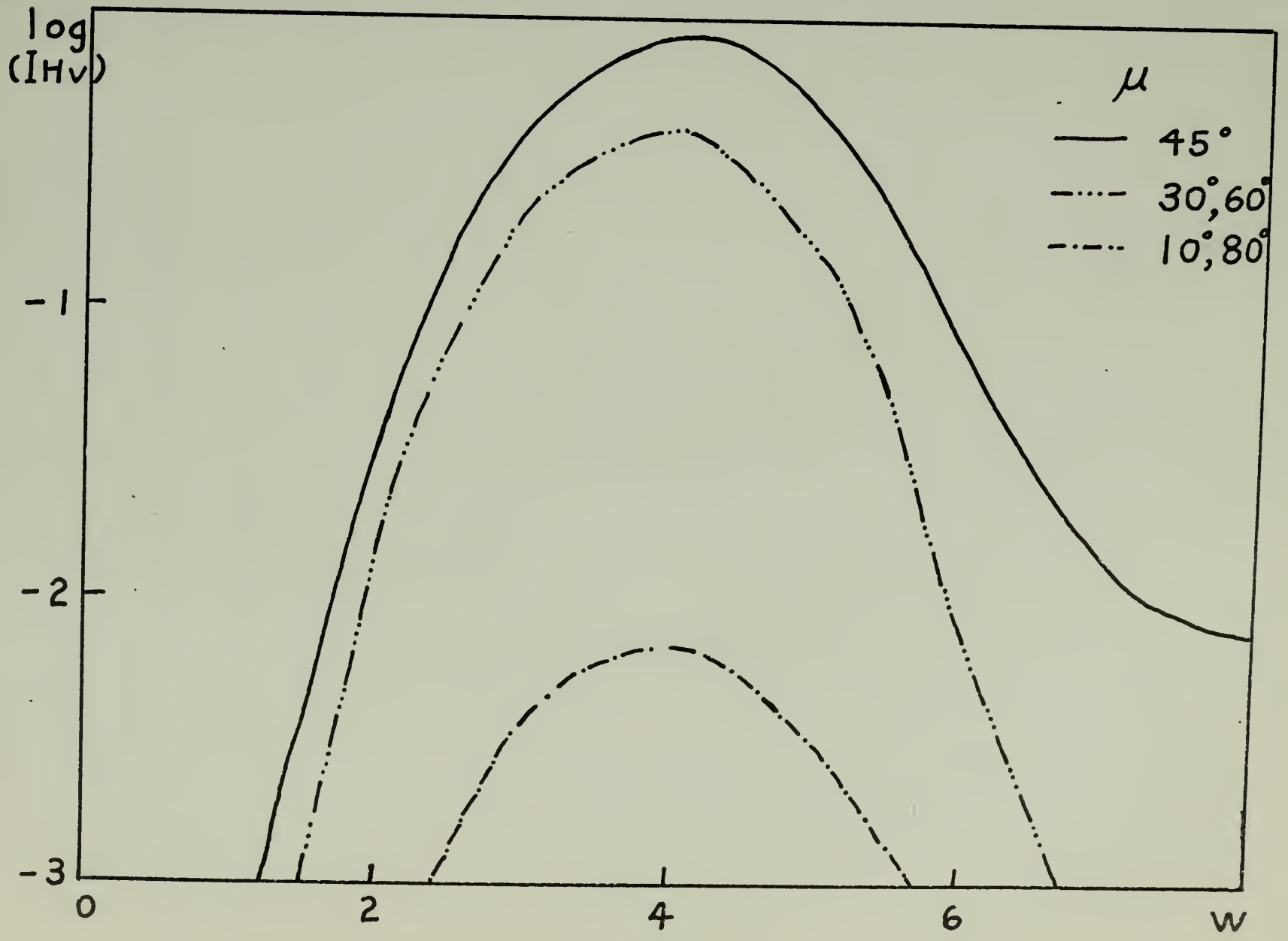

Figure III-2

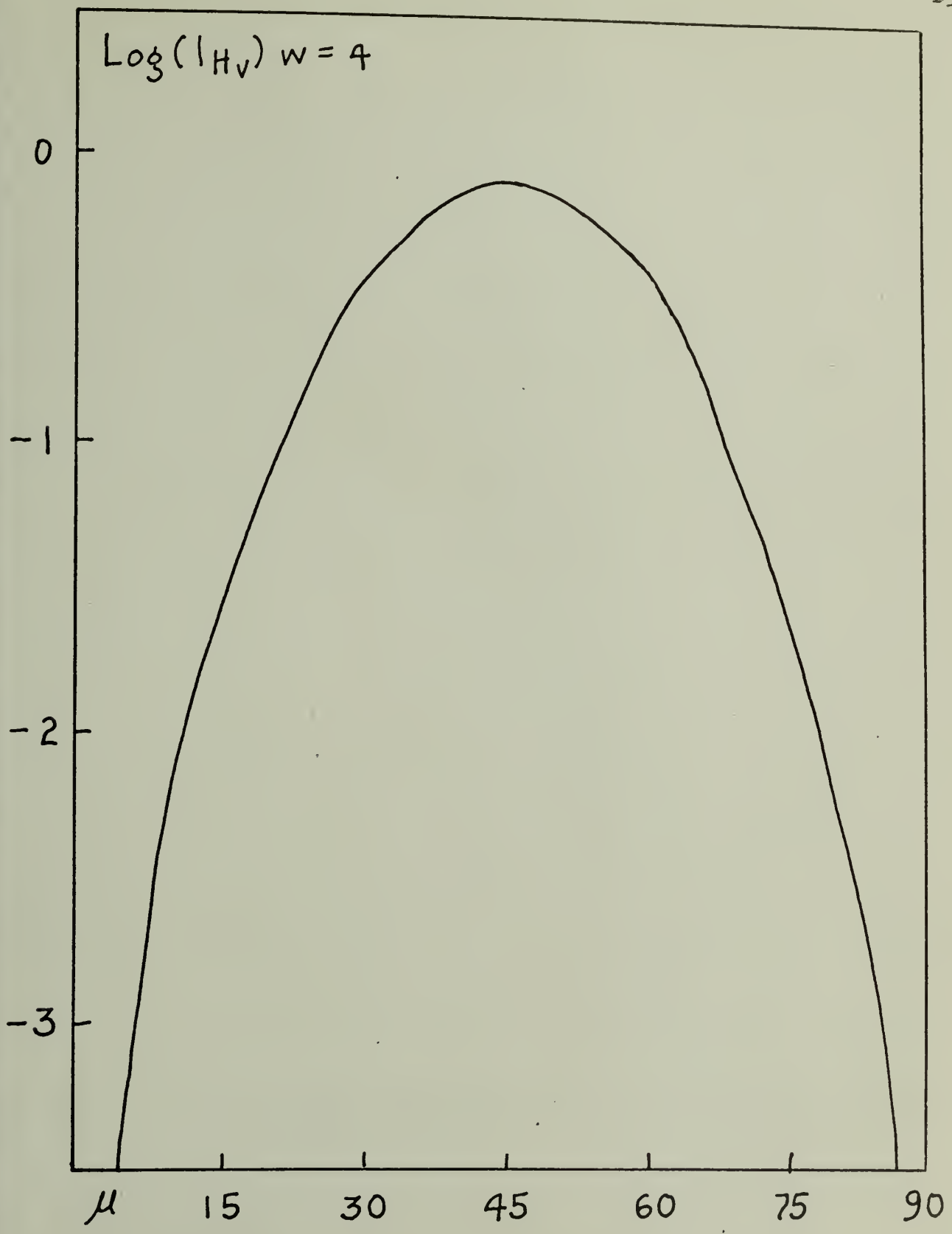

Figure III-3

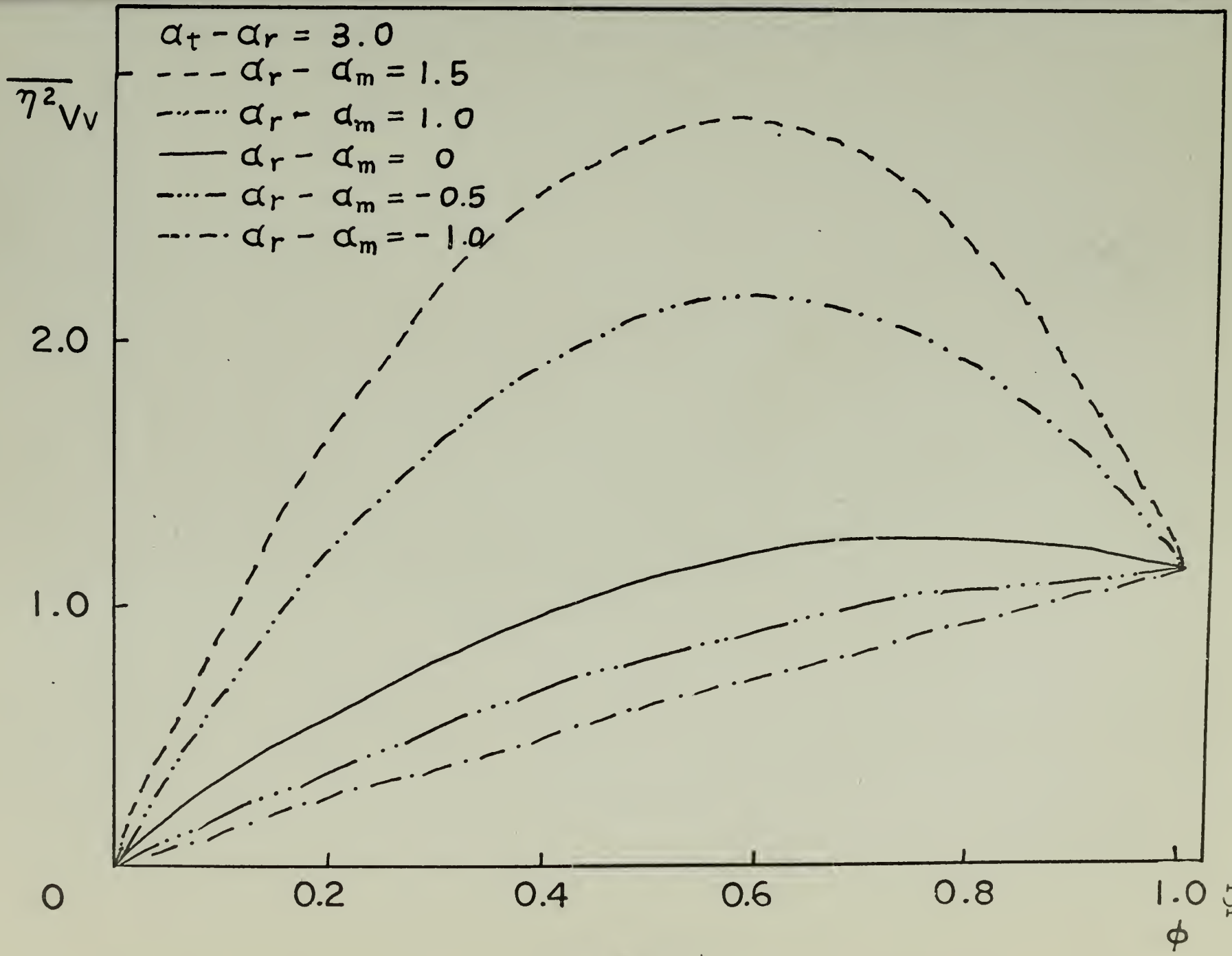
$\alpha_t - \alpha_r = 3.0$
$\alpha_r - \alpha_m = 1.5$
$\alpha_r - \alpha_m = 1.0$
$\alpha_r - \alpha_m = 0$
$\alpha_r - \alpha_m = -0.5$
$\alpha_r - \alpha_m = -1.0$
$\overline{\eta^2}_{Vv}$
2.0
1.0
0
0.2
0.4
0.6
0.8
1.0
ϕ

Figure III-4

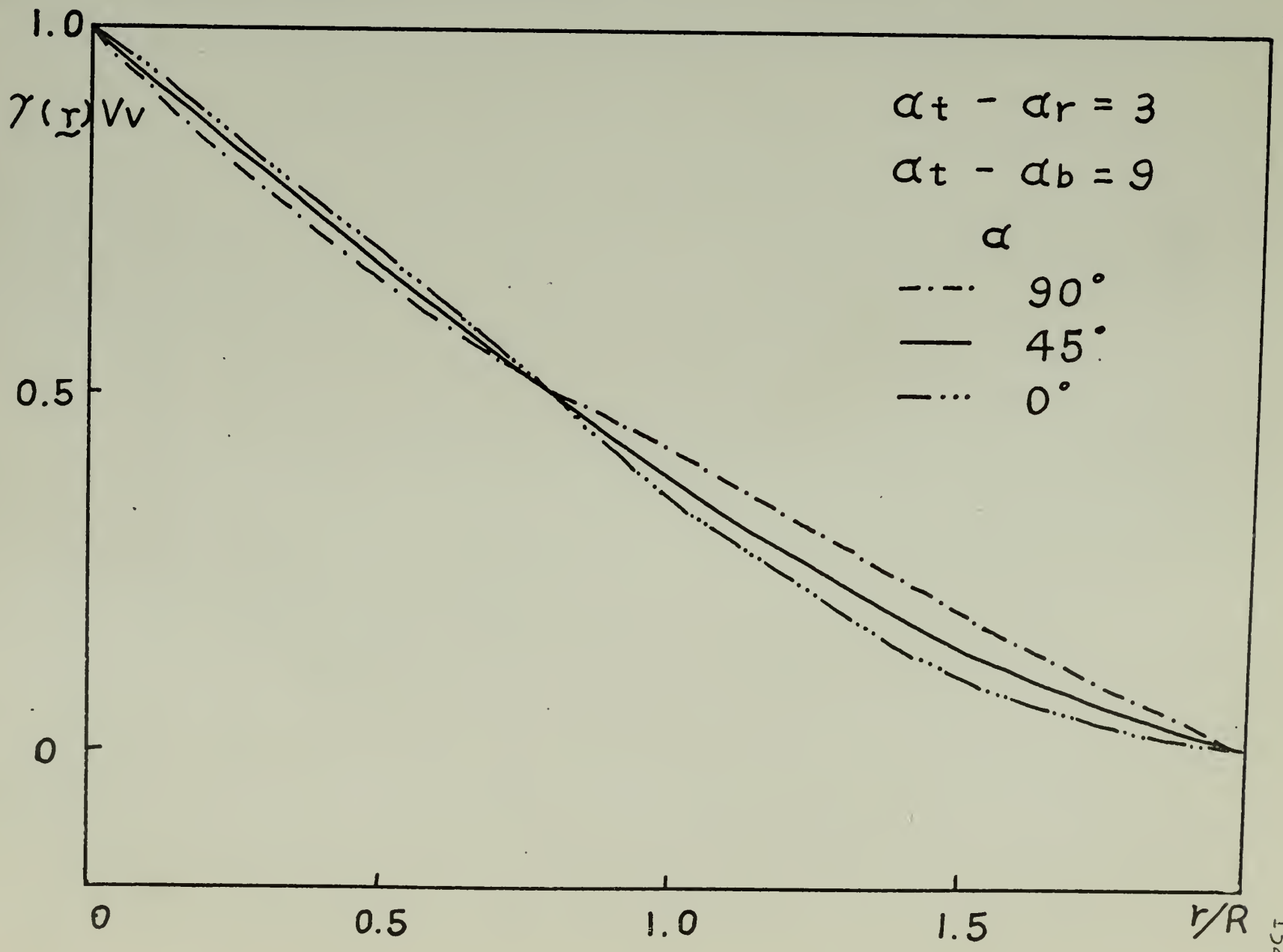
1.0
$\gamma(\underline{r})Vv$
0.5
0
0
0.5
1.0
1.5
r/R
$\alpha_t - \alpha_r = 3$
$\alpha_t - \alpha_b = 9$
α
90°
45°
0°

Figure III-5

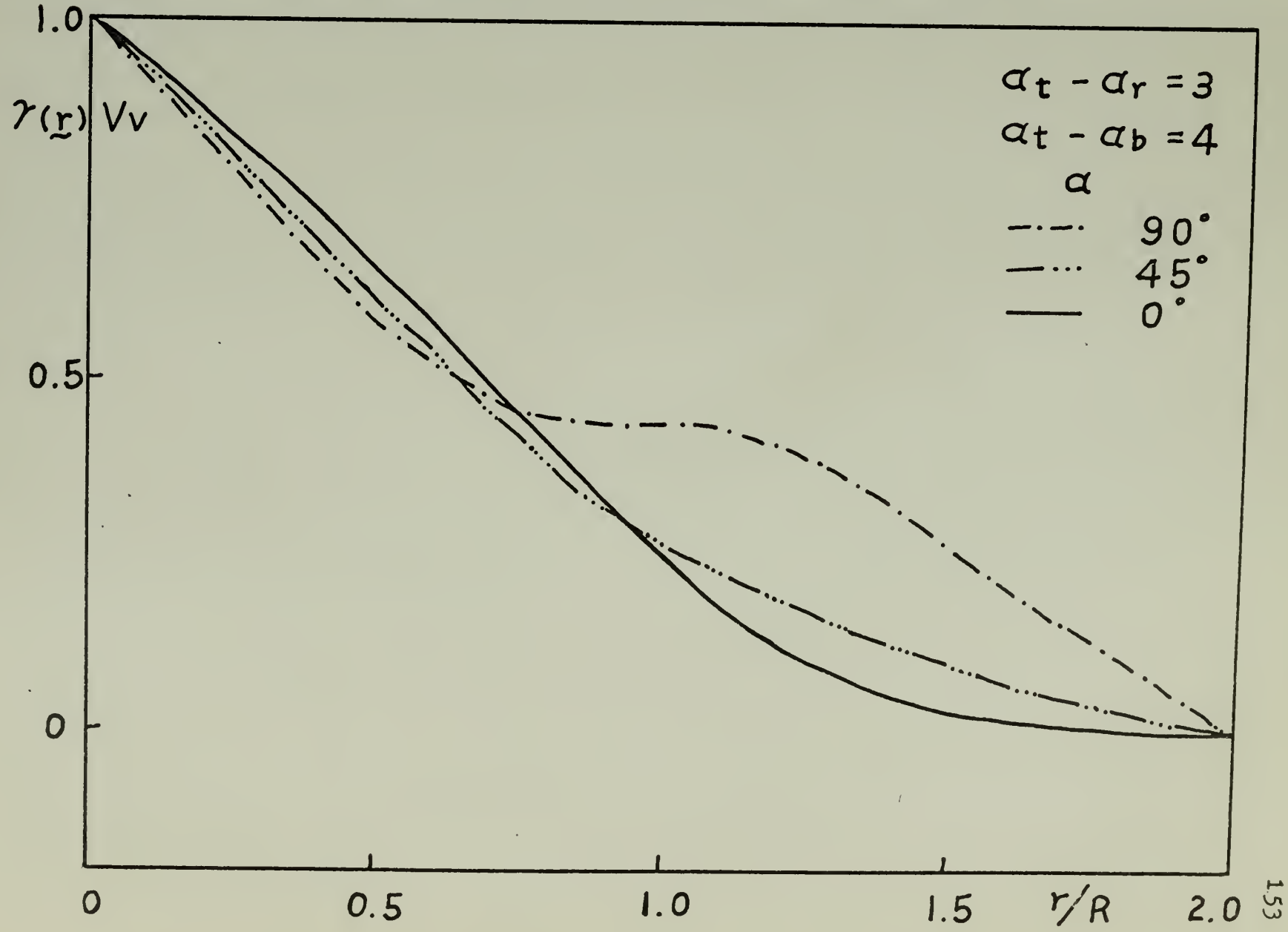
1.0
$\gamma(\underset{\sim}{r})$ Vv
0.5
0
0
0.5
1.0
1.5
r/R
2.0
$\alpha_t - \alpha_r = 3$
$\alpha_t - \alpha_b = 4$
α
90°
45°
0°

Figure III-6

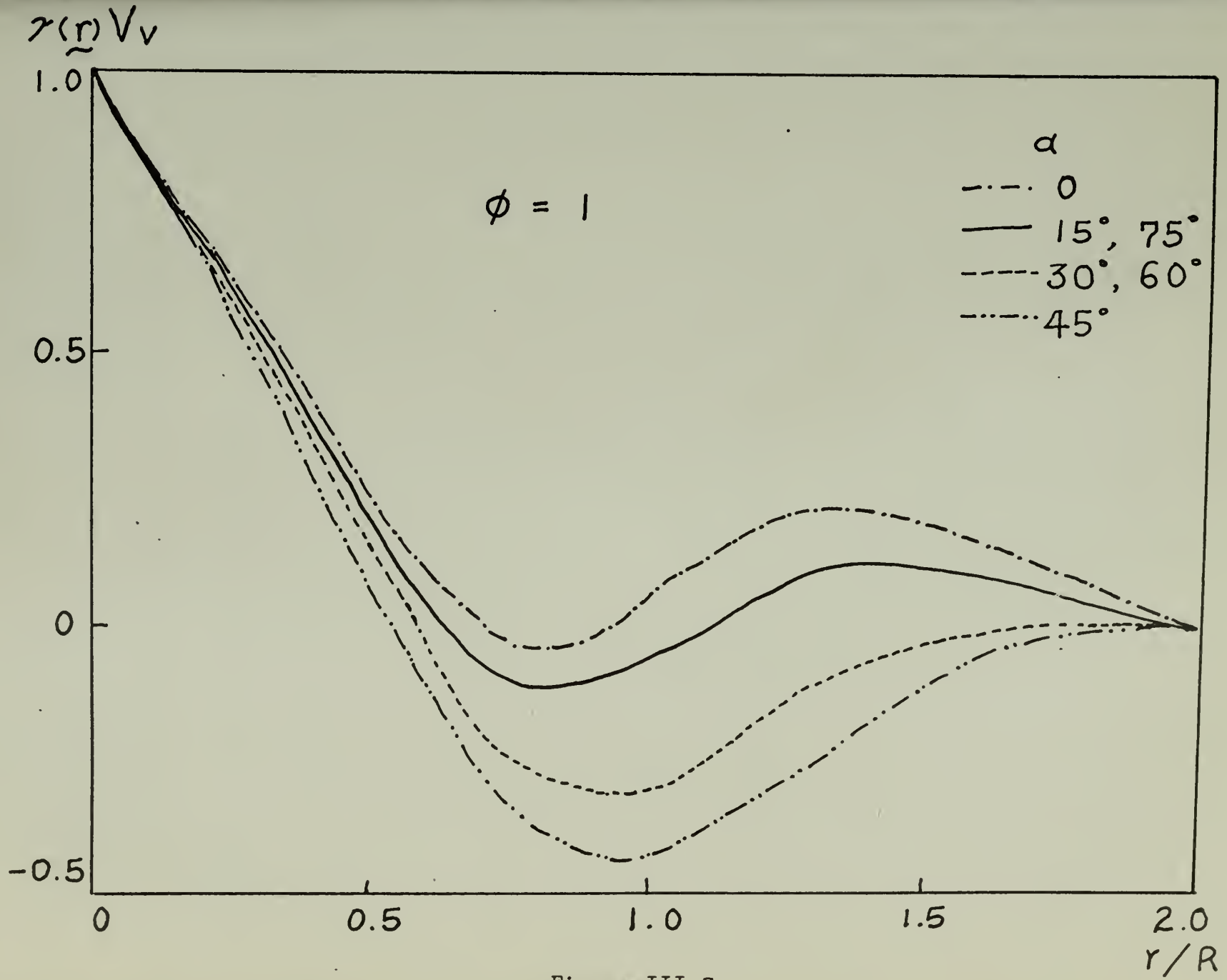

Figure III-7

Figure III-8

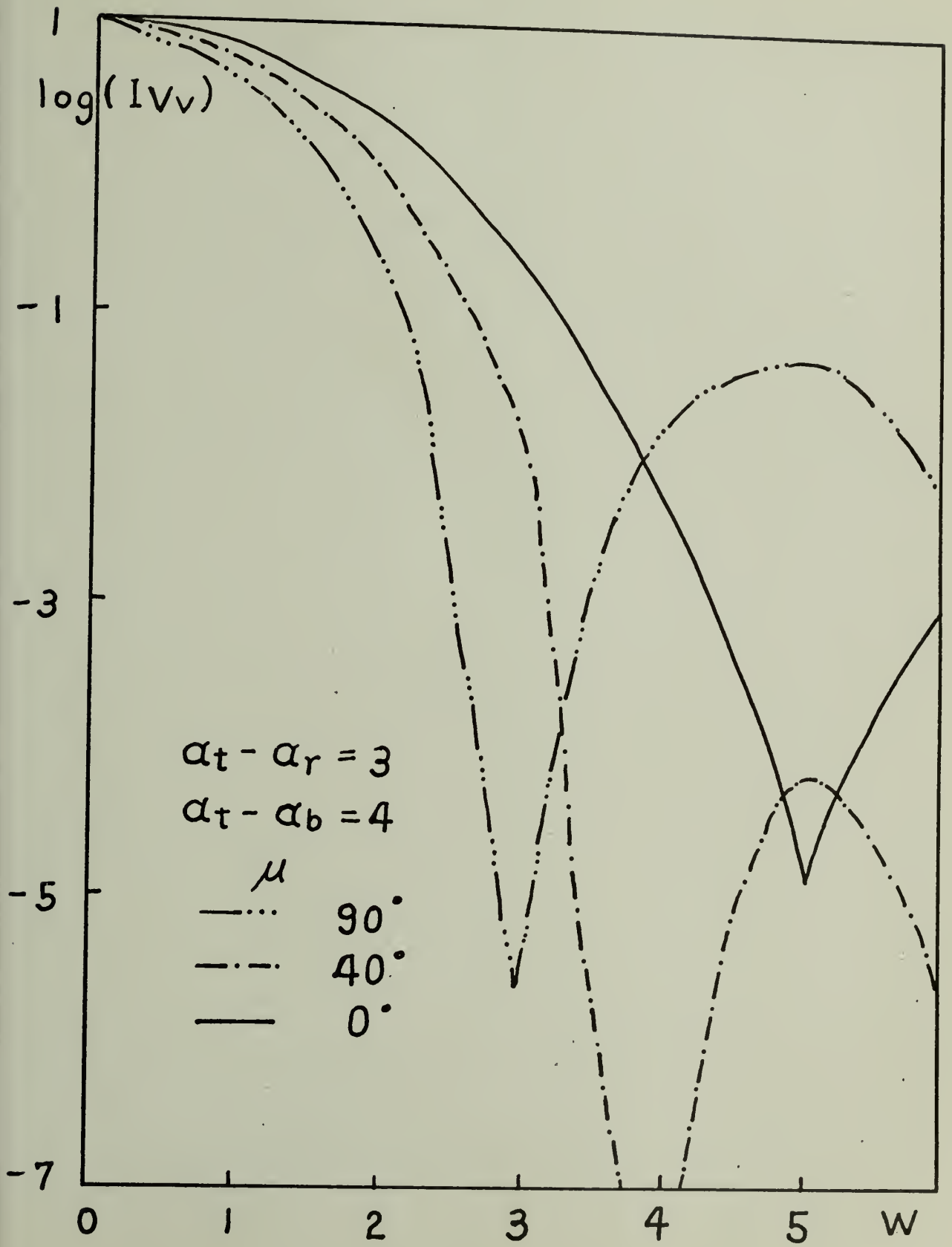

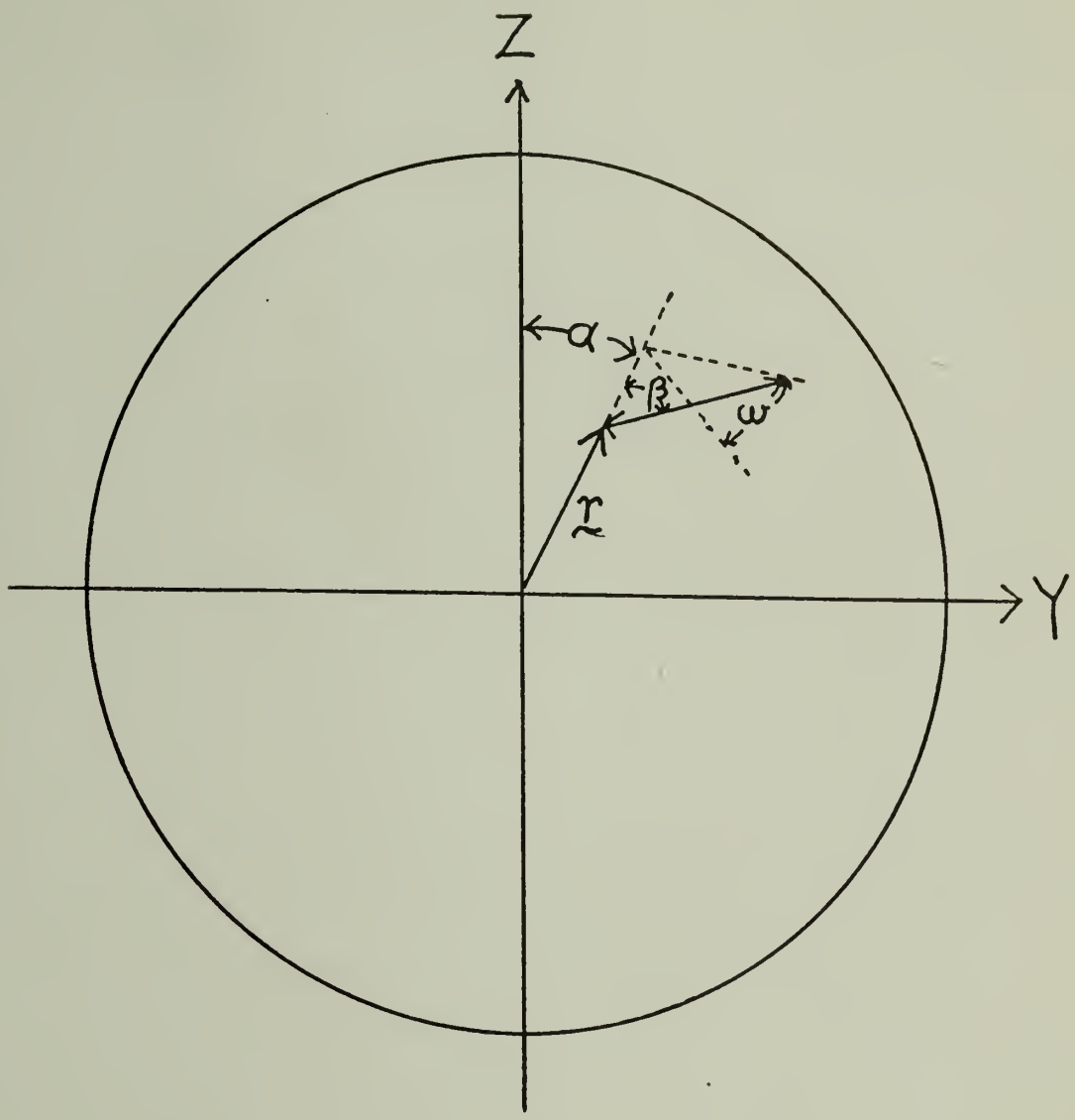

Figure IV-1

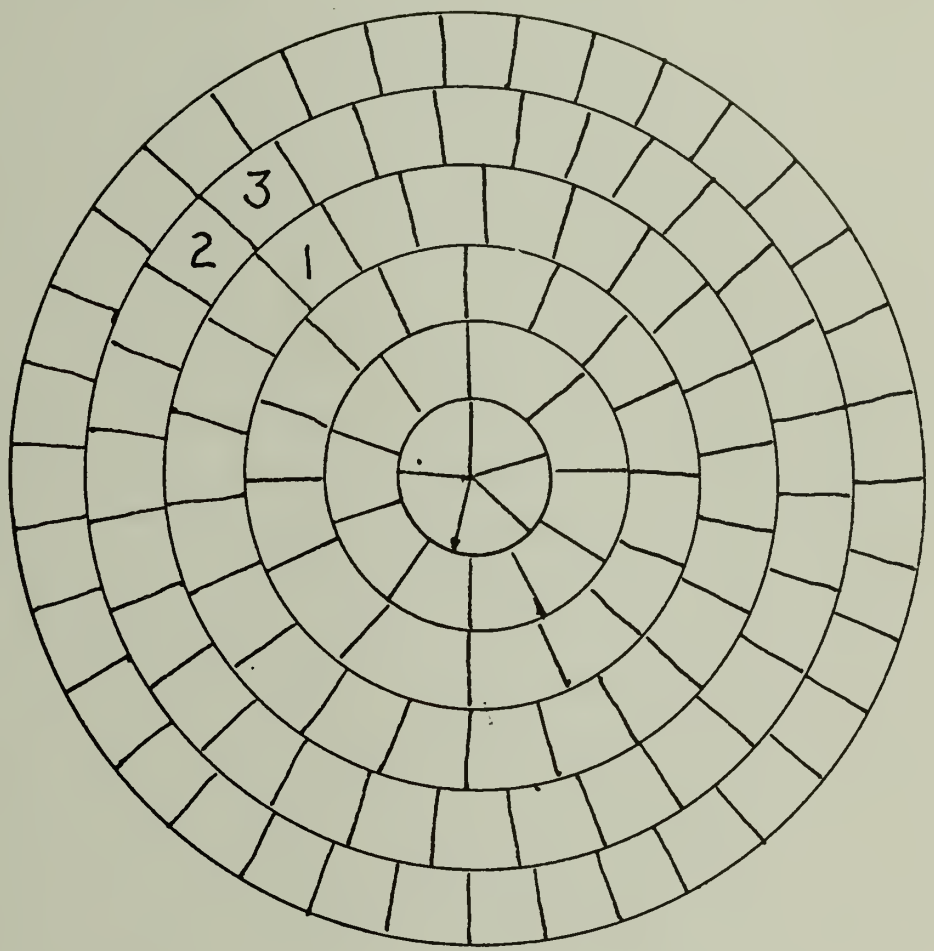

Figure IV-2

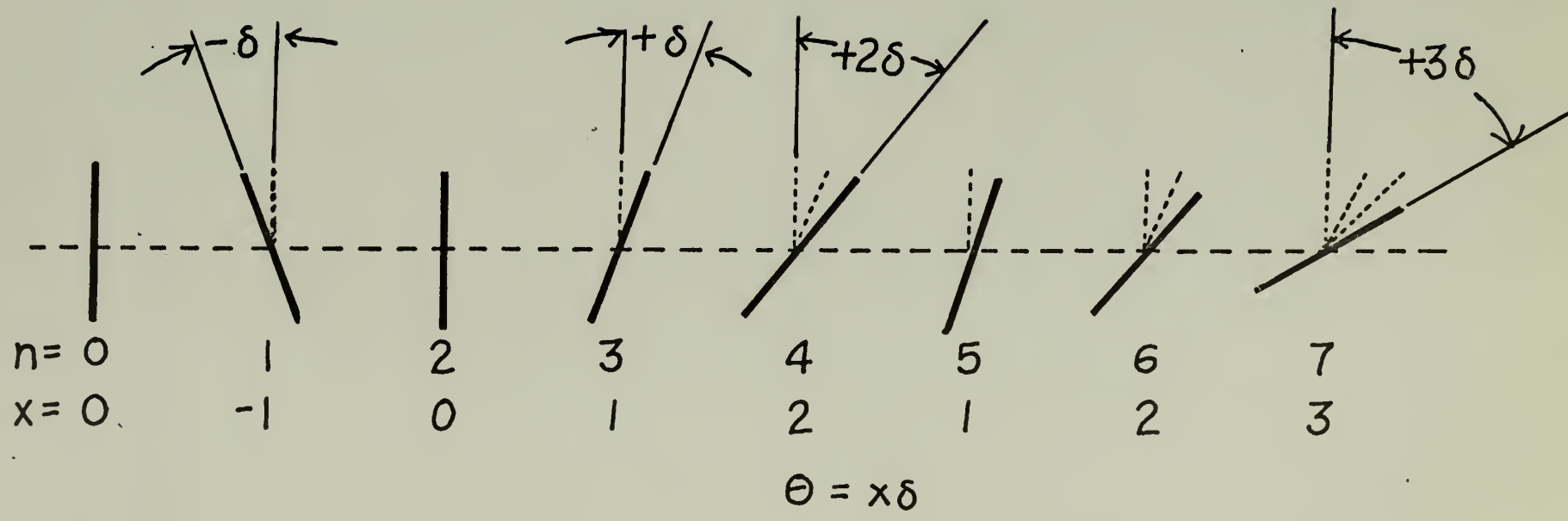

Figure IV-3

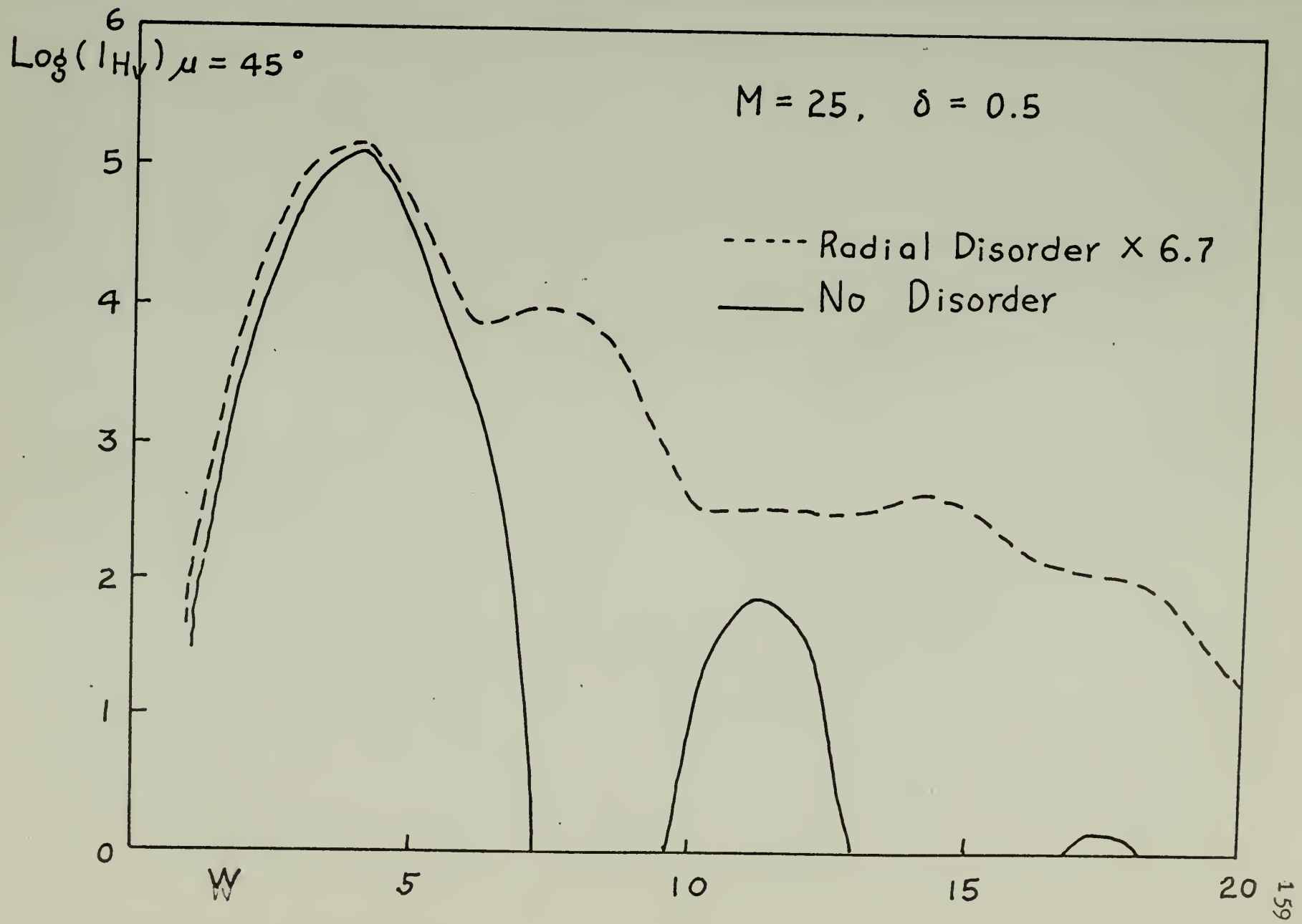
Log(I_{H_V}) $\mu = 45°$
M = 25, δ = 0.5
Radial Disorder X 6.7
No Disorder
6
5
4
3
2
1
0
W
5
10
15
20

Figure IV-4

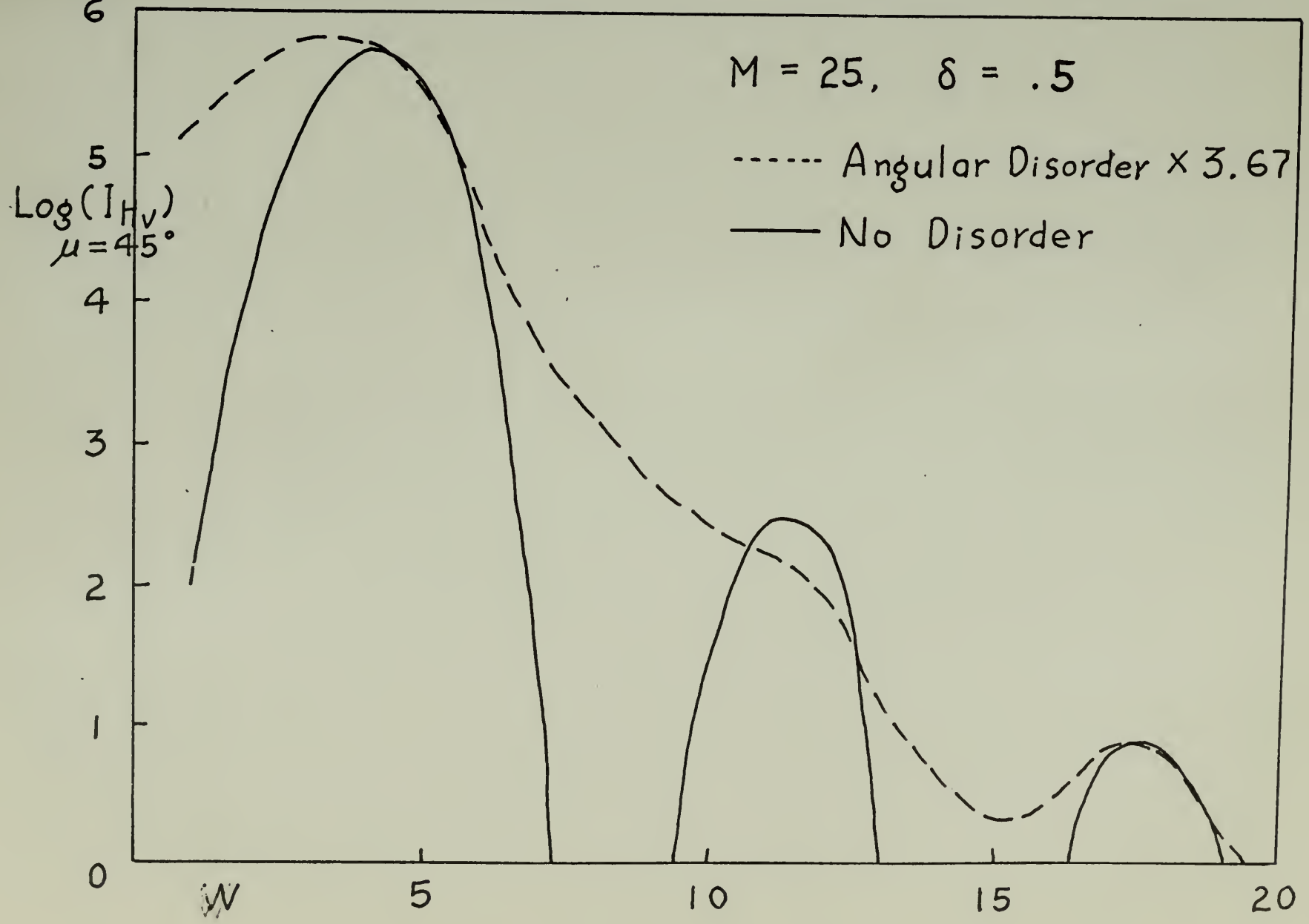
M = 25, δ = .5
----- Angular Disorder × 3.67
—— No Disorder
Log(I_HV)
μ = 45°
6
5
4
3
2
1
0
W
5
10
15
20

Figure IV-5

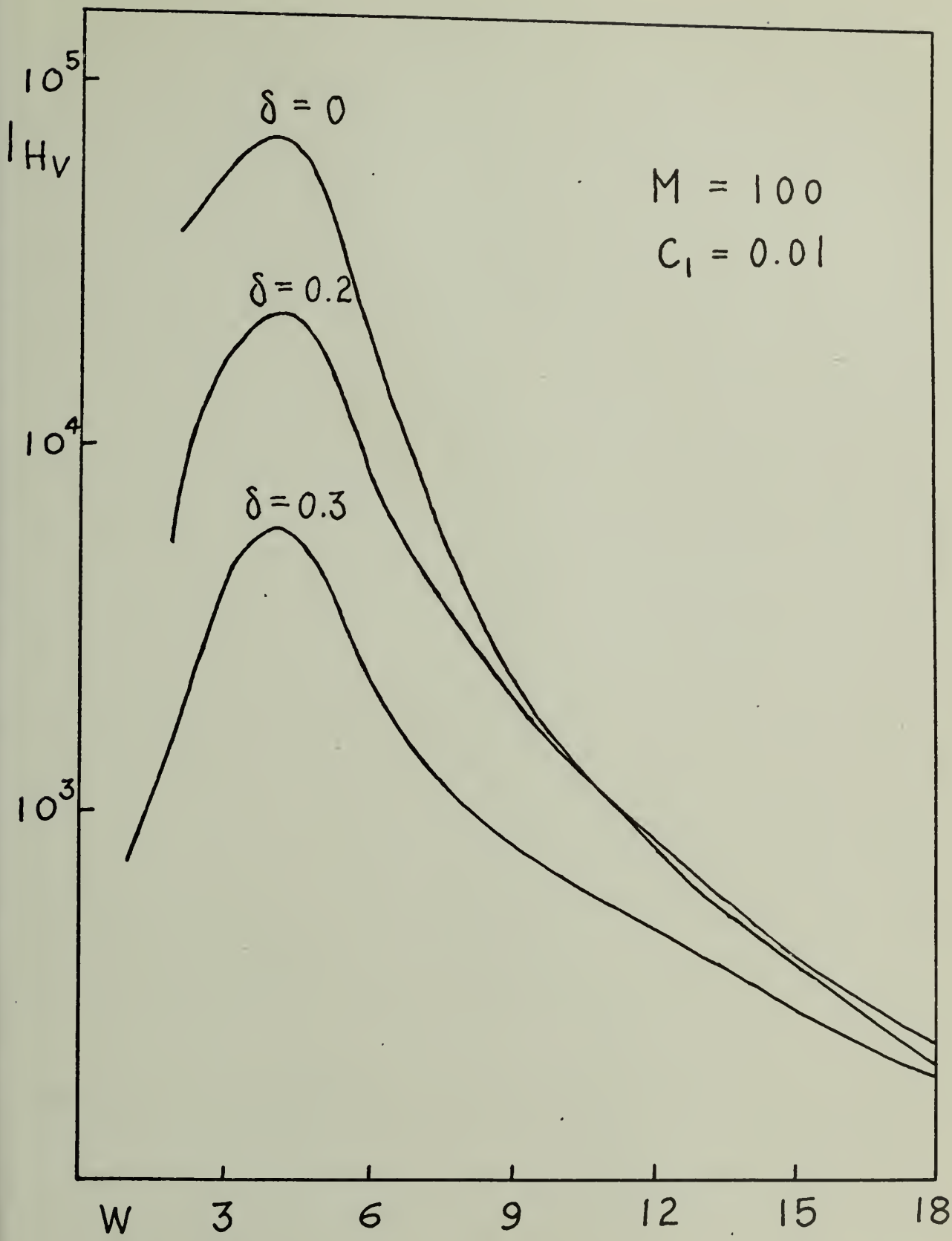
10^5
I_{Hv}
$\delta = 0$
$\delta = 0.2$
$\delta = 0.3$
M = 100
$C_1 = 0.01$
10^4
10^3
W
3
6
9
12
15
18

Figure IV-6

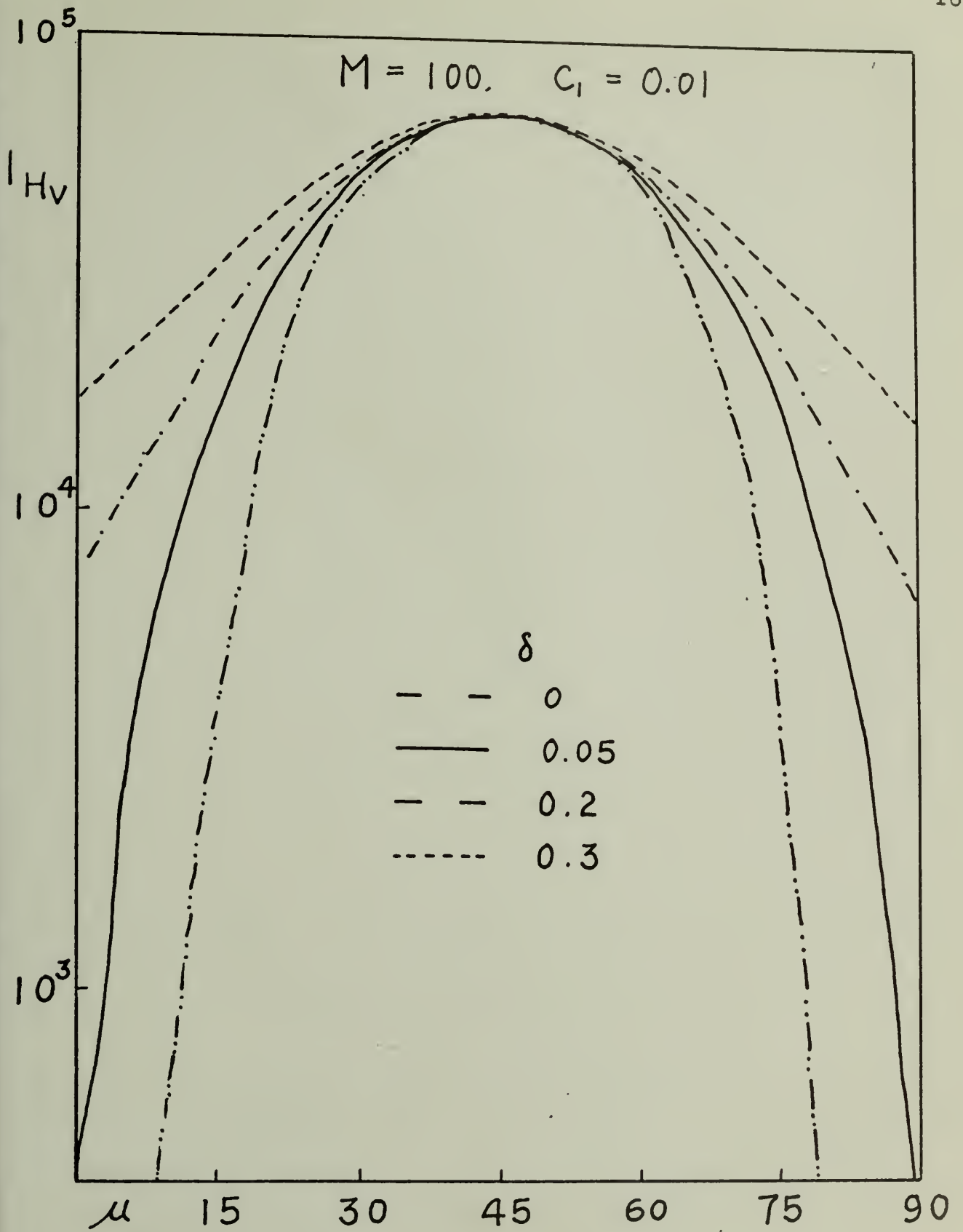

Figure IV-7

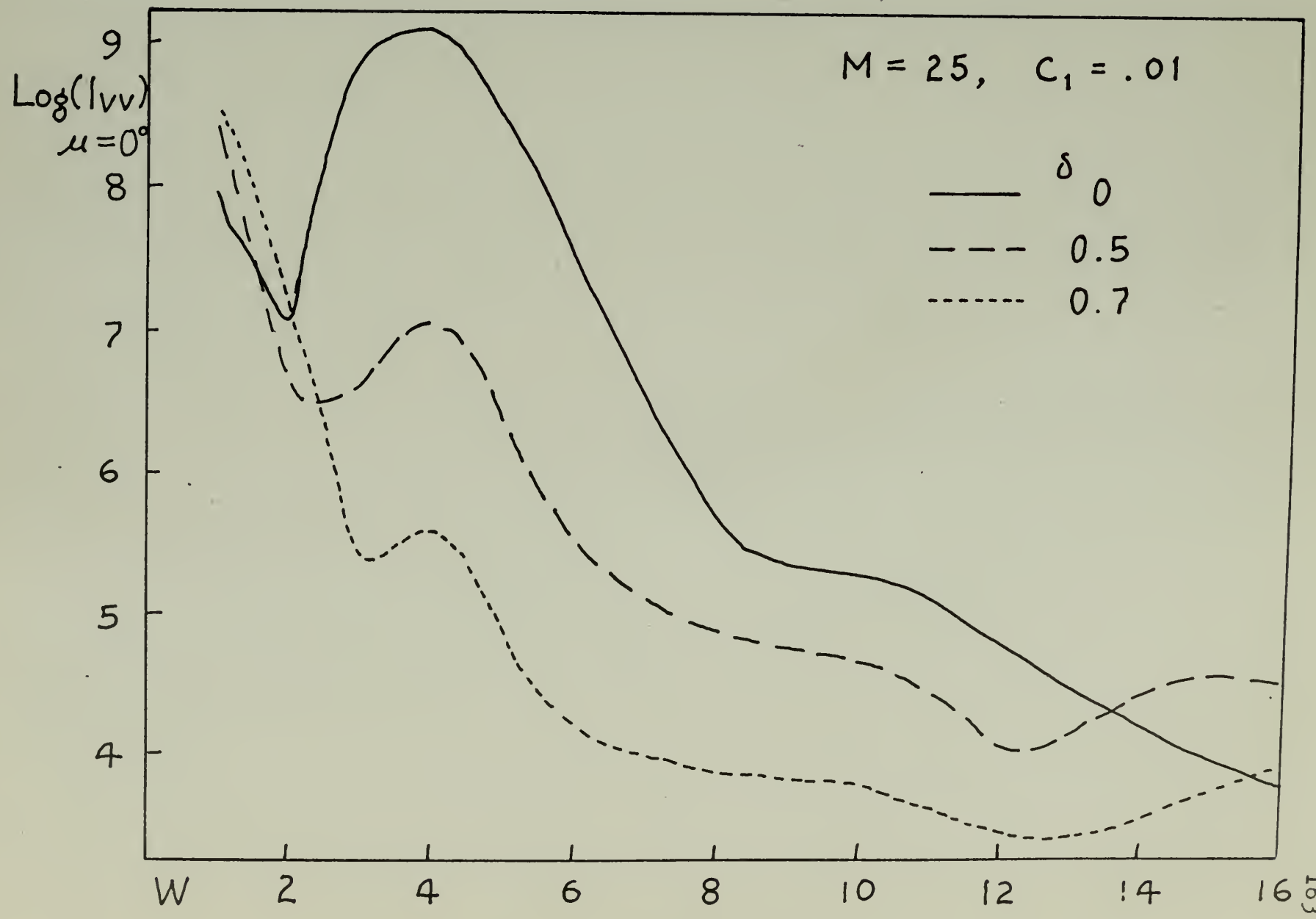

Figure IV-8

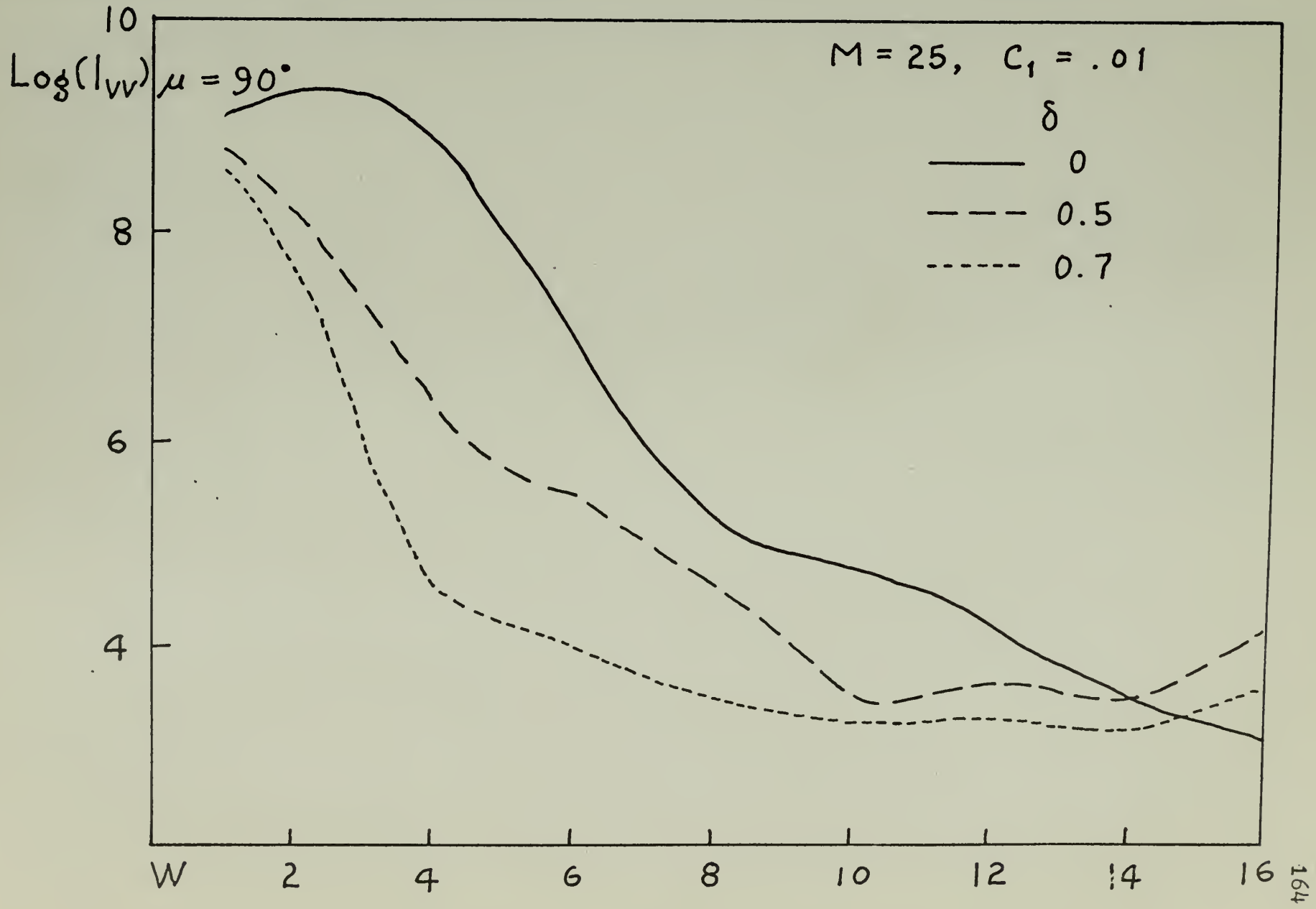

Figure IV-9

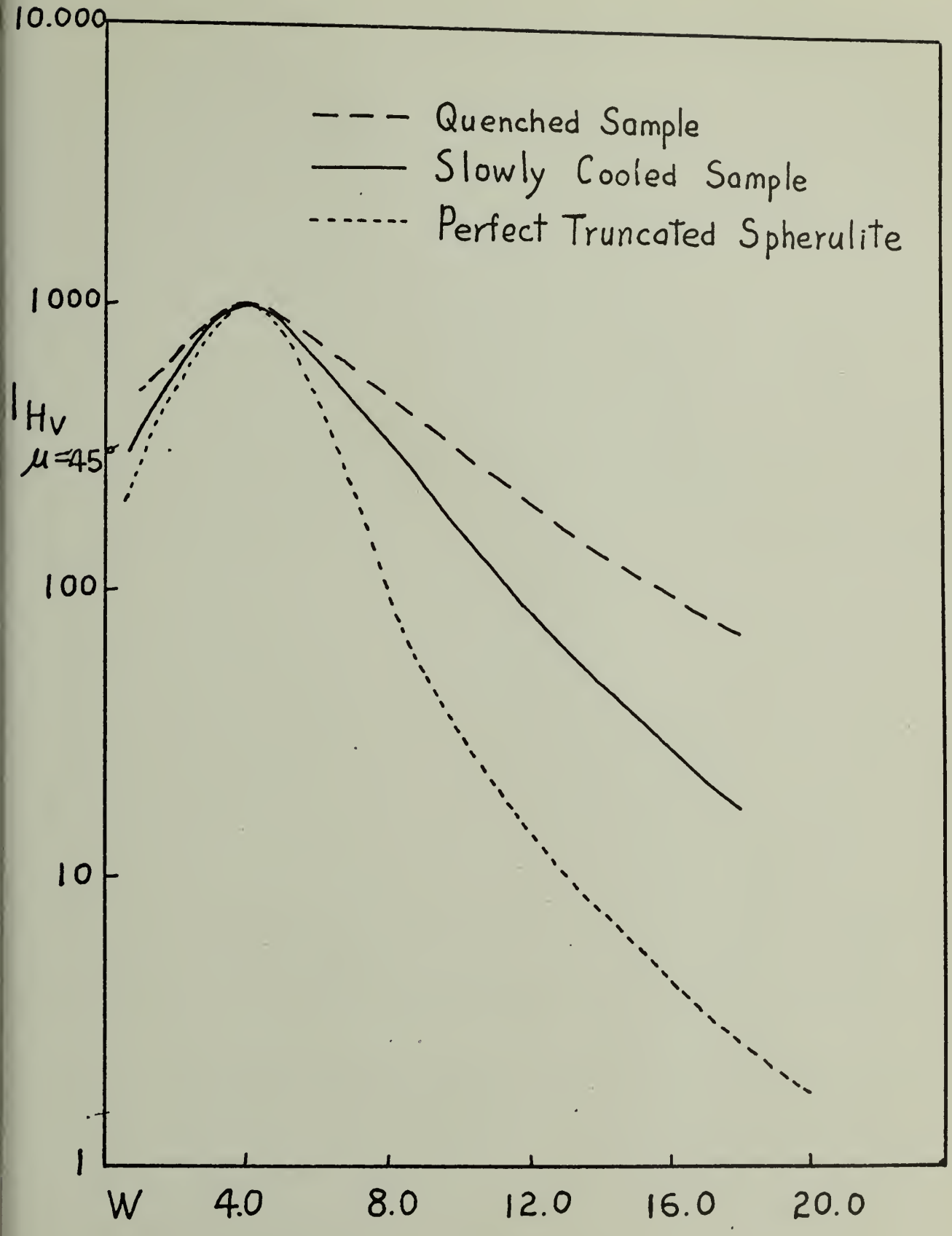
10.000
1000
100
10
1
I_{Hv}
$\mu=45°$
Quenched Sample
Slowly Cooled Sample
Perfect Truncated Spherulite
W
4.0
8.0
12.0
16.0
20.0

Figure IV-10

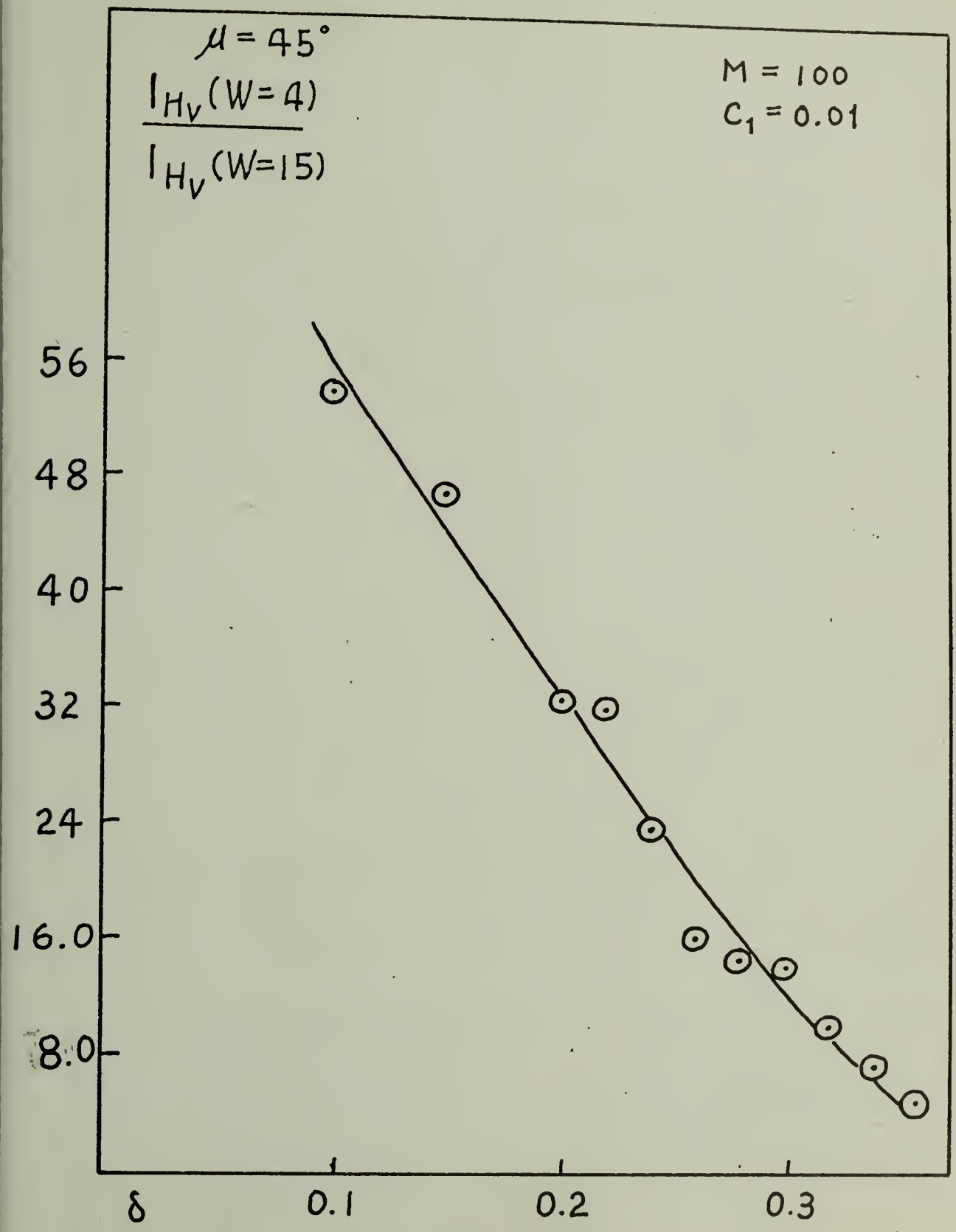

Figure IV-11

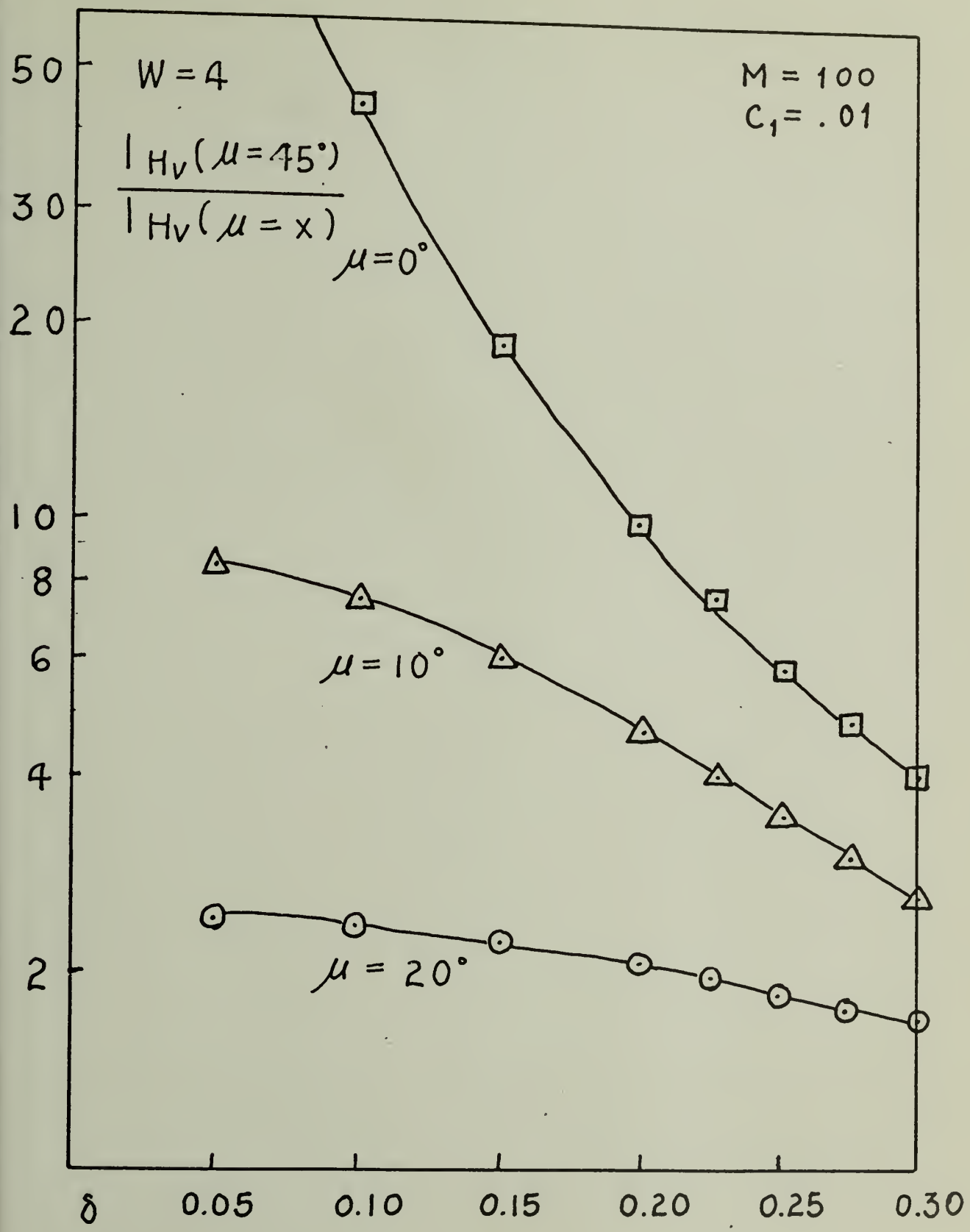
W = 4
M = 100
C_1 = .01
$\frac{I_{Hv}(\mu=45°)}{I_{Hv}(\mu=x)}$
μ = 0°
μ = 10°
μ = 20°
50
30
20
10
8
6
4
2
δ
0.05
0.10
0.15
0.20
0.25
0.30

Figure IV-12

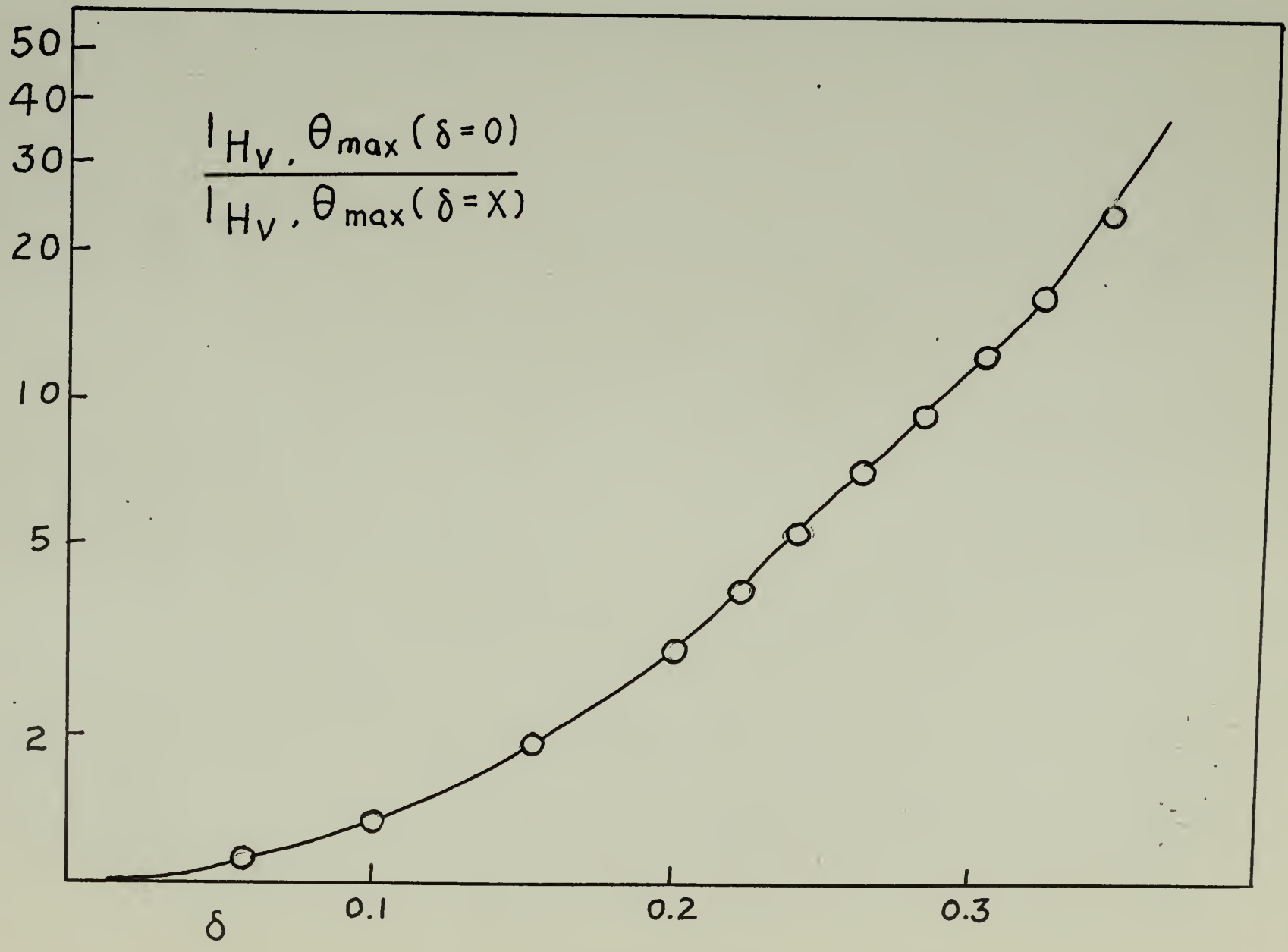
50
40
30
20
10
5
2
$\frac{I_{H_V,\theta_{max}(\delta=0)}}{I_{H_V,\theta_{max}(\delta=X)}}$
δ
0.1
0.2
0.3

Figure IV-13

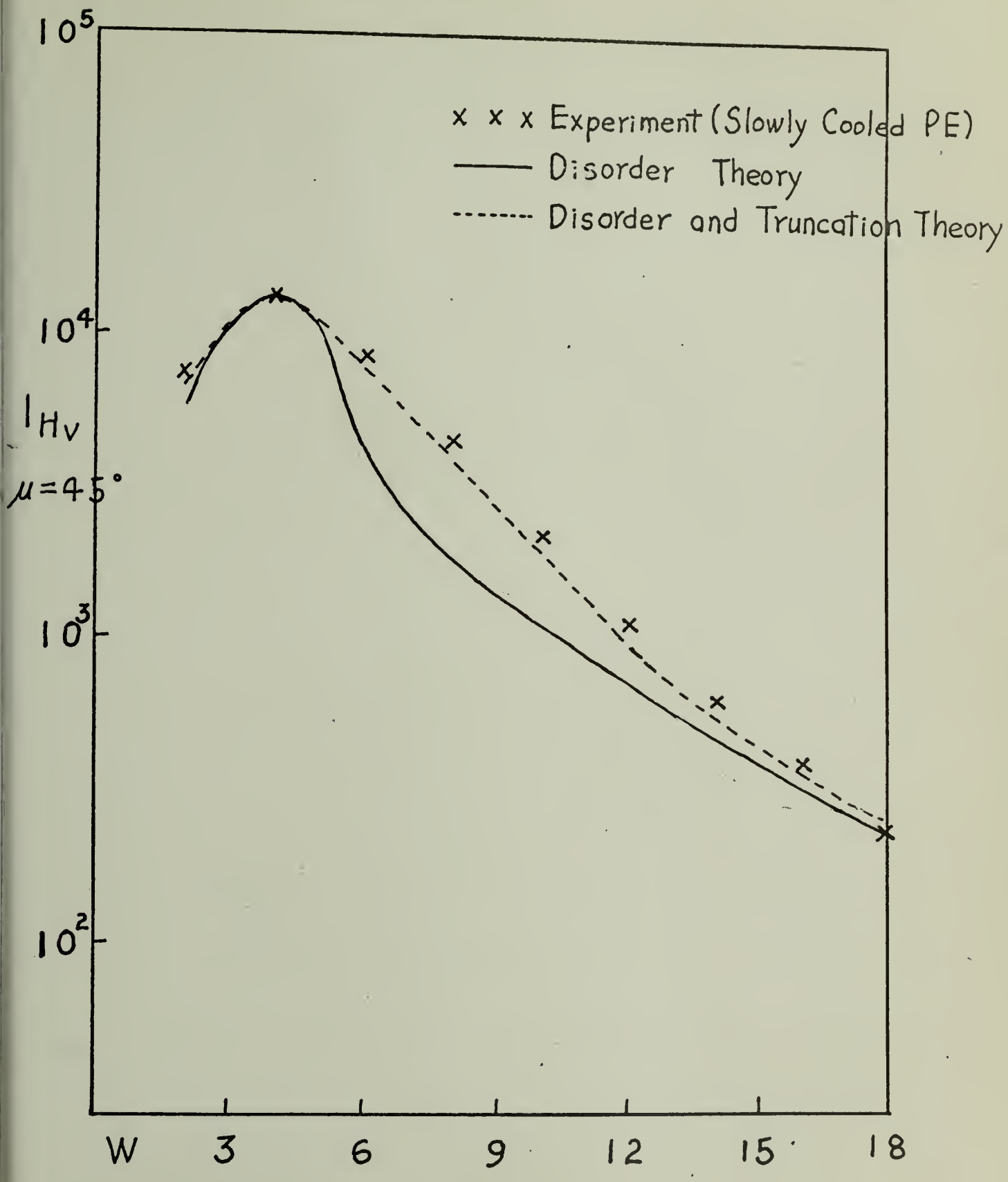
10^5
10^4
10^3
10^2
I_{Hv}
$\mu = 45°$
x x x Experiment (Slowly Cooled PE)
Disorder Theory
Disorder and Truncation Theory
W
3
6
9
12
15
18

Figure IV-14

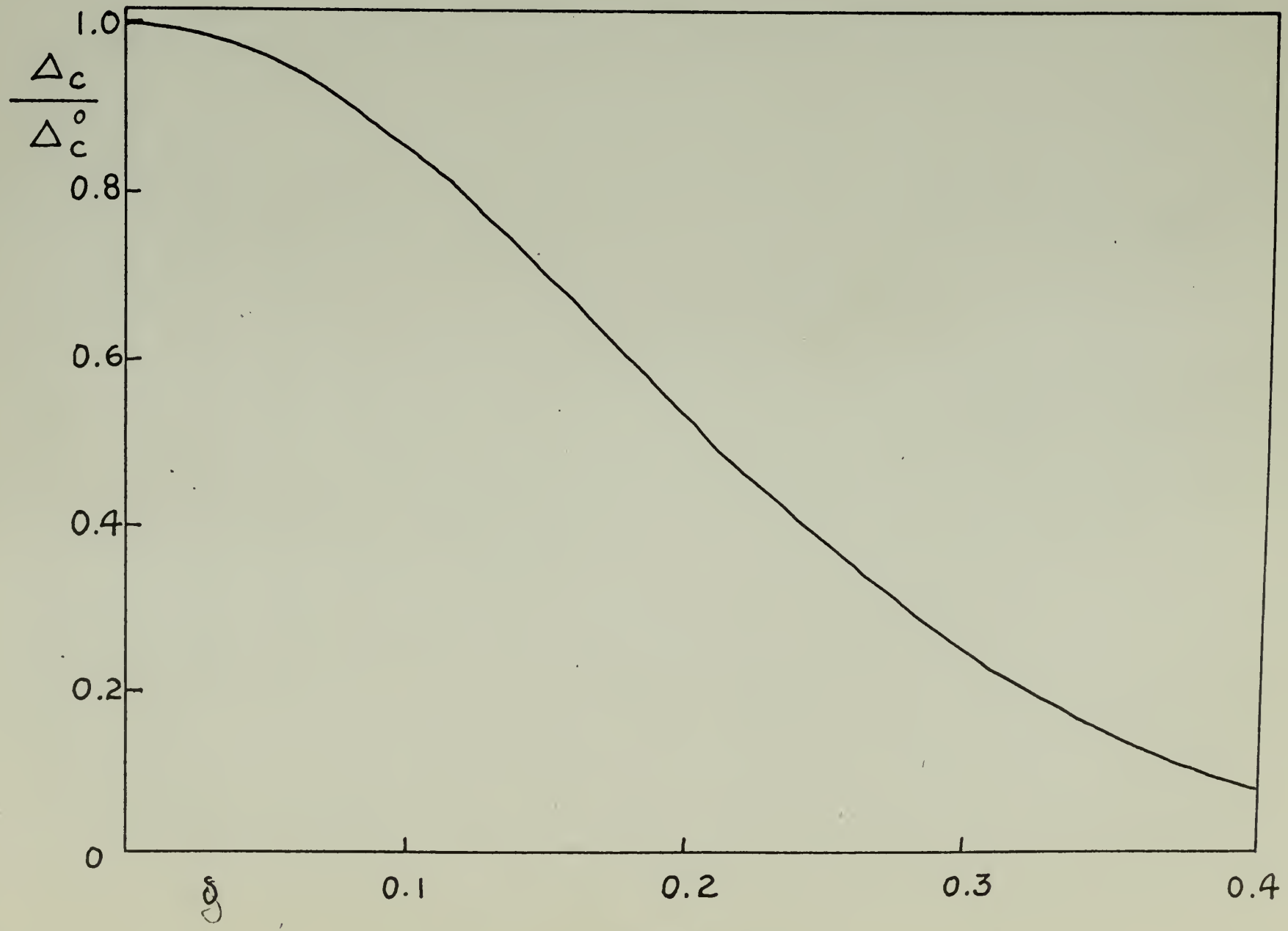

Figure IV-15

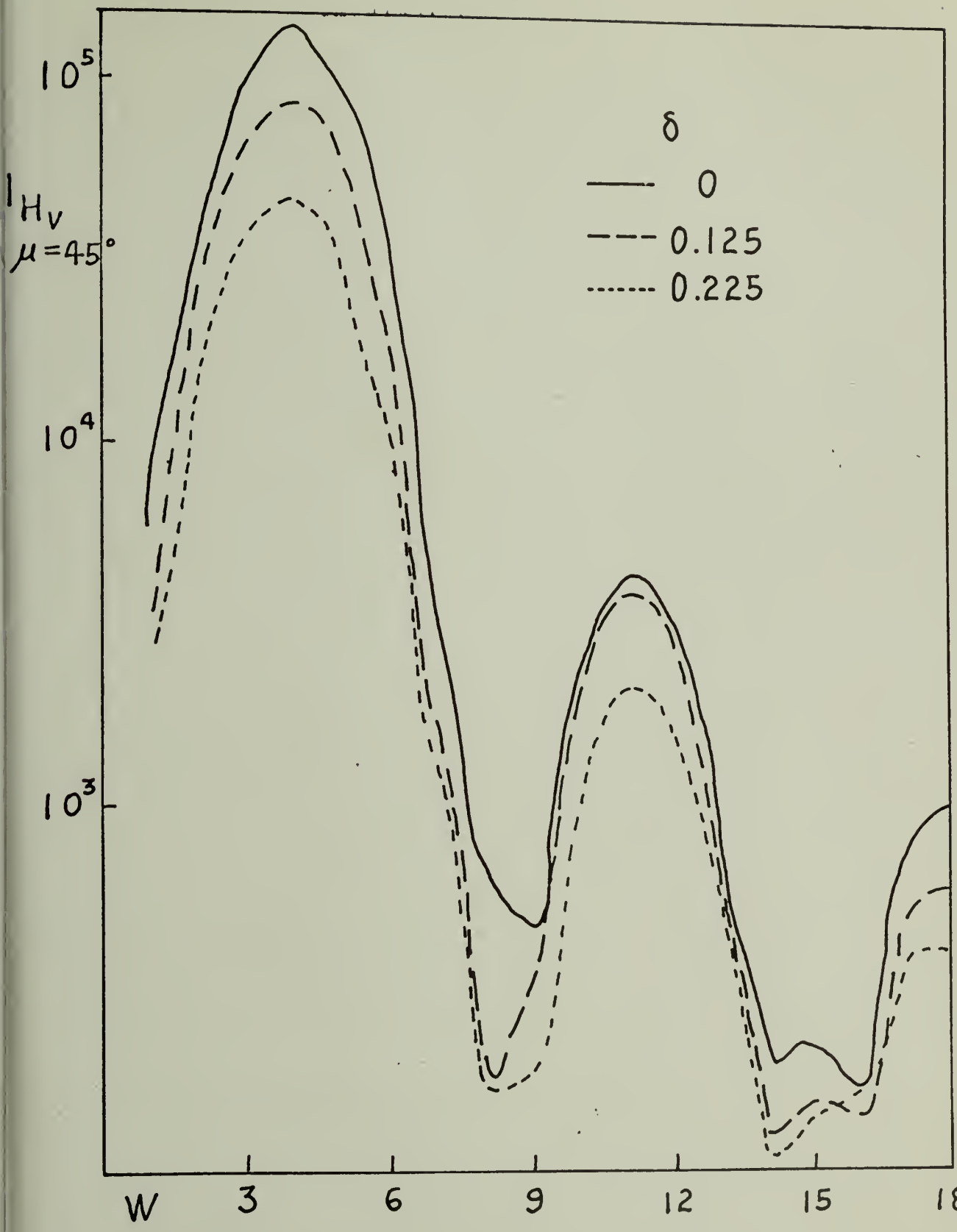

Figure IV-16

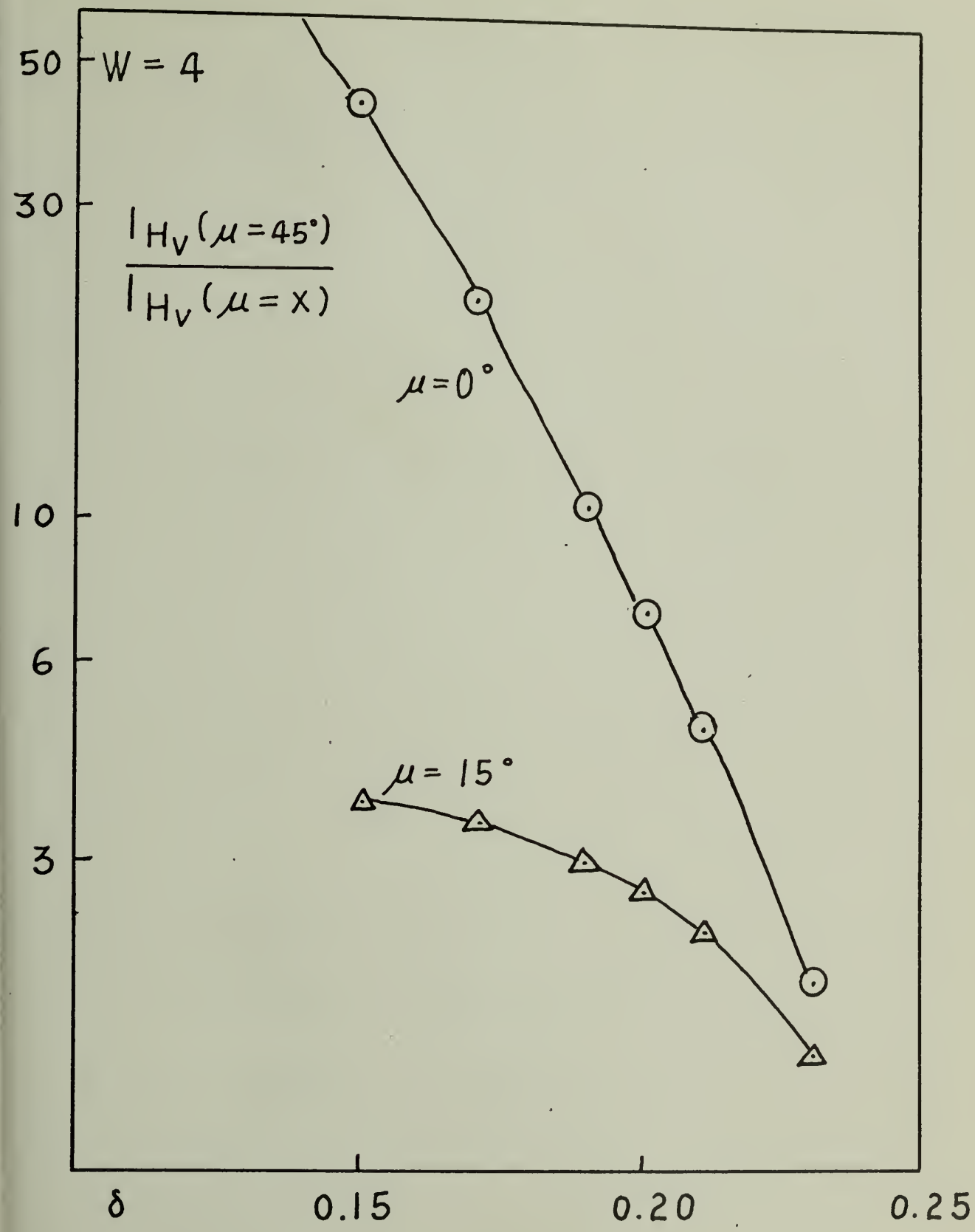

Figure IV-17

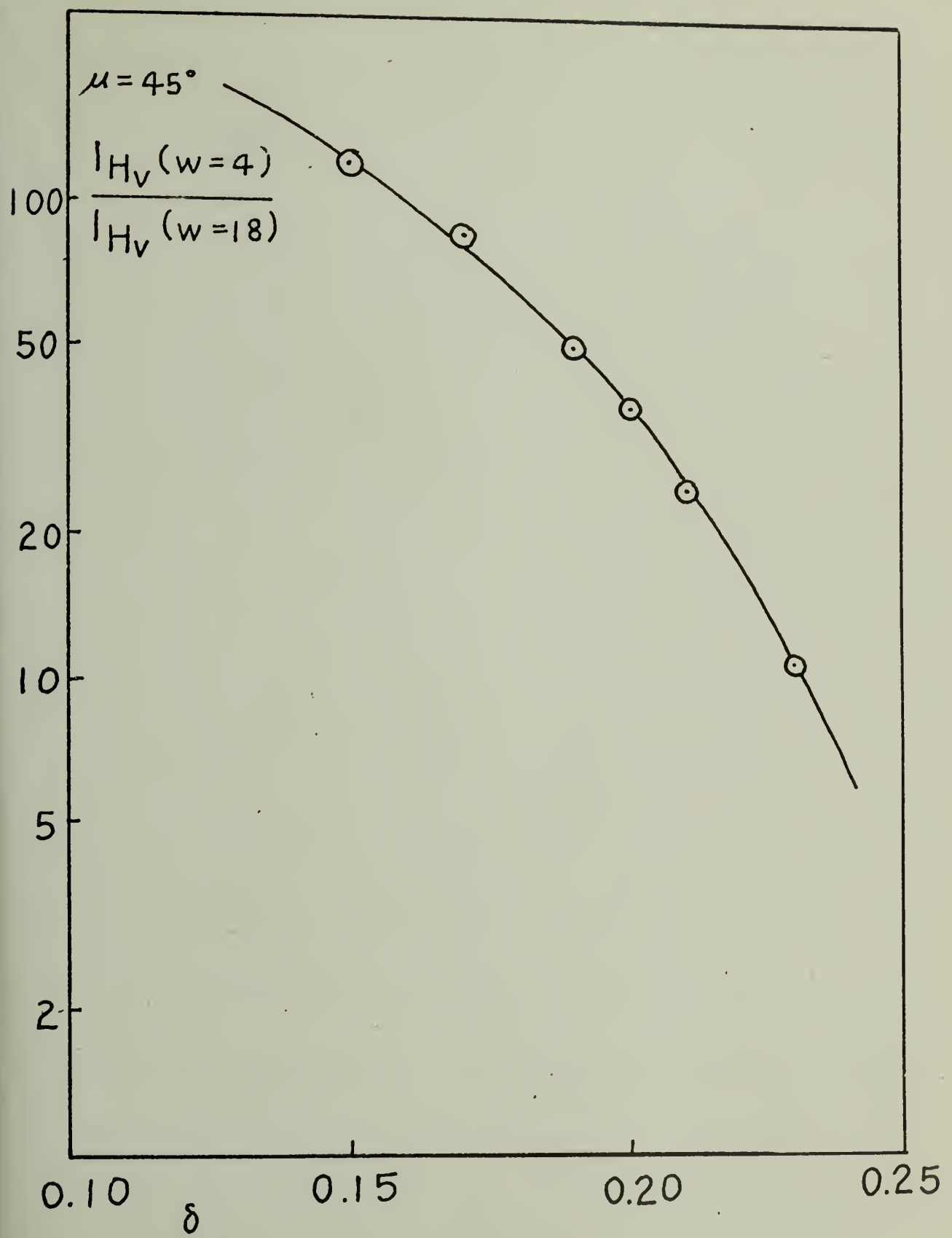

Figure IV-18

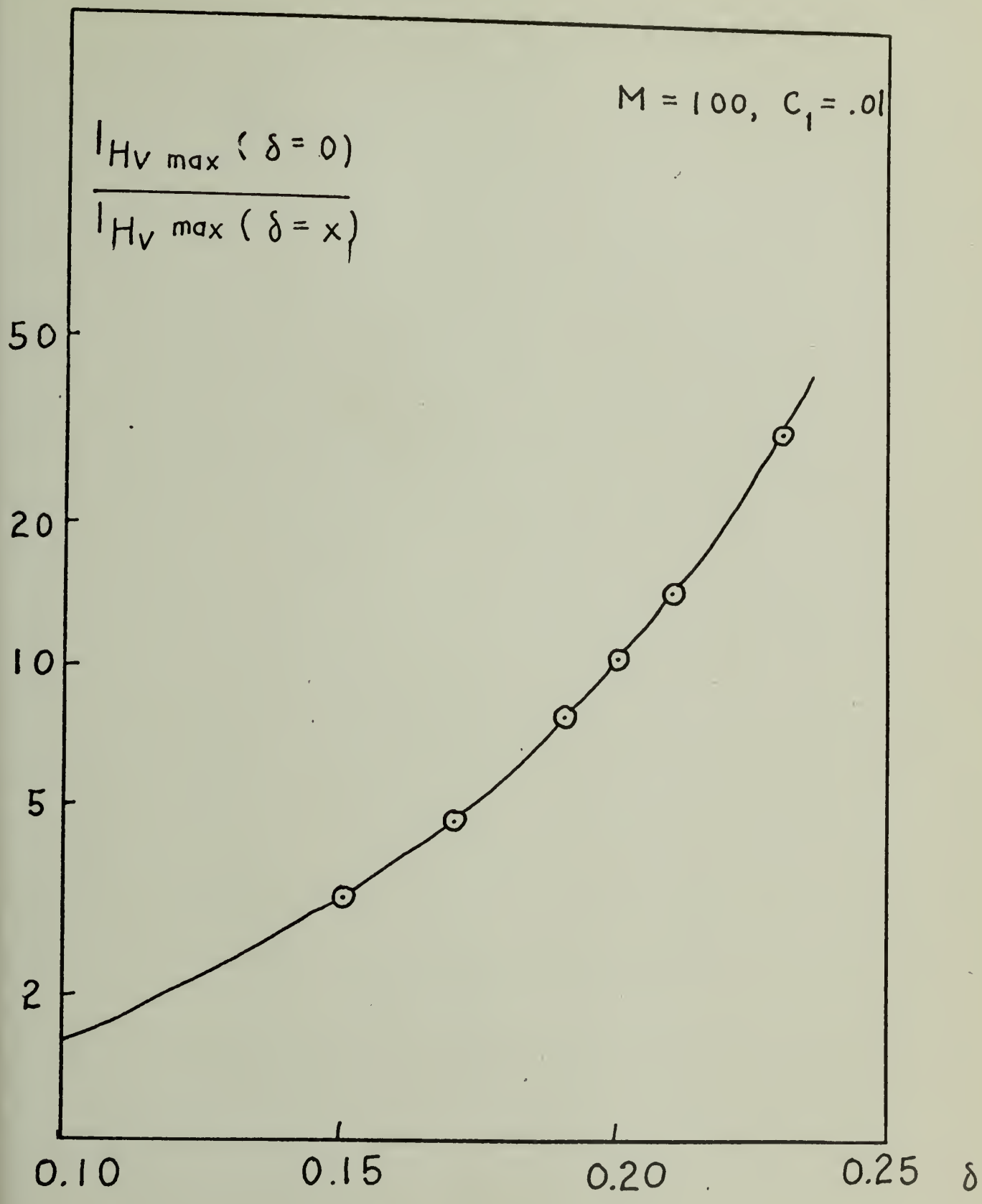
M = 100, C_1 = .01
$\frac{I_{Hv\ max}(\delta = 0)}{I_{Hv\ max}(\delta = x)}$
50
20
10
5
2
0.10
0.15
0.20
0.25
δ

Figure IV-19

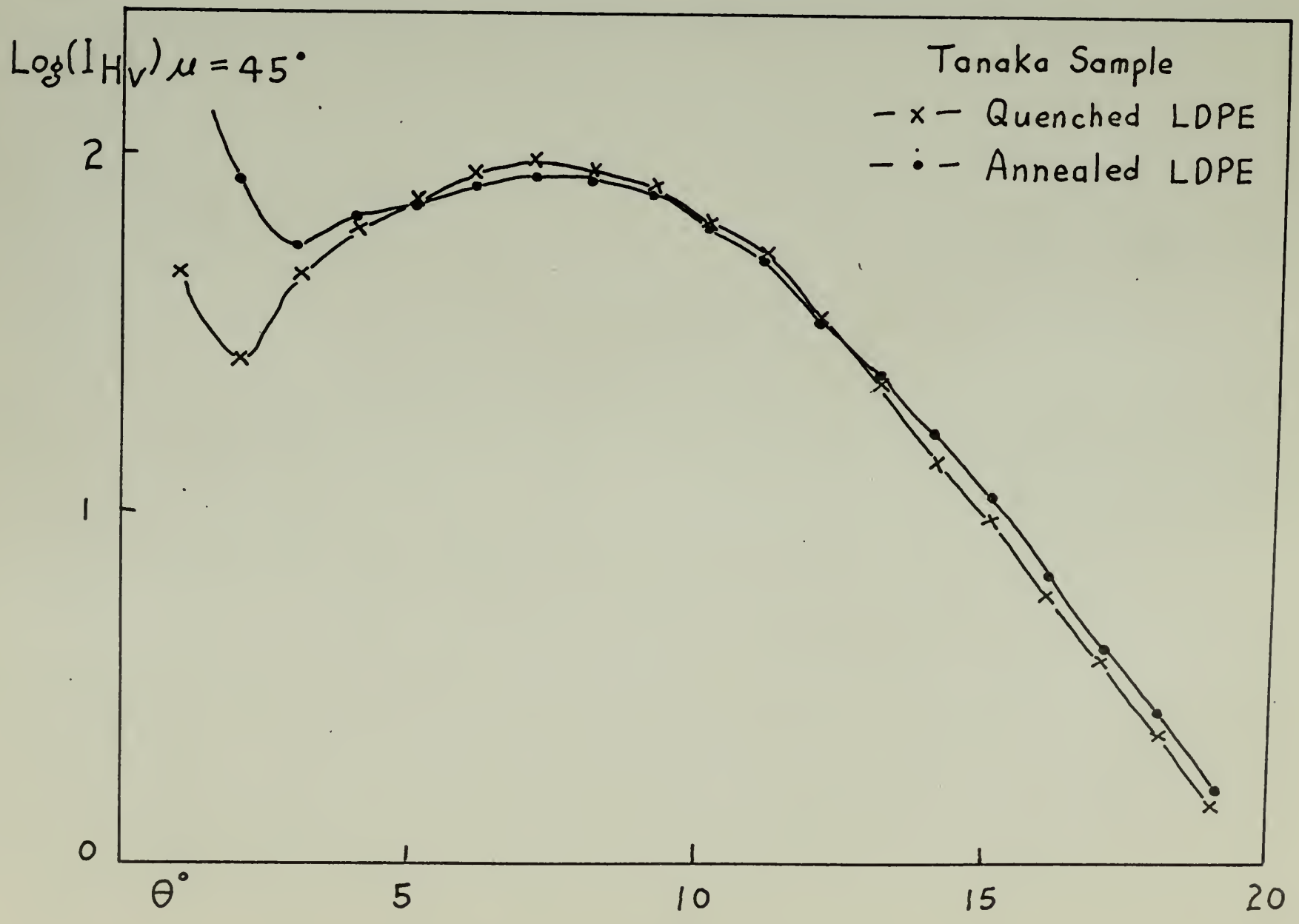
Log(I_HV) μ = 45°
Tanaka Sample
— x — Quenched LDPE
— • — Annealed LDPE
2
1
0
θ°
5
10
15
20

Figure V-1

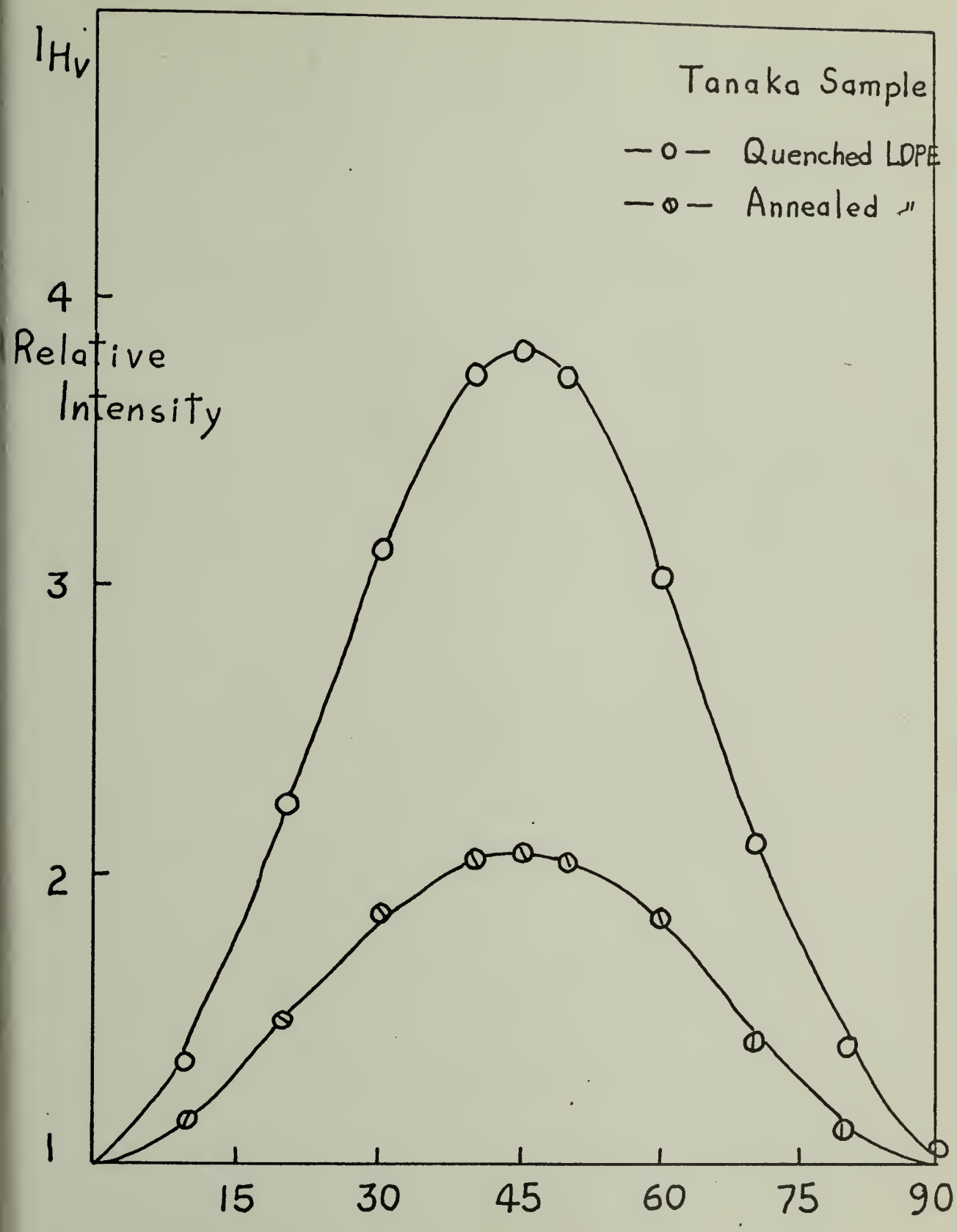
I_{Hv}
Tanaka Sample
—o— Quenched LDPE
—⊘— Annealed "
4
Relative
Intensity
3
2
1
15
30
45
60
75
90

Figure V-2

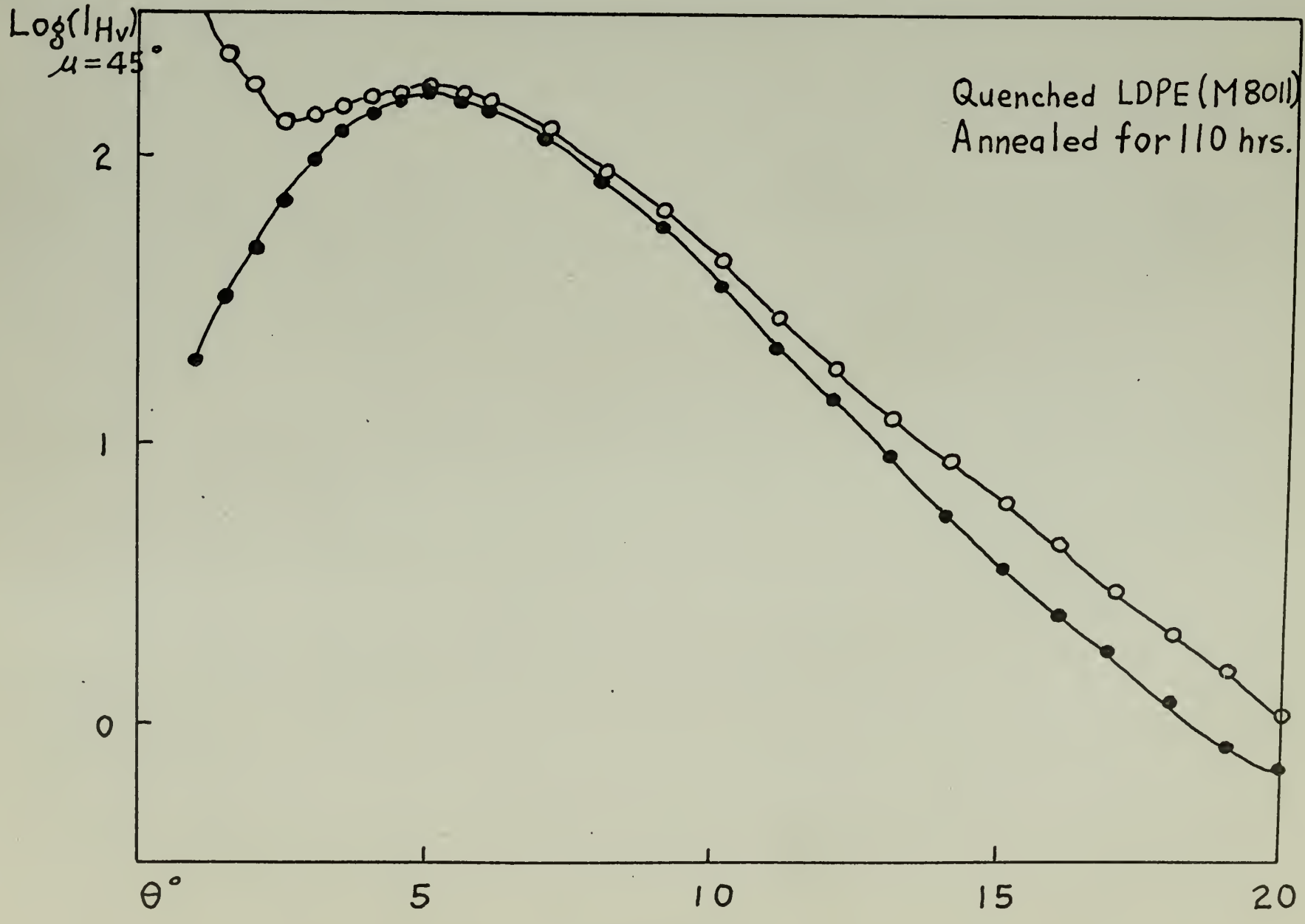
Log(I Hv)
μ=45°
Quenched LDPE (M8011)
Annealed for 110 hrs. ×1.28
2
1
0
θ°
5
10
15
20

Figure V-3

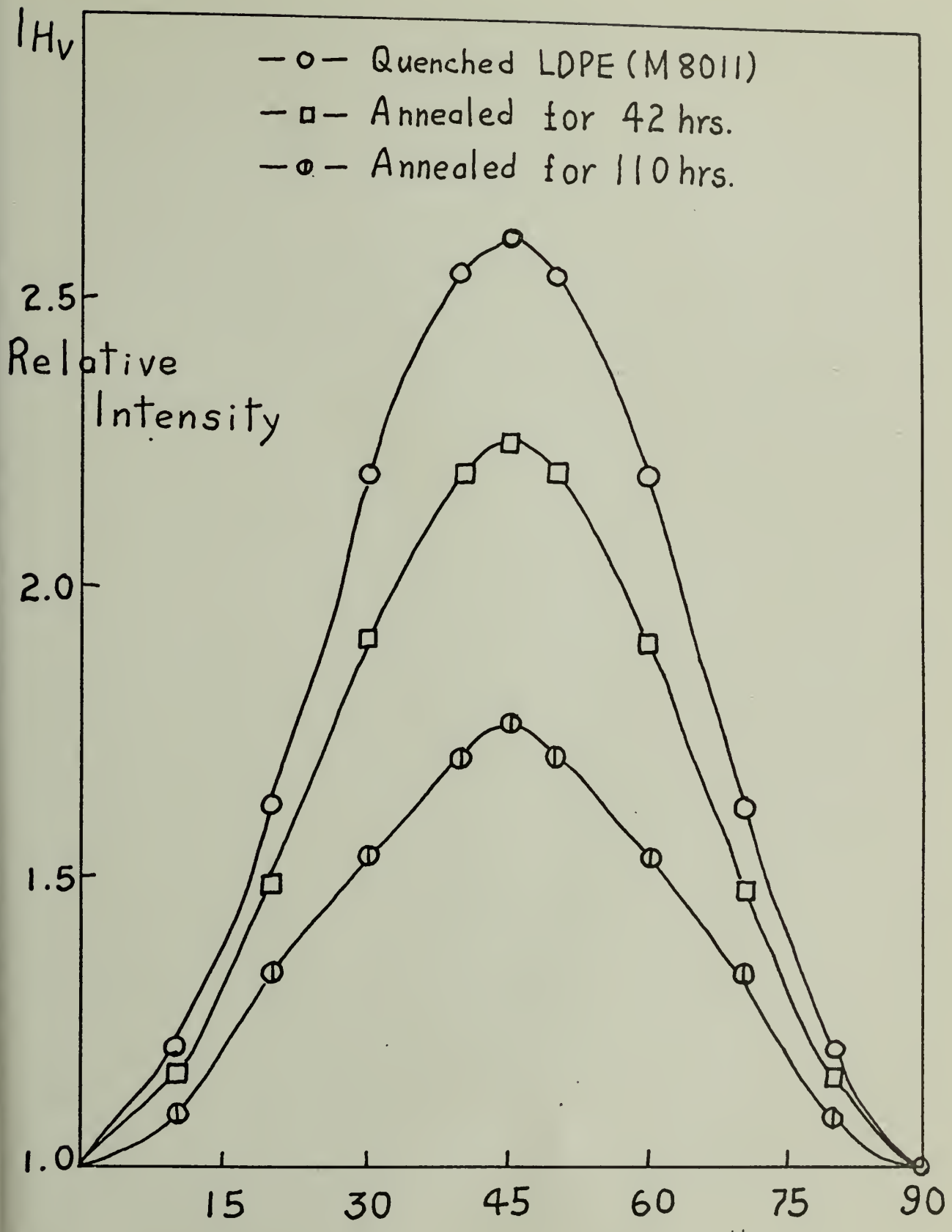
I_{Hv}
— o — Quenched LDPE (M8011)
— □ — Annealed for 42 hrs.
— ⊕ — Annealed for 110 hrs.
2.5
Relative
Intensity
2.0
1.5
1.0
15
30
45
60
75
90

Figure V-4

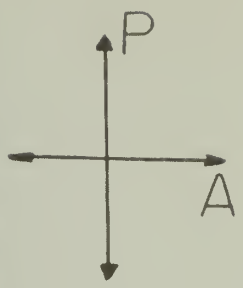

H_V

V_V

UNDEFORMED PE

Figure V-5

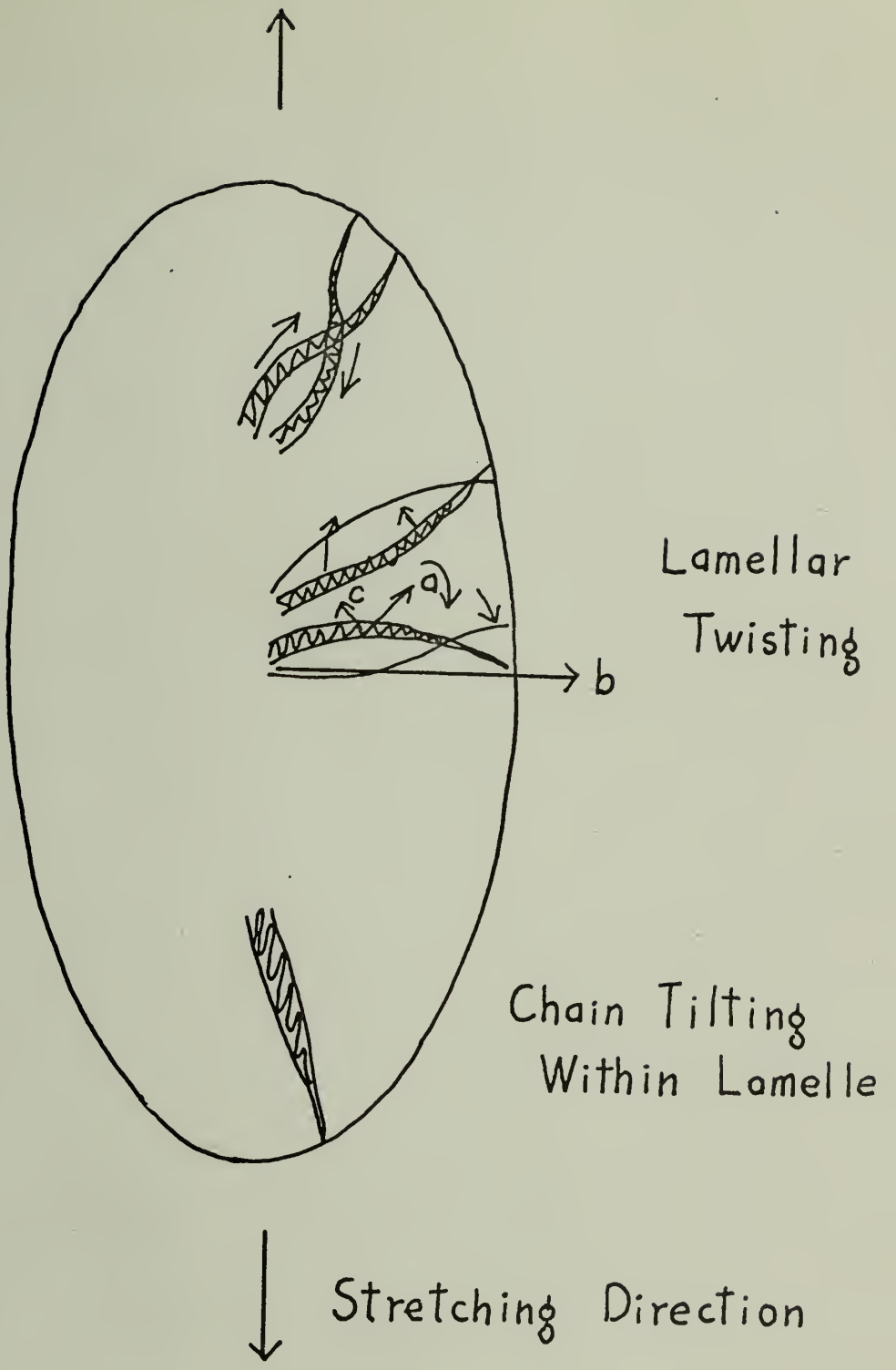
Lamellar
Twisting
b
c
a
Chain Tilting
Within Lamelle
Stretching Direction

Figure VI-1

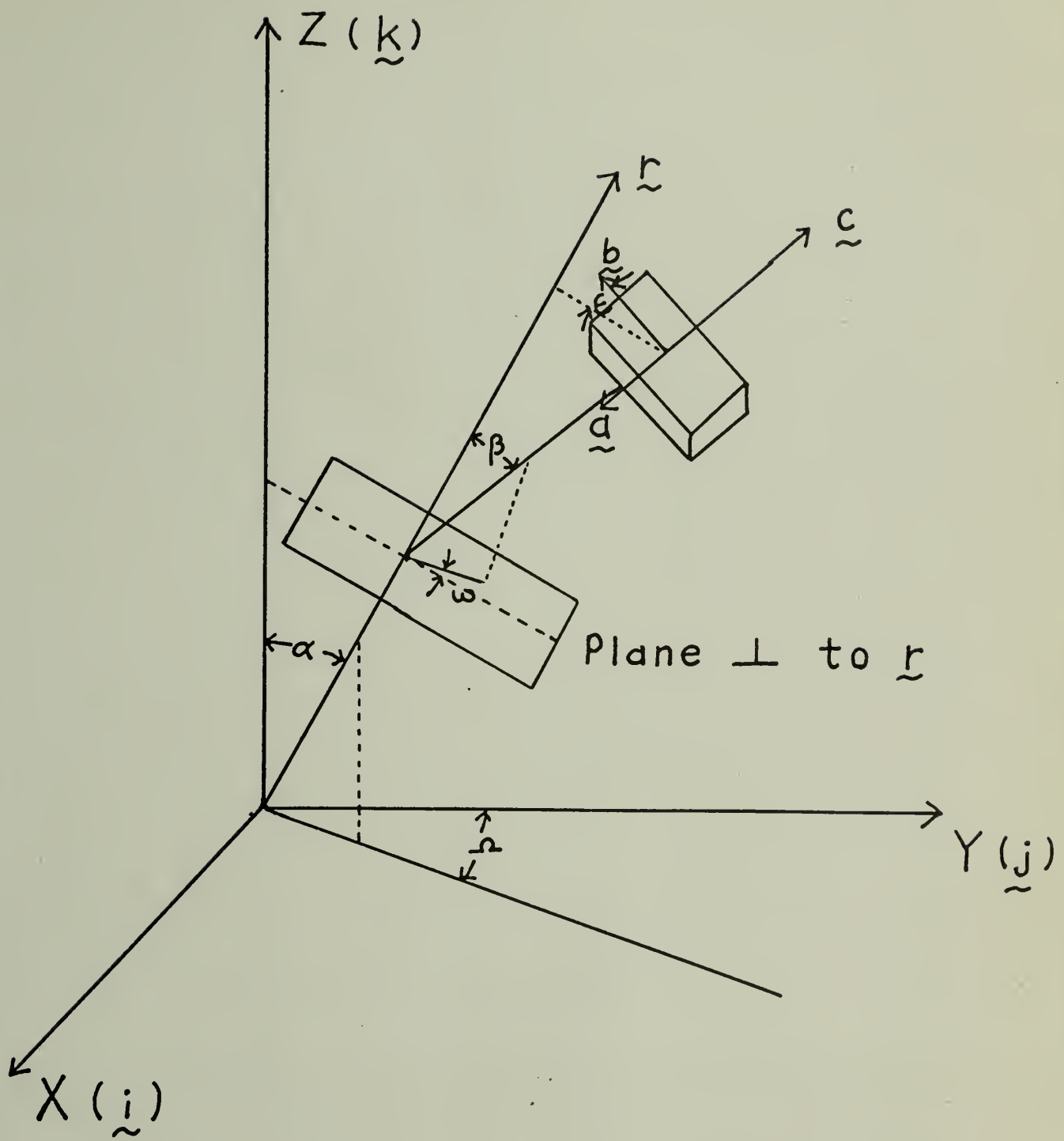

Figure VI-2

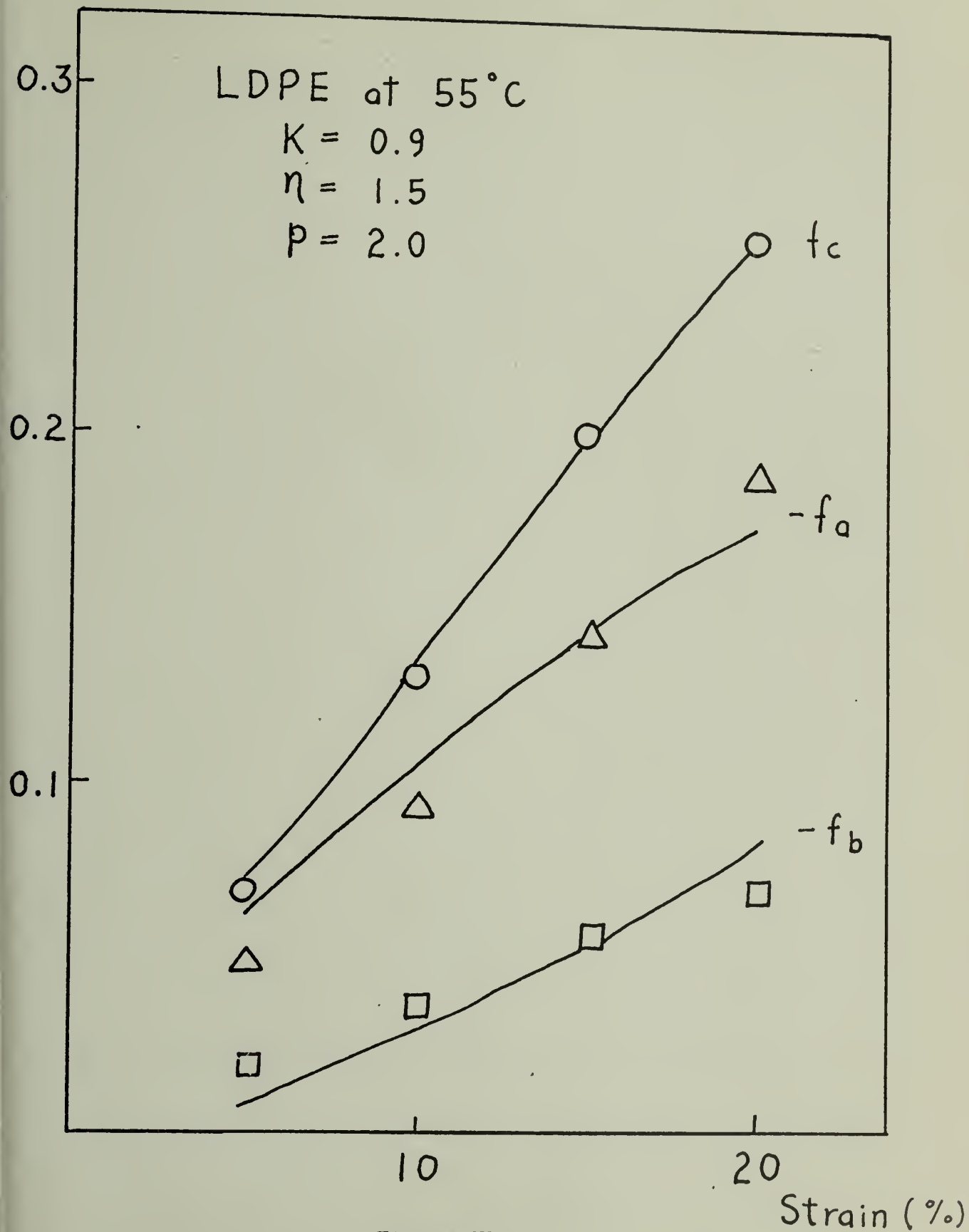

Figure VI-3

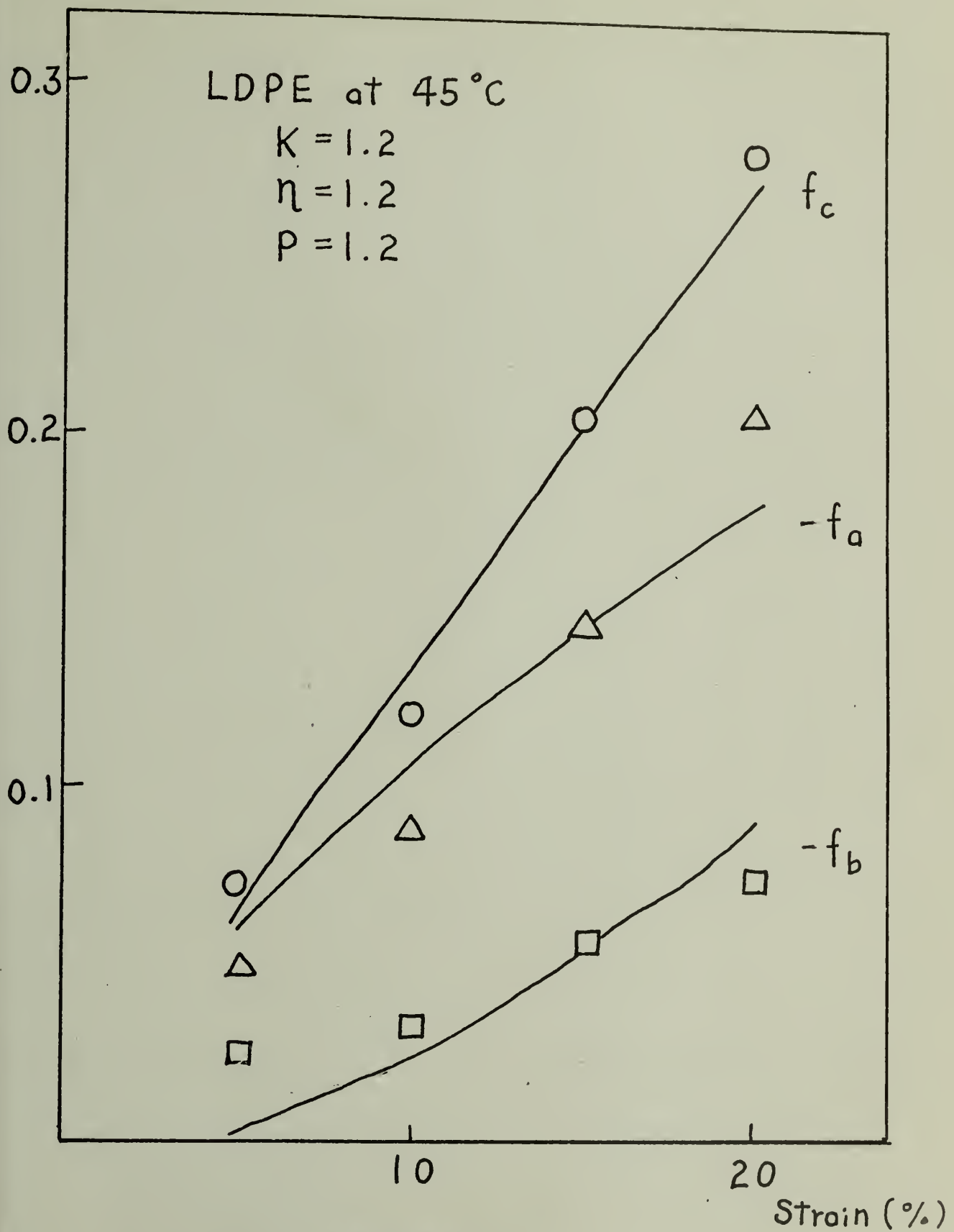

Figure VI-4

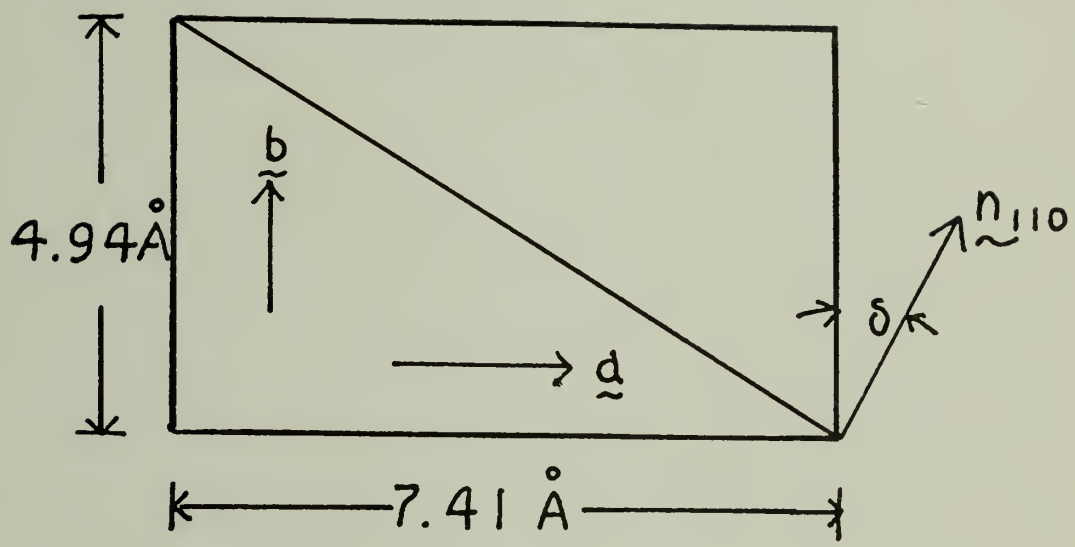

Figure VI-5

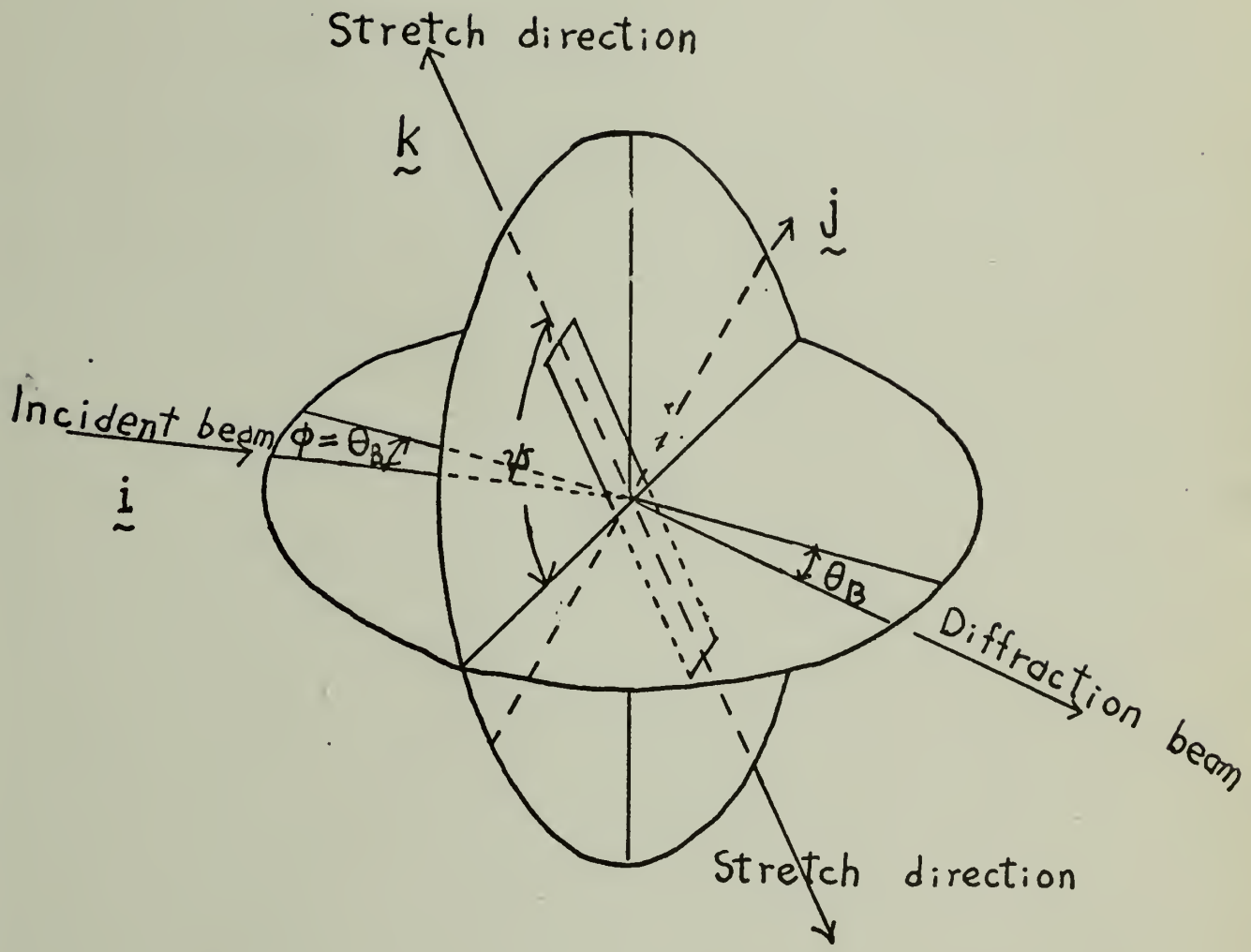
Stretch direction
k
j
Incident beam
Φ=θB
i
2θB
Diffraction beam
Stretch direction

Figure VI-6

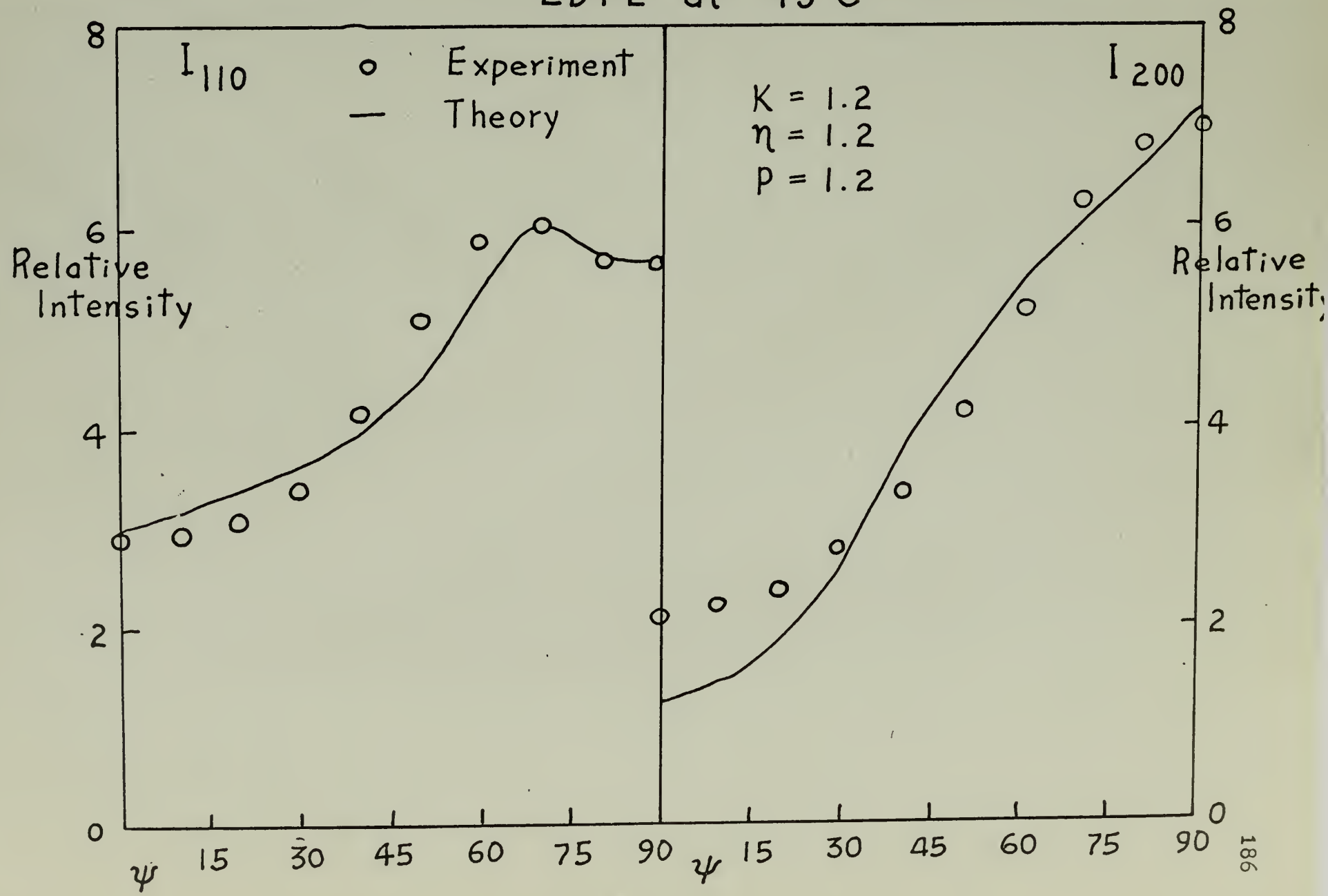
LDPE at 45°C
I_{110}
Experiment
Theory
I_{200}
K = 1.2
η = 1.2
P = 1.2
Relative Intensity
Relative Intensity
8
6
4
2
0
ψ
15
30
45
60
75
90

Figure VI-7

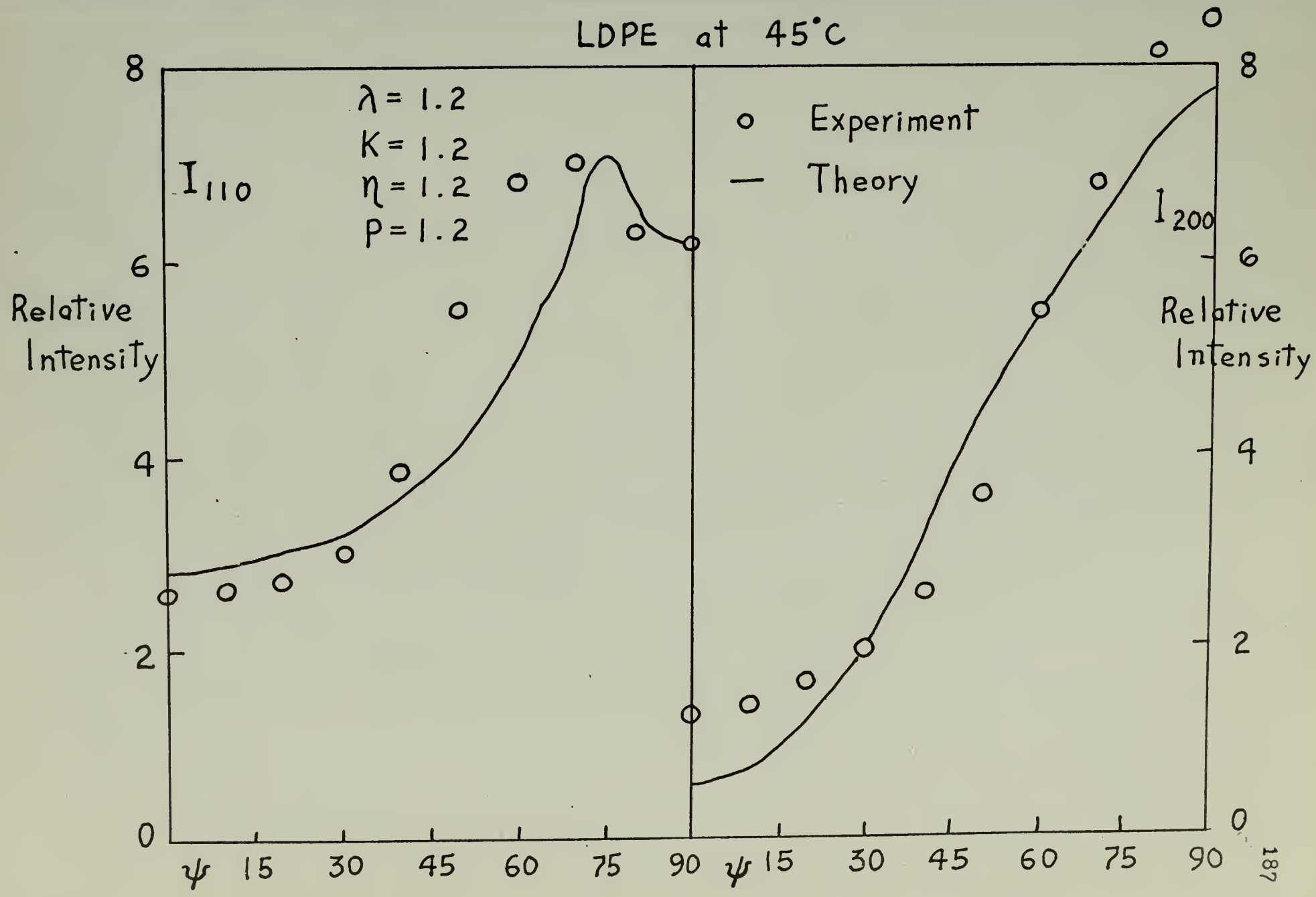
LDPE at 45°C
λ = 1.2
K = 1.2
η = 1.2
P = 1.2
I110
I200
Experiment
Theory
Relative Intensity
Relative Intensity
ψ
ψ
0
2
4
6
8
15
30
45
60
75
90

Figure VI-8

LOW DENSITY POLYETHYLENE (M 8011)

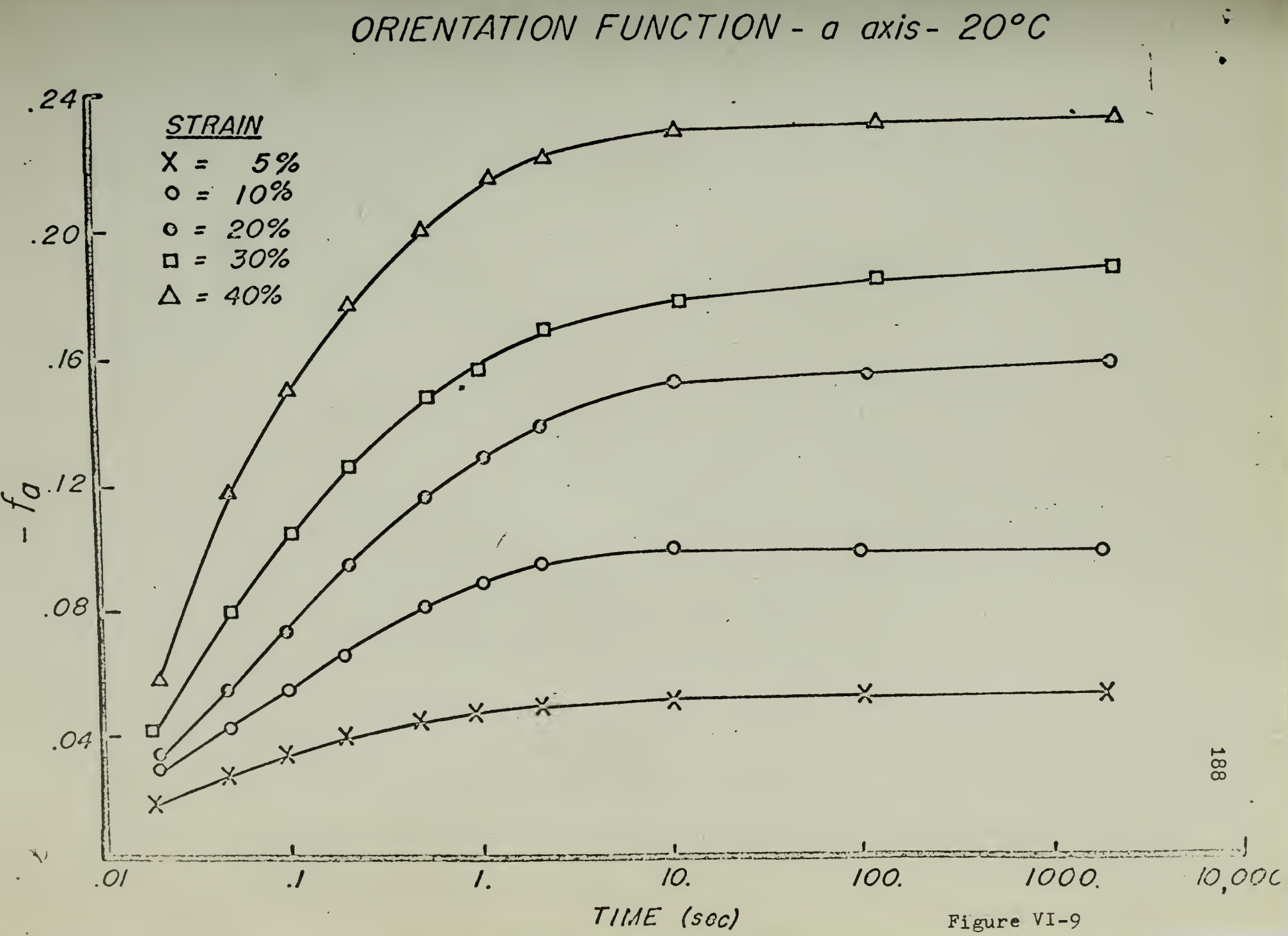

Figure VI-9

LOW DENSITY POLYETHYLENE (M8011)
ORIENTATION FUNCTION - b axis - 20°C

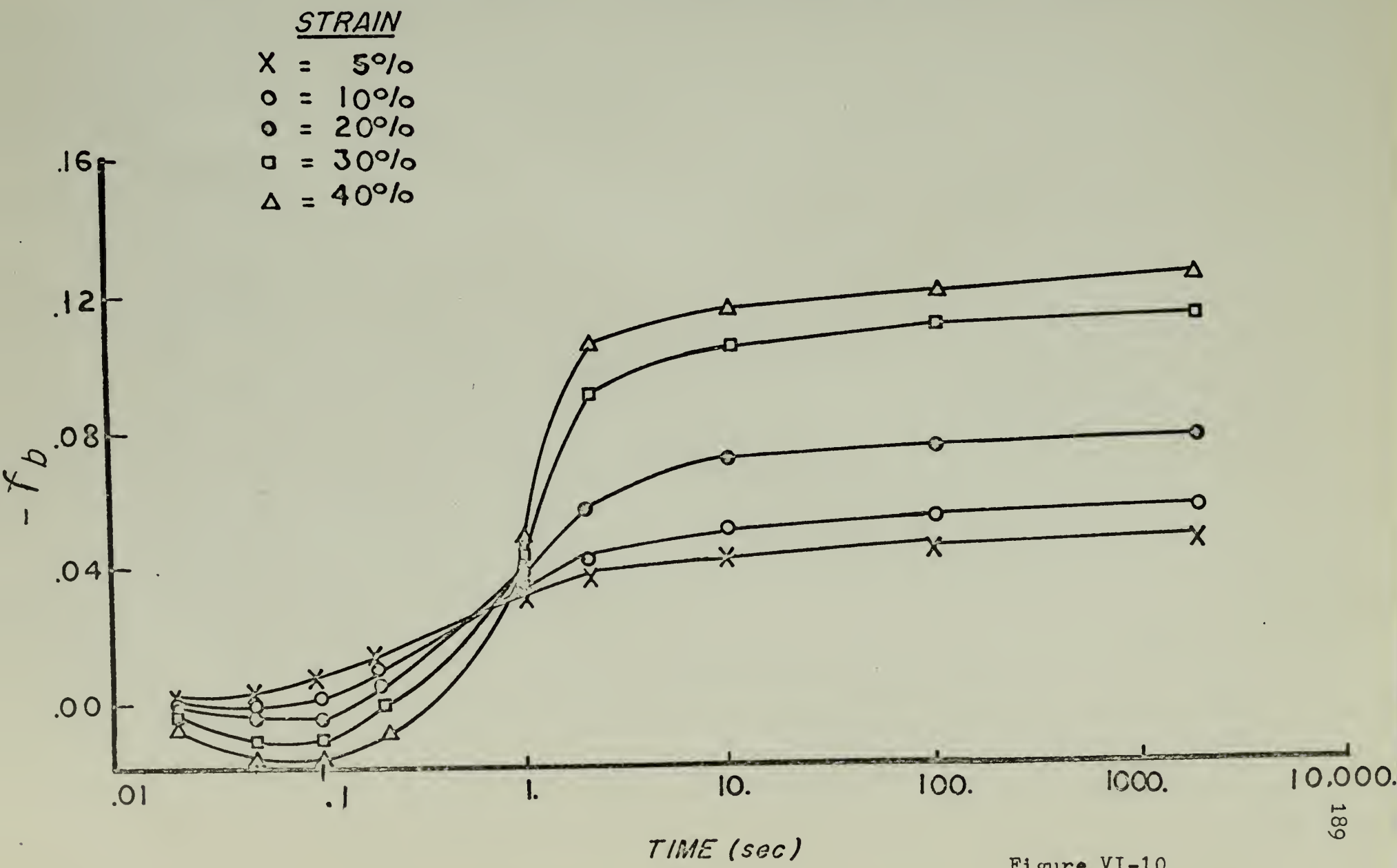

Figure VI-10

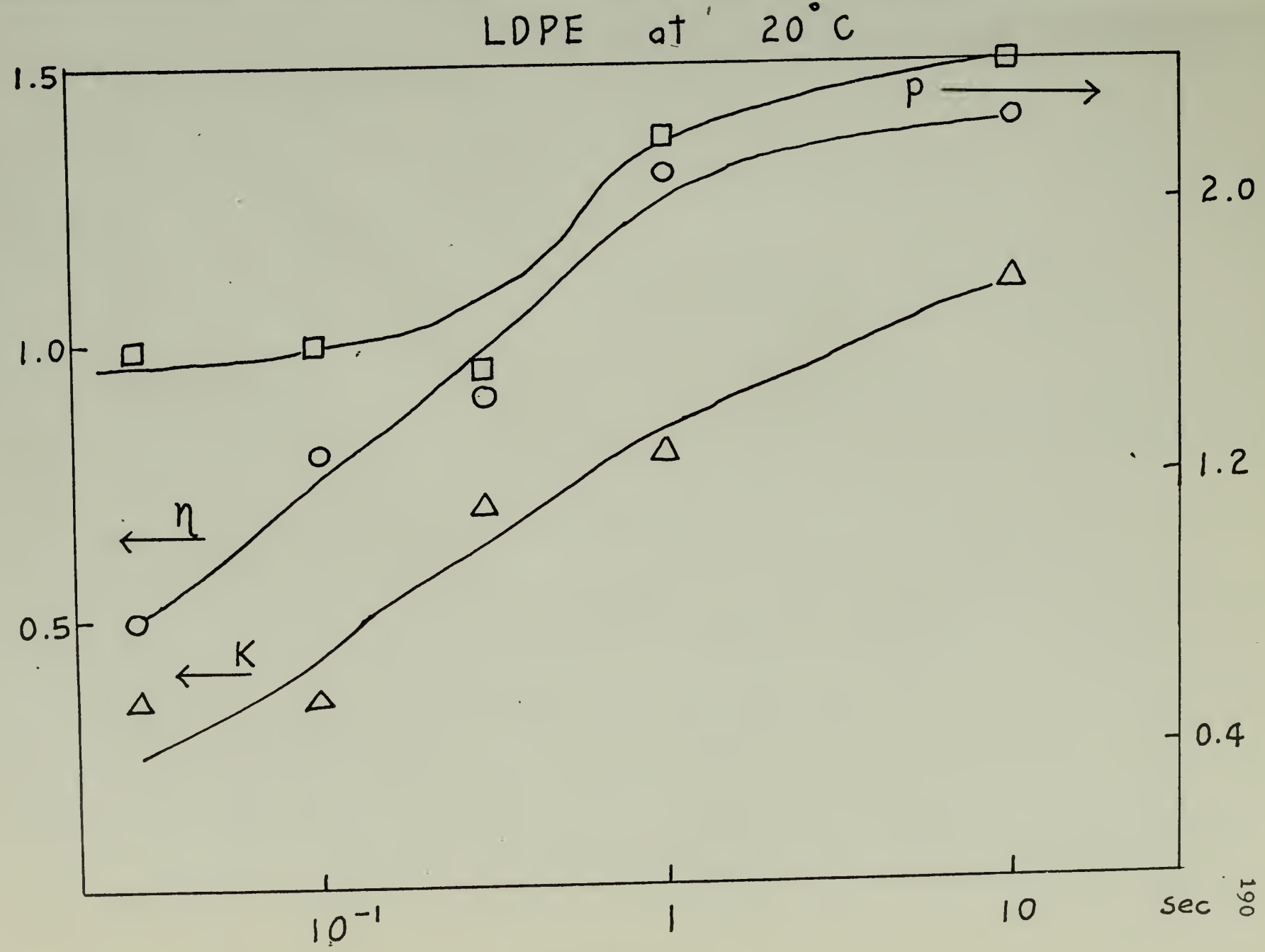

Figure VI-11

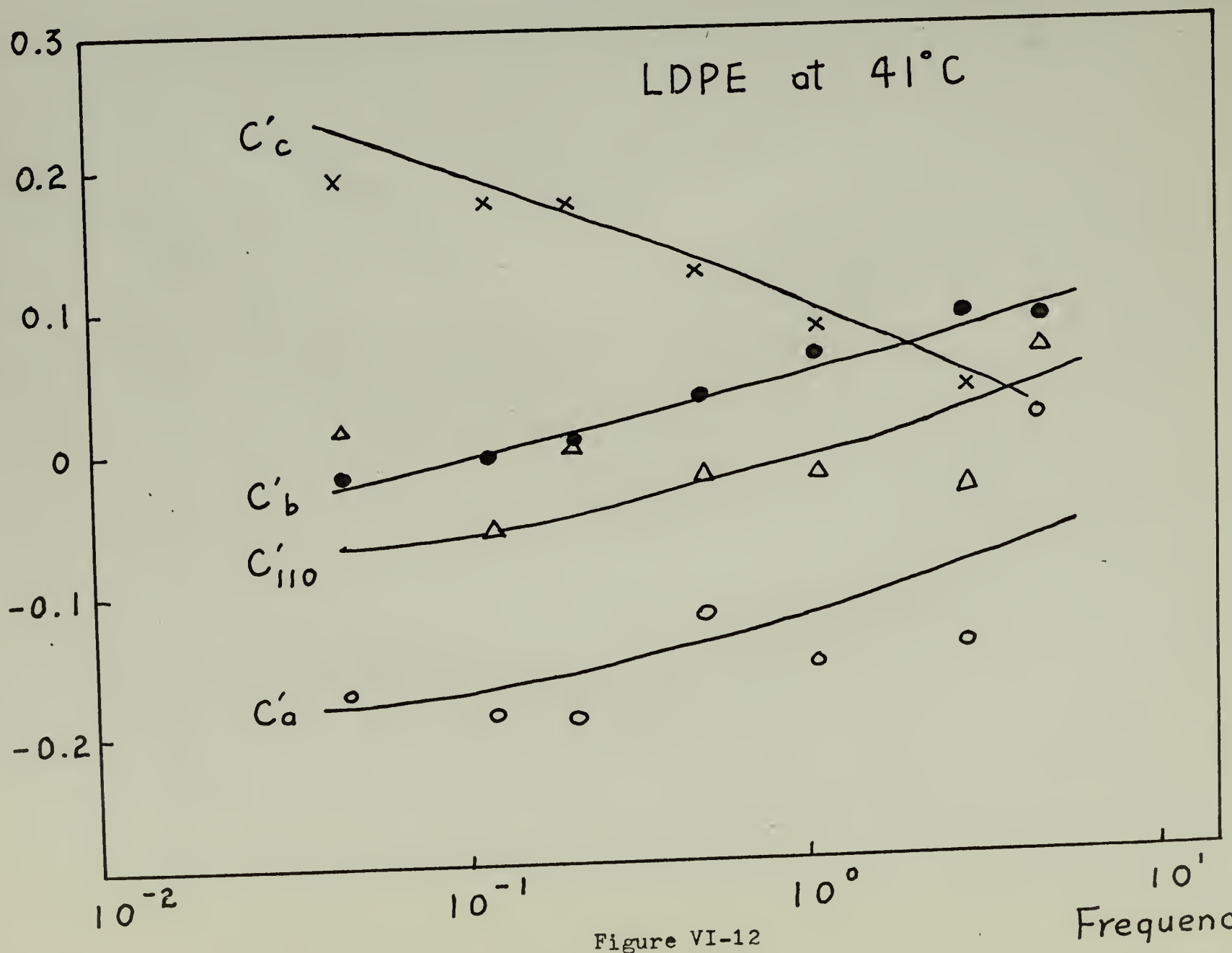
LDPE at 41°C
C'c
C'b
C'110
C'a
0.3
0.2
0.1
0
-0.1
-0.2
10^-2
10^-1
10^0
10^1
Frequency (Hz)

Figure VI-12

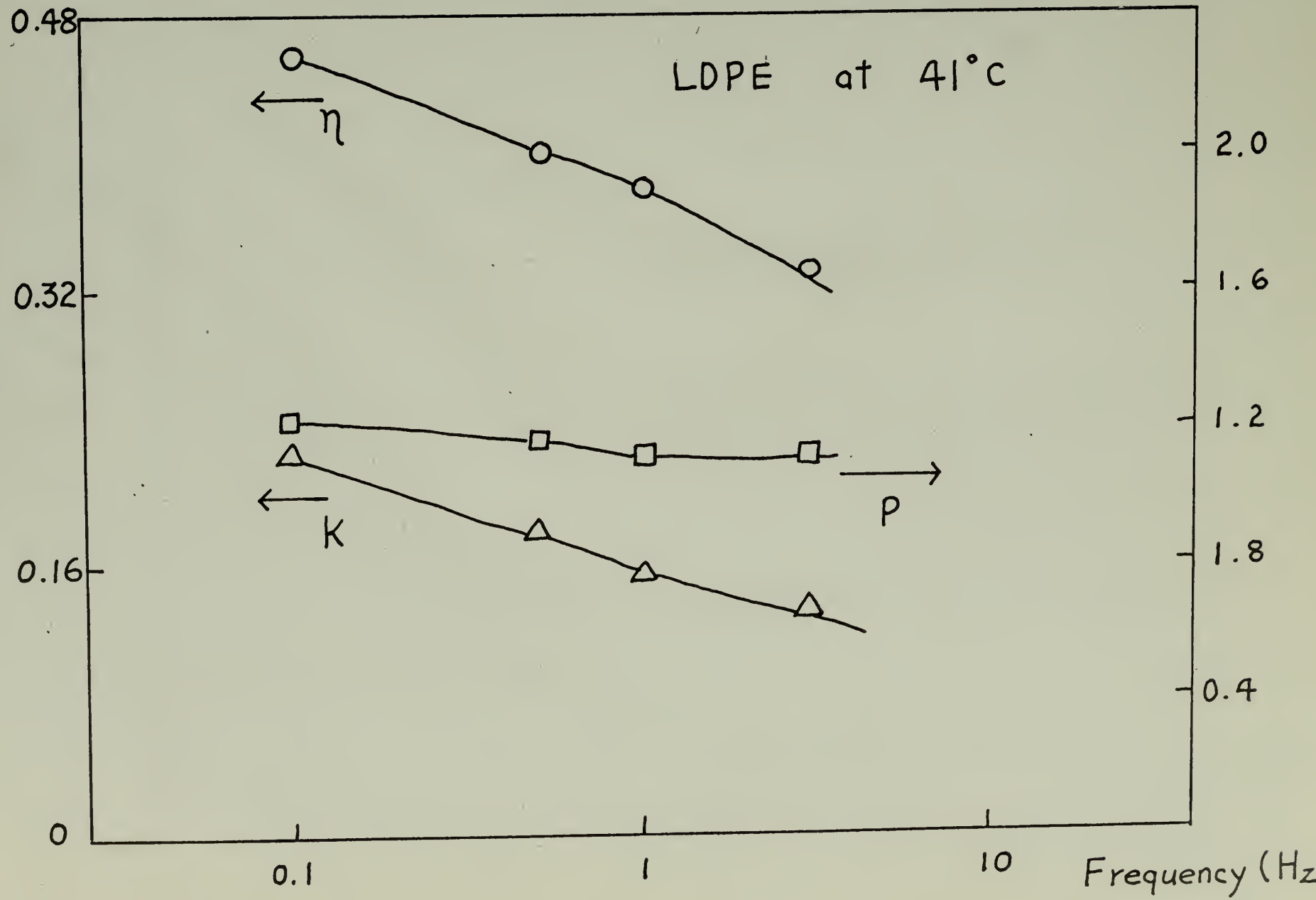

Figure VI-13

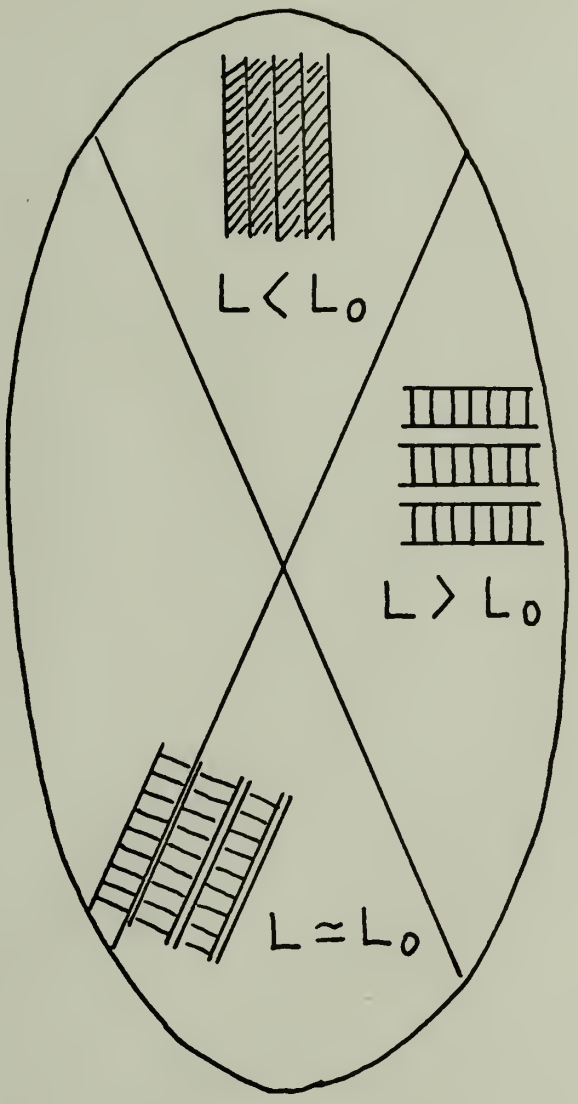

Figure VII-1

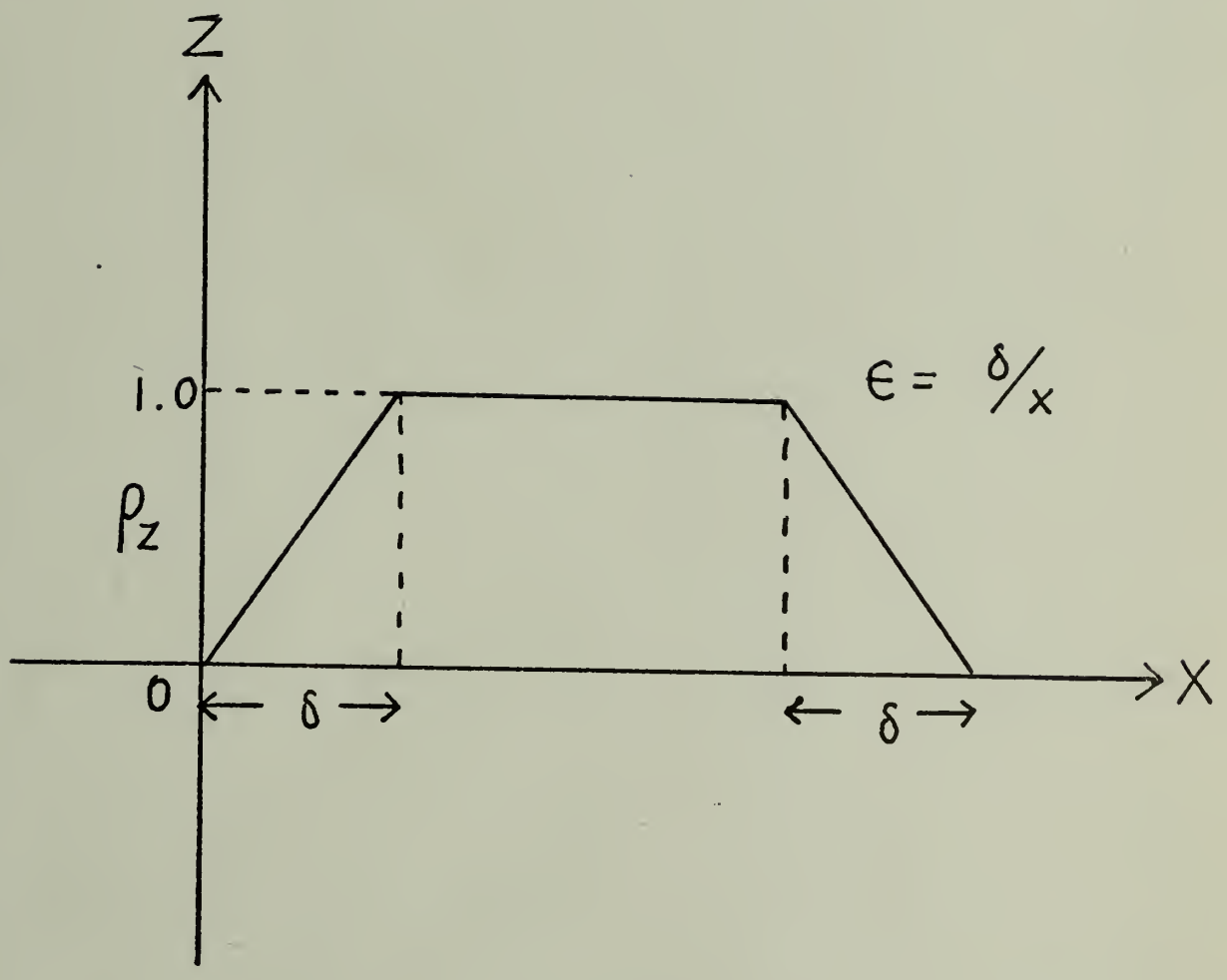

Figure VII -2

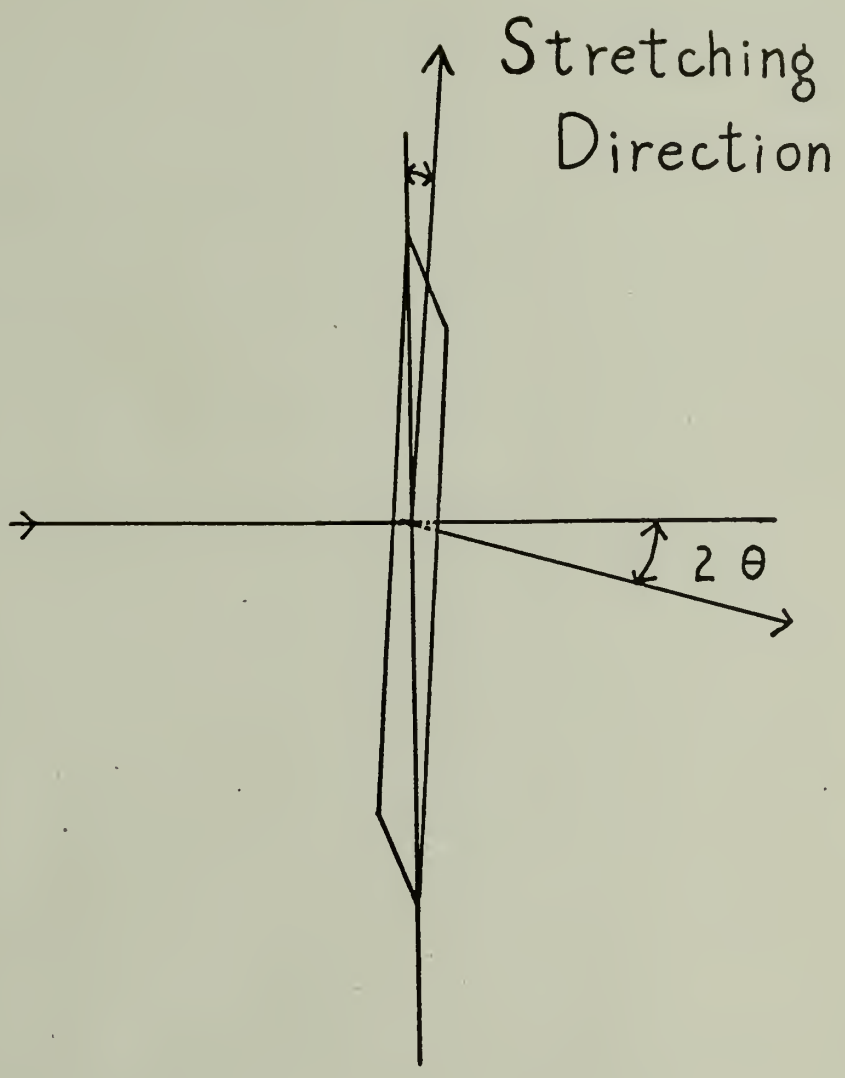

Figure VII -3

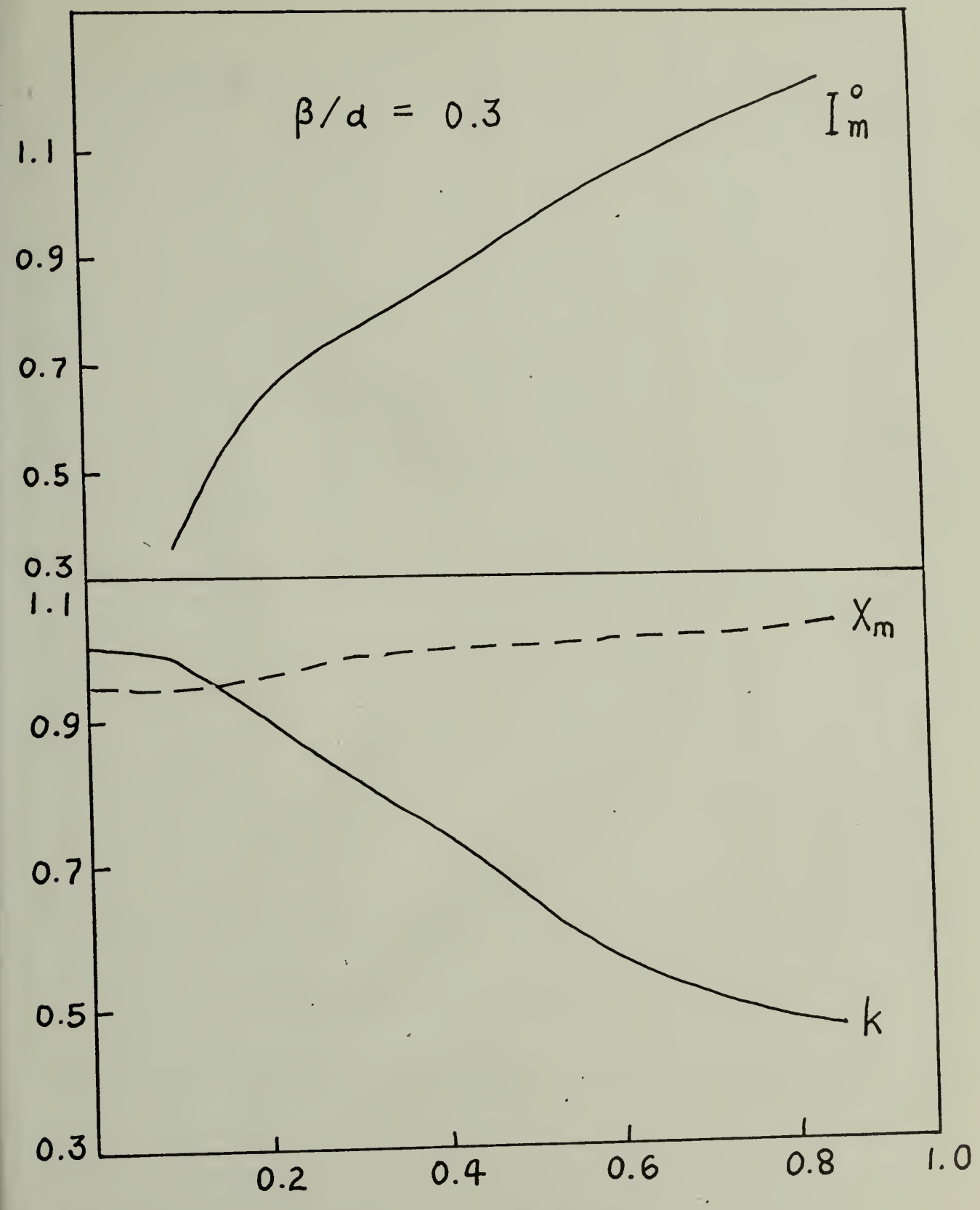

Figure VII-4

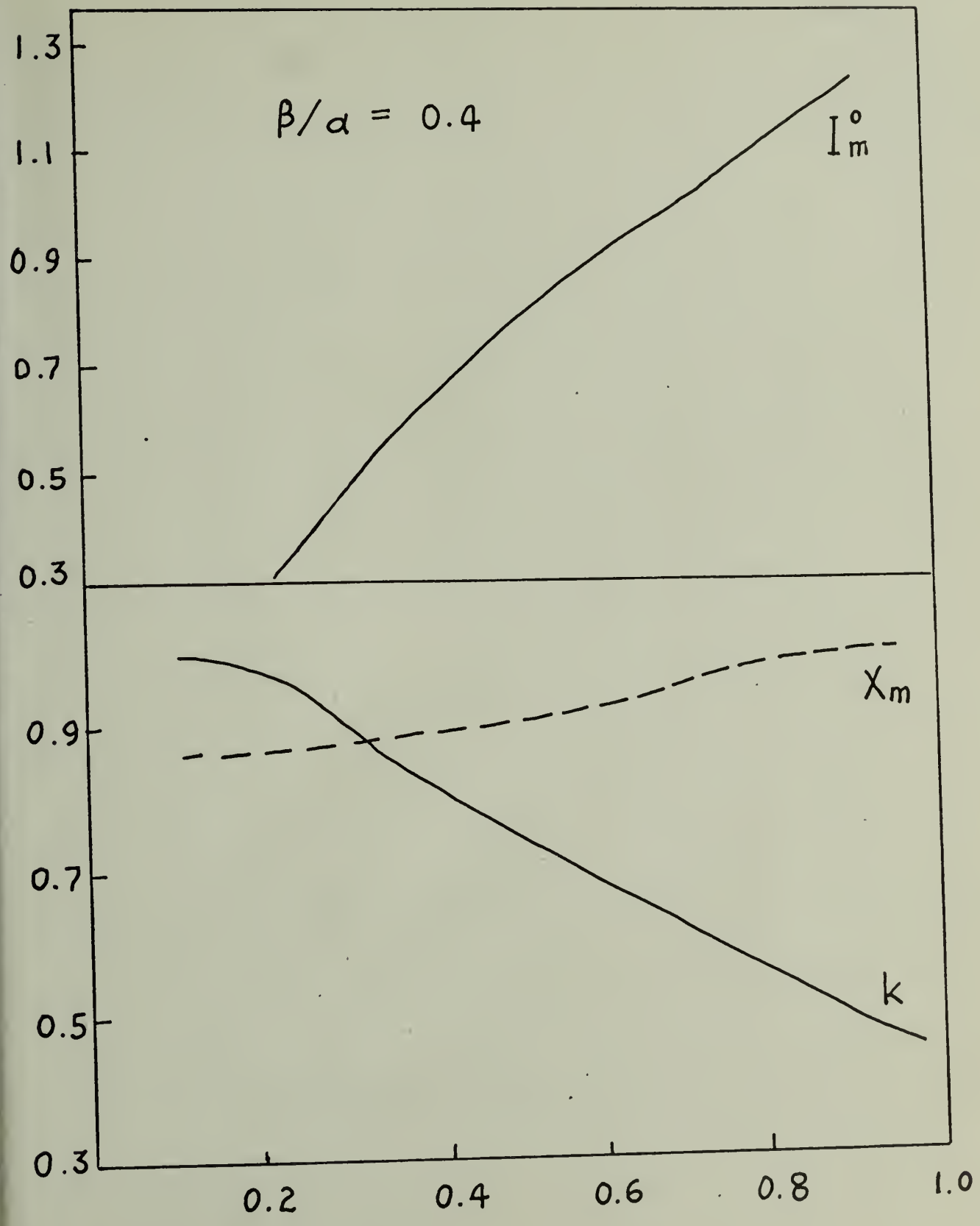

Figure VII-5

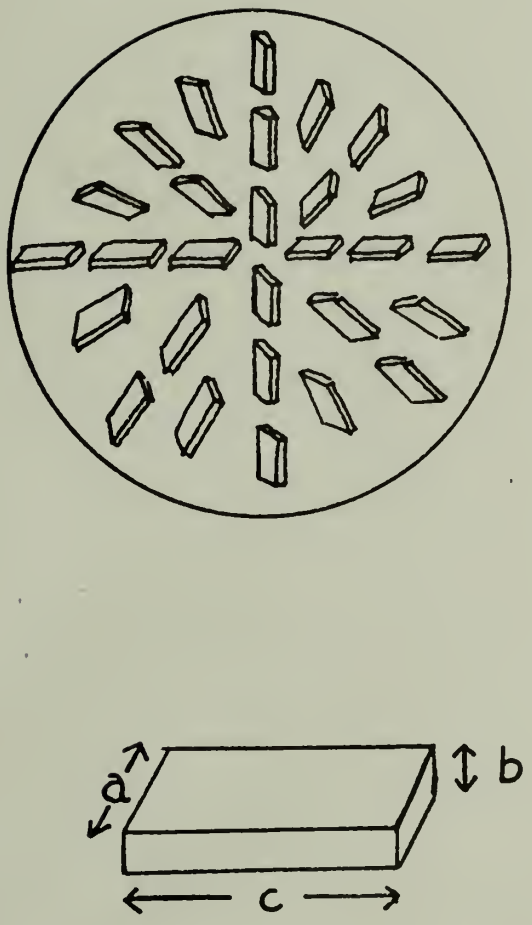

Figure VIII-1

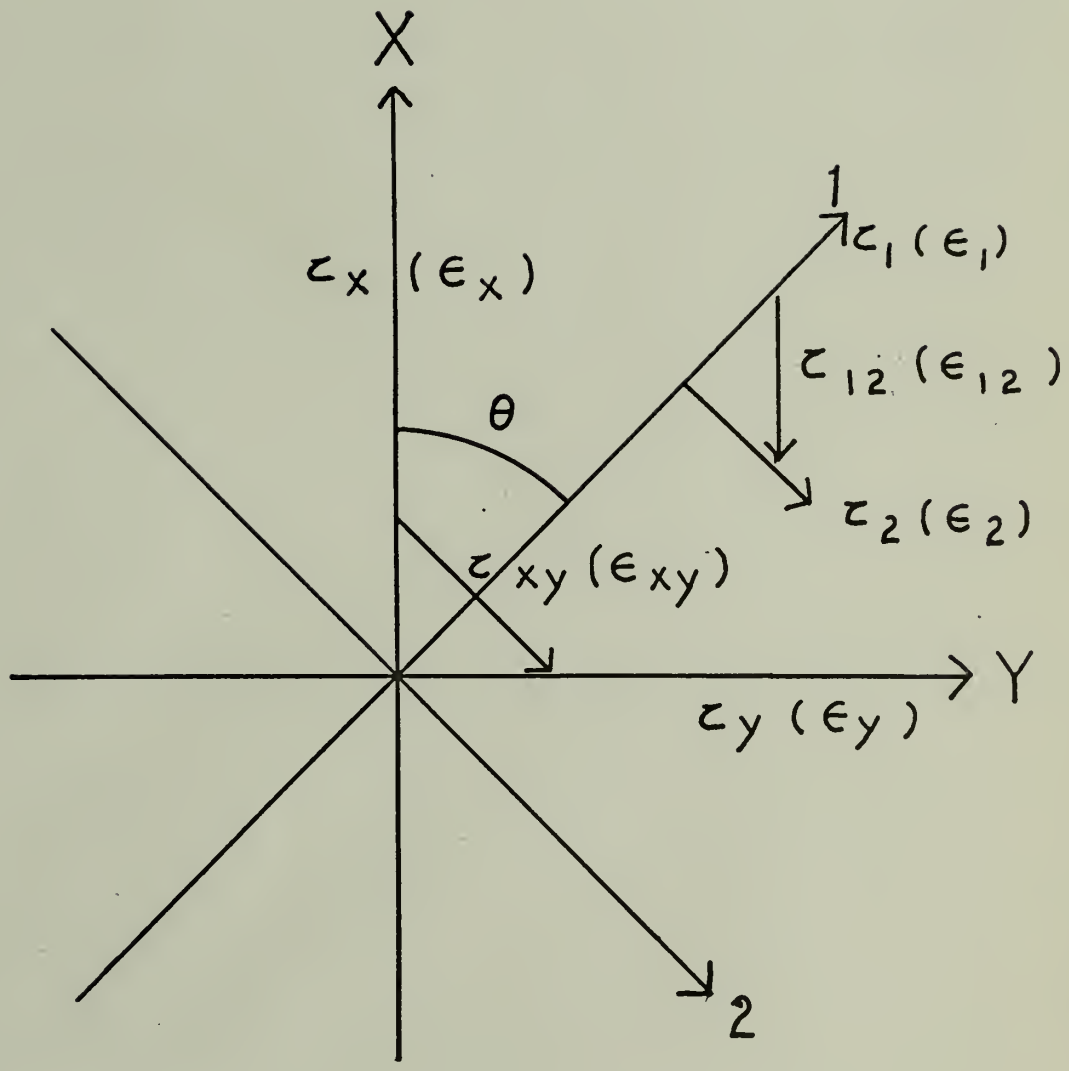

Figure VIII-2

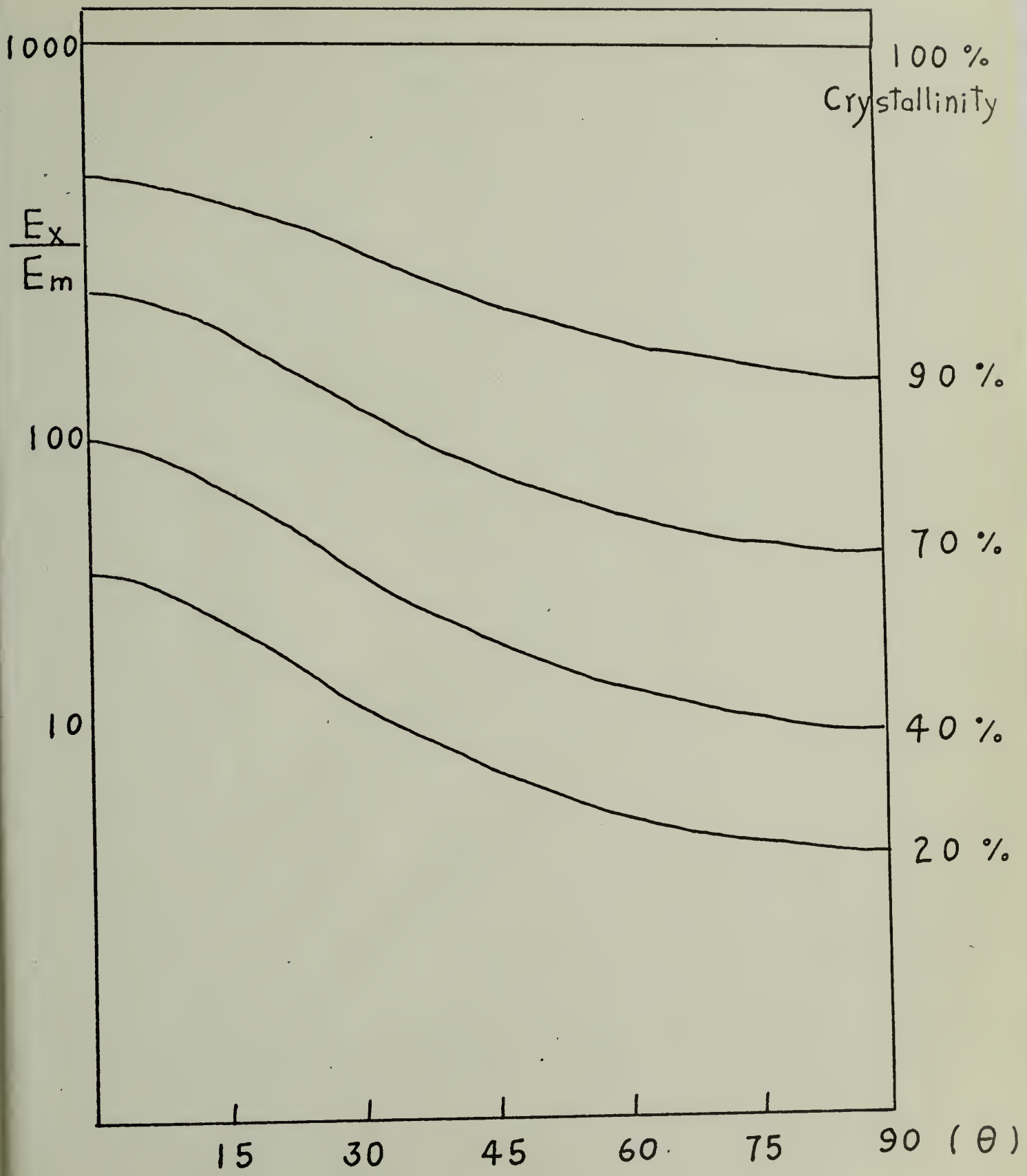

Figure VIII-3

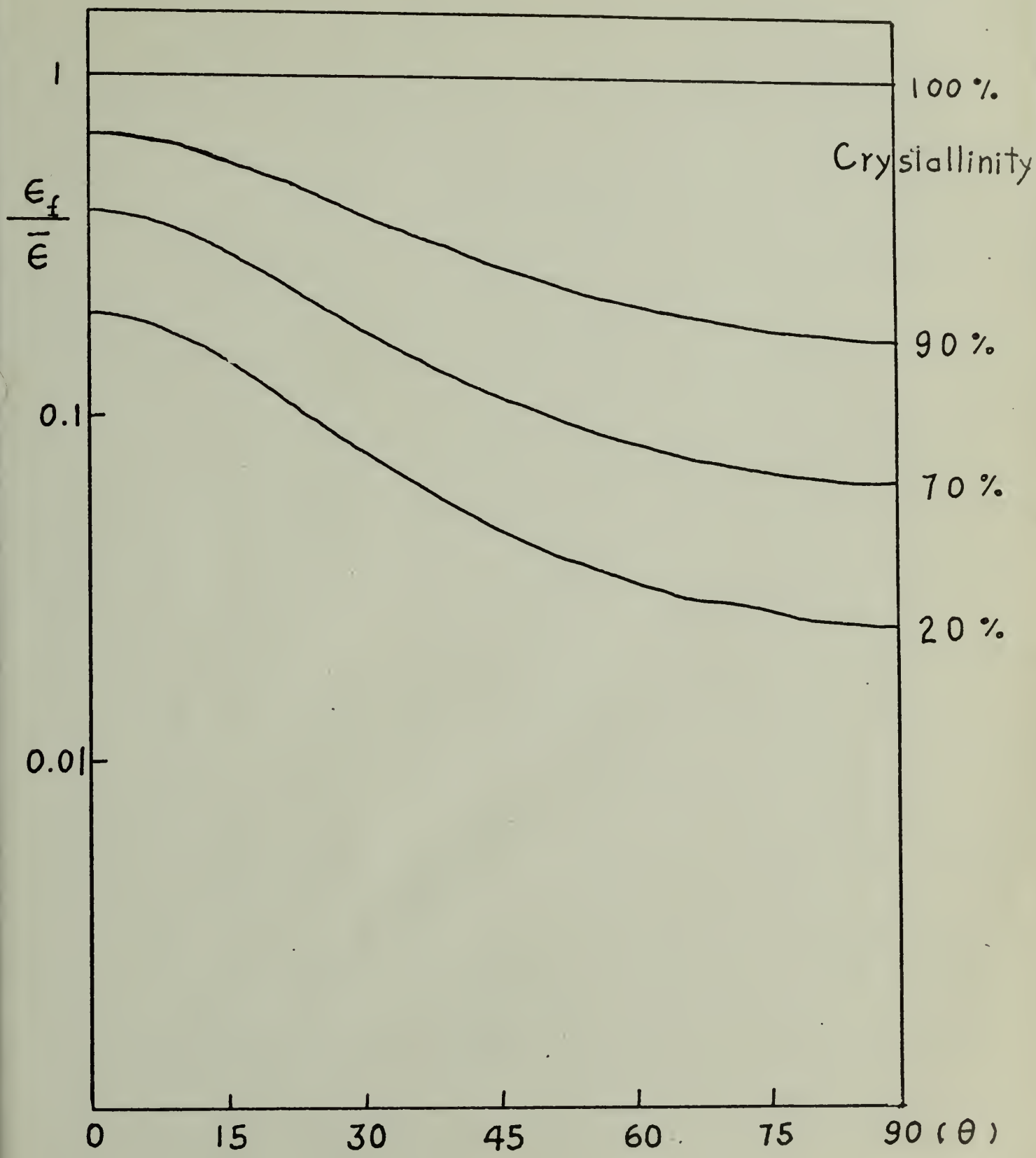

Figure VIII-4

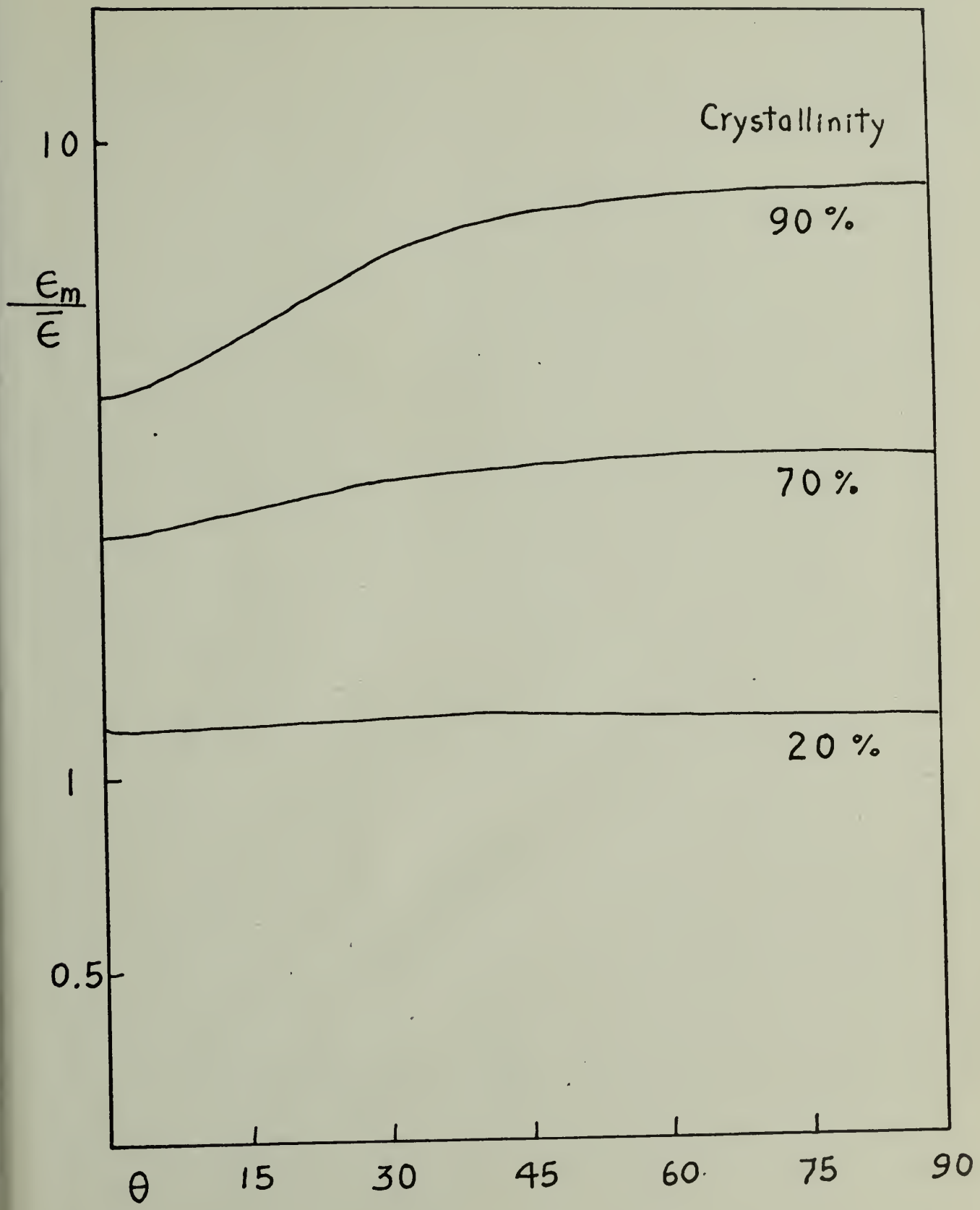

Figure VIII-5

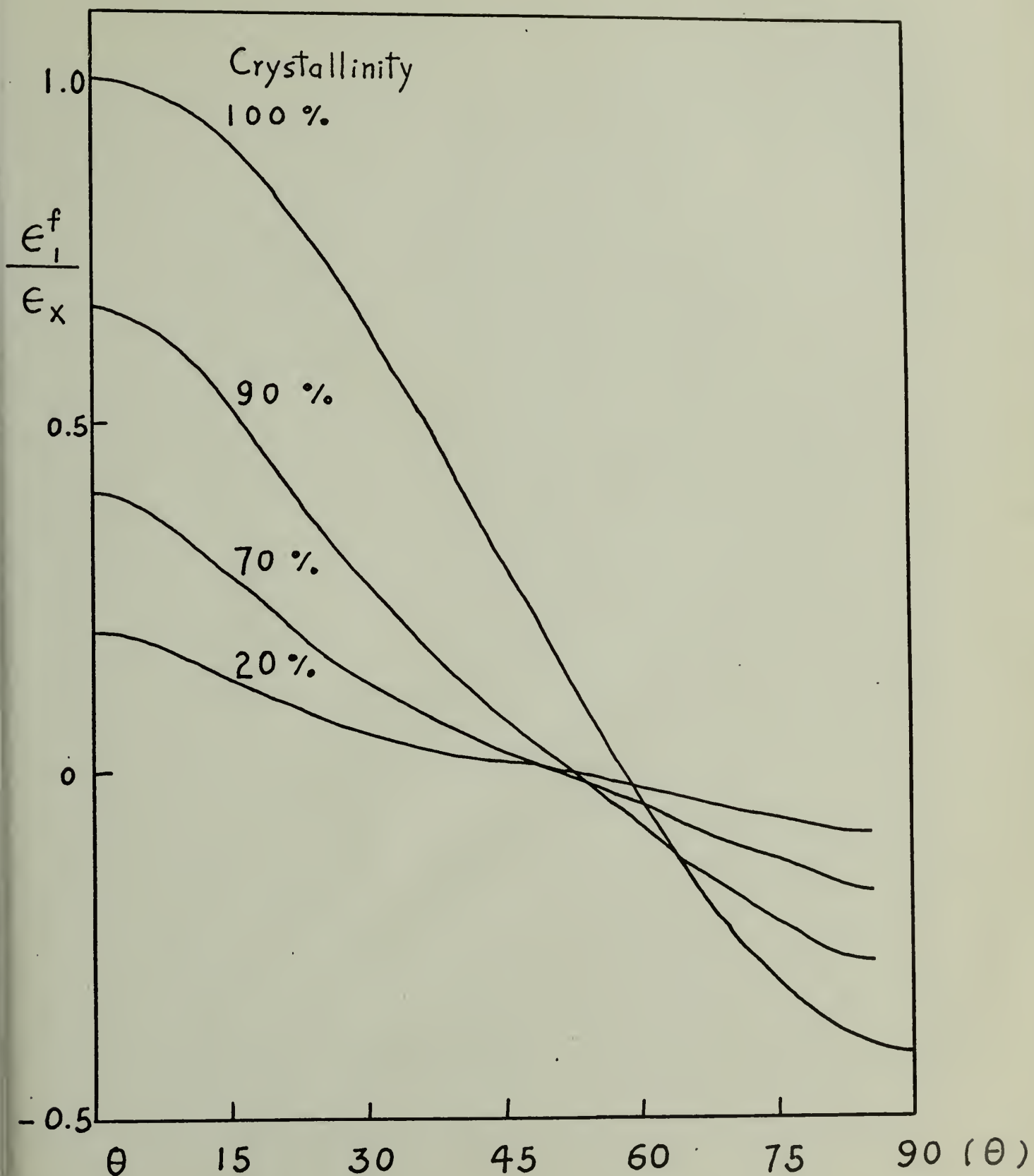

Figure VIII-6

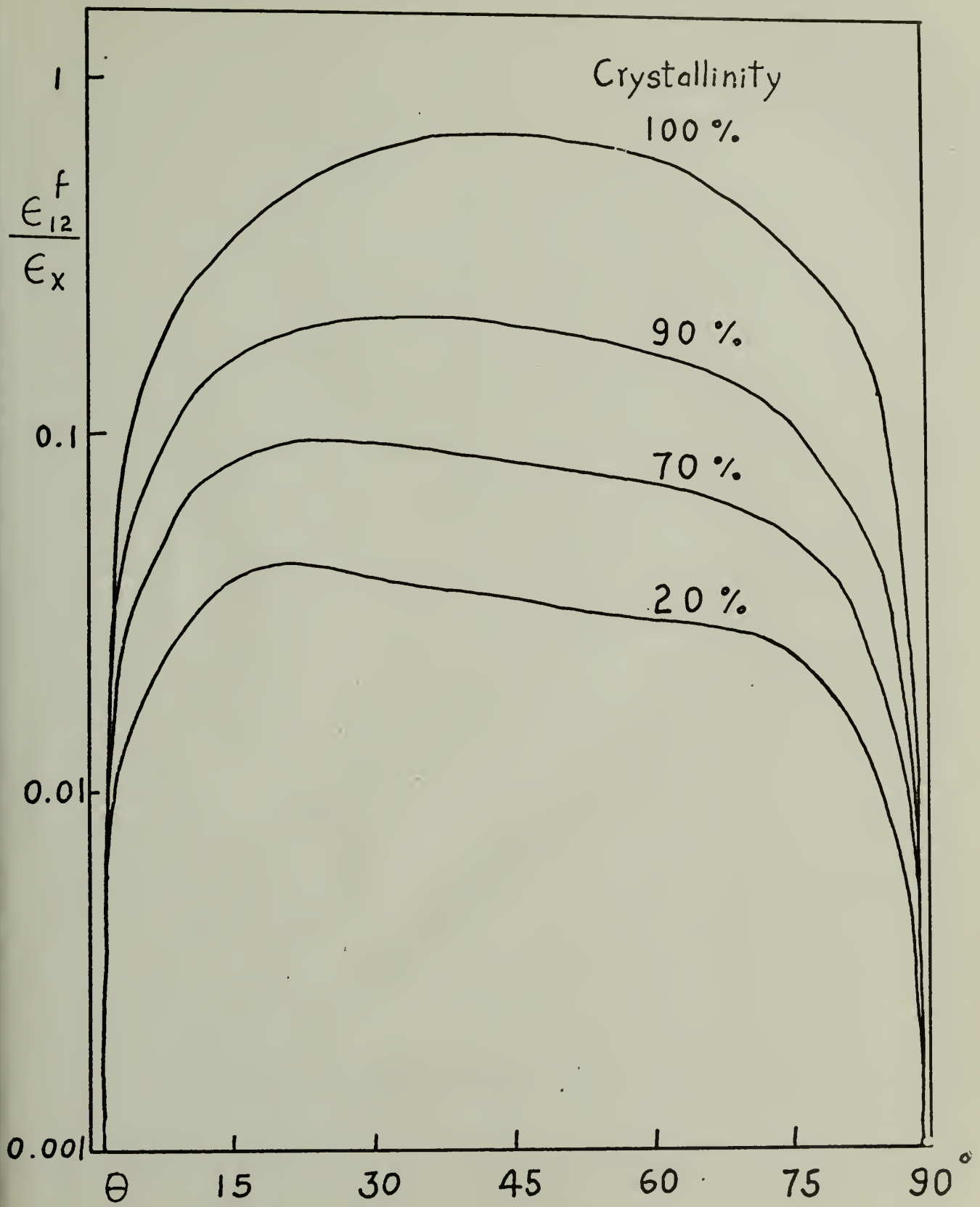

Figure VIII-7

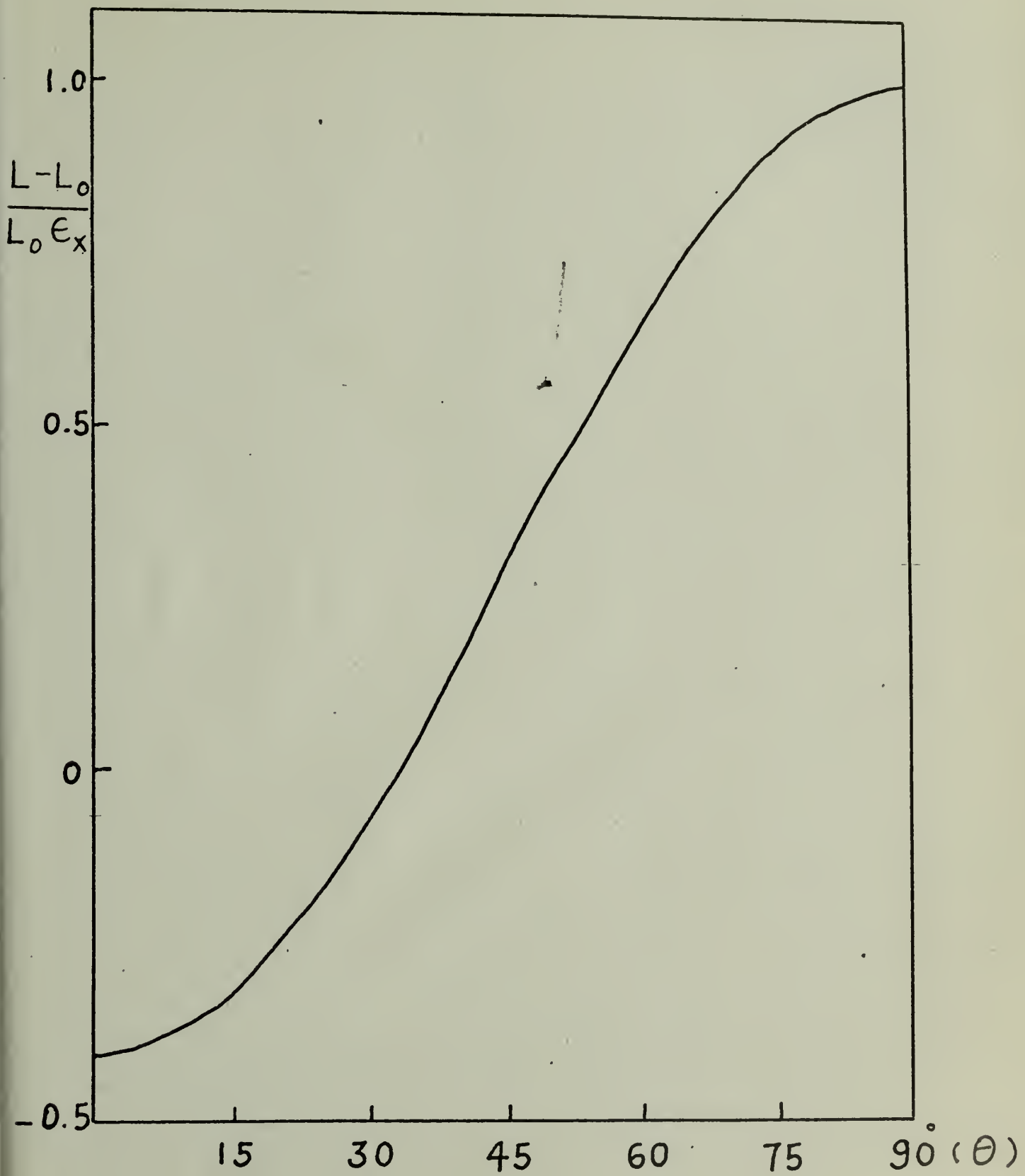

Figure VIII-8

APPENDIX

I-1. The computer program to calculate the light scattering pattern from the randomly oriented sectors.

I-2. The computer program to calculate the light scattering pattern from the disk in which the anisotropic sectors are arranged in a circular array.

II-1. The computer program to calculate the V_V scattering patterns, considering the inter-spherulitic interference.

II-2. The computer program to calculate the V_V scattering pattern from spherulites, considering the effects of the inter-spherulitic interference and truncations.

III-1. The computer program to obtain the correlation function of spherulites, and the light scattering pattern from this correlation.

IV-1. The computer program to calculate the light scattering from the disordered spherulites.

VI-1. The computer program to determine the orientation parameters from the experimental results by comparing the square deviations.

VI-2. The computer program to predict the diffraction intensity distribution for the 110 and 200 plane of the polyethylene from the orienation parameters

VI-3. The computer program to determine the dynamic orientation parameters.

VII-1. The computer program to correct the slit smearing in the small angle x-ray diffraction experiments.

VIII-1. The computer program to calculate the local strain distribution in crystalline polymers, employing the composite theory.

VII-2. The computer program to calculate the relative peak intensity of the small angle angle x-ray scattering as function of the structural parameters.

```
LIST
 10 PROGRAM YOON
 15 DIMENSION ER1(60),EI1(60),XI(60)
 20* THIS IS THE LIGHT SCATTERING FROM A SECTOR*
 30 A1=0.0003
 40 PI=3.1415926
 50 XLAM=0.00005
 60 A=0.0003
 65 BE=60.
 70 C=100000.
 75 DEL=45.
 77 DEL=DEL*PI/180.
 80 DA=0.4
 85 DAM=10.
 90 AA=0.0
 95 XMUMAX=90.
100 XK=2.*PI/XLAM
110 BE=BE*PI/180.
120 XMU1=40.
140 XMU=XMU1*PI/180.
150 A=0.
160 A=A+DA
170 TH=ASINF(1/(XK*A))
220 COSH0=COS(TH)/SQRT(COS(TH)**2+(SIN(TH)*SIN(XMU))**2)
223 M=2
225 XMU=0.
230 GAM=0.
240 DGAM=PI/50.
250 DO 500 I=1,51
260 AL=GAM-BE/2.
270  DAL=BE/50.
300 DO 400 J=1,51
310 TO=AL+DEL
320 Y=SINF(2.*TO)
330 P=COSF(XMU-AL)
350 Z=P*A
370 ER1(J)=Y/(P**2)*(Z*SINF(Z)+COSF(Z)-1.)
380 EI1(J)=Y/(P**2)*(SINF(Z)-Z*COSF(Z))
390 AL=AL+DAL
400 CONTINUE
410 SR=0.
415 SI=0.
420 DO 450 K=1,24
430 SR=SR+4.*ER1(2*K)+2.*ER1(2*K+1)
440 SI=SI+4.*EI1(2*K)+2.*EI1(2*K+1)
450 CONTINUE
460 SR=DAL/3.*(SR+ER1(1)+4.*ER1(50)+ER1(51))
470 SI=DAL/3.*(SI+EI1(1)+4.*EI1(50)+EI1(51))
480 XI(I)=SR**2+SI**2
490 GAM=GAM+DGAM
500 CONTINUE
```

```
520 DO 540 L=1,24
530 XHV=XHV+4.*XI(2*L)+2.*XI(2*L+1)
540 CONTINUE
550 XHV=XHV+XI(1)+XI(50)*4.+XI(51)
560 DEL=-DEL
570 M=M+1
580 IF(M-2)230,230,590
590 XHV=XHV*DGAM/3.
650 XHV=(A1*COSRO/Y**2)**2*XHV
655 XHV=XHV*C**2*(2.*PI/BE)**2
660 XHV=ALOG(XHV)
670  PRINT,XMU1,L,XHV
700 IF(L-LMAX)160,800,800
800 XMU1=XMU1+DXM
810 IF(XMU1-XMUMAX)140,140,820
820 END
850 ENDPROG
```

```
LIST DO3
10 PROGRAM DO
15 DIMENSION ER1(60),ER2(250),EI1(60),EI2(250)
20* THIS IS THE SCATTERING FROM A LIQUID CRYSTAL MODELZZ*
30 A1=0.0003
40 PI=3.1415926
50 XLAM=0.00005
60 W=0.0003
65 R=10.
70 WS=R*W
80 BE=45.
85 C=100000.
100 DEL=45.
105 DEL=DEL*PI/180.
110 DW=0.4
120 WMAX=8.0
130 XK=2.*PI/XLAM
150 BE=BE*PI/180.
160 XMU1=45.
170 XMU=XMU1*PI/180.
180 W=0.
190 W=W+DW
200 TH=ASINF(W/(XK*R))
300 COSRO=COS(TH)/SQRT(COS(TH)**2+(SIN(TH)*SIN(XMU))**2)
310 GAM=0.
315 WS=R*W
320 DGAM=PI/200.
330 DAL=BE/50.
340 DO 600 I=1,201
350 AL=GAM-BE/2.
360 PS=COS(XMU-GAM)
370 ZS=WS*PS
380 ZRS=ZS*SIN(ZS)+COS(ZS)-1.
390 ZIS=-ZS*COS(ZS)+SIN(ZS)
400 DO 530 J=1,51
410 TO=AL+DEL
420 Y=SINF(2.*TO)
430 P=COS(XMU-AL)
440 Z=W*P
450 ZR=Z*SIN(Z)+COS(Z)-1.
460 ZI=-Z*COS(Z)+SIN(Z)
500 ER1(J)=Y/P**2*ZR
510 EI1(J)=Y/P**2*ZI
520 AL=AL+DAL
530 CONTINUE
540 SR=0.
550 SI=0.
560 DO 580 K=1,24
565 SR=SR+4.*ER1(2*K)+2.*ER1(2*K+1)
570 SI=SI+4.*EI1(2*K)+2.*EI1(2*K+1)
580 CONTINUE
585 ER2(I)=DAL/3.*(SI+SR+ER1(1)+4.*ER1(50)+ER1(51))
587 XX=ER2(I)
590 EI2(I)=DAL/3.*(SI+EI1(1)+4.*EI1(50)+EI1(51))
593 ER2(I)=(ER2(I)*ZRS-EI2(I)*ZIS)/PS**2
```

```
597 GAM=GAM+DGAM
600 CONTINUE
610 XR=0.
620 XI=0.
630 DO 670 L=1,99
640 XR=XR+4.*ER2(2*L)+2.*ER2(2*L+1)
670 CONTINUE
680 XI=DGAM/3.*(YF+EI2(1)+4.*EI2(200)+EI2(201))
700 XHV=XR**2+XI**2
720 XHV=(A1*COSH0/(L*LS)**2)**2*XHV
730 XHV=XHV*C**2*(2.*PI/EE)**2
740 XHV=ALOG(XHV)
750 PRINT,XV(1),N,XHV
760 IF(L-NMAX)190,800,800
800 END
850 ENDPROG
```

Definition of symbols in Appendix(I-1), and (I-2):

PI: π

XLAM: The wave length of light in the medium.

R: The radius of the sector.

BE: The aperture angle of the sector.

DEL: The angle between the optic axis direction and the sector radius.

W: $kR\sin\theta$

XMU1: The azimuthal angle

XHV: The I_{Hv} intensity.

RS: The radius of the disk containing the sectors inside.

```
      PROGRAM MODEL1
      DIMENSION X(200),Y(200),DIST(200),G(200),GAMMAR(200)
      DIMENSION COSKRS(200),SINKRS(200),T(90),STORE(85,2)
      DIMENSION XIHV(85,2),XLOGIHV(85,2),AXE(85),AYE(2),EHV(85,2)
      TYPE REAL LAMBDA,MU,MUR,MUMAX,J0W,J1W,FACOR,FACT,FINT
      NU=40
      N=20
      R = 0.0003
      PI=3.1415926
      LAMBDA=0.0000428
      C=100000.
      ARMAT=-0.0003
      A1=-0.0002
      A2=0.0001
      MU=0.
      DELW=0.20
      WMAX=0.001
      PRINT 111
  111 FORMAT(5X,* V,V PATTERN FOR INTERFERENCE LIGHT SCATTERING *)
      PRINT 113,N,NU,R,A1,A2,C
  113 FORMAT(20X,* NUMBER OF SPHERULITES =*,I5,/,10X,* CONSIDERED CONFI
     1GURATION =*,I5,/,10X,* RADIUS OF SPHERULITES =*,F20.7,/,10X,*  A1
     2=*,F10.6,5X,* A2 =*,F10.6,/,10X,* CONSTANT =*,F20.5)
      JI=1
      DO 25 I=1,85
      DO 25 J=1,2
   25 XIHV(I,J)=0.
      KKK=0
   27 W = 0.10
      KKK=KKK+1
      KK=0
      MUR=MU*PI/180.
   26 THETAR = ASIN((W*LAMBDA)/(2.*PI*R))
      KK = KK+1
      COSRHO2 = COS(THETAR)/SQRT(COS(THETAR)**2+SIN(THETAR)**2*SIN(MUR)
     1**2)
      COSRHO1 = COS(THETAR)/SQRT(COS(THETAR)**2+SIN(THETAR)**2*COS(MUR)
     1**2)
      CALL BES(0,W,0,J0W,T)
      CALL BES(1,W,0,J1W,T)
      XX=2*MUR
      EHV(KK,KKK)=C*COSRHO1*PI*R**2*2./W**2*(A1*(1.-J0W)+A2*(W*J1W-(1.-
     1J0W))-(A1-A2)*COS(XX)*(2.*(1.-J0W)-W*J1W))
      W = W + DELW
      IF(W .LE. WMAX)GO TO 26
      FACT = (R**2)*(PI)
      FACT = (N*(FACT**2))
  200 I=1
  500 X=RANF(-1)*0.4
      Y=RANF(-1)*0.4
      D=(X-0.2)**2+(Y-0.2)**2
      IF(D-0.029)509,515,515
  509 X(I)=X
      Y(I)=Y
      I=I+1
  515 IF(N-I)525,500,500
```

```
525 DO 225 J=1,N
    DO 15 I=1,N
    IF (J .EQ. I) GO TO 15
    XX=((X(I)-X(J))**2)+((Y(I)-Y(J))**2)
    DIST(I)=SQRT(XX)
    G(I)=DIST(I)/(2.*R*100.)
    IF(X(J) .GT. X(I))GO TO 17
    XX=((Y(I)-Y(J))/DIST(I))
    XX=ABS(XX)
    IF(XX-1.)5,6,6
  6 IF(Y(J) .GT. Y(I))GO TO 7
    GAMMAR(I)=0.
    GO TO 15
  7 GAMMAR(I)=PI
    GO TO 15
  5 GAMMAR(I)=ACOS(XX)
    GO TO 15
 17 XX=((Y(J)-Y(I))/DIST(I))
 18 GAMMAR(I)=ACOS(XX) + PI
 15 CONTINUE
    KKK=0
205 W=0.1
    KKK=KKK+1
    KK=0
    MUR=MU*PI/180.
210 DO 80 I=1,N
    IF(I .EQ. J)GO TO 80
    COSKRS(I)=(MUR-GAMMAR(I))
    COSKRS(I)=COS(COSKRS(I))
    COSKRS(I)=2*W*G(I)*COSKRS(I)
    COSKRS(I)=COS(COSKRS(I))
 80 CONTINUE
    KK=KK+1
    ZZZ=(EHV(KK,KKK)**2)
    ZZ=0.
    DO 75 I=1,N
    IF(I .EQ. J)GO TO 75
    ZZ=ZZ+(ZZZ*COSKRS(I))
 75 CONTINUE
    XIHV(KK,KKK)=XIHV(KK,KKK)+ZZ*ZZZ
    W=W+DELW
    IF(W .LE. WMAX)GO TO 210
225 CONTINUE
    JI=JI+1
    IF(NU-JI)230,200,200
230 W=0.1
    XNU=NU
    XN=N
    PRINT 64
 64 FORMAT(/////30X,*----------*)
    J=1
    DO 220 I=1,KK
    XIHV(I,J)=XIHV(I,J)/XNU/FACT
    IF(XIHV(I,J) .LE. 0.)GO TO 220
    XLOGIHV(I,J)=ALOG(XIHV(I,J))
    W=W+0.2
```

5.48

04/07/71

```
      PRINT 142,W,XLOGIHV(I,J)
  142 FORMAT(4X,F5.3,4X,F20.10)
  220 CONTINUE
  171 STOP
      END
```

```
      SUBROUTINE BES(NO,X,KODE,RESULT,T)                          BES     1
C     C3 UCSD BES                                                           F 63
      DIMENSION T(90)
  107 FORMAT(55H1NEGATIVE ORDER NOT ACCEPTED IN BESSEL FUNCTION ROUTINE)BES     3
      KLAM=1                                                      BES     4
      KO=NO+1                                                     BES     5
      IF(X) 5,1,5                                                 BES     6
    1 IF(NO) 4,2,3                                                BES     7
    2 T(KO)=1.0                                                   BES     8
      RESULT=1.0                                                  BES     9
      RETURN                                                      BES    10
    4 IF(KO) 5,10,3                                               BES    11
    3 RESULT=0                                                    BES    12
      RETURN                                                      BES    13
   10 RESULT=9.9999999E200                                        BES    14
      RETURN                                                      BES    15
    5 PRINT 107                                                   BES    16
      STOP1                                                       BES    17
    6 IF(NC) 5,7,7                                                BES    18
    7 IF(KODE) 8,9,8                                              BES    19
    8 KLAM=KLAM+1                                                 BES    20
    9 JC=2*XFIXF(X)                                               BES    21
      MC=NC                                                       BES    22
      IF(NO-JC) 11,12,12                                          BES    23
   11 MC=JC                                                       BES    24
   12 MC=NO+11
      T(MO)=0.                                                    BES 26
      LOR=MO-1                                                     BES 27
      T(LOR)=1.0E+300                                             BES    28
      GO TO (23,51),KLAM                                          BES    29
   23 F=2*LOR                                                     BES    30
      NO=NO-3                                                     BES    31
      I2=NO                                                       BES    32
   24 F=F-2.                                                      BES    33
      T(I2+1)=F/X*T(I2+2)-T(I2+3)                                 BES    34
      IF(I2)25,26,25                                              BES    35
   25 I2=I2-1                                                     BES    36
      GO TO 24                                                    BES    37
   26 SUM=T(1)                                                    BES    38
      DO40 J=3,NO,2                                               BES    39
   40 SUM=SUM+2.*T(J)                                             BES    40
      F=1./SUM                                                    BES    41
      DO 50 J= 1,KO                                               BES    42
   50 T(J)=T(J)*F
      RESULT=T(KO)                                                BES    44
      RETURN                                                      BES    45
   51 F=2*LOR-2                                                   BES    46
      NO=NO-3                                                     BES    47
      I2=NO                                                       BES    48
  511 T(I2+1)=F/X*T(I2+2)+T(I2+3)                                 BES    49
      IF(I2)52,53,52                                              BES    50
   52 I2=I2-1                                                     BES    51
      F=F-2.                                                      BES    52
      GO TO 511                                                   BES    53
   53 SUM=T(1)                                                    BES    54
      DO 70 J=2,NO                                                BES    55
```

```
      SUM=SUM+2.*T(J)
      F=1./SUM*EXPF(X)
      DO 60 J=1,KO
      T(J)=T(J)*F
      RESULT=T(KO)
      RETURN
      END
```

```
BES   56
BES   57
BES   58
BES   59
BES   60
BES   61
BES   62
```

```
      PROGRAM MODELE 1
      DIMENSION X(20),Y(20),DIST(20,20),G(20,20),GAMMAR(20,20)
      DIMENSION ESTAR(20,20),EHV2(20,20)
      DIMENSION EHV1(20,20),TR1(50),TI1(50),SUMHVR(20),SUMHVI(20)
      DIMENSION XIHV(20),T(90),Z(50),YIHV(20),ZIHV(20)
      DIMENSION SINKRS(20,20),COSKRS(20,20)
      DIMENSION XXIHV(85,2),XLOGIHV(85,2),AXE(85),AYE(2)
      TYPE REAL LAMBDA,MU,MUR,NUMAX,J0R,J1R,FACUP,FACT,FINT
      N=20
      NN=N-1
      NINCR=50
      R=0.0001
      MU=40
      PI=3.1415926
      LAMBDA=0.000428
      C=100000.
      ARMAT=-0.0003
      ARMAT1=-0.0002
      ARMAT2=0.0001
      ARMAT3=0.0003
      RRRR=10**(-20)
      DELW=0.4
      WMAX=0.001
      MU=0.
      PRINT 2
    2 FORMAT(//////30X,*LIGHT SCATTERING     TRUNCATED SPHERULITES*)
      PRINT 3,N,R,ARMAT,C
    3 FORMAT(/////30X,*NUMBER OF SPHERULITES CONSIDERED = *,3X,I3,//30X,
     1*RADIUS OF SPHERULITES = *,3X,E9.1,3X,*(CM)*,//30X,*WAVE LENGTH =
     2 4280 A*,//30X,*POLARISABILITIES DIFFERENCE =*,3X,E10.2,//30X,
     3*CONSTANT C = *,3X,E9.1)
      DO 130 I=1,85
      DO 130 J=1,2
  130 XXIHV(I,J)=0.
      JI=1
  111 I=1
  112 XX=RANF(-1)*0.4
      YY=RANF(-1)*0.4
      DD=(XX-0.2)**2+(YY-0.2)**2
      IF(DD-0.029)113,115,115
  113 X(I)=XX
      Y(I)=YY
      I=I+1
  115 IF(N-I)180,112,112
  180 PRINT 12
   12 FORMAT(/////30X,*COORDINATES OF THE SELECTED POINTS IN MM.*,//32X,
     1*X*,10X,*Y*,//)
      PRINT 13,(X(I),Y(I),I=1,N)
   13 FORMAT(10(33X,F5.3,5X,F5.3,/))
      DO 15 I=1,NN
      II=I+1
      DO 15 J=II,N
      XX=((X(I)-X(J))**2)+((Y(I)-Y(J))**2)
      DIST(I,J)=SQRT(XX)
      G(I,J) = DIST(I,J)/(2.*R*100.)
      IF(X(I) .GT. X(J))GO TO 17
```

```
      XX=((Y(J)-Y(I))/DIST(I,J))
      IF(XX-1.)5,6,6
    6 GAMMAR(I,J)=0.000
      GO TO 15
    5 IF(ABS(XX).GT.1.0)GO TO 7
      GAMMAR(I,J)=ACOS(XX)
      GO TO 15
    7 GAMMAR(I,J)= PI
      GO TO 15
   17 XX=((Y(I)-Y(J))/DIST(I,J))
      GAMMAR(I,J)=ACOS(XX) + PI
   15 CONTINUE
      DO 19 I=1,NN
      II=I+1
      DO 18 J=II,N
      GAMMAR(J,I) = GAMMAR(I,J) + PI
   18 G(J,I) = G(I,J)
      DO 22 I=1,N
      DO 22 J=1,N
      IF (I .EQ. J)GO TO 22
      IF(G(I,J) .LT. 1.)GO TO 21
      ESTAR(I,J) = 0.
      GO TO 22
   21 ESTAR(I,J) = ACOS(G(I,J))
   22 CONTINUE
      FACT=0.0
      DO 30 I=1,N
      DO 30 J=1,N
      IF(I .EQ. J)GO TO 30
      XX=(2*ESTAR(I,J))
      FACOR=(XX-SIN(XX))
      FACT=FACT+FACOR
   30 CONTINUE
      FACT = (R**2)*(PI-(FACT/(2*N)))
      PRINT 31, FACT
   31 FORMAT(////30X,*CORRECTION FACTOR = *,4X,E12.3,///)
      FACT = (N*(FACT**2))
      PRINT 31, FACT
      KKK=0
   27 W=0.1
      KKK=KKK+1
      KK=0
      MU=KK*PI/180.
   26 THETAR = ASIN((W*LAMBDA)/(2.*PI*R))
      COSRHO2 = COS(THETAR)/SQRT(COS(THETAR)**2*SIN(THETAR)**2*SIN(MUR)
     1**2)
      COSRHO1 = COS(THETAR)/SQRT(COS(THETAR)**2*SIN(THETAR)**2*COS(MUR)
     1**2)
      CALL BES(0,W,0,J0W,T)
      CALL BES(1,W,0,J1W,T)
      ERV=C*COSRHO1*PI*R**2*2./W**2*(ARMAT1*(1.-J0W)+ARMAT2*(W*J1W+J0W
     1-1.)+ARMAT3*COS(MUR)**2*(2.*(1.-J0W)-W*J1W))
      COEF=COSRHO1*R**2
      DO 40 I=1,N
      DO 40 J=1,N
      IF(I .EQ. J)GO TO 40
```

```
      IF(G(I,J) .LT. 1.)GO TO 45
      EHVR1(I,J) = 0.
      EHVI1(I,J) = 0.
      GO TO 40
   45 CONTINUE
      DELALPHR = (2.*ESTAR(I,J))/FLOAT(NINCR-1)
      GAMMAR1 = GAMMAR(I,J) + .002
      ALPHAR1=GAMMAR1-ESTAR(I,J)
      DO 55 JJ=1,NINCR
      XX=(MUR-ALPHAR1)
      XX=COS(XX)
      WX=W*XX
      WX2 = WX**2
      XX=ABS(WX2)
      IF(XX .LE. RRRR)GO TO 60
      RRR=(ALPHAR1=GAMMAR1)
      XR2=COS(RRR)
      RRR=ABS(RRR)
      IF(XR2 .LE. RRRR)GO TO 60
      GO TO 61
   60 PRINT 56
   56 FORMAT(///30X,*DENOMINATOR EQUALS ZERO*)
      PRINT 57, WX,WX2,GAMMAR1,ALPHAR1,MUR
   57 FORMAT(//30X,*WX = *,2X,F5.3,//30X,*WX2 = *,2X,F6.3,//30X,
     1*GAMMAR1 = *,2X,F6.3,//30X,*ALPHAR1 = *,2X,F6.3,//30X,*MUR = *,
     22X,F6.3)
      STOP
   61 XX=ALPHAR1-GAMMAR1
      XX=COS(XX)
      SECANG = 1/XX
      XC = G(I,J)*WX*SECANG
      XX=COS(ALPHAR1)
      WX=SIN(WX)
      WWW=COS(WX)
      CC=COS(XC)
      CCC=SIN(XC)
      TR1(JJ)=C*(ARMAT*XX**2+ARMAT2)/WX**2*(WWW*CC+WX*WW-XC*CCC)
      TI1(JJ)=C*(ARMAT*XX**2+ARMAT2)/WX**2*(WW-CCC-WX*WWW+XC*CC)
   55 ALPHAR1 = ALPHAR1 + DELALPHR
      CALL USF(DELALPHR,TR1,Z,NINCR)
      EHVR1(I,J) = COEF*Z(NINCR)
      CALL USF(DELALPHR,TI1,Z,NINCR)
      EHVI1(I,J) = COEF*Z(NINCR)
   40 CONTINUE
      DO 69 I=1,N
      SUMHVR(I) = 0.
   69 SUMHVI(I) = 0.
      DO 70 I=1,N
      DO 70 J=1,N
      IF(I .EQ. J)GO TO 70
      SUMHVR(I) = SUMHVR(I) + EHVR1(I,J)
      SUMHVI(I) = SUMHVI(I) + EHVI1(I,J)
   70 CONTINUE
      DO 80 I=1,N
      DO 80 J=1,N
      IF(I .EQ. J)GO TO 80
```

```
      COSKRS(I,J) = (THUR-GAMMAR(I,J))
      COSKPS(I,J) = COS(COSKRS(I,J))
      COSKRS(I,J) = 2*W*G(I,J)*COSKRS(I,J)
      SINKRS(I,J) = SIN(COSKRS(I,J))
      COSKRS(I,J) = COS(COSKPS(I,J))
   80 CONTINUE
      DO 75 I=1,N
      XIHV(I) =((EHV-SUMHVR(I))**2)+ (SUMHVI(I)**2))
      YIHV(I) = 0.0
      ZIHV(I) = 0.0
      DO 76 J=1,N
      IF(I .EQ. J)GO TO 76
      YIHV(I) = YIHV(I) + (EHV*EHV-2*EHV*SUMHVR(I)+SUMHVR(I)*SUMHVR(J)
     1+SUMHVI(I)*SUMHVI(J))*COSKPS(I,J)
      ZIHV(I) =((EHV*SUMHVI(J)-SUMHVR(I)*SUMHVI(J)-EHV*SUMHVI(I)
     1+SUMHVR(J)*SUMHVI(I))*SINKPS(I,J)) + ZIHV(I)
   76 CONTINUE
      XIHV(I) = (XIHV(I)+YIHV(I)+ZIHV(I))
   75 CONTINUE
      KK=NK+1
      DO 90 I=1,N
   90 XXIHV(KK,KKK)=XXIHV(KK,KKK)+XIHV(I)/(FACT*NU)
   95 CONTINUE
      W = W + DELW
      IF(W .LE. WMAX)GO TO 20
      JI=JI+1
      IF(JI-NJ)111,111,120
  120 W=-0.5
      PRINT 64
   64 FORMAT(/////30X,*=-----------=---=-------=--*)
      DO 140 I=1,KK
      W=W+DELW
      PRINT 151,W,XXIHV(I,1)
  151 FORMAT(10X,F10.5,F30.10)
      IF(XXIHV(I,1).LE.0.)GO TO 140
      XLOGIHV(I,1)=ALOG(XXIHV(I,1))
      PRINT 145,W,XLOGIHV(I,1)
  145 FORMAT(10X,F10.5,10X,F20.7)
  140 CONTINUE
  171 STOP
      END
```

```
      SUBROUTINE QSF(H,Y,Z,NDIM)
C     DESCRIPTION OF PARAMETERS
C     H               = THE INCREMENT OF ARGUMENT VALUES.
C     Y               = THE INPUT VECTOR OF FUNCTION VALUES.
C     Z               = THE RESULTING VECTOR OF INTEGRAL VALUES.
C     NDIM            = THE DIMENSION OF VECTORS X AND Y.
      DIMENSION Z(NDIM),Y(NDIM)
      HT=.333333*H
      IF(NDIM-5)7,8,1
    1 SUM1=Y(2)+Y(2)
      SUM1=SUM1+SUM1
      SUM1=HT*(Y(1)+SUM1+Y(3))
      AUX1=Y(4)+Y(4)
      AUX1=AUX1+AUX1
      AUX1=SUM1+HT*(Y(3)+AUX1+Y(5))
      AUX2=HT*(Y(1)+3.875*(Y(2)+Y(5))+2.625*(Y(3)+Y(4))+Y(6))
      SUM2=Y(5)+Y(5)
      SUM2=SUM2+SUM2
      SUM2=AUX2+HT*(Y(4)+SUM2+Y(6))
      Z(1)=0.
      AUX=Y(3)+Y(3)
      AUX=AUX+AUX
      Z(2)=SUM2-HT*(Y(2)+AUX+Y(4))
      Z(3)=SUM1
      Z(4)=SUM2
      IF(NDIM-6)5,5,2
C                          INTEGRATION LOOP
    2 DO 4 I=7,NDIM,2
      SUM1=AUX1
      SUM2=AUX2
      AUX1=Y(I-1)+Y(I-1)
      AUX1=AUX1+AUX1
      AUX1=SUM1+HT*(Y(I-2)+AUX1+Y(I))
      Z(I-2)=SUM1
      IF(I-NDIM)3,6,6
    3 AUX2=Y(I)+Y(I)
      AUX2=AUX2+AUX2
      AUX2=SUM2+HT*(Y(I-1)+AUX2+Y(I+1))
    4 Z(I-1)=SUM2
    5 Z(NDIM-1)=AUX1
      Z(NDIM)=AUX2
      RETURN
    6 Z(NDIM-1)=SUM2
      Z(NDIM)=AUX1
      RETURN
C                                END OF INTEGRATION LOOP
    7 IF(NDIM-3)12,11,8
    8 SUM2=1.125*HT*(Y(1)+Y(2)+Y(2)+Y(2)+Y(3)+Y(3)+Y(3)+Y(4))
      SUM1=Y(2)+Y(2)
      SUM1=SUM1+SUM1
      SUM1=HT*(Y(1)+SUM1+Y(3))
      Z(1)=0.
      AUX1=Y(3)+Y(3)
      AUX1=AUX1+AUX1
      Z(2)=SUM2-HT*(Y(2)+AUX1+Y(4))
      IF(NDIM-5)10,9,9
```

```
    9 AUX1=Y(4)+Y(4)
      AUX1=AUX1+AUX1
      Z(5)=SUM1+HT*(Y(3)+AUX1+Y(5))
   10 Z(3)=SUM1
      Z(4)=SUM2
      RETURN
   11 SUM1=HT*(1.25*Y(1)+Y(2)+Y(2)-.25*Y(3))
      SUM2=Y(2)+Y(2)
      SUM2=SUM2+SUM2
      Z(3)=HT*(Y(1)+SUM2+Y(3))
      Z(1)=0.
      Z(2)=SUM1
   12 RETURN
      END
```

Definition of symbols in Appendix(II-1), and (II-2):

R: The radius of spherulites.

LAMBDA: The wavelength of light in the medium.

NU: The number of sets of spherulites.

N: The number of spherulites in each set.

MU: The azimuthal angle.

W: $kR\sin\theta$

XIHV: The I_{V_V} intensity.

A1: $\alpha_r - \alpha_s$

A2: $\alpha_t - \alpha_s$

J1W: The first order Bessel function.

J0W: The zero order Bessel function.

FACT: The normalization parameter to compare with the single spherulite case.

RANF(-1): The random number generator between 0 and 1.

X, Y: The coordinate for the center of spherulite.

GAMMAR: The angle between the vector connecting the centers of two spherulites and the polarization direction of the polarizer.

ESTAR: The angle of the truncation.

```
LIST
10 PROGRAM DEBYE
13 DIMENSION R(30,30),A(30),B(30),FC(30),FS(30)
15 E1=0.
20 PI=3.1415926
25 DO 29 I=1,21
26 DO 29 J=1,21
27 R(I,J)=0.
29 CONTINUE
30 DO 500 X=1.,51.
35 PRINT 37,X
37 FORMAT(1X,F5.2)
40 DO 490 Y=1.,51.
50 Z=(X-1.-25.)**2+(Y-1.-25.)**2
60  IF(Z-625.)75,75,490
75 A1=Y-1.-25.
80 A2=SQRT(Z)
85 BB=A1/A2
87 IF(ABSF(BB)-1.)90,90,120
90 IF(X-26.)93,93,100
93 AL1=PI+ACOS(-BB)
95 GO TO 130
100 AL1=ACOSF(BB)
105 GO TO 130
120 IF(BB)122,122,127
122 AL1=PI
125 GO TO 130
127 AL1=0.
130 AL2=2.*AL1
135 EE1=-3.*COSF(AL1)**2+4.
140 E1=E1+EE1**2
150 XR=0.
155 DO 480 I=1,11
160 ALP=0.
165 DO 470 J=1,7
170 XX=X+XR*SINF(ALP)
175 YY=Y+XR*COSF(ALP)
180 ZZ=(XX-1.-25.)**2+(YY-1.-25.)**2
183 IF(ZZ-625.)185,185,460
185 AA1=YY-1.-25.
190 AA2=SQRT(ZZ)
195 CC=AA1/AA2
197 IF(ABSF(CC)-1.)200,220,220
200 IF(XX-26.)202,202,210
202 AAL1=PI+ACOSF(-CC)
205 GO TO 230
210 AAL1=ACOSF(CC)
215 GO TO 230
220 IF(CC)223,223,227
223 AAL1=PI
225 GO TO 230
227 AAL1=0.
230 AAL2=2.*AAL1
235 EE2=-3.*COSF(AAL1)**2+4.
```

```
240 R(I,J)=R(I,J)+EE1*EE2
460 ALP=ALP+PI/12.
470 CONTINUE
475 XR=XR+5.
480 CONTINUE
490 CONTINUE
500 CONTINUE
510 DO 550 I=1,11
520 DO 550 J=1,7
530 R(I,J)=R(I,J)/E1
535 PRINT 540,I,J,R(I,J)
540 FORMAT(1X,2I6,F15.4)
550 CONTINUE
600 INPUT,XU
605 XU=XU/180.*PI
610 W=0.
615 XR=0.
620 DO 800 I=1,11
640 AL=0.
645 DO 730 J=1,25
647 JX=J-1
650 J1=JX/12
655 J2=JX-J1*12
657 IF(J2-6)670,670,660
660 J2=12-J2
670 J3=J2+1
675 Y1=COSF(XU-AL)
680 Y2=W*XR*Y1
685 Y3C=COSF(Y2)
690 Y3S=SINF(Y2)
700 A(J)=R(I,J3)*Y3C
710 B(J)=R(I,J3)*Y3S
720 AL=AL+PI/12.
730 CONTINUE
740 C1=0.
750 S1=0.
760 DO 780 K=1,11
765 C1=C1+4.*A(2*K)+2.*A(2*K+1)
770 S1=S1+4.*B(2*K)+2.*B(2*K+1)
780 CONTINUE
785 FC(I)=PI/36.*(C1+A(1)+4.*A(24)+A(25))
786 FC(I)=FC(I)*XR
787 FS(I)=PI/36.*(S1+B(1)+4.*B(24)+B(25))
789 FS(I)=FS(I)*XR
790 XR=XR+0.2
800 CONTINUE
810 GC=0.
815 GS=0.
820 DO 840 L=1,4
830 GC=GC+4.*FC(2*L)+2.*FC(2*L+1)
835 GS=GS+4.*FS(2*L)+2.*FS(2*L+1)
840 CONTINUE
```

```
850 GC=0.2/3.*(GC+FC(1)+4.*FC(10)+FC(11))
855 GS=0.2/3.*(GS+FS(1)+4.*FS(10)+FS(11))
860 HV=GC**2+GS**2
870 XHV=ALOG(HV)
880 PRINT 890,W,XHV
890 FORMAT(1X,F5.1,10X,F10.4)
900 W=W+1.
910 IF(W-9.)615,615,600
950 END
960 ENDPROG
```

Definition of symbols in Appendix(III-1):

E1: The total suare fluctuation for a spherulite.

R(I,J): The sum of products of fluctuations between the volume elements separated by the Ith angular coordinate and the Jth separation distance coordinate in a spherulite.

X, Y: The coordinates representing the location of volume elements in a spherulite.

AL1: The orientation of optic axis at the location(X,Y).

EE1: The fluctuation at (X,Y) position in a spherulite (the equation shows the case for the V_v scattering when $(\alpha_r-\alpha_t)$ is -3, and $(\alpha_t-\alpha_b)$ is 4.)

EE2: The fluctuation at the position separated by the Ith angular coordinate and the Jth distance coordinate from the volume element at (X,Y).

XU: The azimuthal angle.

XHV: The scattering intensity.

* In this numerical calculation, the center of spherulite is located at the position(25,25), and the radius is 25 in the scale used.

```
LIST
 5 PROGRAM DISK
 10 DIMENSION A(700),D(700),E1(10,20),E2(10,20),AYH(10,20)
 11 DIMENSION SI1(40),COT(40),ABC(100,20)
 13 M1=100
 14 AM1=M1
 15 M2=100/X1
 17 M3=1
 20 CA=0.01
 22 PI=3.141592654
 24 DA=0.3
 26 AMU=PI/4.
 27 R=3.
 28 DO 34 K=1,20
 29 XK=K
 30 ST=XK*0.35/(R*2.*PI)
 31 SI1(K)=ST*SINF(AMU)/SQRT(1.-ST**2+ST**2*SINF(AMU)**2)
 32 COT(K)=SQRT(1.-SI1(K)**2)
 34 CONTINUE
 35 DO 38 L=1,10
 36 DO 38 L5=1,20
 37 AYH(L,L5)=0.
 38 CONTINUE
 40 DO 48 K=1,10
 41 DO 48 K5=1,20
 43 E1(K,K5)=0.
 45 E2(K,K5)=0.
 48 CONTINUE
 49
 50 X1R=1.
 51 DO 65 J=1,100
 52 XJ=J
 53 DO 65 L=1,20
 55 XXL=L
 57 S2=XJ*XXL/100.
 59 ABC(J,L)=S2
 65 CONTINUE
 67 DO 705 I=1,M1
 69 X1=I
 71 L=I-1
 73 X=2.*PI*X1
 75 I1=X
 77 IT=I/20
 78 ITI=IT*20
 80 IF(I-ITI)83,83,85
 83 PRINT 84,I
 84 FORMAT(1X,I3)
 85 I2=RANF(-1)*X
 90 IF(L)95,95,105
 95 A(I2)=0.
 100 GO TO 200
```

```
105 IG=(L*I2)/I
110 IF(D(IG))115,115,125
115 B=0.5-0.5*(1.-EXPF(D(IG)*CA))
120 GO TO 130
125 B=0.5+0.5*(1.-EXPF(-D(IG)*CA))
130 AA=RANF(-1)
150 IF(AA-B)160,160,180
160 A(I2)=D(IG)-1.
170 GO TO 200
180 A(I2)=D(IG)+1.
200 K1=1
205 K2=I2
210 K1=K1+1
215 IF(K1-I1)220,220,500
220 K2=K2+1
225 IF(K2-I1)230,230,250
230 J=K2
240 GO TO 255
250 J=K2-I1
253 IF(J-1)260,260,255
255 I3=(L*J)/I
256 K3=J-1
258 GO TO 280
260 I3=1
270 K3=I1
280 IF(L)290,290,310
290 BB=A(K3)
300 GO TO 320
310 BB=(D(I3)+A(K3))/2.
320 IF(BB)330,330,350
330 B=0.5-0.5*(1.-EXPF(BB*CA))
340 GO TO 360
350 B=0.5+0.5*(1.-EXPF(-BB*CA))
360 XX=RANF(-1)
400 IF(XX-B)410,410,450
410 A(J)=BB-1.
420 GO TO  210
450 A(J)=BB+1.
460 GO TO 210
500 GO TO 510
510 M3=2.*PI*X1R
513 XM3=M3
515 AL=0.
520 DAL=2.*PI/XM3
525 M4=M3/I1
530 DO 670 J1=1,M3
535 M5=(J1-1)/M4+1
540 IR=M1R
550 SIA2=SINF(2.*AL)
553 XMU=PI/4.
```

```
555 COM=COSF(XMU-AL)
560 KKK=2
563 DO 655 K5=1,10
565 S3=ARC(IR,KKK)*COM
566 S3C=COSF(S3)
567 S3S=SINF(S3)
568 DA=0.
570 DO 650 L=1,6
585 DEL=A(K5)*DA
590 S1=(3.*SINF(DEL)**2-1.)/2.*SIA2
595 E1(L,K5)=E1(L,K5)+S1*S3C
600 E2(L,K5)=E2(L,K5)+S1*S3S
640 DA=DA+0.05
650 CONTINUE
653 KKK=KKK+2
655 CONTINUE
660 AL=AL+DAL
670 CONTINUE
673 X1R=X1R+1.
675 M6=(X1R-1.)*XM1/100.+1.
677 IF(M6-I)510,510,685
685 DO 700 K=1,I1
690 D(K)=A(K)
700 CONTINUE
705 CONTINUE
725 DD2=1.
727 DO 750 J5=1,10
730 DO 750  J=1,6
740 XYH(J,J5)=XYH(J,J5)+(E1(J,J5)**2+E2(J,J5)**2)*DD2
750 CONTINUE
770 N3=N3+1
775 PRINT,N3
780 IF(N3-5)40,40,800
800 DO 850 J=1,6
810 DO 850 J5=1,10
820 WW=XYH(J,J5)*0.0001
825 WW1=ALOG(WW)
830 PRINT 835,J,J5,WW,WW1
835 FORMAT(1X,2I5,F20.5,F20.5)
850 CONTINUE
900 END
910 ENDPROG
```

Definition of symbols in Appendix(IV-1).

M1: The number of lattice cells along the radius.

CA: The parameter representing the tendency to return to the original orientation of optic axis.

R: The radius of spherulite in μ.

ST: sin θ

XYH(I,J): The scattering intensity at the Jth W position for the Ith disorder parameter δ.

BB: The average fluctuation of the nearest neighbors.

A(I): The orientation fluctuation of crystal in the Ith lattice cell of the lattice layer in consideration.

D(I): The set of orientation fluctuation of crystals in the previous lattice layer.

XMU: The azimuthal angle.

B: The probability to have negative fluctuation.

RANF(-1): The random number generator between 0 and 1.

DA: The orientation fluctuation parameter δ.

DEL: The orientation fluctuation in the lattice cell.

* The sample program shown here was used to calculate the light scattering from disordered spherulite Case(3), where the twisting angle fluctuates randomly. Other cases can be easily calculated by changing the statement 590.

```
LIST
10 PROGRAM PARAM
15 DIMENSION FE(10),FEE(10)
20 DIMENSION AL(10),FC(10),FA(10)
22 DIMENSION FCC(10),FAA(10),AN(100)
23 DIMENSION ZSA(60,6),ZCA(60,6),ZG(60,6),ZBE(60,6)
25 N=4
30 READ 35,(AL(I),FC(I),FA(I),FE(I),I=1,N)
35 FORMAT(5,4F7.3)
40 PRINT 45,(AL(I),FC(I),FA(I),FE(I),I=1,N)
45 FORMAT(1A,4F10.3)
50 DK=0.025
60 DM=0.025
70 DF=0.05
75 SAM=1.
80 AMK=1.3
90 AMM=1.4
95 AEC=0.002
100 AMF=1.5
105 BE0=3.1415926/2.
110 AK=1.1
115 DAL=3.1415926/50.
120 AMU=1.0
125 A1=0.03
127 A2=0.03
130 I=1
140 AL2=SQRT(1./AL(I))
150 AL=0.
160 DO 300 K=1,51
163 CO=COSF(AL)
165 SI=SINF(AL)
170 CA=AL(I)*CO/SQRT((XL2*SI)**2+(XL(I)*CO)**2)
175 ZCA(K,I)=CA
180 X=AK*(XL(I)**2-XL2**2)*CA**2
190 BE=BE0*EXPF(-X)
195 ZBE(K,I)=BE
200 SA=XL2*SI/SQRT((XL2*SI)**2+(XL(I)*CO)**2)
205 ZSA(K,I)=SA
210 Y=XMU*(XL(I)**2-XL2**2)*SA**2
220 G=1.-EXPF(-Y)
225 ZG(K,I)=G
230 CC=(1.+G)/2.*(SIN(BE)*SA)**2+(COS(BE)*CA)**2
240 AN(K)=CC*SI
290 AL=AL+DAL
300 CONTINUE
310 DD=0.
320 DO 350 J=1,24
330 DD=DD+4.*AN(2*J)+2.*AN(2*J+1)
350 CONTINUE
360 DD=DAL/3.*(DD+AN(1)+4.*AN(50)+AN(51))
370 AA=DD/2.
380 OF=(3.*AA-1.)/2.
390 IF(OF.LE.FC(I)+A1.AND.OF.GE.FC(I)-A1)GO TO 500
400 XMU=XMU+DM
410 IF(XMU-XMM)420,420,430
```

```
420 GO TO 130
430 AK=AK+DK
435 PRINT,AK
440 IF(AK-AMK)450,450,1030
450 GO TO 120
500 I=I+1
505 FCC(I-1)=0.
510 IF(I-N)140,140,540
540 P=1.0
550 I=1
560 AL2=SQRT(1./AL(I))
570 AL=0.
580 DO 700 L=1,51
590 CA=ZCA(L,I)
610 BE=ZBE(L,I)
620 SA=ZSA(L,I)
640 G=ZG(L,I)
650 H=EXP(-P*(AL(I)**2-AL2**2)*CA**2)
660 CC=SIN(BE)**2*CA**2*(1.-H)/2.
665 CC=CC+SA**2*(1.+H)/2.*(1.-G)/2.+(COS(BE)*SA)**2*(1.+G)*
666A (1.-H)/4.
680 AN(L)=CC*SIN(AL)
690 AL=AL+DAL
700 CONTINUE
710 DD=0.
720 DO 740 M=1,24
730 DD=DD+4.*AN(2*M)+2.*AN(2*M+1)
740 CONTINUE
750 DD=DAL/3.*(DD+AN(1)+4.*AN(50)+AN(51))
760 AA=DD/2.
770 FF=(3.*AA-1.)/2.
780 IF(FF.LE.FA(I)+A2.AND.FF.GE.FA(I)-A2)GO TO 850
790 P=P+DP
800 IF(P-AMP)550,550,400
850 I=I+1
855 FAA(I-1)=FF
860 IF(I-N)560,560,870
870 I=1
880 FBB(I)=-FCC(I)-FAA(I)
890 IF(FBB(I).LE.FB(I)+A2.AND.FBB(I).GE.FB(I)-A2)GO TO 910
900 GO TO 790
910 I=I+1
920 IF(I-N)880,880,953
953 SM1=0.
955 SM2=0.
957 SM3=0.
960 DO 970 J=1,N
963 SM1=SM1+(FC(J)-FCC(J))**2
965 SM2=SM2+(FA(J)-FAA(J))**2
967 SM3=SM3+(FB(J)-FBB(J))**2
970 CONTINUE
973  SM1=SM1+SM2+SM3
975 IF(SMM-SM1)790,790,980
980 AKK=AK
982 AMUU=AMU
985 APP=P
```

```
990 SRM=SR1
1000 PRINT 1010,AKK,AMUU,XPP,SRM
1010 FORMAT(1X,3F7.2,F10.6)
1020 GO TO 790
1030 END
1040 ENDPROG
```

```
LIST
10 PROGRAM XRAY
20 DIMENSION G(200),BE(200),ATH(200),ATH(200),AN(200)
22 DIMENSION H(101),ZCA(101),ZSA(101)
30 DIMENSION AL(100),ZTH(100)
35 DIMENSION A4TH(60),BTH(60),B4TH(60)
40 DTH=3.1415926/50.
50 P=2.0
60 PI=3.141592654
70 DEE=PI/25.
80 DOM=PI/25.
85 I=1
90 AL3=1.15
95 AL(I)=AL3
100 AL2=1./SQRT(AL3)
105 BE0=3.1415926/2.
110 AK=0.9
115 DAL=3.1415926/50.
120 AMU=1.5
125 DO 135 J=1,51
130 ATH(J)=0.
133 ZTH(J)=0.
135 CONTINUE
140 Z=ATANF(4.94/7.41)
143 CZ=COSF(Z)
145 SZ=SINF(Z)
150 AL=0.
160 DO 300 K=1,51
163 CO=COSF(AL)
165 SI=SINF(AL)
170 CA=AL3*CO/SQRT((AL2*SI)**2+(AL3*CO)**2)
175 ZCA(K)=CA
180 X=AK*(AL(I)**2-AL2**2)*CA**2
190 BE(K)=BE0*EXPF(-X)
200 SA=AL2*SI/SQRT((AL2*SI)**2+(AL3*CO)**2)
205 ZSA(K)=SA
210 Y=AMU*(AL(I)**2-AL2**2)*SA**2
220 G(K)=1.-EXPF(-Y)
230 H(K)=EXPF(-P*(AL3**2-AL2**2)*CA**2)
290 AL=AL+DAL
300 CONTINUE
310 AL=0.
320 DO 600 K=1,50
330 XBE=BE(K)
335 RBS=SINF(XBE)
340 RBC=COSF(XBE)
343 QS=SINF(AL)
350 CA=ZCA(K)
360 SA=ZSA(K)
370 XH=H(K)
```

```
380 XG=G(K)
390 OM=0.
400 DO 550 N=1,50
403 SOS=SINF(OM)
405 SOC=COSF(OM)
407 SO2=COSF(2.*OM)
410 EE=0.
415 AA=0.5+XG*SO2
420 DO 520 L=1,50
423 SES=SINF(EE)
425 SEC=COSF(EE)
427 SE2=COSF(2.*EE)
430 CC=SES*CA*SES+SA*(SEC*SOS+SEC*SOC*SES)
431A
435 C1=SES*SEC*CA-SA*(SOS*SES-SOC*SEC*SEC)
438  CD=CZ*C1+SZ*CC
450 YY=0.5+XH*SE2
455 DA=ACOS(CC)*50./PI+1.
460 DD=ACOS(CD)*50./PI+1.
465 MA=DA
470 M=DD
475 Z1H(MA)=Z1H(MA)+AA*YY*QS
480 X1H(M)=X1H(M)+AA*YY*QS
490 EE=EE+DEE
520 CONTINUE
530 OM=OM+DOM
550 CONTINUE
590 AL=AL+DAL
595 PRINT,K
600 CONTINUE
610 DO 700 L=1,51
630 X1=L-1
640 1H=X1*PI/50.+D1H/2.
650 A1H(L)=X1H(L)*COS(1H)**2
655 A41H(L)=X1H(L)*COS(1H)**4
660 B1H(L)=Z1H(L)*COS(1H)**2
665 B41H(L)=Z1H(L)*COS(1H)**4
666A
700 CONTINUE
710 F11=0.
715 F12=0.
720 F14=0.
725 F21=0.
730 F22=0.
735 F24=0.
740 DO 800 M=1,24
745 F11=F11+4.*X1H(2*M)+2.*X1H(2*M+1)
750 F12=F12+4.*A1H(2*M)+2.*A1H(2*M+1)
755 F14=F14+4.*A41H(2*M)+2.*A41H(2*M+1)
760 F21=F21+4.*Z1H(2*M)+2.*Z1H(2*M+1)
```

```
765 F22=F22+4.*B1H(2*M)+2.*B1H(2*M+1)
770 F24=F24+4.*B41H(2*M)+2.*B41H(2*M+1)
800 CONTINUE
810 F11=F11+A1H(1)+4.*A1H(50)+A1H(51)
815 F12=F12+A1H(1)+4.*A1H(50)+A1H(51)
820 F14=F14+A41H(1)+4.*A41H(50)+A41H(51)
825 F21=F21+Z1H(1)+4.*Z1H(50)+Z1H(51)
830 F22=F22+B1H(1)+4.*B1H(50)+B1H(51)
835 F24=F24+B41H(1)+4.*B41H(50)+B41H(51)
840 C11=F12/F11
845 C14=F14/F11
850 C21=F22/F21
855 C24=F24/F21
860 F012=(3.*C11-1.)/2.
865 F014=(35.*C14-30.*C11+3.)/8.
870 F022=(3.*C21-1.)/2.
875 F024=(35.*C24-30.*C21+3.)/8.
880 PRINT 885
885 FORMAT(1X,5X,* AZIMUTHAL ANGLE*,5X,*      110*,  5X,*  200*)
900  DO 950 L=1,51
910 X1=L-1
920 TH=X1*PI/50.+D1H/2.
925 T1=TH*180./PI
930 X1=A1H(L)/(F11*SIN(TH))
935 X2=Z1H(L)/(F21*SIN(TH))
945 PRINT 947,T1,X1,X2
947 FORMAT(1X,F15.2,F8.4,F15.4)
950 CONTINUE
960 PRINT 970,XL3,XK,XMU,P
970 FORMAT(1X,* SIMAIN =*,F5.2,*     K=*,F5.2,    *  XMU=*,
971A F5.2,*       P=*,F5.2)
980 PRINT 985,F012,F014,F022,F024
985 FORMAT(1X,* F110=*,F7.3,*  F1104=*,F8.3,*    F200=*,F8.3,
986A *    F2004=*,F8.3)
1000 END
1010 ENDPROG
```

```
LIST
10 PROGRAM PARAM
15 DIMENSION FB(10),FBB(10)
20 DIMENSION XL(10),FC(10),FA(10)
22 DIMENSION FCC(10),FAA(10),XN(100)
23 DIMENSION ZSA(60,6),ZCA(60,6),ZG(60,6),ZBE(60,6)
25 N=2
27 READ,ST1,OFA,OFB,OFC,AK1,XMU1,XP1
29  ST2=ST1**2-1./ST1
30 READ 35,(XL(I),FC(I),FA(I),FB(I),I=1,N)
35 FORMAT(5,4F7.3)
40 PRINT 45,(XL(I),FC(I),FA(I),FB(I),I=1,N)
45 FORMAT(1X,4F10.3)
50 DK=0.01
51 ASK=ST2*AK1
52 ASM=ST2*XMU1
53 ASP=ST2*XP1
60 DM=0.01
70 DP=0.01
75 SHM=1.
80 AMK=2.0
90 XMM=1.0
95 ABC=0.002
100 XMP=2.0
105 BEO=3.1415926/2.
110 AK=0.
115 DAL=3.1415926/50.
120 XMU=0.
125 A1=0.01
127 A2=0.01
130 I=1
140 XL2=SQRT(1./XL(I))
145 ST3=XL(I)**2-XL2**2
147 ST4=XL(I)-ST1
150 AL=0.
160 DO 300 K=1,51
163 CO=COSF(AL)
165 SI=SINF(AL)
170 CA=XL(I)*CO/SQRT((XL2*SI)**2+(XL(I)*CO)**2)
175 ZCA(K,I)=CA
180 X=(ASK+(ST3-ST2)*AK)*CA**2
190 BE=BEO*EXPF(-X)
195 ZBE(K,I)=BE
200 SA=XL2*SI/SQRT((XL2*SI)**2+(XL(I)*CO)**2)
205 ZSA(K,I)=SA
210 Y=(ASM+(ST3-ST2)*XMU)*SA**2
220 G=1.-EXPF(-Y)
225 ZG(K,I)=G
230 CC=(1.+G)/2.*(SIN(BE)*SA)**2+(COS(BE)*CA)**2
240 XN(K)=CC*SI
290 AL=AL+DAL
300 CONTINUE
310 DD=0.
320 DO 350 J=1,24
330 DD=DD+4.*XN(2*J)+2.*XN(2*J+1)
```

```
350 CONTINUE
360 DD=DAL/3.*(DD+AN(1)+4.*AN(50)+AN(51))
370 AA=DD/2.
380 OF=(3.*AA-1.)/2.
383 OF=OF-OFC
385 OF=OF/S14
390 IF(OF.LE.FC(I)+A1.AND.OF.GE.FC(I)-A1)GO TO 500
400 AMU=AMU+DM
410 IF(AMU-AMM)420,420,430
420 GO TO 130
430 AK=AK+DK
435 PRINT,AK
440 IF(AK-AMK)450,450,1030
450 GO TO 120
500 I=I+1
505 FCC(I-1)=OF
510 IF(I-N)140,140,540
540 P=0.
550 I=1
560 AL2=SQRT(1./XL(I))
565 S13=XL(I)**2-XL2**2
567 S14=XL(I)-S11
570 AL=0.
580 DO 700 L=1,51
590 CA=ZCA(L,I)
610 BE=ZBE(L,I)
620 SA=ZSA(L,I)
640 G=ZG(L,I)
650 H=EXPF((XSP+(S13-S12)*P)*(-1.)*CA**2)
660 CC=SIN(BE)**2*CA**2*(1.-H)/2.
665 CC=CC+SA**2*(1.+H)/2.*(1.-G)/2.+(COS(BE)*SA)**2*(1.+G)*
666A (1.-H)/4.
680 AN(L)=CC*SIN(AL)
690 AL=AL+DAL
700 CONTINUE
710 DD=0.
720 DO 740 M=1,24
730 DD=DD+4.*AN(2*M)+2.*AN(2*M+1)
740 CONTINUE
750 DD=DAL/3.*(DD+AN(1)+4.*AN(50)+AN(51))
760 AA=DD/2.
770 FF=(3.*AA-1.)/2.
773 FF=FF-OFA
775 FF=FF/S14
780 IF(FF.LE.FA(I)+A2.AND.FF.GE.FA(I)-A2)GO TO 850
790 P=P+DP
800 IF(P-XMP)550,550,400
850 I=I+1
855 FAA(I-1)=FF
860 IF(I-N)560,560,870
870 I=1
880 FBB(I)=-FCC(I)-FAA(I)
890 IF(FBB(I).LE.FB(I)+A2.AND.FBB(I).GE.FB(I)-A2)GO TO 910
900 GO TO 790
910 I=I+1
```

```
920 IF(I-N)880,880,953
953 SM1=0.
955 SM2=0.
957 SM3=0.
960 DO 970 J=1,N
963 SM1=SM1+(FCC(J)-FCC(J))**2
965 SM2=SM2+(FAA(J)-FAA(J))**2
967 SM3=SM3+(FBB(J)-FBB(J))**2
970 CONTINUE
973  SR1=SM1+SM2+SM3
975 IF(SRM-SR1)790,790,980
980 AKK=AK
982 AMUU=AMU
985 APP=P
990 SRM=SR1
1000 PRINT 1010,AKK,AMUU,APP,SRM
1010 FORMAT(1X,3F7.2,F10.6)
1015 PRINT,XL(1),FCC(1),FAA(1),FBB(1)
1017 PRINT,XL(2),FCC(2),FAA(2),FBB(2)
1020 GO TO 790
1030 END
1040 ENDPROG
```

Definitions of symbols in Appendix(VI-1), (VI-2) and (VI-3):

XL(I): The strain in the Ith experimental data.

FC(I),FA(I),FB(I): The c, a, and b axis orientation function of the Ith experimental data.

XMK,XMM,XMP: The maximum limit of the orientation parameters.

XK,XMU,P: The starting values of the orientation parameters (K, η, P).

A1, A2: Accepted limit of deviation on comparing the theoretical and experimental orientation functions.

BE0: Initial value of the c axis tilting angle.

XL2: The transverse strain.

FCC(I),FAA(I),FBB(I): The theoretical values of the c, a, b axis orientation functions.

SR1: The total square deviations between the experimental and the theoretical results.

BE: The tilting angle of caxis, β.

OM: The lamellar twisting angle, ω.

EE: The rotational angle around the c axis, ϵ.

XTH(L),ZTH(L): The distribution of total number of the 110 and 200 plane normal.

X1,X2: The distribution of the 110 and 200 diffraction intensity of deformed spherulites of polyethylene.

TH: The azimuthal angle of the diffracted beam.

ST1,OFA,OFB,OFC: Static values of λ_3, f_a, f_b, f_c.

XK1,XMU1,XP1: Static values of the orientation parameters, K, η, P

SLIT-LENGTH COLLIMATION CORRECTION FOR GAUSSIAN WEIGHTING FUNCTION
(REVISED MARCH, 1969)

THIS PROGRAM SAXSC IS USED FOR CORRECTING SMALL ANGLE X-RAY SCATTERING INTENSITY FROM A FINITE SLIT SYSTEM WITH A GAUSSIAN WEIGHTING FUNCTION. THE USER IS REFERRED TO (P.W.SCHMIDT, ACTA CRYSTA.19,938 (1965)) FOR THE PROCEDURE AND INPUT DATA ARE EXPLAINED AS FOLLOWS.

THE ANGULAR INCREMENT IS A MILLIRADIANS. THE INTENSITY VALUES F(I) ARE GIVEN FOR SCATTERING ANGLES FROM A THROUGH A*IMAX. (THE FORTRAN SYMBOL * WILL BE USED TO DENOTE MULTIPLICATION. ZEROES ARE USED FOR F(I) FOR INTENSITIES AT WHICH EXPERIMENTAL DATA ARE NOT AVAILABLE.) FIVE INTENSITY VALUES ARE PUT ON EACH CARD IN (5E11.4) FORMAT.

THE PROGRAM CALCULATES CORRECTED INTENSITIES FROM J0*A MILLIRADIANS THROUGH N1*A MILLIRADIANS WITH AN ANGULAR INCREMENT N2*A MILLIRADIANS. CORRECTED INTENSITIES ARE COMPUTED NEXT FROM (N1 + N4)*A MILLIRADIANS THROUGH N3*A MILLIRADIANS WITH AN INCREMENT N4*A, AND THEN FROM (N3 + N6)*A MILLIRADIANS THROUGH N5*A MILLIRADIANS WITH AN INCREMENT N6*A, PROVIDED N6 DOES NOT EXCEED IMAX. CORRECTED INTENSITIES ARE NOT CALCULATED FOR ANGLES EXCEEDING IMAX*A MILLIRADIANS, REGARDLESS OF THE VALUES OF THE NUMBERS ON CARD 3 BELOW. (THIS IMAX VALUE IS THE VALUE FOR THE CURVE BEING CORRECTED.)

IN THE USE OF THIS PROGRAM, THE CARDS ARE ARRANGED AS FOLLOWS.

CARD 1. A

CARD 2. J0 AND IMAX. (THE VALUE OF J0 ON THIS CARD MUST EQUAL THE SMALLEST J0 VALUE USED WITH ANY OF THE SCATTERING CURVES BEING CORRECTED. THE IMAX VALUE ON THIS CARD MUST EQUAL THE LARGEST IMAX VALUE USED FOR ANY OF THE CURVES BEING CORRECTED.)

CARD 3. N1, N2, N3, N4, N5, N6

CARD 4. J0 AND IMAX FOR THE FIRST CURVE

CARD 5. THE FIRST CARD OF THE SET OF CARDS WITH THE INTENSITIES F(I)

THE OTHER CARDS FOR THIS CURVE THEN FOLLOW. FOR EXAMPLE, IF THERE ARE 80 F(I) IN THE FIRST CURVE, IMAX = 80, AND THERE 16 CARDS IN THE SET. FOR EACH SUCCEEDING CURVE, THE SET OF F(I) CARDS IS PRECEDED BY A CARD GIVING J0 AND IMAX FOR THIS CURVE.

AFTER THE LAST CURVE HAS BEEN CORRECTED, THE COMPUTER GIVES A STATEMENT INDICATING THAT THE END OF THE DATA HAS BEEN REACHED.

USUALLY IT IS MOST CONVENIENT TO HAVE THE VALUES OF N3 AND N5 BE AT LEAST AS LARGE AS N1 AND N3, RESPECTIVELY, WITH N2 AND N4 BEING NO LESS THATN N4 AND N6, RESPECTIVELY. HOWEVER, THESE CONDITIONS ARE NOT NECESSARY. FOR EXAMPLE, IF CORRECTED VALUES ARE DESIRED ONLY FOR A SINGLE ANGULAR INCREMENT, THE APPROPRIATE VALUES OF N1 AND N2 CAN BE CHOSEN, AND N3, N4, N5, AND N6 CAN ALL BE SET EQUAL TO ZERO, OR THESE POSITIONS CAN BE LEFT BLANK ON CARD 3.

THE LARGEST VALUES ALLOWED FOR THE NUMBERS ON CARDS 2, 3, AND 4 ARE DETERMINED BY THE DIMENSION STATEMENT AT THE BEGINNING OF THE PROGRAM. (THIS STATEMENT CAN BE CHANGED WHEN NECESSARY.) NO IMAX VALUE ON CARDS 2 OR 4 CAN EXCEED J00, AND NO INPUT CURVES CAN HAVE MORE THAN 400 DATA POINTS, ACCORDING TO THE DIMENSION STATEMENT USED IN THIS PROGRAM. WITH THE NUMBER 50 USED IN THE SECOND SUBSCRIPT OF T(I,JJ) IN THE DIMENSION STATEMENT, CORRECTED INTENSITIES CAN BE CALCULATED AT UP TO 50 ANGLES. THE ANGLES AT WHICH CORRECTED DATA ARE OBTAINED ARE SPECIFIED BY THE NUMBERS ON CARDS 2, 3, AND 4.

THE WIDTH OF THE GAUSSIAN WEIGHTING FUNCTION IS DETERMINED BY THE CONSTANT SL DEFINED EARLY IN THE PROGRAM. FOR A BEEMAN-TYPE FOUR-SLIT COLLIMATION SYSTEM WITH 50 CM. BETWEEN SUCCESSIVE SLITS AND WITH THE X-RAY BEAM UNIFORMLY ILLUMINATING THE ENTIRE LENGTH OF THE ENTRANCE SLIT, SL IS EQUAL TO THE SLIT LENGTH IN CENTIMETERS. THE CONSTANT SL MUST BE SPEC-

```
IFIED FOR EACH SLIT SETTING FOR WHICH CORRECTIONS ARE CALCULATED.
    IN OUR CASES, THE WIDTH OF THE GAUSSIAN WEITHTING FUNCTION IS
THEORETICALLY CALCULATED BY THE METHOD REPORTED BY P.W.HENDRICKS AND P.W.
SCHMIDT (1966).  WE HAVE A SEPARATED PROGRAM CALLED WEIGHT FOR THIS
CALCULATION.
      THE CONSTANTS L0, L1, AND L2 IN THE INPUT AND OUTPUT STATEMENTS MUST
BE DEFINED AT THE BEGINNING OF THE PROGRAM.
      IN STEP 103, ALOG IS A NATURAL LOGARITHM.  THIS NOTATION MAY HAVE TO
BE CHANGED FOR SOME COMPUTERS.
  ****2 BANKS ARE REQUIRED FOR UMASS SYSTEM****

  COMPUTATION OF LEAST SQUARES FIT TIJ
  DIMENSION T(220,100), E(200)
  DIMENSION EA(200)
  DIMENSION IMA(4),JJM(4),AT(4)
  DOUBLE PRECISION SL, PDELH, SQPI, A, SJ1(220), SJ2(220),
 1 SJ3(220), B, C, D, E, DD, EE, H, UIJ, V32IJ,V33IJ,
 2 T31IJ, DEL51, DEL52, DEL53, DEL42, VV
  L0=60
  L1=61
  L2=62
  PI=3.1415927D 00
  A1=3600.D 00
  SQPI = 1.7724538561D00
  PDELH=SQPI*10.81070 00
1 FORMAT(F6.4)
2 FORMAT(2I4)
3 FORMAT(6I4)
4 FORMAT(1H1,4X,10HANGLE(RAD),9X,10HANGLE(DEG),8X,14HCORRECTED INT.,
 19X,14HMEASURED INT. )
5 FORMAT(5E13.7)
6 FORMAT(1X,F12.6,8X,F12.6,4X,E20.8,2X,E18.6)
7 FORMAT(5X,F10.6,F15.6,5X,F10.6,2F15.6)
  READ (L0,1) A
  READ (L0,2) J0, IMAX
  READ (L0,3) N1, N2, N3, N4, N5, N6
  A=(A*PI)/A1
  N = N1
  NN = N2
  J00 = J0
  JJ = 0
0 DO 105 J = J0, N, NN
  IM = IMAX - J + 12
  JJ = JJ + 1
  DO 102 I = 6, 10
  SJ1(I) = 0.0
  SJ2(I) = 0.0
2 SJ3(I) = 0.0
  B = J
  IM1 = IM + 1
  DO 104 I = 11, IM1
  C = I - 10
  D = C*C + 2D0*C*B
  E = (C-1D0)*(C-1D0)+2D0*B*(C-1D0)
  DD=DSQRT(D)
  EE= DSQRT(E)
3 SJ1(I)=DLOG((C+B+DD)/(C+B-1D0+EE))
  SJ2(I)=(C+B-0.5D0)*SJ1(I)-DD+EE
4 SJ3(I)= 0.5D0*((C+B)**2-1D0/3D0+0.5D0*B**2)*SJ1(I)
 1  -0.75D0*(C+B)*DD+(0.75D0*(C+B)+0.25D0)*EE
```

```
      H = A * DDELH
      KA=0
      DO 605 I = 10, IM
      C = I - 12
      UIJ=DEXP(-(H*H)*(C*C+2D0*B*C))/(H*SDBI)
      V32IJ=SJ2(I-1D0)-2D0*SJ2(I-2D0)+SJ2(I-3D0)
      V33IJ=SJ3(I)-3D0*SJ3(I-1D0)+3D0*SJ3(I-2D0)-SJ3(I-3D0)
      T31IJ=UIJ* (SJ1(I-1D0)-SJ1(I-2D0)+V32IJ+V33IJ)
      DEL51= SJ1(I+1D0)-5D0*SJ1(I)+10D0*SJ1(I-1D0)-10D0*SJ1(I-2D0)+5D0*
     1 SJ1(I-3D0)-SJ1(I-4D0)
      DEL52 = SJ2(I+1D0)- 5D0* SJ2(I)+10D0*SJ2(I-1D0)-10D0*SJ2(I-2D0)
     1 + 5D0*SJ2(I-3D0)-SJ2(I-4D0)
      DEL53=SJ3(I+1)-5D0*SJ3(I)+10D0*SJ3(I-1)-10D0*SJ3(I-2)
     1 +  5D0*SJ3(I-3)-SJ3(I-4)
      DEL42=SJ2(I)-4D0*SJ2(I-1)+6D0*SJ2(I-2)-4D0*SJ2(I-3)+SJ2(I-4)
      VV=-2D0*DEL51+DEL52+6D0*DEL42+7D0*DEL53
      T(I,JJ) = T31IJ + (5.*UIJ*VV)/126.
      KA=KA+1
      IMA(KA)=I
      JJM(KA)=JJ
      AT(KA)=T(I,JJ)
      IF(KA.LT.4) GO TO 605
      WRITE(L1,400)
  400 FORMAT(14HCTIJ ELEMENTS /)
      WRITE(L1,601)(IMA(K),JJM(K),AT(K),K=1,4)
  601 FORMAT(4(3X,2I3,E16.8))
      KA=0
  401 FORMAT(5X,2I4,F16.8)
  605 CONTINUE
      IF(KA.GE.4) GO TO 105
      WRITE(L1,400)
      WRITE(L1,601)(IMA(K),JJM(K),AT(K),K=1,KA)
  105 CONTINUE
      IF (N - N3) 110, 111, 111
  110 N = N3
      NN = N4
      J0 = N1 + N4
      J01 = JJ - 1
      GO TO 100
  111 IF (N - N5) 112, 200, 200
  112 N = N5
      NN = N6
      J0 = N3 + N6
      J02 = JJ - 1
      GO TO 100
      SLIT LENGTH CORRECTION
  200 READ (L0,2) J0, IMAX
      READ (L0,5) (F(I), I = 1, IMAX)
      WRITE(L1,301)
  301 FORMAT(29H0 MEAS. INT. CORR. FOR BACKG.  //)
  302 WRITE(L1,303)(F(I),I=1,IMAX)
  303 FORMAT((5X,E13.7) )
      WRITE (L1,4)
      IF (J0 - N1) 201, 204, 204
  201 NN = N2
      JJ = (J0 - J00)/N2
      IF (N1 - IMAX) 202, 203, 203
  202 N = N1
      GO TO 220
  203 N = IMAX
```

```
      GO TO 220
  204 IF (J0 - N3) 205, 208, 208
  205 NN = N4
      JJ = J01 + (J0 - N1)/N4
      IF (N3 - IMAX) 206, 207, 207
  206 N = N3
      GO TO 220
  207 N = IMAX
      GO TO 220
  208 NN = N6
      JJ = J02 + (J0 - N3)/N6
      IF (N5 - IMAX) 209, 210, 210
  209 N = N5
      GO TO 220
  210 N = IMAX
  220 DO 230 J = J0, N, NN
      IMAX1 = IMAX + 12 - J
      JJ = JJ + 1
      SUM = 0.0
      DO 225 I = 10, IMAX1
      K = J + I - 12
  225 SUM = SUM + F(K)*T(I,JJ)
      X = J
      X=A*X
      Y = X*57.29578
      FA(J)=SUM
  230 WRITE (L1,6) X,Y,SUM,F(J)
      DO 300 IA=J0,N
      AC=(FLOATF(IA)*A)**2
  300 FA(IA)=FA(IA)*AC
      WRITE(6,500)
  500 FORMAT(40H0 INTENS. CORR. FOR LORENTZ-GEOM. FACTOR /)
      WRITE(L1,501)(FA(I),I=J0,N)
  501 FORMAT((5X,F16.8))
      IF (N - IMAX) 251, 200, 200
  251 IF(N - N3) 252, 261,261
  252 J0 = N1 + N4
      GO TO 205
  261 IF(N - N5) 262, 200, 200
  262 J0 = N3 + N6
      GO TO 208
      END
         SCOPE
@LOAD
@RUN,5,
3.
    2  27
    3   1  27   1
    2  27
     0.000          0.000          1.560          1.560          1.590
     1.650          1.720          1.850          1.990          2.070
     2.070          1.980          1.840          1.670          1.470
     1.260          1.030          0.810          0.650          0.520
     0.420          0.340          0.280          0.220          0.180
     0.140          0.110
@@GG
```

APPENDIX VII-2

```
LIST
10 PROGRAM L[illegible]ELL
30 A[illegible]=1.5[illegible]
50 PI=3.1415926
60 ALF=0.2
70 INPUT,XK,X4
80 AL=XK/(1.-XK)
90 [illegible]F=AL[illegible]*AL
100 [illegible]=[illegible]*2.*PI/(1.+AL)
110 FF=0.2
130 PFY=[illegible]*[illegible]
140 ALY=AL*Y
150 X1=([illegible]**2+[illegible]**2[illegible]**2-SINF(PFY)**2)/(SINF(PFY)**2+[illegible]**2+
151 [illegible]**2*[illegible]**2-2.*[illegible]*(COSF(ALY)*SINF(PFY)+2.*PFY*[illegible]*SINF(ALY)+
152 SINF(PFY))
170 [illegible]=((SINF((1.-[illegible])*[illegible])/((1.-F[illegible])*PFY)*(COSF((1.-FF)*ALY)+
171 SINF([illegible])*[illegible]COSF([illegible]ALY)/([illegible])-SINF([illegible])/[illegible]*COSF(ALY)
172 -1.)**2+(SINF((1.-F[illegible])*[illegible])/((1.-F[illegible])*PFY)*SINF((1.-FF)*ALY)+
173 SINF(FF*PFY)/(FF*PFY)*SINF(FF*ALY)-SINF(PFY)/PFY*SINF(ALY))**2)
175 [illegible]=F[illegible]/(F[illegible]**2*ALY**2)
180 FF1=1.-FF
190 FF2=1.-2.*FF
200 [illegible]=(4.+2.*[illegible]SINF(F[illegible]2*[illegible])/(F[illegible]2*[illegible])*COSF(F[illegible]2*ALY)-4.*SINF(FF1*
201 PFY)/(FF1*PFY)*COSF(FF1*ALY)-4.*SINF(FF*PFY)/(FF*PFY)*COSF(
202 FF*ALY)+2.*SINF(PFY)/PFY*COSF(ALY))/(FF**2*ALY**4)
230 XL1=[illegible]-F[illegible]+X1*[illegible]
240 PRINT,XK,X4,XL1
250 GO TO 70
300 END
310 ENDPROG
```

Definition of symbols in Appendix(VII-2):

AMB: The wavelength of the beam.

ALB: The structural parameter, β/α.

XKK: The linear crystallinity.

XM: Maxium scattering angle represented by $(c\sin 2\theta/\lambda)$.

EP: ϵ

BE: β

XLI: The diffraction intensity.

```
LIST
10 PROGRAM COMP
15 DIMENSION XAS(30),XCS(30)
20* THIS IS TO CALCULATE THE LOCAL STRAIN IN CRYSTALLINE POLY
21* MER USING THE COMPOSITE THEORY*
50 CO=0.
60 AOR=10.
100 XLD=100.
120 EEF=1000.
130 EEM=1.
140 G1M=0.5
150 G1F=0.3
160 H1F=EEF/(2.*(1.+G1F))
170 H1M=EEM/(2.*(1.+G1M))
175 PRINT 180
180 FORMAT(1X,* CRYSTALLINITY*,3X,* ASPECT RATIO*,3X,* CRYSTAL
181A MODULUS*,3X,* AMORPHOUS MODULUS*)
185 PRINT 190,CO,XLD,EEF,EEM
190 FORMAT(1X,F10.2,F17.2,F13.2,F15.2,/,)
200 P1=2.*XLD
210 CALL HAL(EEM,EEF,CO,P1,E11)
230 P2=2.*AOR
240 CALL HAL(EEM,EEF,CO,P2,E22)
250 P3=EXPF(ALOG(AOR)*3.**0.5)
260 CALL HAL(H1M,H1F,CO,P3,G12)
300 GG1=G1F*CO+G1M*(1.-CO)
310 GG2=GG1*E22/E11
320 Q11=E11/(1.-GG1*GG2)
330 Q22=E22/(1.-GG1*GG2)
350 Q12=GG2*E11/(1.-GG1*GG2)
360 Q66=G12
365 PRINT,Q11,Q22,Q66
370 S11=1./E11
380 S22=1./E22
390 S12=-1.*GG1/E11
400 S66=1/G12
410 U1=(3.*Q11+3.*Q22+2.*Q12+4.*Q66)/8.
420 U5=(Q11+Q22+4.*Q66-2.*Q12)/8.
430 SI1=(3.*S11+3.*S22+2.*S12+S66)/8.
440 SI2=(S11-S22)/2.
450 SI3=(S11+S22-2.*S12-S66)/8.
460 EAL=4.*U5*(U1-U5)/U1
470 GAI=U5
480 PAL=(U1-2.*U5)/U1
485 PRINT,GAL,PAL
490 AAS=(EAL-EEF)/(EEM-EEF)/(1.-CO)
500 ACS=(EAL-EEM)/(EEF-EEM)/CO
510 AAT=(1./EAL-1./EEF)/(1./EEM-1./EEF)/(1.-CO)
520 ACT=(1./EAL-1./EEM)/(1./EEF-1./EEM)/CO
530 PRINT 535
535 FORMAT(1X,5X,*  E11*,5X,* E22*,5X,* ISOTROPIC MODULUS*)
536A
540 PRINT 541,E11,E22,EAI
541 FORMAT(1X,F12.3,F8.3,F14.3,/,)
543 PRINT 545
```

```
545 FORMAT(1X,14X,* AVGE STRAIN*,3X,* AVGE STRESS*,3X,* CRY
546A STRAIN*,3X,* CRY STRESS*)
547 PRINT 548,AAS,AAT,ACS,ACT
548 FORMAT(1X,7X,4F15.4,/,)
550 PRINT 553
553 FORMAT(1X,* ANGLE*,2X,* E(TH)*)
555 TH1=0.
560 DO 685 I=1,19
565 TH=TH1/180.*3.1415926
570 AS1=SI1+SI2*COSF(2.*TH)+SI3*COSF(4.*TH)
590 AE=1./AS1
600 AE=(AE-CEM)/(CEE-CEM)/CO
605 XCS(I)=AE
610 AM=(AE-CEE)/(CEM-CEE)/(1.-CO)
615 XAS(I)=AM
620 PE=(1./AE-1./CEM)/(1./CEE-1./CEM)/CO
630 PM=(1./AE-1./CEE)/(1./CEM-1./CEE)/(1.-CO)
651A
660 PRINT 670,TH1,AE,AM,PM,AE,PE
670 FORMAT(1X,F5.1,F8.2,F9.4,F15.4,F15.4,F15.4)
680 TH1=TH1+5.
685 CONTINUE
690 PRINT 695
695 FORMAT(1X,*  XLC1*,3X,*  XLC12*,3X,*  XLC2*,3X,*  XLA2*,
696A 6X,*  XX2*)
700 CONTINUE
702 XLX=1.0
703 XLY=0.4
704 XLY=-0.4
705 TH2=0.
707 DO 740 J=1,19
708 TH=TH2/180.*3.1415926
709 PRINT,TH2
710 XLAX=XLX*XAS(J)
711 XLAY=XLY*XAS(19-J)
713 XLCX=XLX*XCS(J)
715 XLCY=XLY*XCS(19-J)
717 C2=COS(TH)**2
718 S2=SIN(TH)**2
719 XLA2=S2*XLAX+C2*XLAY
720 XLC1=C2*XLCX+S2*XLCY
722 XLC2=S2*XLCX+C2*XLCY
724 XLC12=-SIN(TH)*COS(TH)*XLCX+SIN(TH)*COS(TH)*XLCY
725 XX2=CO*XLC2+(1.-CO)*XLA2
728A
730 PRINT 733,XLC1,XLC12,XLC2,XLA2,XX2
733 FORMAT(1X,F5.3,3F9.3,F13.3)
735 TH2=TH2+5.
740 CONTINUE
745 END
750 SUBROUTINE HAL(F1,F2,CO,F3,F4)
760 F5=(F2/F1-1.)/(F2/F1+F3)
770 F4=F1*(1.+F3*F5*CO)/(1.-F5*CO)
780 RETURN
790 END
800 ENTRPG
```

Definitions of symbols in Appendix(VIII-1):

CO: The crystallinity.

AOB: The ratio of the transverse dimension and thickness of lamellae.

XLD: The ratio of the length and thickness of lamellae.

GEF, GEM: The elastic modulus of the reinforcement and matrix phase.

GlF, GlM: The Poisson ratio of the crystalline and amorphous phase.

TH1: The orientational angle of the lamellae.

XLX: The macroscopic strain along the stretching direction.

XLY: The macroscopic strain along the transverse direction.

AAS: The strain in the amorphous phase.

ACS: The strain in the crystalline phase.

XX2: The variation of the long period.

XLC1: The crystalline strain along the lamellar axis.

XLC12: The crystalline shear strain in the lamellar coordinate.